STRUCTURAL PROPERTIES OF SOLID IONIC HALIDES

A Thesis submitted for the Degree of Doctor of Philosophy

by

DEMETRIOS ZACHARIA DEMETRIOU

****

Department of Chemistry
University College, London

February 1991

THIS THESIS IS DEDICATED TO
MY SON RAPHAEL

"IF I HAVE EVER MADE ANY VALUABLE DISCOVERIES, IT HAS BEEN OWING MORE TO PATIENT ATTENTION THAN TO ANY OTHER TALENT"

SIR ISAAC NEWTON

ACKNOWLEDGEMENTS

It is a pleasure firstly to thank my Supervisor, Professor C.R.A. Catlow, for his advice and guidance with all aspects of the work reported in this thesis. I am also grateful to Professor A.V. Chadwick and Dr. A.D. Murray for their generous assistance with the major proportion of this study. Indeed I would like to extend my general gratitude to Dr. A.N. Fitch for his guidance with the X-ray powder diffractometer at the Chemistry Department of the University of Keele and Dr. G.J. McIntyre at the ILL concerning the single crystal neutron work.

I offer my thanks to my brother S.Z. Demetriou and all our friends for their tremendous support throughout this study.

ABSTRACT

In this thesis the structural properties of solid ionic halides and in particular several classes of fluorite structured materials have been investigated. The systems studied include: rare-earth fluorides and the anion excess alkaline earth fluorides, perovskite and elpasolite structured halides. The aim of this work is to understand and investigate:

1) The complex defect structures of the CaF_2 - $(Ln)F_3$ systems where Ln = La, Er and Nd. Chapter 3 of this thesis determines the effects of ageing (investigated by annealing samples at high temperatures for variable times) and dopant ion radius on the defect structures of the solid solutions of composition 95-50 mole per cent CaF_2-$(Ln)F_3$. The prepared and annealed compounds of all the three systems where characterized by X-ray powder diffraction.

2) The anion disorder of the perovskite fluoride $KCaF_3$. Chapter 4 describes a series of experiments using single crystal neutron diffraction on the D9 diffractometer at the ILL. The aim is to identify the nature and concentration of these defects, as has been achieved using single crystal neutron techniques for the high temperature superionic fluorites. This experiment therefore has offered an excellent opportunity to investigate a simple member of a

potentially larger and important class of high temperature superionics.

3) Several elpasolite structured halides, of general formula A_2BReX_6 (where A and B are monovalent ions and Re is a rare-earth cation). We present in Chapter 5 a study of several members of the A_2BReX_6 system which have been investigated by High Resolution X-ray Diffraction using the synchrotron radiation source at the Daresbury Laboratory. This work provides a basis for the further systematic investigation of these systems.

CONTENTS

Introduction

In this thesis we investigate the structural properties of a number of compounds which are chemically and structurally related to, or are themselves, good ionic conductors. This rapidly expanding field of solid state science has led to major new areas of scientific research and many applications in modern technology.

Solids which exhibit high ionic conductivities comparable to those of molten salts, are an important class of materials with a number of possible applications in technological systems ranging from high-energy-density batteries to lasers [1]. Consequently the investigation of these solids which are termed "solid electrolytes" or "fast-ion conductors" or "superionic conductors" is currently one of the most active areas of scientific research. The interest in this field is reflected in the numerous studies reported in review articles [2-5]. Among solid electrolytes, fast fluorine ion conductors particularly, have become a research field of growing importance. Materials with very good electrical performances have been prepared in this work with particular emphasis on fluorite-type materials. Solids with the fluorite structure are chosen because they are good models for superionic materials due to their relative structural simplicity and availability as large single crystals. Such materials have useful applications in

thermodynamic measurements, specific electrodes, solid-state batteries, electrochromic devices, gas sensors etc.

The performance of electrolytic oxides such as those derived from ZrO_2 with CaF_2-type structure, whose conduction is due to O^{2-} migration, is only good at high temperatures (t>600°C) [6-8]. In contrast, isostructural fluorides have a significant anionic conduction at relatively low temperatures [9]. This property is obviously a consequence of the higher mobility of F^- as a result of smaller size, but even more of lower electric charge and less covalent bonding. As a consequence, fluorides can be predicted to be the best anionic conductors. The hope therefore of discovering a suitable solid with a high F^- ion conductivity is not beyond reach. Furthermore, these materials are very often electronic insulators, an essential property for their use as electrolytes in electrochemical batteries [10-12].

An essential feature is the role which defects play in determining the macroscopic properties of technologically important materials. Knowledge of the nature and behaviour of defects is vital in order to gain detailed understanding of solid state phenomena in Chemistry, Physics, Metallurgy, Geology and in the production of catalysts, ceramics, semiconductor components and solid electrolytes.

The mechanisms affecting ion transport are almost invariably associated with point defects [13]. In addition to these thermally produced defects, other point defects can be formed by incorporation of aliovalent impurities in the crystal. Charge compensation requires the generation of extrinsic defects to preserve overall electrical neutrality. For instance, trivalent cations in alkaline-earth fluorides can produce F^- interstitials, whereas monovalent cations produce F^- vacancies. Fluorine ion vacancies can also result from the presence of divalent anions such as oxygen. Ionic diffusion in solids usually proceeds by the motion of these defects within the lattice [14].

The introduction of both experimental and theoretical techniques together with major development in existing methods have greatly increased the understanding of the defective solid state in the last decade.

The structural properties of solid ionic halides and in particular several classes of fluorite structured materials have been investigated. The systems studied include: rare-earth fluorides and the anion excess alkaline earth fluorides, perovskite and elpasolite structured halides.

The aim of this work is to understand and investigate:
1) The complex defect structures of the CaF_2-$(Ln)F_3$ systems where Ln=La, Er and Nd. Interest in these systems

(or, more precisely, in $Ca_{1-x}Ln_xF_{2+x}$ solid solutions with the fluorite structure type) grew after Goldschmidt [15] proposed a scheme of heterovalent isomorphous substitutions of Ca^{2+} by Ln^{3+} in the fluorite structure type. This scheme envisaged valency compensation by additional interstitial fluoride ions in the centres of the empty cubes of the fluorite structure and offered a basis for the isolation of a new type of "isomorphism with the occupation of space" in ionic crystals. Furthermore, interest in these systems has been stimulated by the use of their phases to produce laser materials [16-22], converters of infrared quanta to visible light [23-32], photochromic materials [33,34], thin-film capacitors [35,36] etc.

Many authors have investigated the phase equilibria between alkaline-earth fluorides and rare-earth trifluorides [23,37-44]; in particular, the BaF_2-RF_3 [43] and CaF_2-RF_3 [41] systems have been exhaustively examined by Sobolev and his co-workers. Despite intensive investigations of these classic disordered solid phases, there remain several puzzles in understanding their complex defect structures. Early work using both neutron diffraction [45] and computer modelling methods [46] supported the formation of dopant/interstitial dim ers and trim ers in systems containing 5-10 mole per cent of the trivalent ion dissolved substitutionally in the fluorite structured host.

More recent work [47] has proposed more complex structures, in particular the cubo-octahedral structure containing 6 dopant ions. Computer modelling studies [48] have suggested that the relative stability of the different cluster types depends on the radius of the dopant ion, with clusters of the 2:2:2 and 4:3:2 type being stable for the larger dopant ions (e.g. La^{3+}) and the cubo-octahedral aggregates having greater stability for the smaller dopant ions (e.g. Y^{3+}, Er^{3+}). These predictions have been supported by EXAFS studies [49], and by recent single crystal neutron diffraction work [50,51].

Chapter 3 of this thesis determines the effects of ageing (investigated by annealing samples at high temperatures for variable times) and dopant ion radius on the defect structure of the solid solutions 95-50 mole per cent CaF_2-$(Ln)F_3$ where Ln=La, Er and Nd. The possible importance of temperature effects has been highlighted by conductivity work [52], whilst a preliminary X-ray diffraction study undertaken at University College London has suggested that ageing may lead to substantial effects on the cluster structures, as would be expected in view of the very low dopant ion diffusion coefficients.

The prepared and annealed compounds of all the three systems under investigation w ere characterized by X-ray diffraction at the Chemistry Department of the University of Keele.

2) The anion disorder of the perovskite fluoride $KCaF_3$. Perovskite Fluorides, ABF_3 (A = alkali metal, B = divalent cation) have invoked considerable interest following the suggestion [53] that the perovskite structure is conduc ive to fast anion conduction. In this context it was noted that high pressure $MgSiO_3$ has a distorted perovskite structure; fast ion conduction in this material, which is thought to be a major constituent of the earth's inner mantle could have important geophysical implications. Indeed fast-ion motion has been claimed in $NaMgF_3$ [53], however, more recent work [54] did not show the phenomenon to be present in $NaMgF_3$ and $KMgF_3$. There is good evidence for high temperature fast ion conduction in $KCaF_3$ [54] and $CsPbF_3$ [55] suggesting that the nature of the B ion plays an important role in transport. At low temperatures the mobile defect is the F^- vacancy [54]. However, little is known about the defect structures.

The general aim of this experiment dealt with in Chapter 4 of this thesis is to identify the nature and concentration of these defects, as has been achieved using single crystal neutron techniques for the high temperature superionic fluorites [56]. The high temperature defect structure was identified in single crystal neutron diffraction experiments on the D9 diffractometer at the ILL. This experiment therefore has offered an excellent opportunity to investigate a simple member of a potentially larger and important class of high temperature superionics.

3) Several elpasolite structured halides, of general formula A_2BReX_6 (where A and B are monovalent ions and Re is a rare-earth cation). These materials, are known to be good fluoride ion conductors [57] with a perovskite related structure. Several members of this class of materials undergo a number of phase transitions involving distortion of the ReX_6 octahedra. The majority of the compounds A_2BReF_6 and A_2BReCl_6 crystallise with the elpasolite structure of space group O_h^5 [58] and are of great interest. Only a very small number of insulating rare-earth compounds with cubic point symmetry are known (mainly spinels and divalent fluorites RF_2) and the present isostructural series provides a basis for the systematic study of the effect of changing the rare-earth ion. The symmetry is the same as in previously examined rock-salt structures for which physical phenomena associated with crystal field effects have been very satisfactorily explained using theoretical models. There have been several studies of the crystallographic [58-62], optical [63,64], magnetic [65-67], and spectroscopic [68,69] properties of these classes of compounds. The main theme of Chapter 5 of this thesis is concerned with the structural studies of several members of the A_2BReX_6 system which have been investigated by High Resolution X-ray Diffraction using the synchrotron radiation source at the Daresbury Laboratory. Furthermore, this work provides a basis for the further systematic investigation of these systems.

CHAPTER 1

STRUCTURAL CONSIDERATIONS OF IONIC CRYSTALS

1.1 Nature and Occurrence of Point Defects

A crystal is a regularly repeating three dimensional array of atoms or ions or molecules. Ionic crystals, however, consist of arrays of different charged ions which are attracted together mainly by electrostatic forces. These ions rearrange themselves in a manner such that the coulombic attractions of oppositely charged ions overcome the repulsion of like ions. Once the centres of these oppositely charged ions come within a certain close proximity, the repulsive overlap of the outer of the electron clouds reaches equilibrium with the electrostatic attractive forces and a stable crystal structure is formed.

An important group of ionic solids with the formula MF_2 crystallize in what is known as the fluorite structure (section 1.2.2). The structure of the fluorite lattice is shown in Figure (1.1). In a compound MF_2 each anion is surrounded by four cations disposed tetrahedrally, whereas each cation is surrounded by eight anions at the corners of a cube [70]. The lattice can be described as a simple cubic array of anions with a cation at every alternate cubic centre.

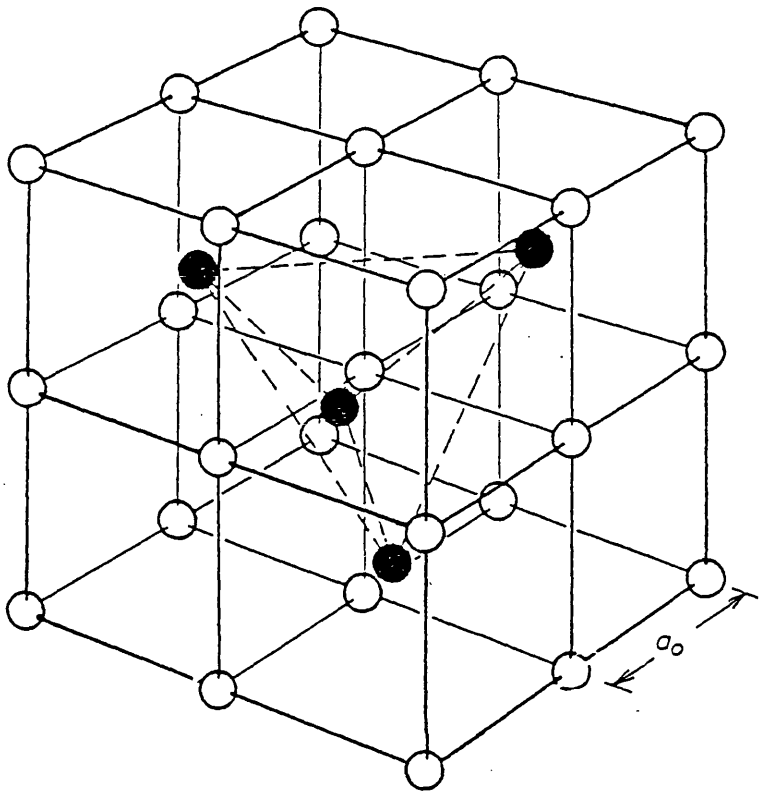

FIG. 1.1: THE STRUCTURE OF THE FLUORITE MF_2 LATTICE. ○ F^- anions, ● M^{2+} cations.

A perfect lattice such as that described above in which each ion occupies the site assigned to it on the basis of the crystal structure and where none of these sites is empty, does not exist at temperatures above absolute zero. In real crystals the lattice will deviate to some extent from the ideal lattice, not only disturbed by thermal atomic vibrations but also by the appearance of lattice imperfections. Important among other lattice imperfections present in solids are:

a) gross defects

b) point defects.

The gross defects extend over many interatomic distances where the regular infinite array of the perfect lattice breaks down. They can be classified as: line defects (e.g. dislocations), plane defects (e.g. grain boundaries, shear structures, surfaces) and volume defects (e.g. voids, inclusions of second phase). Gross defects are of a non-equilibrium nature in the sense that they cannot exist in measurable concentrations as thermodynamically stable imperfections. Of particular importance are the dislocations as they may play an important role in determining many of the physical properties of the crystals. However, in well annealed single crystals they would have negligible effect on the lattice diffusion, except at the low temperatures.

We shall be concerned here with the so-called <u>point-defects</u>, i.e. those of atomic size. Impurity atoms taking

the place of normal atoms or in interstitial positions of the lattice are examples of point defects. Intrinsic point defects are spontaneously produced in a crystal at non-zero temperatures when atoms leave their normal lattice sites to occupy some other places as a result of thermal agitation. The two most important types of intrinsic point defects are vacant lattice sites or vacancies and atoms placed in sites that are normally not occupied, so called interstitials.

Intrinsic defects occur in all crystalline solids and in ionic crystals these defects in general carry an effective electric charge. Thus, defects of one kind would leave the crystal charged or would produce high electric fields between the interior and the surface of the crystal. Consequently, positive and negative charged defects must be produced in the different sublattices in quantities that guarantee charge neutrality.

1.2 Defects in Solid Fluorides

1.2.1 Introduction

Many of the important properties of crystalline solids are controlled by defects. For example, transport properties (electrical conductivity and diffusion) are due to the migration of point defects [14,71]. Furthermore the thermodynamic and mechanical behaviour of solids arises as a result of their defect structure. Solid fluorides, despite the relative simplicity of their crystal

structures, range from highly perfect to highly disordered solids and are relevant in explaining many important features of solid-state chemistry such as superionic conduction and photochromism. Alkaline earth fluorides (e.g. CaF_2, SrF_2 and BaF_2) show an exceptional variation in their defect chemistry. At low temperatures, the pure fluorides are typical ionic solids with low levels of intrinsic disorder due to the high electronegativity of fluorine. On the other hand, these materials at high temperatures show superionic properties [72,73] i.e. ionic conductivity values of the same order of magnitude as those of molten salts. Doping of fluorides with trivalent rare earth cations e.g. La^{3+} will induce appropriate concentrations of charge-compensating defects. The structural properties of heavily defective phases are among the most intensively studied topics of solid-state chemistry [74]. In addition, properties of irradiated materials are of great interest. The electronic defects created have been studied using spectroscopic and theoretical methods [75]. The photochromism of the doped materials is of special interest [76]. Other disordered fluorides such as high temperature rare-earth fluorides which have superionic properties are also of great interest. In addition, to the fluorides already mentioned, other compounds also adopt the fluorite structure:-

(i) CdF_2, β-PbF_2 and $SrCl_2$

(ii) Oxides (e.g. CeO_2, ThO_2, UO_2 and stabilised ZrO_2)

(iii) Oxides (e.g. Li_2O) and sulphides (e.g. Na_2S) which adopt the related anti-fluorite structure.

Several fluorite-structured materials are of technological importance e.g. UO_2 is used as a fuel in nuclear reactors, stabilised ZrO_2 as an electrolyte in fuel cells and oxygen sensors [77] and the fluorides in solid state lasers [78] and as fluoride ion conductors [9].

1.2.2 The Fluorite Lattice

The structure of the fluorite lattice is shown in Fig. (1.1). In a compound MF_2 each anion is surrounded by four cations disposed tetrahedrally whereas each cation is surrounded by eight anions at the corners of a cube [70]. The lattice can be described as a simple cubic array of anions with a cation at every alternate cubic centre. The presence of the unoccupied anion cubes means that it is a very "open" structure and this leads to very interesting defect behaviour. The occupied cubes are connected (as are the vacant cubes) by edge sharing: i.e. the cations form a <110> net in the simple cubic anion array. This manner of describing the fluorite structure enables us to envisage defect structures more easily. It can be seen that the most obvious site for incorporation of interstitials is at the centre of one of the vacant anion cubes whilst other point defects (vacancies and substitutionals) are at the regular cation and anion sites of the lattice. Fig.(1.2)

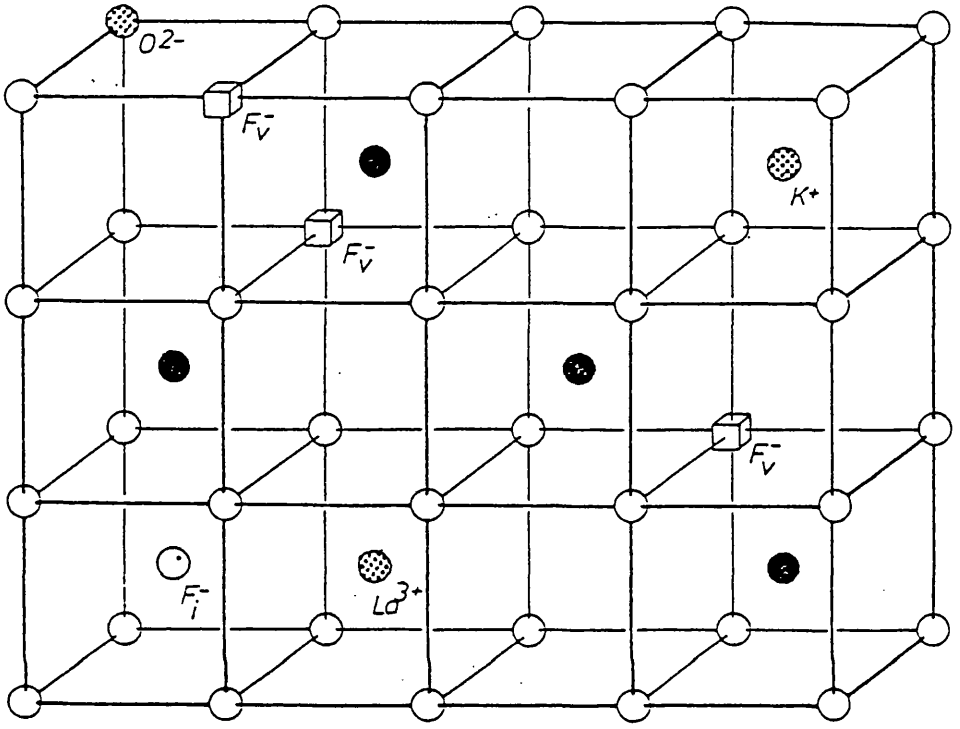

FIG.1.2: THE FLUORITE LATTICE CONTAINING POINT DEFECTS.
F_v^- vacancy, F_i^- interstitial, impurity ion

shows the various point defects likely to occur in a fluorite lattice.

1.2.3 Intrinsic Point Defects

There are two major possibilities to be considered for the dominant point defect structures in pure CaF_2, as have been predicted by simple theoretical models:

(a) anion-Frenkel pairs (anion vacancies and anions on the cube-centre interstitial sites) and

(b) Schottky triplets (cation and anion vacancies).

With respect to the perfect lattice, the effective charges of these defects are +1e, -1e and -2e (where e is the charge of a proton) for the anion vacancy, anion interstitial and the cation vacancy respectively. If the anion-Frenkel pairs are the dominant defects, then doping the cation sub-lattice with M^{3+} ions (effective charge +1e) will increase the anion interstitial concentration; doping, however, with M^{+} ions (effective charge -1e) will increase the anion vacancy concentration. On the other hand, if Schottky triplets dominate, doping with M^{3+} will increase the cation vacancy concentration and doping with M^{+} will again result in an increase in the anion vacancy concentration. Long-range Coulomb interactions need to be taken into account, since the aliovalent dopant ions and the defects they create have opposite effective charges. At low temperatures or high dopant concentrations, these lead to the formation of impurity-defect complexes with the two series on neighbouring sites. Some simple complexes

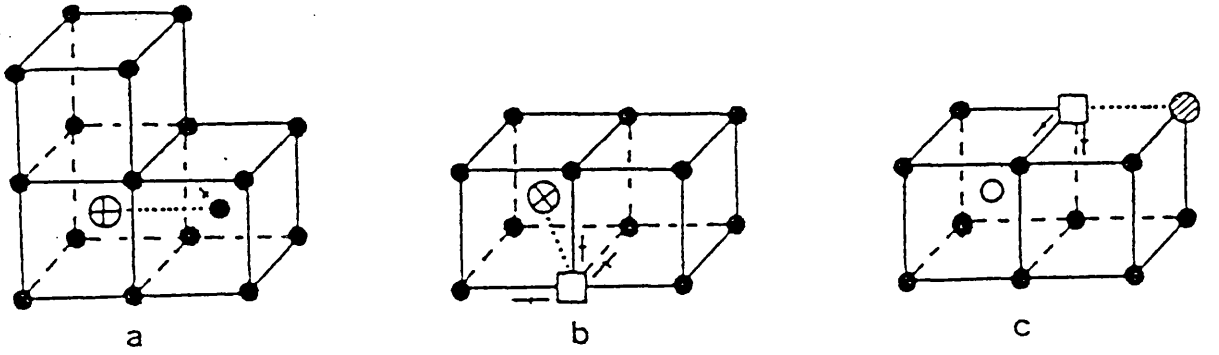

FIG. 1.3: Simple impurity-defect complexes in CaF_2. The filled circles represent the anions, the open circles the cations and the open squares the anion vacancies. The arrows indicate the direction in which the defects move when the complex reorients. (a) M^{3+} - interstitial anion nearest neighbour complex ($\oplus$ = M^{3+} ion); (b) M^{+} - vacancy nearest neighbour complex ($\otimes$ = M^{+} ion); (c) O^{2-} - vacancy nearest neighbour complex ($\circledcirc$ = O^{2-} ion).

expected at low impurity concentrations of less than 1 mole percent are given in Fig. (1.3).

1.2.4 Solid State Diffusion Mechanisms in Fluorite Lattices

Ionic movement in solids can take place when defects are present in the crystal lattice. The different types of defects give rise to different mechanisms of diffusion. These are illustrated schematically in Fig. (1.4) for fluorine motion in a fluorite lattice:

(i) Vacancy Mechanism: The diffusion is said to take place by the vacancy mechanism if an ion in any lattice site adjacent to a vacancy exchanges places with the vacancy. The vacancy wandering through the lattice in this way leaves behind a trail of ions displaced over one or more lattice steps, when the vacancy has passed the ion site. In a fluorite lattice, the more likely vacancy jumps of fluorine ions are the simple ⟨100⟩ jumps Fig.(1.4a).

(ii) Interstitial Mechanism: in which an interstitial ion hops to any one of the neighbouring interstitial sites without permanently displacing any other ion. Thus, in contrast with the vacancy mechanism, it causes a longer-range migration of single ions. This is also called a direct interstitial mechanism Fig.(1.4b).

(iii) Interstitialcy mechanism: in which an interstitial ion displaces a neighbouring lattice ion (of its own kind) into a new interstitial position and itself takes up the vacated lattice site Fig.(1.4c). In this mechanism, the

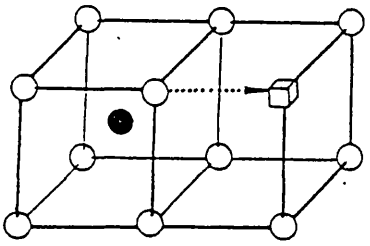

a) VACANCY MECHANISM
⟨100⟩ JUMPS

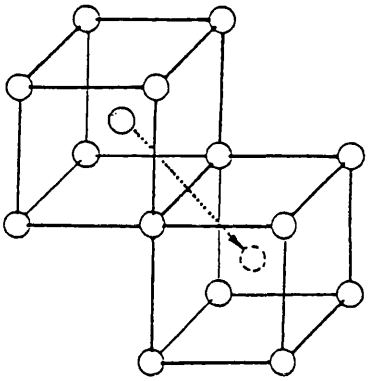

b) INTERSTITIAL MECHANISM
⟨110⟩ JUMPS

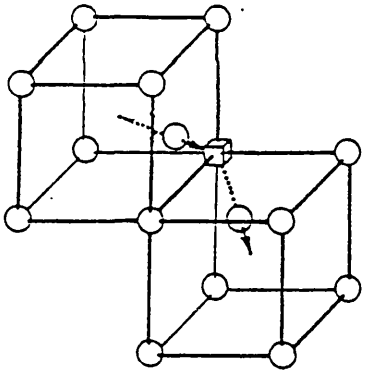

c) INTERSTITIALCY MECHANISM
(NON-COLLINEAR)

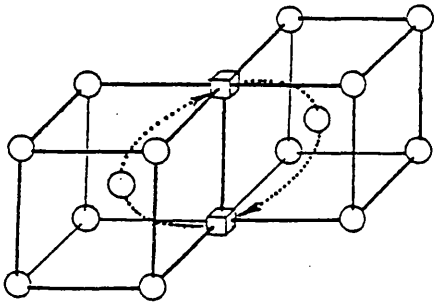

d) EXCHANGE MECHANISM

FIG.1.4: DIFFUSION MECHANISMS IN FLUORITE LATTICES
● Cation M^{2+}; ○ Anion F^-; ◻ F^- Vacancy.

interstitial defect cuts a trajectory through the lattice, hitting lattice sites and the individual ions along the path are effectively displaced by one or more lattice steps. If the ion on the normal lattice site is pushed in the same direction as that of the interstitial ion, the jump is termed collinear. If the ion is pushed in any other direction to one of the other neighbouring sites, the jump is termed non-collinear. The non-collinear jumps can occur in a forward direction or in a backward direction. In a fluorite lattice the collinear and the backward non-collinear modes of the interstitialcy mechanism are forbidden for fluorine motion since these jumps are blocked by the M^{2+} ions. For the same reason, the direct ⟨100⟩ interstitial jumps are also discarded. Thus, we are left with only two possible diffusion mechanisms for the interstitial ions; the interstitial mechanism involving ⟨100⟩ jumps through a cube edge to a neighbouring interstitial site Fig.(1.4b) and the non-collinear forward interstitialcy mechanism. Simple considerations based on the lattice geometry and size of the ions might indicate that the direct ⟨110⟩ interstitial jump is the less likely mechanism because the lattice distortion would become large enough to make it inoperative. This assumption is supported by theoretical calculations of migration energies in alkaline earth fluorides.

Non-defect assisted processes have also been suggested. There is the ring diffusion where atoms roughly situated in

a ring move together so that the whole ring rotates by one atomic distance. This seems unlikely in ionic crystals. Nevertheless, a non-defect assisted mechanism very likely to occur in a fluorite lattice is the direct exchange of two neighbouring fluorine ions. This mechanism has been proposed by Catlow [79] based on theoretical calculations and proceeds by a concerted migration of two lattice ions via interstitial sites passing through the saddle point shown in Fig. (1.4d). The calculated Arrhenius energies for the direct exchange indicate that it may be operative in the intrinsic region of the defect assisted diffusion. The preceding description has been restricted to mechanisms of lattice diffusion within solids. Diffusion also takes place along dislocations, grain boundaries and surfaces and it is generally agreed that diffusion along such imperfections is more rapid than lattice diffusion. Dislocations can act as sources and sinks for point defects. Thus, if for example it requires less energy to form a F^- vacancy than a F^- interstitial in these regions, more vacancies than interstitials will diffuse into the bulk of the crystal. This would leave an excess of charge at the dislocation and an electrostatic potential is set up which influences in turn the energy of formation of the defects.

1.2.5 Superionic Fluorides

Fluorite-structured materials appear to show a diffuse phase transition, manifested by a λ-type specific heat

anomaly [80,81]. within a few hundred degrees of their melting point. Typical data are illustrated in Fig. (1.5) for PbF_2. The materials show exceptionally high ionic conductivity, above the phase transition temperature T_c, with the Arrhenius plot levelling off as shown in Fig. (1.5). The overall view is that the diffuse phase transition and the superionicity are due to the generation of disorder on the anion sublattice, but the extent and nature of this disorder have been a matter of considerable controversy. Derrington et al., [82], in earlier work, proposed disordering of the anion sublattice at T_c and the term sublattice melting was used to describe this process. The extent of disorder has been shown, however, using diffraction studies [83] to be (far) more limited than implied by this term. These studies have shown that in the superionic phase most anions (>90%) are still located at the regular lattice sites. This has also been given further support from evidence obtained from dynamic computer simulation studies [84,85]. Furthermore, energetic considerations of the generation of high levels of disorder were shown, by Catlow [72], to be incompatible with enthalpy values of the diffuse transitions as obtained from the specific heat data. Consequently, it appears that the diffuse phase transition involves the generation of about 1 to 5 mol% of anionic defects, the high mobility of which is responsible for the superionic properties of the high-temperature phase. The question raised however, by such models is why the generation of disorder does not

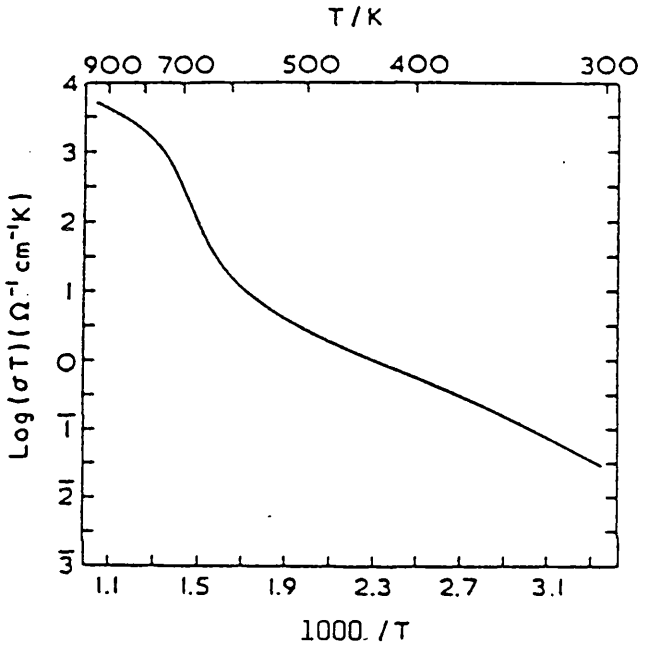

FIG. 1.5: Arrhenius plot of the conductivity of PbF_2. Note the levelling off of the plot above the phase transition temperature T_c.

continue beyond the diffuse phase transition, as is suggested by both the specific heat data and the flatness of the Arrhenius plot of the conductivity above T_c illustrated in Fig (1.5). Dickens et al. [86] suggested a possible solution to this problem. He proposed that in the superionic phase there were significant concentrations of interstitial-vacancy clusters of the type illustrated in Fig. (1.6). These clusters are similar to the dopant-interstitial clusters discussed in section 1.2.6. Energy calculations by Catlow and Hayes [87] have shown these to be stable. Their formation provides a good explanation of the observed features of quasi-elastic and Bragg scattering data. It may be argued therefore, that in the neighbourhood of T_c, the vacancy and interstitial concentrations have reached sufficient levels to produce such clusters. Repulsive interactions between these bulky defects, however, prevent further large-scale generation of disorder above T_c. A great deal of theoretical and experimental work needs to be carried out before such models are universally accepted.

There has been speculation that superionic behaviour is present in high temperature LaF_3 and YF_3 and in the former case there is also clear evidence for a specific heat excess [88], which starts at ~1100°C and continues up to the melting point (unlike the λ-type anomaly observed for the fluorites). There is, however, no definite knowledge of the defect structure in these superionic phases.

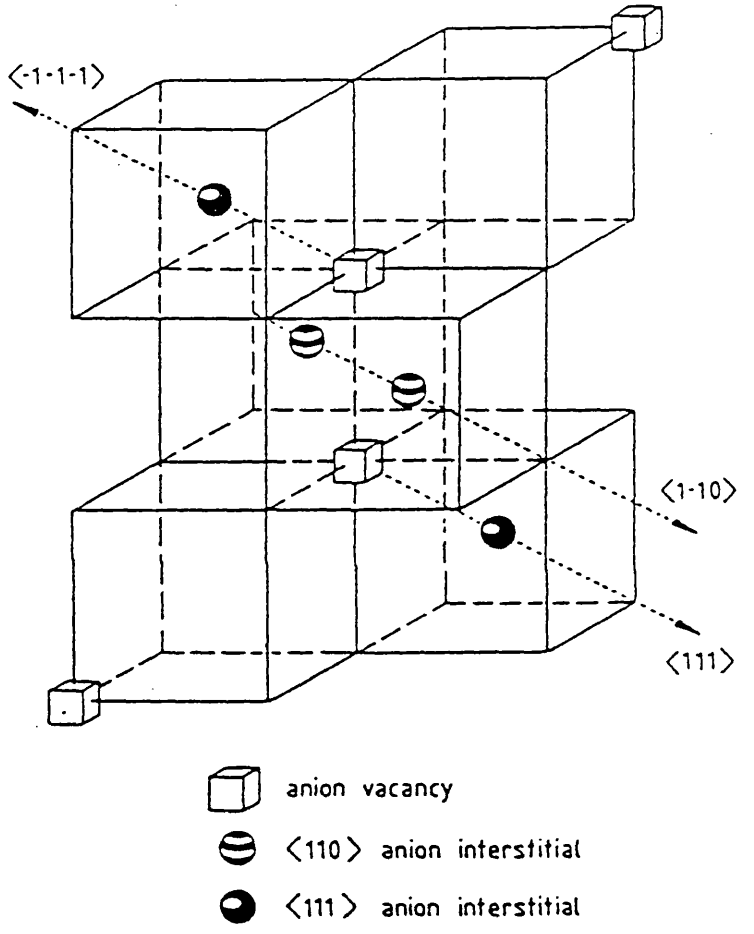

FIG. 1.6: Interstitial-vacancy complex proposed by Dickens et al. (1982) for high-temperature fluorites.

Note the similarity to the dopant-interstitial complexes shown in Fig. 1.9

In addition to high temperature superionic behaviour in LaF_3 and YF_3 [88], doped fluorite structured fluorides may also show high ionic conductivity. This property arises from the very high levels of disorder that can be induced by doping of alkaline-earth fluorides by trivalent ions.

1.2.6 Doped Alkaline-Earth Fluorides

Alkaline-earth fluorides have the capacity to form solid solutions, retaining the fluorite structure, with high concentrations (up to 40 mol%) of rare-earth fluorides. The rare-earth cations enter the lattice at cation sites; electroneutrality is restored by the creation of anion interstitials, which in heavily doped materials are consequently present in high concentrations.

Much of the interest in these materials has concentrated on the structural features of the high interstitial concentrations. For low dopant concentrations (<1 mol%), the defect structure appears to be simple. Spin resonance studies [89], have shown the formation of simple pair clusters, see Fig.(1.7). Here, the interstitials are bound to sites neighbouring the dopant, owing to the coulombic interaction between the substitutional dopant and its charge-compensating defect. Diffraction techniques show a more radical structure at more concentrated interstitial solutions (>5 mol% dopant). The presence of interstitials at sites strongly displaced from the body-centre positions of the cubic interstitial site, which are occupied in the

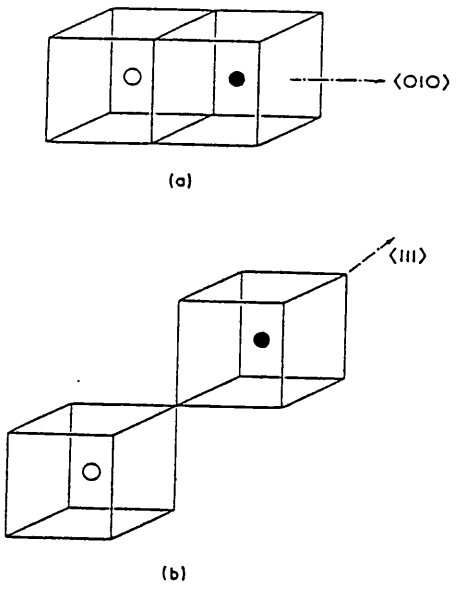

FIG. 1.7: Simple cluster of trivalent ions and interstitials in doped alkaline-earth fluorides: (a) nearest-neighbour pair: (b) next-nearest-neighbour pair.

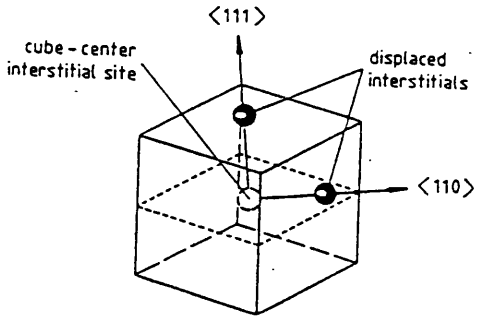

FIG.1.8: Interstitial position [110] and [111] in anion-excess fluorides.

low-concentration region, where revealed from refinements of neutron Bragg diffraction data by Cheetham et al. [45] and Catlow et al.[50,51]. There are two types of displaced interstitial: one is displaced along the [110]; and the other along the [111] direction Fig.(1.8). In addition the Bragg diffraction data showed the presence of vacancies.

Cheetham et al. [45] argued that their results on Y^{3+} - doped CaF_2 could be explained in terms of the formation of interstitial clusters. The models they proposed are illustrated in Fig.(1.9); the smaller "2:2:2" cluster had been suggested by Willis [90] in studies on the iso-structural nonstoichiometric UO'_{2+x} phase. The cluster includes both [110] and [111] interstitials as well as vacancies, and as such can rationalise the results of the Bragg scattering data. Furthermore, the ratios of the various types of species in the 2:2:2 cluster are compatible with Bragg scattering data on 5 mol% Y^{3+}-doped CaF_2, whereas the 4:3:2 model seems to explain the data for 10 mol% solution. For higher dopant concentrations, however, it is doubtful whether any simple cluster model would be applicable.

The models proposed by Cheetham et al. [45] were supported using calculations of clusters energies by Catlow [46,91]. These studies showed that the clusters were strongly bound when dopant ions were in nearest-neighbour cation position with respect to the interstitial cluster. This work

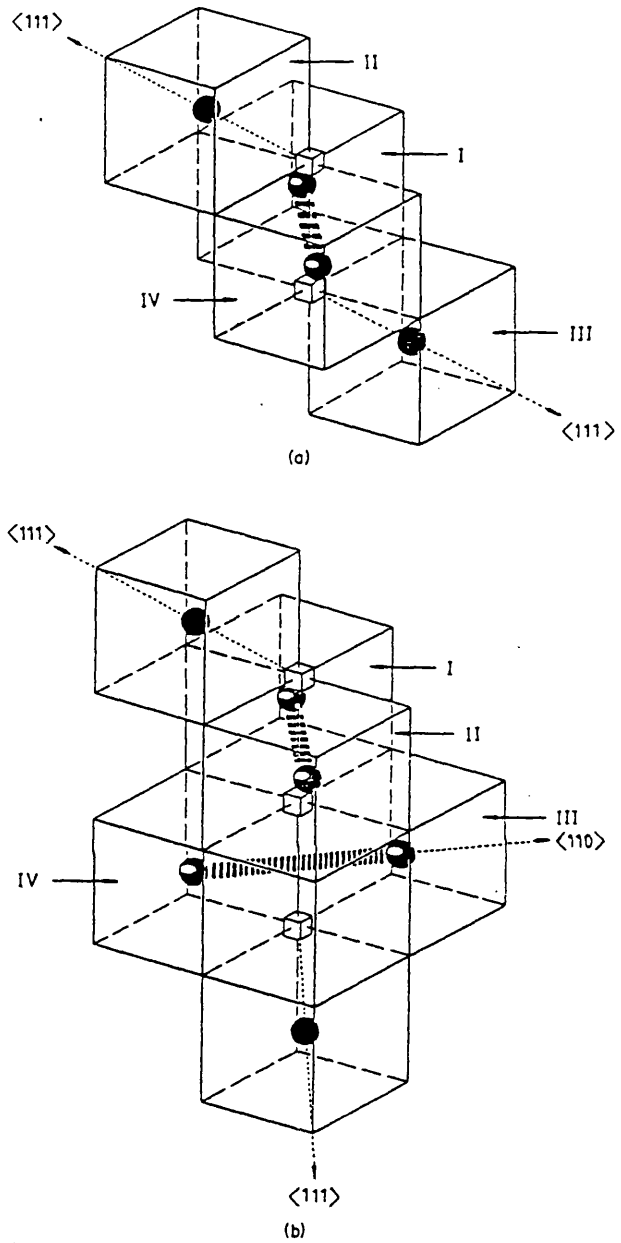

FIG. 1.9: Interstitial clusters "2:2:2" (a) and "4:3:2" (b)

provided a more plausible rationalisation of the structure of these unusual clusters. Thus, the 2:2:2 cluster is essentially a dimer of the simple pair clusters shown in Fig.(1.7). The most obvious structure for such a dimer is shown in Fig.(1.10). However, calculations showed that such clusters were unstable, and the stability required a coupled relaxation in which interstitial ions move inward (to become [110] interstitials) and lattice ions are displaced toward interstitial sites (to become [111] "interstitials" and leaving vacancies).

This process generates the 2:2:2 cluster and was shown by the calculations to be highly favoured energetically. Similar arguments apply to the 4:3:2 cluster. Other workers [92], using x-ray techniques usually in very heavily doped CaF_2, have suggested larger, more complex cluster structures in which six dopant ions are grouped around a central interstitial site. Lattice anion sites surrounding the interstitial position are vacant, but anions are situated above each edge of the cube to give the structure shown in Fig.(1.11). Support for these models is provided by the observation by Bevan et al. [93] of an ordered system($Ca_{14}Y_5F_{43}$, which is a naturally occurring mineral, tveitite). The structure is based on the cubo-octahedral arrangement of trivalent ions within a fluorite-structured host. Mixed-fluoride systems (e.g.$RbBi_3F_{10}$/ KY_3F_{10}) also contain this type of cubo-octahedral anion cluster.

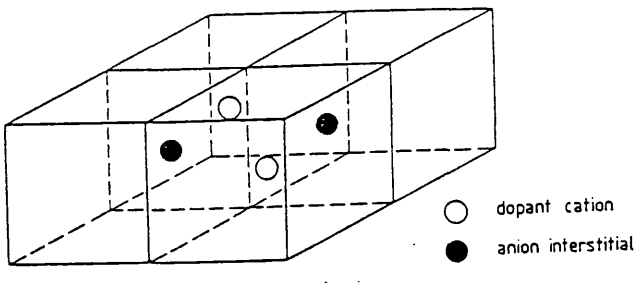

FIG. 1.10: Planar dimer of two dopant-interstitial pairs.

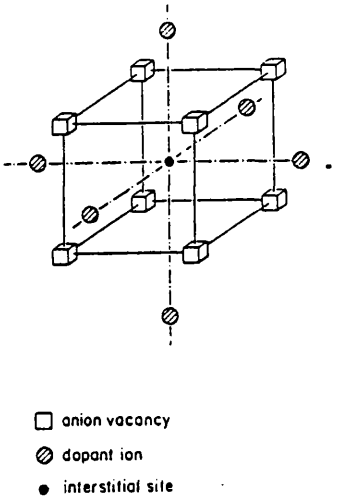

FIG. 1.11: Cubo-octahedral dopant-interstitial cluster. Note that interstitials are present above each cube edge.

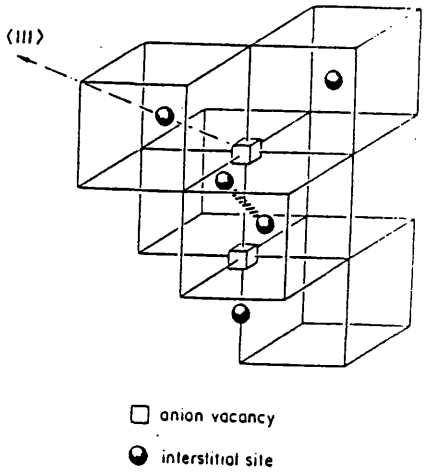

FIG. 1.12: Cluster formed by capture of interstitial by 2:2:2 cluster

Information on the factors controlling the stability of the cubo-octahedral structures has been provided by calculations of their energies [94]. This work showed that the stability of such clusters relative to the 2:2:2 and 4:3:2 models was critically dependent on the size of the dopant ion relative to that of the host-lattice cation. For large cations (e.g. La^{3+}) the 2:2:2 type of model is preferred, whereas smaller cations show greatest stability for the cubo-octahedral clusters. Neutron diffraction studies [50,51] on La^{3+} - and Er^{3+} -doped CaF_2 involves the capture by the 2:2:2 cluster of an additional interstitial to give a different cluster (see Fig. 1.12). The stability of these clusters was strongly supported by calculations [50,51].

On summing up, there appears to be a highly complex range of possible cluster structures for doped fluorite-structured fluorides. What type of structure is adopted depends on the size of the dopant ion and in addition, on factors such as the duration of the high temperature anneal. This factor is relevant because of the low cation mobility in the fluorite structure. It is finally noted that it is possible to dope alkaline-earth fluorides with low-valence ions (e.g. Na^{+}), which induce a charge-compensating vacancy population although the solubility of monovalent dopants is generally less than 1 mol% very much less than that of trivalent ions. Low solubilities of aliovalent dopant ions are also observed with the alkali

metal fluorides; there appears to be high dopant solubilities in LaF_3, although the doped rear-earth fluorides had not been extensively investigated. In view of this, the work described in Chapter 3 investigates further the effects of annealing samples at high temperatures for variable times and in addition the variation of cluster structure with dopant ion radius. Consequently three systems of solid solutions 95-50 mole per cent CaF_2-$(Ln)F_3$ where Ln = La, Er and Nd were studied.

1.2.7 Ionic Conductivity in Heavily Rare-Earth Doped Fluorides

In view of the high interstitial concentrations in heavily doped materials, it might be expected that these materials would show high ionic conductivities. Schoonman and co-workers [95] have therefore performed extensive conductivity studies of heavily doped alkaline-earth fluorides and an interesting feature of their results is the decrease in the activation energy for conductivity with the dopant concentration. Thus, they attribute to the occurrence of relatively easy conduction paths around the clusters. However, the conductivity of these materials is generally not sufficient to justify the use of the term 'superionic materials'.

Further studies by Chadwick et al. [52] on the ionic conductivity of rare-earth doped CaF_2 have shown that conductivity of CaF_2 increases with doping and also depends

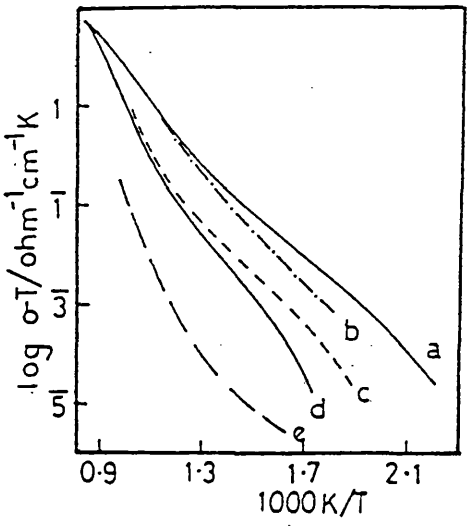

FIG.1.13 : Conductivity plots for $Ca_{0.9}RE_{0.1}F_{2.1}$ RE = Gd(a), La(b), Er(c), Yb(d) and nominally pure (e).

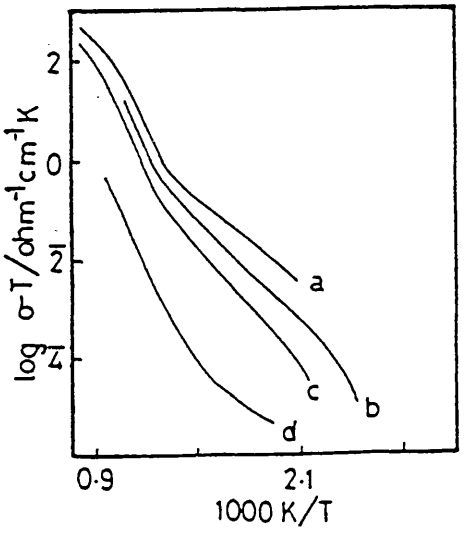

FIG. 1.14: Conductivity plots for $Ca_{1-x}Er_xF_{2+x}$; x = 0.2(a), 0.1(b), 0.05(c), 0.0(d).

on the dopant ion. Fig.(1.13) shows how the conductivity of CaF_2 increases with various rare-earth dopant ions at 10 mole per cent. In addition, Fig.(1.14) shows how the conductivity increases with different mole percentages of Er doped $CaF_2(Ca_{1-x}Er_xF_{2+x})$. From the analysis of their experimental results it has been suggested that doping aids the formation of clusters which consequently increases conductivity. Doping also lowers the activation energy and thus ionic conductivity in doped CaF_2 is possible at lower temperatures.

With the formation of clusters, further disorder in the fluorite lattice is hindered and as a result, conductivity levels off above T_c. Superionic conductivity implies that as temperature increases, conductivity also increases. This appears not to be the case with rare-earth doped fluorides and thus it can be argued that the term 'superionic conductivity' does not apply to these materials.

CHAPTER 2

THEORY OF X-RAY AND NEUTRON DIFFRACTION

2.1 Introduction

The study of solids by diffraction techniques may be regarded as the twentieth-century sequel to classical crystallography and the culmination of the work and ideas of crystallographers during the previous 200 years.

The diffraction method of structure analysis covers vapour-phase, thin-film, and single-crystal electron diffraction, liquid and amorphous and crystalline solid state X-ray diffraction, and solid state neutron diffraction. From these methods a complete description of the structure of a solid is obtained by determining the crystal system, space group, unit cell dimensions, atomic coordinates and finally the actual electron density distribution around the atoms. Amongst the different diffraction techniques, X-ray diffraction has been most commonly used for routine characterisation as well as for detailed structural elucidation. The availability of synchrotron X-radiation of continuously variable wavelength has made X-ray diffraction a still more powerful structural tool for the study of solids. However, solid state chemists are making increasing use of electron diffraction and neutron diffraction to obtain information not provided by X-ray diffraction.

This chapter contains a general account of the theory of X-ray and neutron diffraction relevant to the studies in this thesis. For this reason, magnetic scattering effects have been neglected from the discussion of neutron scattering. In the latter part of the chapter, techniques of structural refinement are discussed and a brief description of the neutron instrument employed in this work is included.

2.2 Diffraction of Particles by Crystals

A crystal is a three-dimensional periodic array of atoms, in which distinct planes can be defined. Particles with wavelength similar to the d-spacing of these planes will be diffracted. Simple geometry is used to deduce Bragg's law,

$$2d\sin\theta = n\lambda \tag{2.1}$$

where d is the spacing of the planes, λ is the wavelength of the beam which is diffracted through an angle 2θ, and n is a positive integer. For most crystal spacings wavelengths of 1-2Å are required.

For electromagnetic radiation, the energy is related to the wavelength as follows:

$$E = \frac{hc}{\lambda} \tag{2.2}$$

If we consider a wavelength of 1Å, giving $E \sim 10^4$eV this

would correspond to the X-ray region of the spectrum. Similarly, for electrons and neutrons

$$E=\frac{h^2}{2\lambda^2 m} \tag{2.3}$$

Where m is the mass of the particle, giving $E\sim10^2$ eV and 10^{-1}eV for electrons and neutrons, respectively, of the same wavelength.

In this work only X-ray and neutron diffraction are considered. The fundamental difference between the two techniques is that in the former, X-rays are scattered by the electron cloud of the atom, whereas, in the latter neglecting magnetic effects, neutrons are scattered by the nucleus.

A more general derivation of the Bragg Law can be given by the concept of reciprocal space. If $\underline{a}_1$, $\underline{a}_2$ and $\underline{a}_3$ are the primitive translational vectors of a space lattice in real space, then the fundamental vectors of the reciprocal lattice $\underline{b}_1$, $\underline{b}_2$, $\underline{b}_3$ are defined as:

$$\underline{b}_1=2\pi\frac{\underline{a}_2\times\underline{a}_3}{\underline{a}_1\cdot\underline{a}_2\times\underline{a}_3};\ \underline{b}_2=2\pi\frac{\underline{a}_3\times\underline{a}_1}{\underline{a}_1\cdot\underline{a}_2\times\underline{a}_3};\ \underline{b}_3=2\pi\frac{\underline{a}_1\times\underline{a}_2}{\underline{a}_1\cdot\underline{a}_2\times\underline{a}_3} \tag{2.4}$$

and a reciprocal lattice vector has the form

$$\underline{G}=h\underline{b}_1+k\underline{b}_2+l\underline{b}_3 \tag{2.5}$$

Where h,k,l are the Miller indices.

The wave equation of a plane wave incident on a lattice is given by

$$\Psi=e^{i\underline{k}\cdot\underline{r}} \tag{2.6}$$

where $\underline{k}$ is the wavevector of the incoming beam $|\underline{k}|=2\pi/\lambda$

The outgoing wave has a wavevector $\underline{k}'$ and the scattering vector $\underline{Q}$ is defined as the difference between the outgoing and incoming wavevector, i.e

$$\underline{Q}=\underline{k}'-\underline{k} \tag{2.7}$$

To satisfy the condition of Bragg diffraction the scattering vector is required to equal a reciprocal lattice vector [96], i.e.

$$\underline{Q}=\underline{G} \tag{2.8}$$

Provided that scattering is elastic, there is no change in magnitude of the wavevector:

$$|\underline{k}|=|\underline{k}'|=(2\pi/\lambda)$$

and therefore the magnitude of the scattering vector at an angle of 2θ is given as

$$|\underline{Q}|=\frac{4\pi\sin\theta}{\lambda} \tag{2.9}$$

If the lattice is assumed to contain N atoms, the

scattering amplitude can be defined as

$$A = N\int_{cell} dV n(r) \exp(-i\underline{Q}.r) \tag{2.10}$$

This expression represents the integral over one cell where n(r) is the scattering density of the cell.

2.3 X-ray Diffraction

For X-ray diffraction, n(r) in equation (2.10) represents the electron density, and can be expressed as

$$n(r) = \sum_{j=1}^{s} n_j(\underline{r}-\underline{r}_j) \tag{2.11}$$

where each cell contains s atoms, and $\underline{r}_j$ is the vector to the centre of atom j, with electron density function n_j. The integral in Equation (2.10) may now be written as integrals over the s atoms of a cell

$$\sum_j \int dV n_j(\underline{r}-\underline{r}_j)\exp(-i\underline{Q}\cdot\underline{r}) = \sum_j \exp(-i\underline{Q}.\underline{r}_j)\int dV n_j(\underline{\rho})\exp(-i\underline{Q}.\underline{\rho}) \tag{2.12}$$

The atomic form factor can now be defined as

$$f_j = \int dV n_j(\underline{\rho}) \exp(-i\underline{Q}.\underline{\rho}) \tag{2.13}$$

integrated over all space. If $n_j(\underline{\rho})$ is an atomic property, f_j is an atomic property.

Combining equations (2.12) and (2.13) the structure factor

is obtained as

$$F = \sum_j f_j \exp(-i\underline{Q}.\underline{r}_j)$$

(2.14)

The scattering amplitude (or Equation 2.10) now becomes

$$A = NF \qquad (2.15)$$

Furthermore, since $\underline{Q} = \underline{G}$, $\underline{Q}.\underline{r}_j$ can be expressed in terms of the Miller indices, and the expression for the structure factor becomes

$$F(hkl) = \sum_j f_j \exp\left[-2\pi i(x_j h + y_j k + z_j l)\right]$$

(2.16)

The structure factor is a complex quantity and need not be real. The scattered intensity I is defined as

$$I = FF^* = |F|^2$$

where F^* is the complex conjugate of F so that FF^* is real and

$$I(hkl) \propto |F(hkl)|^2$$

(2.17)

which implies that the intensity of a reflection is proportional to the square of the structure factor.

2.3.1 The Atomic Form Factor

X-rays are scattered from regions of high electron density and this corresponds to the ion cores. However, atomic

dimensions are of the same order as the X-ray wavelength. This means that interference effects arise from X-rays scattered from different parts of the atom. It is these effects that lead to the atomic form factor expression in Equation (2.13). Assuming a spherically symmetric electron distribution, it is possible to show that

$$f_j = 4\pi \int dr n_j(r) r^2 \frac{\sin Qr}{Qr} \tag{2.18}$$

The effects of the form factor can thus be evaluated.

If the same total electron density were concentrated at r = 0, only Qr = 0 would contribute to the integrand. In this limit (sin Qr)/Qr = 1, and

$$f_j = 4\pi \int dr n_j(r) r^2 = Z \tag{2.19}$$

where Z is the atomic number of the atom.

For small angles of scattering $\underline{Q}$ tends to 0 as $\underline{k}' = \underline{k}$ and f_j tends to Z as above. For large values of $\underline{Q}$, (sinQr)/Qr tends to zero and thus for large values of $(h^2 + k^2 + l^2)$, f_j is reduced. This leads to an angular dependent term for the scattering intensity with f_j small for large values of $\sin\theta/\lambda$.

2.3.2 Temperature Dependence

Earlier Debye realized that the effect of temperature

would not broaden diffraction lines but only reduce their intensity. This has been explained by classical theory as follows:

Let the position of an atom (at time t) nominally at $\underline{r}_j$ contain a term $\underline{u}(t)$ fluctuating in time be given by

$$\underline{r}(t) = \underline{r}_j + \underline{u}(t) \tag{2.20}$$

where $\underline{u}$ represents a random displacement.

Supposing each atom fluctuates independently about its own equilibrium position then the thermal average of the structure factor (2.14) contains terms

$$f_j \exp(-i\underline{Q}.\underline{r}_j)\langle\exp(-i\underline{Q}.\underline{u})\rangle \tag{2.21}$$

where <...> denotes the thermal average, and the enclosed term is known as the Debye-Waller factor.

Expansion of this term [96] gives:

$$\begin{aligned}\langle\exp(-i\underline{Q}.\underline{u})\rangle \approx & \exp\left(-\tfrac{1}{2}\langle\underline{Q}.\underline{u}\rangle^2\right) \\ & = \exp\left(-\tfrac{1}{2}|\underline{Q}|^2\langle u^2\rangle\langle\cos^2\theta\rangle\right) \\ & = \exp\left(-\tfrac{1}{6}|\underline{Q}|^2\langle u^2\rangle\right)\end{aligned} \tag{2.22}$$

where $\langle u^2\rangle$ is the mean square displacement of the atom.

It is normal [97] to define a parameter called the 'temperature (or B) factor' as

$$B=8\pi^2\langle u_B^2\rangle \tag{2.23}$$

and the Debye-Waller factor is defined as

$$\exp[-B(\sin\theta/\lambda)^2] \tag{2.24}$$

It is noted, however, that the mean square displacement term is not identical in each definition. In fact,

$$\langle u_B^2\rangle=\frac{1}{3}\langle u^2\rangle \tag{2.25}$$

Since intensity is proportional to the square of the structure factor, the thermal modification to a reflection I_o is

$$I=I_o\exp[-2B(\sin\theta/\lambda)^2] \tag{2.26}$$

The above evaluation requires the vibration to be spherically symmetric around the lattice site. For this reason, B is known as the isotropic temperature factor.

A modification allows the atom to vibrate anisotropically within the bounds of a thermal ellipsoid. The Debye-Waller factor for reflection hkl is then given by

$$\exp\left[h^2b_{11}+k^2b_{22}+l^2b_{33}+2hkb_{12}+2hlb_{13}+2klb_{23}\right]$$

(2.27)

where the anisotropic thermal parameters b_{11} to b_{23} are the unique elements of the symmetric tensor describing the thermal vibration ellipsoid. The values they can take are governed by the site symmetry [98].

Further modification allows anharmonic terms to describe the thermal motion [99]. The effect of these is to allow vibrations in the form of 'lobes' orientated in defined directions.

2.4 Neutron Diffraction

When neutrons are scattered from the nucleus, there is no intra-atomic interference, as in the case of X-rays, hence there is no atomic form factor. In this case, the scattering strength is represented by a complex quantity b, known as the scattering length. However, the imaginary part is only important for nuclei which have a high absorption coefficient.

The total scattering cross-section due to a single nucleus is isotropic, and is given by

$$\sigma=4\pi b^2$$

(2.28)

From equation (2.19), it is clear that the X-ray scattering amplitude is proportional to atomic number Z.

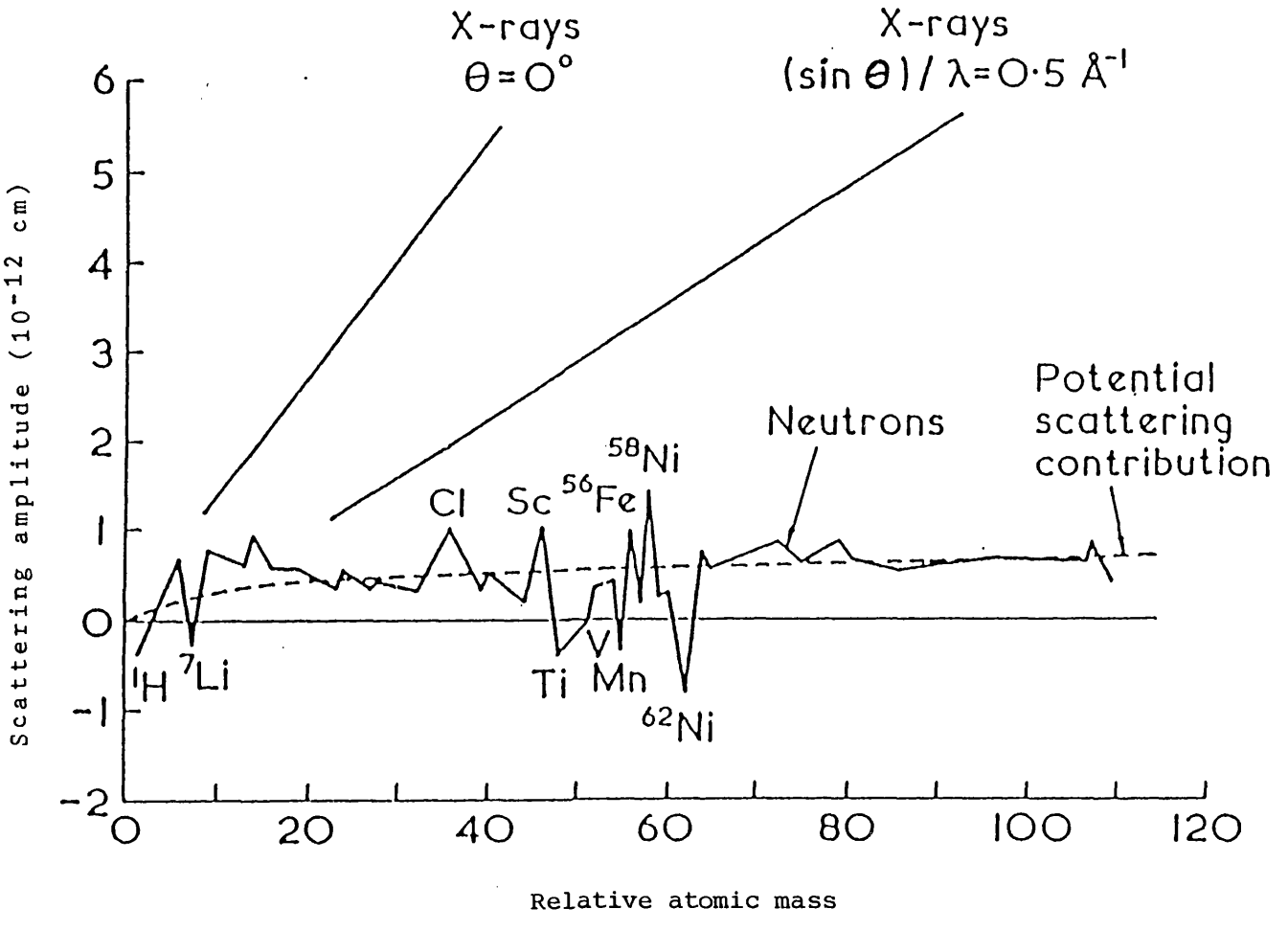

FIG. 2.1: The variation of neutron scattering cross-section with atomic number

For neutrons, however, σ is a quantity that varies irregularly across the periodic table, as shown in Figure 2.1. This gives neutrons the advantage that it is possible to distinguish scattering from atoms with similar atomic numbers which therefore have similar X-ray scattering amplitudes.

2.4.1. Coherent and Incoherent Scattering

Another effect that can influence the diffraction of neutrons is the spin of the scattering nucleus. Consider a lattice of N nuclei, equation (2.14) for the structure factor becomes:

$$F=\sum_{j=1}^{N} b_j \exp(-i\underline{Q}.\underline{r}_j) \qquad (2.29)$$

Neglecting thermal motion, the scattered intensity is proportional to the square of the structure factor thus

$$\begin{aligned} I &= \left|\sum_{j=1}^{N} b_j \exp(-i\underline{Q}.\underline{r}_j)\right|^2 \\ &= \sum_{jj'}^{N} b_j b_{j'} \exp\left[i\underline{Q}.(\underline{r}_j-\underline{r}_{j'})\right] \\ &= \sum_{j} b_j^2 + \sum_{\substack{jj' \\ j\neq j'}} b_j b_{j'} \exp\left[i\underline{Q}.(\underline{r}_j-\underline{r}_{j'})\right] \end{aligned} \qquad (2.30)$$

where Σ indicates a summation not including $j=j'$.

The above separation is possible, because if there is a

non-zero nuclear spin, b varies from one nucleus to another, even for nuclei of the same isotope, due to the random orientation of nuclear spins. Thus there is no correlation between b_j and $b_{j'}$; thus $\langle b_j b_{j'} \rangle = \langle b_j \rangle \langle b_{j'} \rangle = \langle b_j \rangle^2$. The first term in (2.30) is simply $N\langle b^2_j \rangle$, and the second term can be written as

$$N\langle b_j \rangle^2 \sum_{\substack{jj' \\ j \neq j'}}^{N} \exp\left[i\underline{Q}.(\underline{r}_j - \underline{r}_{j'})\right]$$
$$-N\langle b_j \rangle^2 \sum_{j}^{N} \exp\left[i\underline{Q}.(\underline{r}_j - \underline{r}_{j'})\right] - N\langle b_j \rangle^2$$

(2.31)

where j=j' is now included in the summation. Thus

$$I = N\left(\langle b^2 \rangle - \langle b \rangle^2\right) + N\langle b \rangle^2 \left[\sum_{j}^{N} \exp\left(i\underline{Q}.\underline{r}_j\right)\right]^2$$

(2.32)

The first term in equation (2.32) can also be written as $N\langle (b-\langle b \rangle)^2 \rangle$, showing that intensity depends on the mean square deviation of the scattering lengths from their average value. It is known as the incoherent scattering cross-section and is zero for those nuclei with zero spin. If the effect of the Debye-Waller factor is ignored, the incoherent elastic scattering is isotropic and gives a uniform background to the coherent scattering represented by the second term in (2.32). Both coherent and incoherent scattering terms contribute to the intensity, which is attenuated by the Debye-Waller factor. This

factor arises because interference effects between atoms on different sites are smoothed out by thermal vibrations. The coherent scattering takes into account interference effects arising from the phase differences in the scattered radiation due to the relative displacements of the various nuclei in the assembly, and therefore contains information concerning the structural relationships between different atoms. The incoherent scattering cross section, on the other hand, has no phase term and therefore gives no information about relationships between different atoms.

The total scattering cross section per atom can thus be written as

$$\sigma_T = 4\pi\langle b^2\rangle \tag{2.33}$$

The 'coherent scattering cross-section' per atom is

$$\sigma_{coh} = 4\pi\langle b\rangle^2 \tag{2.34}$$

and the difference between the two is the 'incoherent scattering cross-section' per atom.

$$\sigma_{incoh} = 4\pi\left(\langle b^2\rangle - \langle b\rangle^2\right) \tag{2.35}$$

Thus for Bragg scattering by neutrons, the structure factor is given by

$$F(hkl) = \Sigma_j b_j^{coh} \exp[2\pi i(hx+ky+lz)]$$

(2.36)

2.4.2 Non-Stoichiometric Effects

The structure factors from Bragg scattering define only the average unit cell. In other words, the positions and average occupancies of the atomic sites, and their thermal parameters. Defects present in the unit cell, such as fluorine vacancies distributed randomly on a sublattice give rise to partial occupancy of those sites in comparison with the fully occupied sites observed in a stoichiometric material.

It is possible to obtain the fluorine to metal ratio of metal fluorides from the ratio of the cation and fluorine site occupancies. Methods for determining the structural parameters of the average unit cell are described later in this chapter.

Diffraction is not sufficiently sensitive to detect any effects from a material with less than 2-3 mole percent defects, and information on these materials must be obtained by other methods such as conductivity.

2.4.3 Diffuse Scattering

The intensity from a collection of pairs of atoms is proportional to FF^*, and from Equation (2.29)

$$FF^* = \sum_{m,n=1}^{N} \sum b_m b_n \exp\left[i\underline{Q}.(\underline{r}_m - \underline{r}_n)\right]$$

(2.37)

where the summation is made over an assembly of N atoms. This can be expanded to include several different atomic species(v), some of which may be vacancies, as

$$FF^* = \sum_i^v \sum_j^v \sum_m^{N_v} \sum_n^{N_v} \langle b_m \rangle \langle b_n \rangle \exp\left[i\underline{Q}.(\underline{r}_m - \underline{r}_n)\right]$$
$$+ \sum_i^v \sum_j^v \sum_m^{Nv} \sum_n^{Nv} \left(b_m^i b_n^j - \langle b_m^i \rangle \langle b_n^j \rangle \exp\left[i\underline{Q}.(\underline{r}_m - \underline{r}_n)\right]\right)$$

(2.38)

The first term contains contributions from all atoms, and clearly represents Bragg diffraction. The second term represents diffuse scattering, which arises when, for a particular value of $\underline{r}_m - \underline{r}_n$, where $\underline{r}_m$ is the vector distance, there is a difference between the scattering from individual pairs and the average scattering from a pair. That is, $\langle b_m^i b_n^j \rangle = \langle b_m^i \rangle \langle b_n^j \rangle$. The mathematics is very similar to that for the incoherent scattering discussed in section 2.4.1 with the distinction that the term 'incoherent' is used to describe scattering from the random distributions of isotopes or nuclear spin, and the term 'diffuse' is used to describe scattering from other random effects. Clearly, for a random solid solution with a number of different atomic species the two are equivalent [100]. However, an important difference is that the diffuse intensity does contain phase information, and the effect on a Bragg diffraction pattern is to cause

modulations of the background between the Bragg peaks. The normally low concentration of defects and relatively small number of distinct values of $\underline{r}_m - \underline{r}_n$ which contribute, means that, in practice, the diffuse scattering cross-sections are small by comparison with Bragg scattering.

2.4.4 Short Range Order

Evaluation of the diffuse term for random distributions of defects is as already indicated, relatively simple although when there is correlation of defects, termed short range order, these terms are hard to calculate explicitly.

In this case diffuse scattering is generally analyzed by using short range order coefficients [101] which are defined as

$$\alpha_i^A = 1 - P_A(r_i)/X_A \qquad (2.39)$$

where for a binary (AB) solid solution the local environment can be described in terms of a probability $P_A(r_i)$ which is the probability of finding atom A at a distance r_i from atom B when $r_i \to \infty, \alpha_i^A \to o$. The mole fraction of A is given by X_A.

The diffuse intensity from a single crystal can then be represented by

$$I_{(\text{Single Crystal})} = X_A X_B (b_B - b_A)^2 \sum_{n=1}^{N} \propto_i \cos(\underline{Q} \cdot \underline{r}_i)$$

(2.40)

or, for a powder, where the cosine term is averaged over all possible orientations, as:

$$I_{(\text{Powder})} = X_A X_B (b_B - b_A)^2 \sum_{n=0}^{N} s_i \propto_i \sin(Qr_i)/Qr_i$$

(2.41)

where X_a and X_B are the mole fractions of A and B respectively, b_B and b_A are the atomic scattering lengths of B and A nuclei, S_i is the number of atoms at a distance r_i from the origin, and $Q = 4\pi \sin\theta/\lambda$.

2.4.5 Thermal Diffuse Scattering

In addition to the attenuation of Bragg intensities due to increased temperatures, described by the Debye-Waller factor in Section 2.3.2, there is a corresponding increase in the diffuse intensity. This is called thermal diffuse scattering, and is caused by inelastic scattering from one-phonon acoustic modes. It rises to a maximum at the same angular positions as the Bragg reflections, and results in an overestimation of the Bragg intensity [102].

For single crystal X-ray diffraction, the effect is very important and corrections must be made [103]. For powders, however, the thermal diffuse scattering contribution is less [97].

2.5 Bragg Diffraction Experiments

The aim in Bragg diffraction is to measure the intensities and hence the structure factors of as many reflections as possible. The average unit cell is then calculated from these. There are two ways in which the conditions for Bragg's law $\lambda = 2d \sin\theta$ can be achieved:

(a) The wavelength can be held constant and the intensity measured as a function of 2θ. Thus white beams require monochromation. This is usually done by orientation of a crystal such that the Bragg reflection from a set of its crystal planes corresponds to radiation of the required wavelength.

(b) The sample is illuminated with 'white' radiation, and the intensity of the scattered radiation at a fixed angle is then measured as a function of wavelength. The wavelength is related to the energy of the radiation by Equations (2.2) and (2.3), and thus it is convenient to measure intensity as a function of energy.

Method (a) can be referred to as monochromatic, and method (b) as energy-dispersive. In this thesis method (a) was employed.

2.5.1 Single Crystal Methods

The most obvious way of performing a diffraction

experiment is to mount the crystal in a radiation beam and measure the intensity over a wide as possible angular distribution centred on this. This is the principle used in single crystal diffractometers; however, mechanical limitations usually limit the detector to move over a hemispherical surface, and orientation of the crystal can also be accommodated. With the advancement of technology and the advent of computer control the fully automated and computer controlled D9 four-circle diffractometer at the Institute of Laue Langevin in Grenoble France, was used in this work. A description of the instrument is given in section (2.10).

2.5.2 Powder Methods

The powder diffraction method with either X-rays or neutrons is widely used in inorganic structure analysis and in guessing possible structural relationships. In the powder method, a finely ground polycrystalline sample held in a container is illuminated by radiation. The random orientation of the crystallites means that the diffracted beams form the surfaces of Debye-Scherrer cones concentric to the direct beam and making an angle 2θ to it. A detector then scanning a circle centred on the sample will effectively view these cones as lines of intensity, and a plot of counts detected against 2θ will show the Bragg reflections as peaks. This plot of intensity versus 2θ is referred to as a diffraction pattern or profile. Whereas the single crystal method has the advantage that a large

number of independent observations can be made, the powder method does not suffer from systematic effects such as extinction, multiple Bragg and thermal diffuse scattering to anything like the same extent.

The major drawbacks are the relatively small amount of intensity data usually obtained and the difficulty of indexing powder patterns of low symmetry. De Wolff and his school [104] have shown that, given a fairly sophisticated analysis of a set of accurately known line positions, a powder pattern of a low symmetry crystal can usually be indexed if the unit cell is not excessively large (of the order 1000$\AA^3$ in volume). The powder method enables materials for which single crystals cannot be obtained to be identified. Chapter 3 of this thesis is specifically concerned with X-ray powder diffraction studies.

2.6 X-rays and Their Detection

X-rays are electromagnetic radiation emitted, via electronic transitions, from an atom. Thus the simplest method of generation is to accelerate an electron beam onto a target such as copper or molybdenum. The intensity versus wavelength distribution will then have the form shown in Figure 2.2, which is, to some extent, monochromatic.

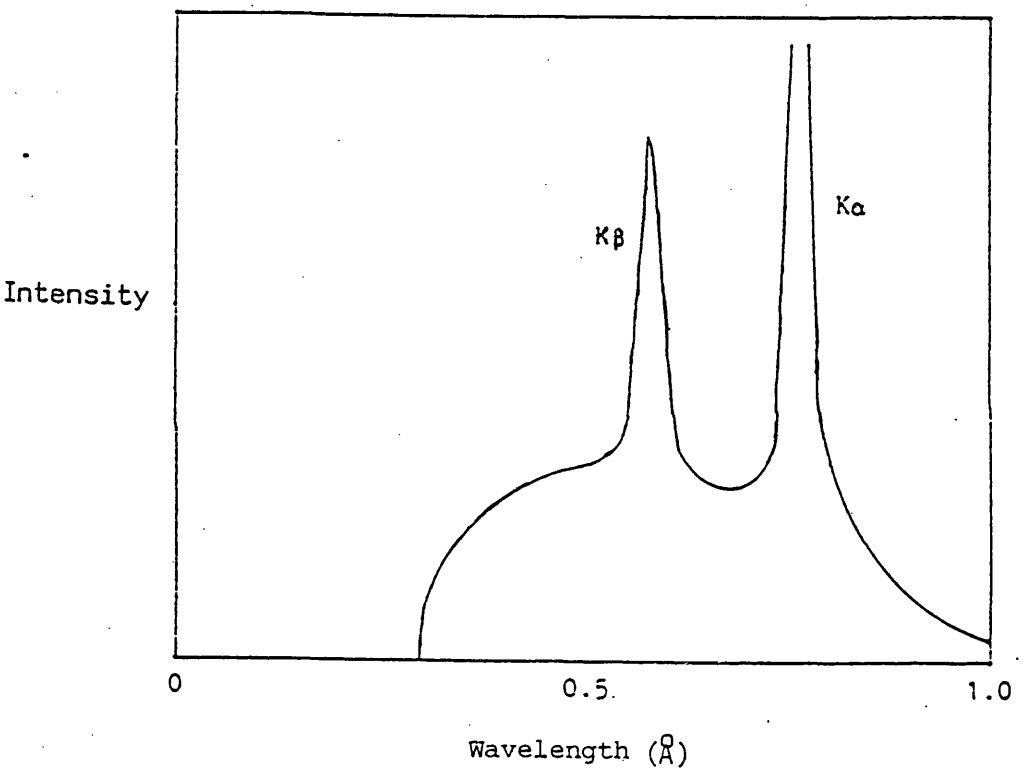

FIG. 2.2: The X-ray spectrum produced by a copper X-ray tube

2.6.1 Synchrotron Radiation

The past decade has seen the development of synchrotron radiation sources worldwide. The properties of this radiation - its intensity and tuneability - are leading to exciting new experiments in chemistry, physics, biology and material science. The intensity is several orders of magnitude greater than the output from a conventional X-ray tube and the wavelength is tunable over the range 0.3 - 2.5Å. Synchrotron radiation (SR) is the intense white source of electromagnetic radiation produced by charged particles i.e. electrons or positrons travelling at relativistic speeds around circular accelerators, e.g. synchrotrons and storage rings. The ideal SR source is a storage ring. The conditions in a storage ring are such that the emitted radiation is confined to a cone, the axis, of which lies in the plane of the ring and its opening angle is approximately γ^{-1}, where the energy of the relativistic electrons is $\gamma\, m_0c^2$ (Fig.2.3a).

The X-ray power emitted by the particles is replenished using the rf power from a klystron. This is coupled to the electron beam via rf cavities around the storage ring (Fig.2.3b). The use of superconducting 'wiggler' magnets to introduce a small kink into the electrons' path causes a shift of the spectrum towards high energy photons, as shown in figure 2.4. The radiation has several unique qualities, the most important of which are:

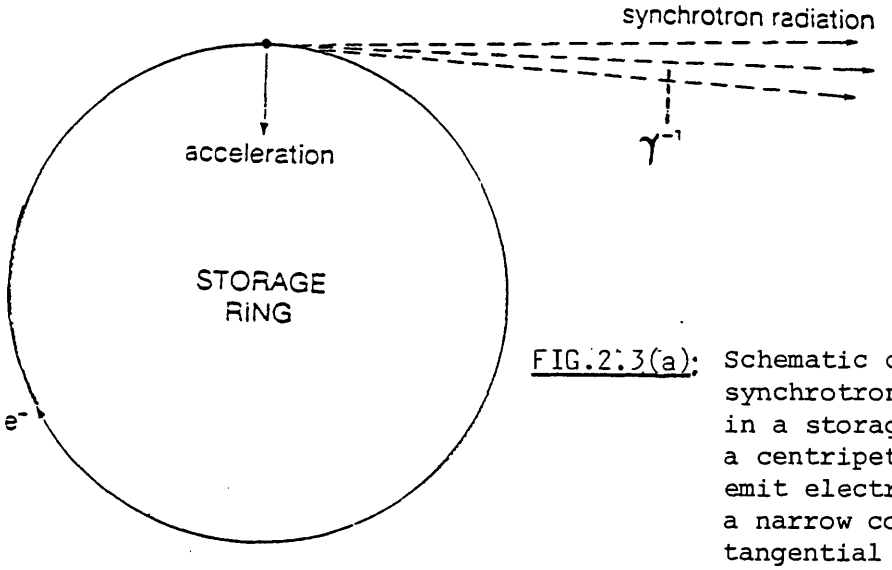

FIG. 2.3(a): Schematic diagram of a synchrotron source. The electrons in a storage ring are subject to a centripetal acceleration and so emit electromagnetic radiation in a narrow cone, whose axis is tangential to the ring. The semi-angle of the cone of radiation is γ^{-1}, where the energy of the electrons is $\gamma m_o c^2$

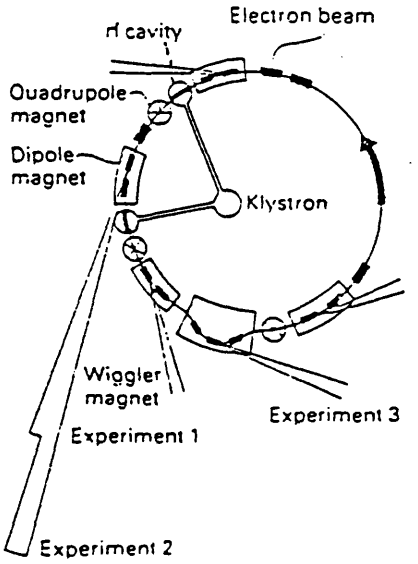

FIG. 2.3(b): A schematic diagram of the storage ring.

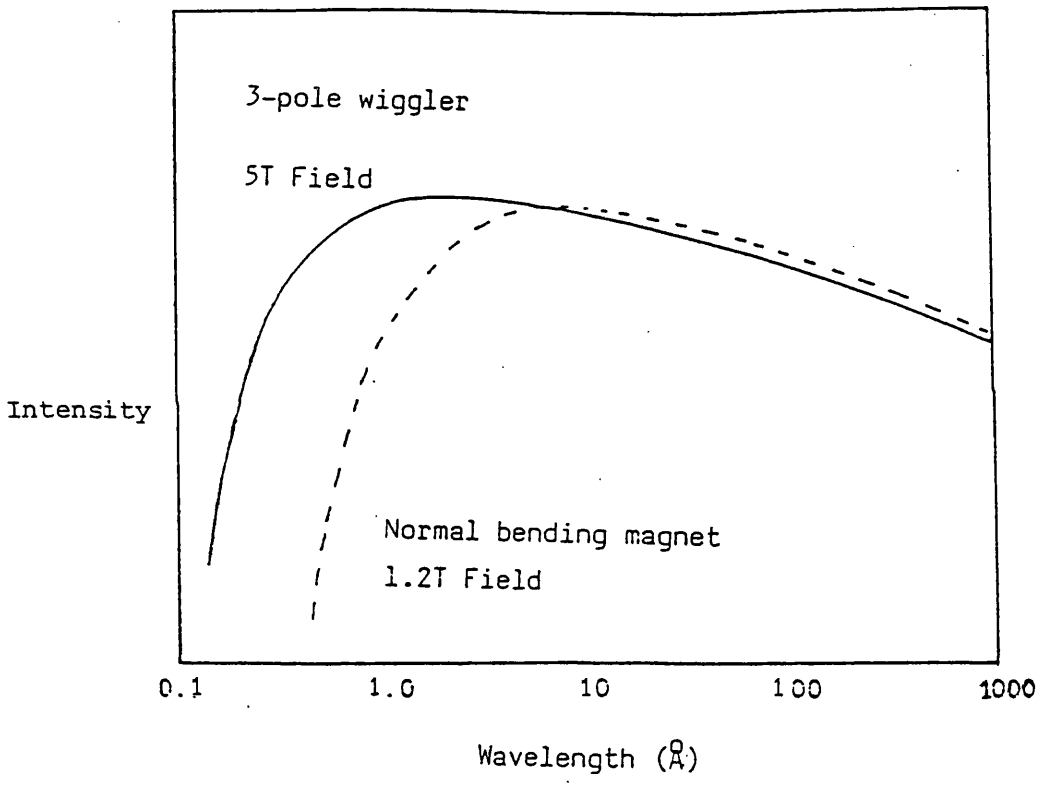

FIG. 2.4: The X-ray spectrum from a synchrotron, showing the effect of a wiggler magnet

(a) Intensity - with currently available sources the intensity of the white radiation is a factor of 10^4-10^6 times greater than that produced from a rotating anode generator - the most powerful laboratory X-ray source.

(b) Tuneability - An enormously wide band of wavelengths - ranging from hard X-rays to microwaves - is available. Moreover, the SR spectrum is smooth, whereas, emission spectra obtained from laboratory sources are broken by characteristic lines.

(c) Collimation - The beam is highly collimated, i.e. it has a very narrow angular divergence in the plane of the accelerator; typical values are 0.01 - 0.02°. Developments in magnet technology are also leading to large reductions in the horizontal divergence of the beam.

(d) Polarisation - At X-ray wavelengths the beam is more than 95% polarised in the plane of the accelerator.

(e) Time structure - The rf coupling breaks the particle beam up into pockets of electrons, so that the light is emitted as a series of pulses with a time duration of less than 10^{-9}s.

The powder diffractometer used for the work described in

Chapter 5 was the 9.1 at the Synchrothron Radiation Sources at Daresbury.

2.6.2 X-ray Detection

Detection of X-rays is achieved by the transfer of the energy to charged particles in the detector. The detector material must be normally electrically neutral and only made conducting by the incoming photons. The materials most commonly used today are semi-conductors such as germanium, often purified by lithium drifting. An incoming photon then produces electronhole pairs which are attracted to opposite ends of the detector by an applied voltage. The resultant current is used to charge capacitors linked to a multi-channel analyzer [105].

2.7 Neutrons and Their Detection

Neutron diffraction arises from interactions with the nucleus instead of the electrons. Hence, neutrons have a number of advantages over X-rays in crystallographic studies:

(i) Neutrons are generally more sensitive to the positions of light atoms, for example, fluorine and oxygen. This arises because of the irregular dependence of neutron scattering power on atomic number (Z), in contrast to linear dependence of Z shown by X-rays, which makes X-rays more suitable for study with regards to positions of heavy metal

atoms, Fig. 2.1.

(ii) Neutron diffraction yields higher angle data, because the neutron scattering amplitude is independent of the Bragg angle θ. This isotropic nature of the scattering arises because neutrons are scattered on the whole by nuclei, except for the small amount of magnetic scattering by any unpaired electron spins in the system. The nuclei act as point scatterers and are small in comparison with the wavelength used, typically 1-5.7Å. As a result, the 'form factor', or atomic scattering factor for neutron scattering is independent of θ. In the case of X-rays, the fundamental scattering body is the electron. The scattered wave from an atom is thus built up from the contributions of the electrons, hence as the Bragg angle increases, the scattered amplitude suffers from interference effects because the size of the scattering centre (i.e. the electronic cloud) is of the order of the wavelength. The atomic scattering factor for X-rays describes the rate of fall, off of the amplitude as depending on $(\sin\theta/\lambda)$, Fig.2.5.

(iii) With neutron diffraction, a well-defined line shape of Bragg reflections occurs. Even for high resolution powder diffractometers, the line shape is that of a simple Gaussian shape and hence the

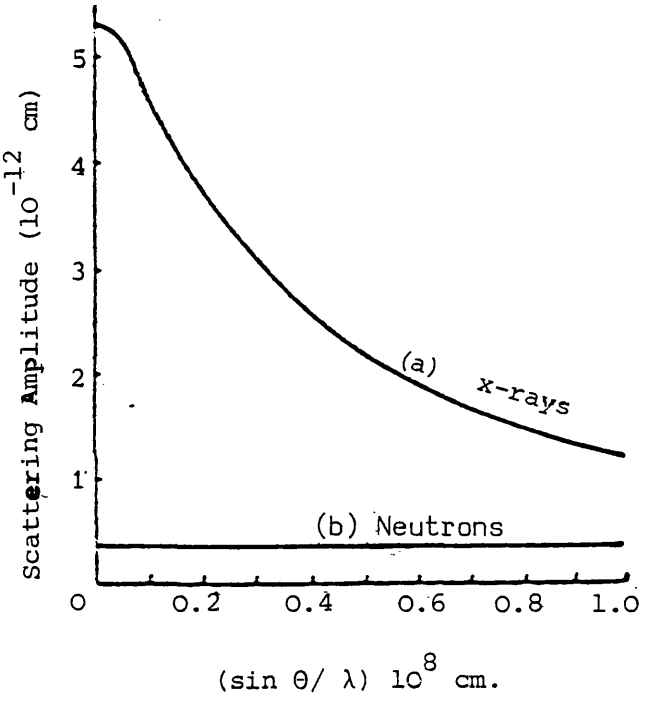

FIG. 2.5: The dependence of X-ray and neutron amplitudes on Bragg Angle θ. (After Bacon)

process of profile refinement is made much simpler. Caglioti, Paoletti and Ricci [106] described the variation of line with θ as:

$$H_k^2 = U\tan^2\theta_k + V\tan\theta_k + W \qquad (2.42)$$

where H_k is the full width of the Gaussian reflection at half height, θ_k is the Bragg angle and U, V, W are half-width parameters independent of θ_k. There is no simple mathematical analogue for x-ray line shapes.

(iv) The technique is able to distinguish neighbouring atoms as in alloys or zeolites due to the non-dependence on Z for scattering power.

(v) It is easy to carry out low and high temperature neutron diffraction studies because of the very low absorption coefficients for neutrons of materials used in the construction of cryostats and furnaces, for example, Al, Cu. In Contrast, x-rays are readily absorbed by metals. For the same reason the neutron diffraction technique may also be used in high pressure studies.

2.7.1 Nuclear Reactors

The most commonly used method of producing neutron beams is by controlled nuclear fission in a reactor. The

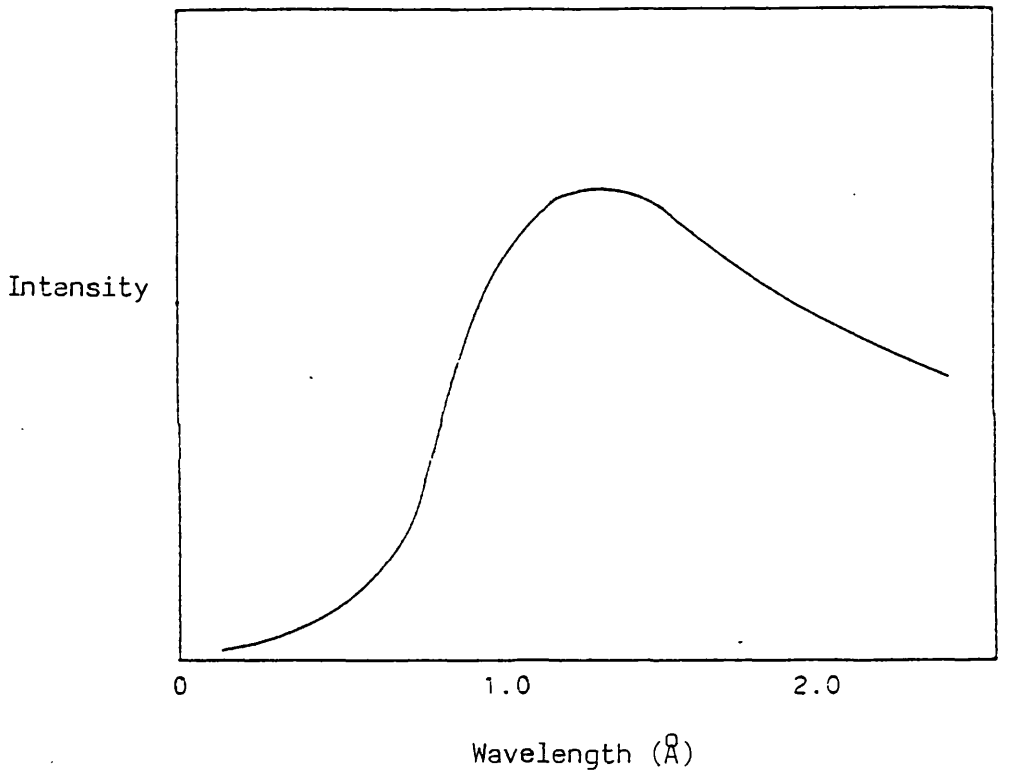

FIG. 2.6: The neutron spectrum emerging from a nuclear reactor

distribution of neutron wavelengths from a reactor is almost Maxwellian and has a peak at a wavelength that is dependent on the moderator temperature, see Fig.2.6. For wavelengths of about 1Å, which is typical of the order of crystal plane spacing, the distribution required corresponds to a moderator temperature of about 300K. These neutrons are known as 'thermal'. The long wavelengths (6-7Å) of cold neutrons is suitable for diffuse scattering. Neutrons are extracted from the reactor core via guide-tubes that operate on the principle of total internal reflection. The beam can then be monochromated by Bragg reflection from crystal planes, and directed to a sample.

The neutron diffraction studies reported in this thesis, were conducted using the 57 MW high flux reactor at the Institute of Laue-Langevin in Grenoble, France.

2.7.2 Pulsed Sources

Another method of producing neutrons is to accelerate bunches of electrons or protons using a linear accelerator (LINAC) or a synchrotron, and cause them to impinge upon a heavy metal target, spraying off neutrons by the resulting fission. The neutrons are slowed down by a moderator and the energy range is extended upwards from that of a reactor making use of the 'epithermal neutrons', that is, neutrons in the act of slowing down. Production of neutrons using pulsed sources was not used in this work,

but there are many accounts in the literature (see [107], for example).

2.7.3 Detection of Neutrons

The three most important reactions of neutron detection are:

$$^{3}He + n \rightarrow {}^{3}H + p + 0.77\ MeV$$

$$^{10}B + n \rightarrow {}^{7}Li + {}^{4}He + 2.3\ MeV$$

$$^{6}Li + n \rightarrow {}^{4}He + {}^{3}He + 4.79\ MeV$$

The first two reactions are used in gas counters. ^{3}He or BF_3 gas enriched with ^{10}B is placed in a steel or copper cylinder with a thin wire anode. This collects electrons from the ionization of the He or BF_3 molecules. ^{6}Li is used in scintillation detectors where it is mixed with a 'phosphor' such as ZnS(Ag). This emits a flash of light as the ionizing particle passes through it, and a photomultiplier is used to collect the photons.

2.8 Analysis of Diffraction Data

As shown in Section 2.3, the intensities of the Bragg reflections are related to the square of the structure factors. The aim is to obtain the crystal structure from the measured structure factors.

2.8.1 Fourier Analysis

Consider a generalized expression of the structure factor

$$F(hkl) = \sum_{N} f_n \exp 2\pi i\left(\frac{hx}{a} + \frac{ky}{b} + \frac{lz}{c}\right)$$

(2.43)

where x,y and z are distances in the a, b, and c directions, respectively, and N is the number of atoms in the cell. In more general terms if instead of discrete atoms, a continuous distribution of electron or nuclear density $\rho(xyz)$ at the point x,y,z is considered then it follows that

$$F(hkl) = \int_0^a \int_0^b \int_0^c \rho(xyz) \exp 2\pi i(hx/a + ky/b + lz/c)\, dxdydz$$

(2.44)

As $\rho(xyz)$ is a periodic function with spatial periods a,b,c, respectively in the three crystallographic directions, it can be expressed as the sum of a three-dimensional series of simple harmonic terms in accordance with Fourier's Theorem. Thus

$$\rho(xyz) = \sum_{h'} \sum_{k'} \sum_{l'} C(h'k'l') \exp 2\pi i(h'x/a + k'y/b + l'z/c)$$

(2.45)

where C(h'k'l') is the coefficient of the Fourier term which has spatial periods a/h',b/k', c/l'. Combining (2.44) and (2.45) gives

$$F(hkl) = \int_0^a \int_0^b \int_0^c \sum_{h'} \sum_{k'} \sum_{l'} C(h'k'l') \exp 2\pi i(h'x/a + k'y/b + l'z/c) \times \exp 2\pi i(hx/a + ky/b + lz/c)\, dxdydz$$

(2.46)

On integration the product of each pair of exponential terms yields zero except for the particular case when $k' = -k$, $l' = -l$, then

$$F(hkl) = vC(\bar{h}, \bar{k}, \bar{l}) \tag{2.47}$$

where v is the unit cell volume. Thus, from experimentally observed structure factors, Equation (2.45) can be used to give $\rho(xyz)$ [108]. The calculated electron or nuclear density is usually presented in the form of a Fourier map of density contours.

There are, however, two difficulties with this method. The first is that F(hkl) is complex, the intensities being proportional to FF^* (Equation (2.17)), and there is no experimental method of finding the phase. Secondly, if experimental limitations prevent the measurement of all intensities, it is possible that termination errors can be introduced into the summation.

This problem can be avoided by using the least squares refinement method, which also has the advantage that computationally, it is a lot faster than the Fourier summation.

2.8.2 Least Squares Refinement

There are three distinct steps to solving a crystal structure:

(i) Indexing, by determining the h,k,l of each reflection in a pattern, and hence the unit cell parameters, from the 2θ values of the reflection.

(ii) Space group determination, by finding the systematic absences in a pattern.

(iii) Refinement, by calculating the atomic positions and thermal parameters within the space group.

This thesis is only concerned with refinement, but there are many texts on the first two steps [109,110]. The least squares refinement method consists of choosing a set of model atomic parameters (x,y,z, occupancy and temperature factor), calculating from these a set of structure factors and comparing them with the experimentally observed structure factors which are calculated from the integrated intensities of the reflections, by means of a reliability, or R, factor:

$$R_I = \frac{\Sigma_i \left| F_i^2(obs) - F_i^2(calc) \right|}{\Sigma_i F_i^2(obs)} \qquad (2.48)$$

The aim is to use the method of least squares to minimize R_I by adjusting the atomic parameters. When minimization is achieved, the model parameters should be equal to those in the experimental sample.

Two types of Fourier map can be used to aid the refinement. The F_{obs} Fourier map is calculated from the observed structure factors. The difference Fourier is calculated from $F_{obs}-F_{calc}$, the difference in the observed and calculated structure factors. Its main use is to show interstitial positions, as any atom observed in the data, but not included in the model structure, will appear as a region of positive density on the map.

Many least squares refinement programs have been written, but in powder diffraction there are severe limitations in their use due to peak overlap. These difficulties can, however, be at least partially overcome by use of the methods discussed in the next section.

2.9 Profile Refinement

The problem of peak overlap is partially overcome by refining against the whole profile using a method originally suggested by Rietveld [111], which is suitable for neutron diffraction because of the Gaussian peak shapes.

For each peak its contribution to the measured profile intensity y_i at $2\theta_i$ will be

$$Y_i = tF_k^2 j_k L_k \frac{2}{H_k}\left(\frac{\ln 2}{\pi}\right)^{1/2} \exp\left\{-4\ln 2\left[(2\theta_i - 2\theta_k)/H_k\right]^2\right\} \qquad (2.49)$$

where

t is the step width of the counter

F_k is the structure factor of the kth reflection

j_k is the multiplicity of the reflection

L_k is the Lorentz factor

$2\theta_k$ is the calculated position of the Bragg reflection corrected for the zero point error of the counter

H_k is the full width at half maximum

This equation can be simplified by putting

$$I_k = iF_k^2 j_k L_k \frac{2}{H_k}\left(\frac{\ln 2}{\pi}\right)^{1/2}$$

$$\text{and} \quad c_k = \frac{4\ln 2}{H_k^2}$$

$$\text{then} \quad y_i = I_k \exp\left[-C_k(2\theta_i - 2\theta_k)^2\right] \qquad (2.50)$$

The half-width of the peak is described by

$$H_k^2 = U\tan^2\theta_k + V\tan\theta_k + W \qquad (2.51)$$

where U, V and W are the half-width parameters.

At low angles the peaks show asymmetry mainly because the use of finite slit and sample height causes vertical divergence [112], with the effect that peak maximum is shifted to lower angles, but the integrated intensity is unchanged. Therefore a semi-empirical correction to Equation (2.50) is introduced:

$$Y_i = I_k \exp\left[-C_k(2\theta_i - 2\theta_k)^2\right] \times\left[1 - P(2\theta_i - 2\theta_k)^2 S/\tan\theta_k\right]$$

(2.52)

Where P is the asymmetry parameter, and S is +1, 0, or -1, depending on $(2\theta_i - 2\theta_K)$ being positive, zero or negative, respectively.

There is also a correction of I for preferred orientation of plate-like crystals:

$$I_{corrected} = I_{obs} \exp(-G\alpha^2)$$

(2.53)

where α is the angle between the scattering vector and the preferred orientation axes, and G is the preferred orientation parameter.

Equation (2.52) can be simplified as

$$Y_i = W_{i,k} F_k^2$$

(2.54)

where $W_{i,k}$ is a measure of the contribution of the Bragg peak at position $2\theta_k$ to the profile y_i at position $2\theta_i$. If the peaks overlap, then more than one peak contributes, and

$$Y_i = \Sigma_k W_{i,k} F_k^2$$

(2.55)

Ignoring overall temperature factors and asymmetry, the structure factor can be written as

$$F_k = A_k^2 + B_k^2 \tag{2.56}$$

with

$$A_k = \Sigma_i n_i b_i \exp\left(-B_i \sin^2\theta_k/\lambda^2\right) \Sigma_r \cos 2\pi\left(hx_{i,r} + ky_{i,r} + lz_{i,r}\right) \tag{2.57}$$

and

$$B_k = \Sigma_i n_i b_i \exp\left(-B_i \sin^2\theta_k/\lambda^2\right) \Sigma_r \sin 2\pi\left(hx_{i,r} + ky_{i,r} + lz_{i,r}\right) \tag{2.58}$$

where

Σ_i represents the sum over all atoms in the asymmetric unit

Σ_r represents the sum over all equivalent positions

b_i is the scattering length atom i

B_i is the individual isotropic temperature factor

n_i is the site occupation

$x_{i,r}$, $Y_{i,r}$, $z_{i,r}$ are the fraction co-ordinates of atom i in the r^{th} equivalent position, and hkl are the Miller indices of F_K.

The parameters to be refined can be divided into two groups:

(i) <u>the profile parameters</u> which define the position and

shape of the peaks. These consist of the zero point error, the cell parameters, the half-width parameters, the asymmetry and preferred orientation parameters,

(ii) the structural parameters which define the contents of the asymmetric unit cell and also include a scale factor c such that y (calc) = cy (obs).

Computationally the process can be divided into two steps:

(i) Determination from the profile parameters of the positions of the peaks and their contribution to the profile intensity.

(ii) Refinement of the structure by calculation of the intensity expected at each point in the profile and derivatives of that intensity with respect to the structural parameters.

For this reason it is usual to use two programs, a Preprofile and a Profile. The least squares equations are constructed in the normal method [113] with the aim to minimize the function

$$X^2 = \Sigma_i w_i |y_i(obs) - y_i(calc)|^2 \qquad (2.59)$$

The weight w_i is assigned as

$$W_i = \left(y_i + B_i^A\right)^{-1}$$

(2.60)

where y_i is the value of the profile point before subtraction of the background B^A_i. The program allows any parameter to be held constant or for constraints to be introduced between a number of them.

Three R factors are calculated in addition to R_I given by Equation (2.48):

The profile R factor,

$$Rp = \frac{100\Sigma_i |y_i(obs) - y_i(calc)|}{\Sigma_i y_i(obs)}$$

(2.61)

the weighted profile R factor,

$$R_{wp} = 100\left[\frac{\Sigma_i w_i [y_i(obs) - y_i(calc)]^2}{\Sigma_i w_i [y_i(obs)]^2}\right]^{1/2}$$

(2.62)

and an expected R factor,

$$R_E = 100\left\{(N-P+C)/\Sigma_i w_i [y_i(obs)]^2\right\}^{1/2}$$

(2.63)

(N-P+C) is the number of degrees of freedom, N is the number of statistically independent observations, P the number of least squares parameters and C the number of constraints functions.

An extension of the Rietveld method is to allow for multipattern refinement [114,115] by use of a program that allows contributions from up to three overlapping patterns in a single profile. These patterns may be due to either impurities or, separate structural phases.

Although there are limitations to the Rietveld method [116], it has been successfully applied to a number of different systems [117]. The method has been extended to analyse X-ray patterns and in principle can be used on any data to which an accurate and consistent peak shape function can be assigned. In this work refinement of data has been obtained using synchrotron radiation where, as in neutron monochromatic diffraction, there is an almost Gaussian peak shape.

2.10 Neutron Instrumentation

The instrument employed in the course of this work is the D9 four-circle diffractometer at the 1.L.L a description of which is given below.

2.10.1 Four-circle Diffractometer D9

The diffractometer (Fig.2.7) is used for measurements requiring wavelengths in the range of 0.35 to 0.85Å, and is situated on the hot source beam tube H3. The instrument has recently been reconstructed replacing the original D9 four-circle diffractometer. D9 is used for precise and accurate measurements of Bragg intensities up

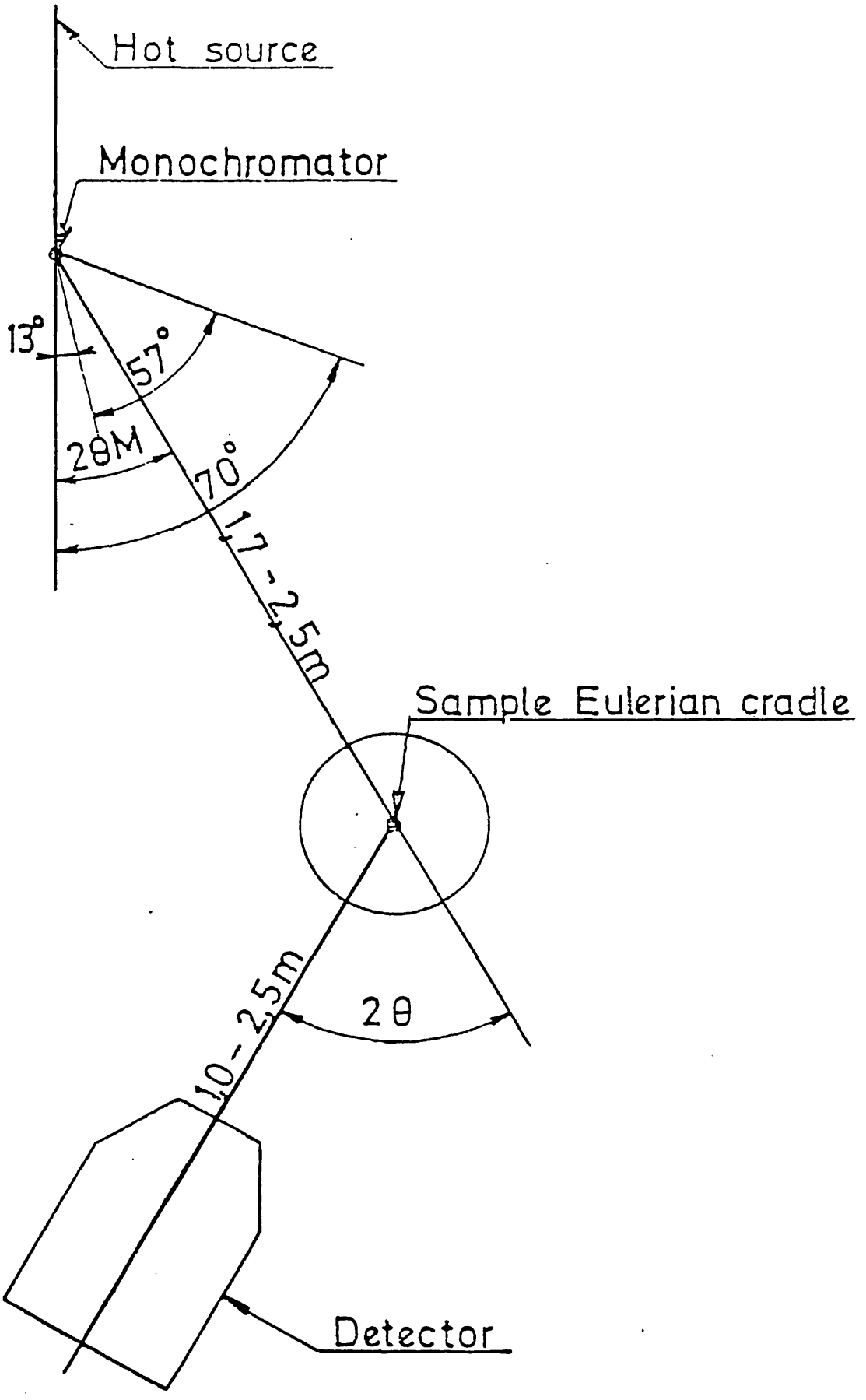

FIG. 2.7: Diffractometer D9

to very high momentum transfer (>2Å^{-1}). The resolution at high scattering angles allow for routine measurements of extended data sets for the detailed study of atomic disorder and atomic thermal motions. This improvement over the previous version of D9 is achieved by going to a higher take-off angle for the monochromator combined with horizontal focusing. The redesign of the diffractometer configuration and the use of beryllium (110) crystals as monochromator increases the flux at the sample position by a factor of 2 to 3. The wavelengths change is fully computerised and facilitates the routine check of extinction effects. The diffractometer is placed on a Tanzboden floor allowing a continuous choice of wavelengths and the change of wavelengths takes only a few seconds. In order to suppress $\lambda/2$ contributions several resonance filters are available at 0.48 Å, 0.55Å, 0.70Å and 0.84Å.

D9 is fully automated and computer controlled (PDP11/34) and is equipped with a 2-stage cryorefrigerator (T min ≈ 15K) mounted on an off-set Eulerian cradle (Fig. 2.8); two furnaces (closed-shell and gas-flow) are available (T max ≈ 1100K).

A small ^{3}He multidetector with 32X32 pixels is also in operation. D9 instrument details are given in table 2.1.

Table 2.1 **D9 Instrument Details**

Beam-tube:	H3 (hot neutrons)
Monochromator Bragg-angle	$13° < 2\theta_m < 55°$
Monochromator crystal:	Be (110) horizontally focussing or Cu(220) in transmission
Maximum flux at sample:	$>10^7 cm^{-2} sec^{-1}$
Maximum beam size at sample:	$0.8X0.8 cm^2$
Incident wavelength:	$0.35 < \lambda(Å) < 0.85$
Incident energies:	$0.11 < E(eV) < 0.67$
Angular ranges:	$-90° < \theta < +150°$ $-95° < w < +80°$ $-110° < X < +110°$ $-180° < \phi < +180°$
Background for normal diffraction geometry:	not yet known

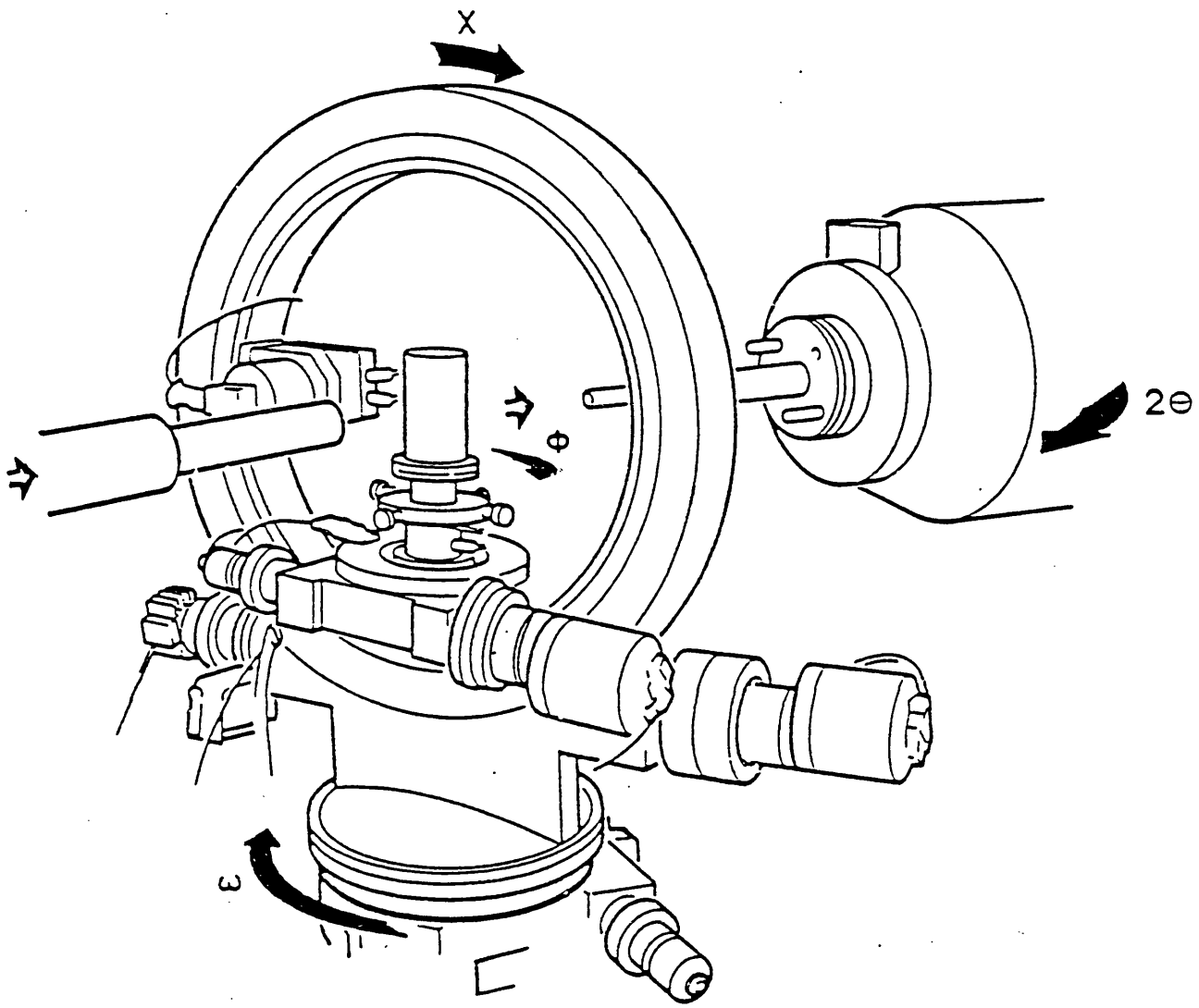

FIG. 2.8: Eulerian cradle with signs of positive rotation

CHAPTER 3

RARE EARTH DOPED ALKALINE EARTH FLUORIDES

3.1 Introduction

The history of experimental investigation of CaF_2-$(Y,Ln)F_3$ systems (Ln= lanthanum and lanthanides) begins in 1914 [118], when the fusion of YF_3 solid solutions in fluorite was found to have a maximum at about 12mol% of yttrium fluoride.

Interest in these systems (or, more precisely, in $Ca_{1-x}Ln_xF_{2+x}$ solid solutions with the fluorite structure type) grew after Goldschmidt [15] proposed a scheme of heterovalent isomorphous substitutions of Ca^{2+} by Ln^{3+} in the fluorite structure type. This scheme envisaged valency compensation by additional interstitial fluoride ions in the centres of the empty cubes of the fluorite structure and offered a basis for the isolation of a new type of "isomorphism with the occupation of space" in ionic crystals.

To test this hypothesis, measurements of the density of solid solutions of the fluorite structure type were made and compared with the theoretically calculated values for various models [24,119-129]. Most of the measurements provided support for the model described in ref.15, but structural studies of $Ca_{0.607}Ce_{0.393}F_{2.393}$ [130] and

$Ca_{0.9}Y_{0.1}F_{2.1}$ [13] showed that the positions of additional fluorine atoms did not conform to the proposal advanced by Goldschmidt. The mechanism of defect interaction in such solid solutions has recently been discussed [46].

The distinctive characteristics of the crystalline structure of solid solutions $Ca_{1-x}R_xF_{2+x}$ with the fluorite structure type find expression in the peculiar spectroscopic behaviour of ion activators in multicomponent matrices [132]. After the production of the first laser on fluorides ($CaF_2:U^{3+}$ [133]) a large number of mixed materials for lasers based on MF_2 with the fluorite structure type were obtained. A detailed characterization of these materials is available [134].

Many authors have investigated the phase equilibria between alkaline-earth fluorides and rare-earth trifluorides [23,37-44]; in particular, the BaF_2-RF_3 [43] and CaF_2-RF_3 [41] systems have been exhaustively examined by Sobolev and his co-workers. In Sobolev's work generally the diagrams are complex in most cases and crystal growth reports have concentrated on either solid solution, usually with the fluorite structure, or on the congruently melting compounds in the series. From the literature it follows that the most characteristic phases in the systems MF_2-$(Y,Ln)F_3$ (M=Ca,Sr,Ba; Ln=lanthanum and the lanthanides) are solid solutions with the fluorite structure or one of its derivatives which are formed in all the systems.

The second most common structural type of the variable - composition phases is the tysonite structure (LaF_3). Tysonite phases are formed by substitution of Ln^{3+} for M^{2+} with formation of vacancies in the anion group; however, they are of various natures and have different types of fusion. The formation of phases with the tysonite structure in the subsolidus of the systems MF_2- $(Y,Ln)F_3$ with rare earth trifluorides not having modifications with this structure [135] indicated that these phases might be berthollides.

As stated earlier fluorides of the elements of group 2 have been widely used as laser host materials. The rare-earth elements are usually added as activators in these systems [16]. Among other potential uses for the solid solutions are the conversion of infrared quanta into visible radiation [136], optical information processing [33,34, 137], solid electrolytes with high ionic conductivity [138,139], thin film condensers [35], photochromic materials [33,34], etc. A pronounced effect of Ln^{3+} impurities on the mechanical characteristics of fluorite [140] was noted. The fusibility of these systems is of interest for an understanding of the electroslag melting of certain metals [39] and the physico-chemical basis of the process of thermal reduction of lanthanide fluorides by calcium [141].

The main emphasis of this work on these systems ie. CaF_2-$(Ln)F_3$ (where Ln=La,Er,Nd), is on structural properties. Despite intensive investigations of these classic disordered solid phases, there remain several puzzles in understanding their complex defect structures.

Early work using both neutron diffraction [45] and computer modelling methods [46] supported the formation of dopant/interstitial dimers and trimers in systems containing 5-10 mole per cent of the trivalent ion dissolved substitutionally in the fluorite structured host. More recent work [47] has proposed more complex structures, in particular the cubo-octahedral structure containing 6 dopant ions.

Computer modelling studies [48] have suggested that the relative stability of the different cluster types depends on the radius of the dopant ion, with clusters of the 2:2:2 and 4:3:2 type being stable for the large dopant ions (eg. La^{3+}) and the cubo-octahedral aggregates having greater stability for the smaller dopant ions (eg. Y^{3+}, Er^{3+}). These predictions have been supported by EXAFS studies [49] and by recent single crystal neutron diffraction work [50,51].

A short-range order model that is suitable for a range of compositions observed in the $Ca_{1-x}Y_xF_{2+x}$ solid solution has been provided by a new polyhedral cluster built up on the

basis of a square antiprism labelled 4:4:3. It also avoids distances for F'_{II}-F'_{II} which are too short in spite of locally closer packing of the anions [142]. The largest clusters (ie., the ordered microdomains observed for samples annealed for a long time) [143] could arise from such 4:4:3 clusters.

Knowledge of the nature of the clusters within anion-excess solid solutions and of transformations with increasing x of small clusters into superclusters is vital for understanding transport properties [52]. The example of $A_{1-x}Bi_xF_{1+2x}$ solid solutions is significant and suggests stronger bonding for superclusters than for smaller ones.

Further neutron work is, however, needed with the following aims (i) to increase our knowledge of the variation of cluster structure with dopant radius, (ii) to study the effects of the host lattice parameter on cluster structure experiments on doped SrF_2 and BaF_2, (iii) to investigate the temperature dependence of the cluster structure.

(iv) The aim of this chapter is to determine the effects of ageing (investigated by annealing samples at high temperatures for variable times) and dopant ion radius on the defect structure of the solid solutions 95-50 mole percent CaF_2 - $(Ln)F_3$ where Ln = La, Er and Nd. The possible importance of temperature effects had been highlighted by conductivity work [52] whilst a premilinary

X-ray diffraction study undertaken at UCL has suggested that ageing (investigated by annealing samples at high temperatures for variable times) may lead to substantial effects on the cluster structures, as would be expected in view of the very low dopant ion diffusion coefficients.

The possibility of very rapid data collection on D9 offers the unique opportunity of solving these problems of obtaining a definitive understanding of the structural properties of these important and complex solid solutions. The single crystal neutron work should be carried out in conjunction with computer modelling and EXAFS studies - a combination which has proved particularly effective in the recent work on these systems [49]. The feedback from these studies into the analysis of existing high quality conductivity data will enable the mechanisms of F^- transport in these systems to be resolved.

In addition, n.m.r studies should be done to ascertain the local environments of the paramagnetic rare earth ions. This technique has considerable potential as a structural tool and should be thoroughly tested here against well-characterized systems.

3.2 Experimental

3.2.1 Preparation of Doped CaF_2/LnF_3 (where Ln=La,Er,Nd) Compounds

The preparation of the doped CaF_2/LnF_3 compounds was carried out at the Chemical laboratory of the University of Kent.

The apparatus used was an r.f. induction furnace manufactured by Electroheating Limited (London). It is provided with rotation and lift motors with gear boxes and was originally designed to operate by the Czochralski method [144]. This technique was not found to be convenient for the present work because of the relatively high melting temperatures of the materials. It was consequently decided to employ the Stöckbarger method [145].

The main features of the apparatus are shown in Fig. 3.1. Two end plates carry flat silicon rubber gaskets sealed against a quartz chamber (70mm bore, 460mm long). Both plates are water cooled and have parts for vacuum or gas entries. A vertical rod supporting the crucible passes through a long water cooled region of the upper work-chamber plate. The rod has a groove out to carry an o-ring seal which slides in a water-cooled housing against a lubricated surface. The rod carrying the crucible is driven by a Velodyne motor through a gearbox and a precision lead screw to provide lowering rates in the range

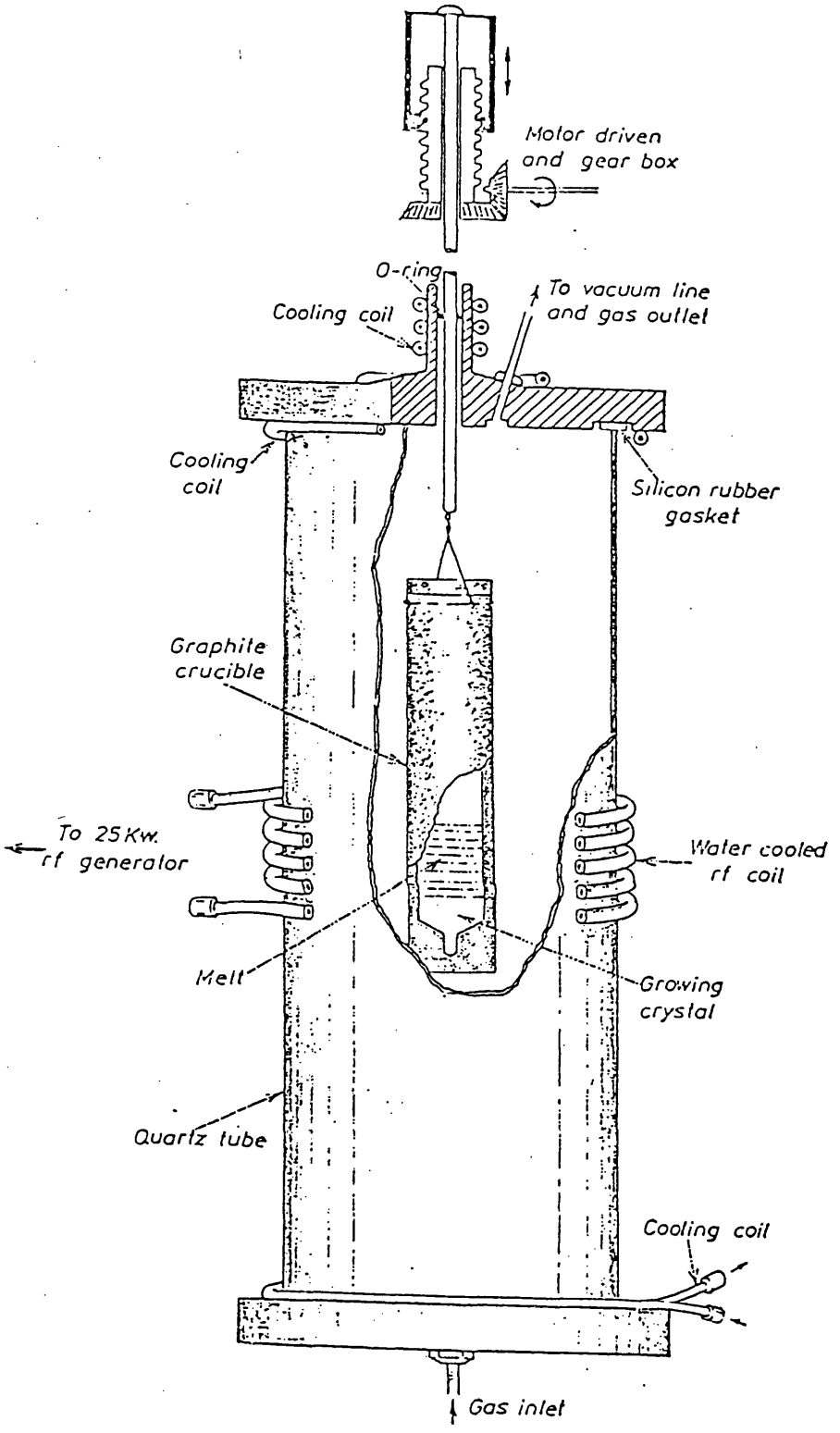

FIG. 3.1: Crystal-growing apparatus
(Not to scale)

of 0.01 to 1.00mm/min. Typical lowering rates for rare earth fluoride systems were 0.2mm/min.

Radio-frequency power at 300kHz was provided by a generator with a capability of 25kw of continuous power. An r.f coil of 6 turns was used; this was made of copper tube and water-cooled.

The crucibles were made by machining graphite rods (Ultra-Carbon and overall length 180mm) with a conical bottom and a capillary (~1mm bore) seeding tip.

The usual procedure was to fill the crucible with powder at the required composition ie. 95-50 mole per cent CaF_2/LnF_3 for all three systems. The crucible was then attached to the drive rod and positioned so that its base was in the centre of the r.f coil. The work chamber was then evacuated and flushed several times with argon (B.O.C. Ltd) and finally left in a slow stream of argon. The r.f. was turned on and the power increased until the powder had melted. This was judged by readings from an optical pyrometer. The drive motor was turned and the crucible allowed to descend through the r.f. coil. When all the melt had been judged to have crystallized, the r.f. power was reduced to zero and the sample removed from the crucible.

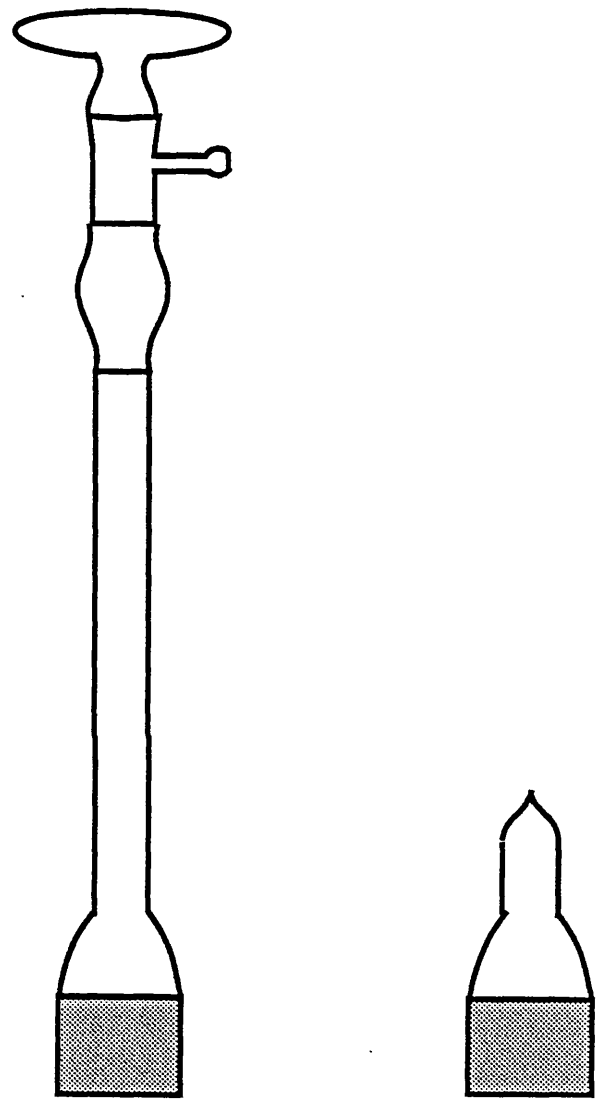

(a) (b)

Fig. 3.2: Device for annealing

3.2.2 Annealing of the Doped CaF_2/LnF_3 (where Ln=La,Er and Nd) Compounds

The prepared compounds from the molten systems of the general formula $Ca_{1-x}Ln_xF_{2+x}$ (where x=0.05 - 0.50) with a minute quantity of PbF_2 (which acts as an O_2 getter) where placed in a graphite crucible positioned at the base of a narrow necked pyrex tube which was connected to a vacuum pump via an adaptor figure 3.2(a) Once under vacuum the lower part of the tubes' neck was sealed Figure 3.2(b) The sealed tubes with the contents where placed in a muffle furnace and annealed at a 1000°C for 3 days.

The prepared and three-day annealed compounds where characterized by X-ray diffraction at the Chemistry Department of the University of Keele. The data were collected on a Phillips PW1050 diffractometer using CuKα radiation with the output in the form of a trace of intensity versus 2θ. After careful consideration according to noticeable changes in the diffraction patterns the molar percentages for each system which were worth further investigation where prepared and annealed for 9 days and 21 days respectively. X-ray diffractograms of the samples were obtained for both annealing times.

3.2.3 Results and Discussion

The X-ray data for the 95 mole% - 50 mole% CaF_2/LnF_3 (Ln=La, Er, Nd) for all three systems are given in the following order:-

(1) Parent compounds - Table 3.1 (a)

(2) The CaF_2/LaF_3 System - Table 3.1 (b)

(3) The CaF_2/ErF_3 System - Table 3.1 (c)

(4) The CaF_2/NdF_3 System - Table 3.1 (d)

In addition the molar percentages of the solid solutions of all three systems which were further investigated by annealing for 9 days and 21 days respectively are also given in Tables 3.1(a), 3.1 (b), 3.1 (c), 3.1 (d) and are the following:

(1) CaF_2/LaF_3 system:-

90 mole% - 80 Mole% CaF_2/LaF_3

and 65 mole% - 55 mole% CaF_2/LaF_3

(2) CaF_2/ErF_3 system:-

65 mole% - 55 mole% CaF_2/ErF_3

(3) CaF_2/NdF_3 system:-

85 mole% CaF_2/NdF_3

75 mole% CaF_2/NdF_3

65 mole% CaF_2/NdF_3

The stick-diagrams of the above molar percentages of all three systems for the samples which were prepared, annealed for 3-days, annealed for 9-days and annealed for 21-days respectively including also the stick-diagrams of the parent compounds are given in the following order:-

(1) Stick-diagrams of parent compounds - Fig.3.3(a)

(2) Stick-diagrams of selected molar percentages in the CaF_2/LaF_3 system - Fig.3.3(b).

(3) Stick-diagrams of selected molar percentages in the CaF_2/ErF_3 system - Fig.3.3(c).

(4) Stick-diagrams of selected molar percentages in the CaF_2/NdF_3 system - Fig.3.3(d).

A careful examination of the results given in Tables 3.1(a), (b), (c) and (d) shows that with small 2θ values the d-spacing changes very rapidly consequently making assignment of peaks very difficult because of the shifting of the peaks. With large 2θ values, however, the d-spacing changes only slightly thus making assignment difficult again. Considering this difficulty, of assigning the peaks using the d-spacing only, both 2θ values and d-spacing were taken into account.

In all three systems on moving from 95-50 mole% CaF_2 the peaks which belong to either parent shift towards a lower 2θ value. This can be explained in terms of one parent compound influencing the other i.e. changes in the internal structure. In addition the CaF_2 peaks begin to disappear quickly on increasing the mole percentage of the other parent compound. In the annealed compounds the intensities

are generally slightly higher and the peaks more clearly visible (Tables 3.1(a), (b), (c) and (d)) which means that more X-rays are diffracted through a certain angle indicating a more regular structure.

A very interesting and important observation is the presence of two-fold and three-fold peaks. The peaks with one shoulder appear in all three systems and are more predominant in the CaF_2/LaF_3 system. This indicates either the presence of two phases or distortion of the cubic phase. The three-fold peaks on the other hand are generally absent in the CaF_2/LaF_3 system but evident in the CaF_2/ErF_3 system and even more predominant in the CaF_2-NdF_3 system. This again indicates either more phases or further distortion of the cubic phase.

Both two-fold and three-fold peaks are generally more clearly visible in the annealed compounds. This confirms the fact that with annealing, the dopant compound penetrates the open CaF_2 lattice. In the CaF_2/LaF_3 system (Table 3.1(b)), considering both the prepared and annealed compounds, new peaks, represented by a dash begin to appear in the 90 mole% CaF_2 compounds, with a considerable increase up to 80 mole% CaF_2. In the 75-50 mole% CaF_2 region there appears to be a gradual decrease in the number of new peaks, although it is interesting to observe the increase in question-marks assigned in the 65-55 mole% CaF_2 region. New compounds may be present, therefore, in the

region of 90-80 mole% CaF_2 and 65-55 mole% CaF_2. Looking at the stick-diagrams of these two regions Fig 3.3(b) prolonged annealing clearly shows ion and vacancy movements.

It can also be seen that annealing initially decreases the symmetry, perhaps by domain formation although the final annealing product ie. the three-week annealed compounds, again has a relatively simple cubic structure. In general a minor phase seems to have been pushed out. It is therefore worthwhile investigating these two regions even further by undertaking a High Resolution X-ray diffraction study.

In the CaF_2/ErF_3 system, (Table 3.1.(c)), new peaks appear in the 65-55 mole% CaF_2 prepared and annealed compounds with a decrease in the 50 mole% CaF_2 compounds. It is interesting to note however the substantial amount of new peaks present in the 65 mole% CaF_2 three-week annealed compound. Thus a new compound may be present in the 65-55 mole% CaF_2 region. The stick-diagrams of this region Fig 3.3(c) show that prolonged annealing produces new phases within the lattice. In this case however we are not dealing with a simple tetragonal distortion of the lattice but with a possible orthorhombic or even domain formation of a new phase. Again the 65-55 mole% CaF_2 region is worth investigating further.

In the CaF_2/NdF_3 system, (Table 3.1.(d)), the majority of the peaks which appear in the doped and doped-annealed compounds can be assigned to either parent and a new compound is not clearly evident; although the few new peaks which arise indicate a small amount of new compound.

Due to this reason prolonged annealing of three possible compounds namely 85, 75 and 65 mole% CaF_2 was undertaken and the stick-diagrams are shown in Fig 3.3(d). It can be seen from the figure that annealing has made things more complicated ie. either a new phase or more domains of impurities. For this reason further investigation of this system by High Resolution X-ray diffraction is required.

It is worthwhile mentioning that the results presented in this chapter are also consistent with radius-ratio considerations. The Nd^{3+} ion (ionic radius -0.99Å) has the same ionic radius size as the Ca^{2+} ion (ionic radius -0.99Å). A higher solubility is thus expected and consequently it is easier to form a simple solid solution. This coincides with the results which indicate no evidence of a new compound.

On the other hand Ca^{2+} and Er^{3+} (ionic radius - 0.88Å) and Ca^{2+} and La^{3+} (ionic radius - 1.06Å) show a mismatch in the ionic radius size. Therefore the bigger the mismatch the lower is the solubility and again this is in agreement with

the results since the greater the mismatch the greater the driving force in forming new compounds from annealing ie. this bigger mismatch opposes the system remaining in the ordinary fluorite structure.

X-ray Diffraction Data for the cooled melts from the CaF_2 : LnF_3 Systems (Ln=La,Er,Nd)

Parent Compounds:

Assignment (a) CaF_2, (b) LaF_3 (c) ErF_3 (d) NdF_3 (a)

2θ	d spacing (Å)	$I^{(rel)}$
28.3	3.153	100
32.8	2.730	1
47.0	1.933	88
55.8	1.647	26
58.5	1.578	1
68.7	1.366	8
75.8	1.255	7
78.2	1.222	1
87.4	1.116	10
94.2	1.052	5
105.8	0.967	3
113.0	0.925	4
115.6	0.911	1
126.1	0.865	5
135.1	0.834	2
138.5	0.824	1

Table 3.1 (a)

X-ray Diffraction Data
for the cooled melts from the
CaF_2 : LnF_3 Systems (Ln=La,Er,Nd)

(b)

2θ	d spacing (Å)	$I^{(rel)}$
24.2	3.678	41
24.7	3.604	29
27.6	3.232	100
34.9	2.571	9
37.9	2.374	2
40.2	2.243	2
43.6	2.076	46
44.7	2.027	59
49.6	1.838	5
50.5	1.807	31
52.4	1.746	18
54.6	1.681	1
56.2	1.637	4
57.0	1.616	3
64.2	1.451	13
64.4	1.447	7
68.1	1.377	10
68.3	1.373	6
68.9	1.363	7
69.1	1.359	6
70.4	1.337	13
70.6	1.334	8
73.7	1.285	1
73.9	1.282	1
74.4	1.275	2
74.6	1.272	1
77.9	1.226	2
80.0	1.199	4
80.3	1.196	3
80.8	1.189	11
81.1	1.186	6
83.2	1.161	2
83.5	1.158	1
85.2	1.139	8
85.4	1.137	4
89.7	1.093	2
90.0	1.090	1
93.8	1.056	5
94.1	1.053	3
95.9	1.038	2
96.2	1.036	1
99.4	1.011	1
99.6	1.009	3
100.0	1.006	2
100.2	1.005	4
100.6	1.002	2
101.0	0.999	8

Table 3.1 (a) (continued)

X-ray Diffraction Data
for the cooled melts from the
CaF_2 : LnF_3 Systems (Ln=La,Er,Nd)

(b) continued

2θ	d spacing (Å)	$I^{(rel)}$
101.3	0.997	5
102.4	0.989	5
102.8	0.986	3
106.4	0.963	1
106.8	0.960	1
113.1	0.924	4
113.5	0.922	2
115.7	0.911	2
116.3	0.908	3
117.0	0.904	3
117.4	0.902	1
119.5	0.892	2
120.0	0.890	1
123.1	0.873	1
128.2	0.857	3
128.7	0.855	1
131.9	0.844	2
132.6	0.842	1
132.9	0.841	2
133.6	0.839	1
136.0	0.831	3
136.7	0.829	2
138.1	0.825	4
138.9	0.823	2
140.2	0.820	4
141.0	0.818	2

Table 3.1(a) (continued)

X-ray Diffraction Data
for the cooled melts from the
CaF_2 : LnF_3 Systems (Ln=La,Er,Nd)

(c)

2θ	d spacing (Å)	$I^{(rel)}$
24.1	3.693	24
24.6	3.619	68
26.0	3.427	75
27.9	3.198	100
31.0	2.885	66
34.9	2.571	3
36.1	2.488	22
37.3	2.411	3
38.7	2.327	2
41.1	2.196	9
43.6	2.076	2
44.0	2.058	16
45.7	1.985	16
47.1	1.929	35
47.7	1.907	23
49.2	1.852	34
49.6	1.838	16
51.5	1.774	11
52.4	1.746	13
53.5	1.713	11
55.1	1.667	13
58.2	1.585	5
59.8	1.546	5
60.3	1.535	3
60.8	1.523	2
62.2	1.492	1
62.5	1.486	4
63.2	1.463	6
63.8	1.459	6
64.7	1.441	4
65.2	1.431	4
65.4	1.427	4
66.0	1.415	6
67.2	1.393	2
67.5	1.388	1
69.7	1.349	2
70.9	1.329	2
71.4	1.321	2
71.6	1.318	2
72.4	1.305	2
73.8	1.284	2
74.0	1.281	4
74.5	1.274	5
75.6	1.258	2
77.0	1.238	5
79.8	1.202	4
83.0	1.163	2

Table 3.1(a) (continued)

X-ray Diffraction Data
for the cooled melts from the
CaF_2 : LnF_3 Systems (Ln=La,Er,Nd)

(c) continued

2θ	d spacing (Å)	$I^{(rel)}$
85.0	1.141	3
87.8	1.112	2
89.9	1.091	2
90.1	1.089	2
91.6	1.075	2
91.9	1.073	2
93.0	1.063	3
94.9	1.046	3
97.1	1.029	2
100.8	1.001	2
104.0	0.978	2
109.6	0.943	2
111.2	0.934	2
112.8	0.926	2

Table 3.1(a) (continued)

X-ray Diffraction Data
for the cooled melts from the
CaF_2 : LnF_3 Systems (Ln=La,Er,Nd)

2θ	(d) d spacing (Å)	$I^{(rel)}$
24.8	3.590	47
25.4	3.507	29
28.3	3.153	100
35.7	2.515	10
44.7	2.027	45
45.8	1.981	50
50.7	1.801	5
51.7	1.768	27
53.7	1.707	16
53.8	1.704	10
57.5	1.603	3
57.7	1.598	2
58.4	1.580	1
65.9	1.417	10
66.1	1.414	6
69.9	1.346	8
70.1	1.342	5
70.7	1.332	6
70.9	1.329	5
72.3	1.307	10
72.5	1.304	6
75.7	1.256	1
75.9	1.254	1
76.4	1.247	2
76.6	1.244	1
80.0	1.199	1
82.3	1.172	5
82.5	1.169	2
83.1	1.162	8
83.4	1.159	5
85.5	1.136	1
85.6	1.135	1
87.6	1.114	6
87.8	1.112	5
92.3	1.069	1
92.6	1.066	1
96.6	1.033	3
96.9	1.030	1
98.8	1.015	3
102.1	0.991	1
102.4	0.989	1
102.7	0.987	2
103.4	0.982	2
104.2	0.977	6
104.6	0.974	3

Table 3.1(a) (continued)

X-ray Diffraction Data
for the cooled melts from the
CaF_2 : LnF_3 Systems (Ln=La,Er,Nd)

(d) continued

2θ	d spacing (Å)	$I^{(rel)}$
105.8	0.967	5
106.2	0.964	2
117.1	0.904	5
117.6	0.901	3

Table 3.1(a) (continued)

X-ray Diffraction Data for the cooled melts from the CaF_2 : LnF_3 Systems (Ln=La,Er,Nd)

The CaF_2/LaF_3 System:

95 mole% CaF_2 /LaF_3

2θ	d spacing (Å)	$I^{(rel)}$	Assignment
28.3	3.153	100	a
32.7	2.739	1	a
44.7	2.027	7	b
46.8	1.941	61	a
55.6	1.653	12	a
58.2	1.585	1	a
58.4	1.580	1	a
68.3	1.373	3	b
68.5	1.370	2	a,b
75.4	1.261	6	a
75.6	1.258	3	a
77.8	1.228	1	b
86.9	1.121	7	a
87.1	1.119	4	a
93.6	1.058	4	b
93.9	1.055	2	b
104.9	0.972	3	a
105.3	0.970	1	a
112.1	0.929	2	a,b,?
124.8	0.870	1	-
125.4	0.868	1	a
133.6	0.839	2	b
134.1	0.837	1	b

Table 3.1(b)

X-ray Diffraction Data for the cooled melts from the CaF_2 : LnF_3 Systems (Ln=La,Er,Nd)

95 mole% CaF_2 / LaF_3 (annealed for 3 days)

2θ	d spacing (Å)	$I^{(rel)}$	Assignment
28.2	3.164	100	a
31.4	2.849	1	a ?
32.7	2.739	2	a
36.4	2.468	1	b ?
44.7	2.027	4	b
46.9	1.937	71	a
55.5	1.656	22	a
58.2	1.585	2	a
58.3	1.583	1	a
68.3	1.373	5	b
68.5	1.370	3	a,b
75.4	1.261	8	a
75.6	1.258	4	a
77.7	1.229	1	b
86.8	1.122	10	a
87.0	1.120	5	a
93.6	1.058	6	b
93.9	1.055	3	b
105.0	0.972	2	a
105.4	0.969	1	a
112.1	0.929	4	a,b,?
112.5	0.927	2	a
114.5	0.917	1	b ?
115.0	0.914	1	a,b
124.9	0.869	4	-
125.4	0.868	2	a
133.6	0.839	3	b
134.2	0.837	2	b

Table 3.1(b) (continued)

X-ray Diffraction Data
for the cooled melts from the
CaF_2 : LnF_3 Systems (Ln=La,Er,Nd)

90 mole% CaF_2 / LaF_3

2θ	d spacing (Å)	$I^{(rel)}$	Assignment
28.2	3.164	100	a
32.5	2.755	2	a
44.7	2.027	7	b
46.6	1.949	41	a
55.2	1.664	23	a
57.9	1.593	5	a
58.0	1.590	3	a
67.9	1.380	2	b
68.1	1.377	1	b
75.0	1.266	4	b
75.2	1.263	3	a,b
77.3	1.234	1	b
86.4	1.126	10	-
86.6	1.124	5	a
93.2	1.061	5	b
93.4	1.059	3	b
104.3	0.976	2	a ?
104.7	0.974	1	a ?
111.2	0.934	3	a ?
111.7	0.932	2	a ?
113.7	0.961	1	b
123.9	0.874	2	b ?
124.2	0.872	2	b ?
132.5	0.842	2	b
133.1	0.840	1	b
135.4	0.833	1	a

Table 3.1(b) (continued)

X-ray Diffraction Data for the cooled melts from the CaF_2 : LnF_3 Systems (Ln=La,Er,Nd)

90 mole% CaF_2 / LaF_3 (annealed for 3 days)

2θ	d spacing (Å)	$I^{(rel)}$	Assignment
28.0	3.187	100	a
32.4	2.763	3	a
44.7	2.027	6	b
46.5	1.953	47	a
55.1	1.667	14	a
57.8	1.595	1	b ?
67.8	1.382	4	b
67.9	1.380	3	b
74.9	1.268	6	b
75.1	1.265	4	b
77.2	1.236	1	b
86.2	1.128	9	a,b,?
86.5	1.125	5	a
92.9	1.064	3	b
93.2	1.061	2	b
104.2	0.977	3	a ?
104.6	0.974	1	a ?
111.2	0.934	3	-
111.6	0.932	1	-
113.6	0.921	1	b
123.9	0.874	2	b ?
124.4	0.871	1	-
132.4	0.843	2	b
133.0	0.841	1	b
135.5	0.833	1	a

X-ray Diffraction Data
for the cooled melts from the
CaF_2 : LnF_3 Systems (Ln=La,Er,Nd)

90 mole% CaF_2 / LaF_3 (annealed for 9 days)

2θ	d spacing (Å)	$I^{(rel)}$	Assignment
28.1	3.175	100	a
32.5	2.755	1	a
46.6	1.949	50	a
55.2	1.664	8	a
57.9	1.593	3	a
58.1	1.588	2	a
67.9	1.380	3	b
68.1	1.377	2	b
75.0	1.266	13	b
75.2	1.263	6	a,b
79.2	1.209	1	a,b
88.2	1.108	2	a
88.5	1.105	1	-
94.9	1.046	3	a,b
95.2	1.044	2	b
106.2	0.964	1	b
106.3	0.963	2	b
106.7	0.961	1	b
113.2	0.923	2	a,b
113.6	0.921	1	b
115.6	0.911	2	a,b
116.0	0.909	1	a,b
125.8	0.866	2	a
126.3	0.864	1	a
134.2	0.837	1	b
137.4	0.827	1	b

Table 3.1(b) (continued)

X-ray Diffraction Data
for the cooled melts from the
CaF_2 : LnF_3 Systems (Ln=La,Er,Nd)

90 mole% CaF_2 / LaF_3 (annealed for 3 weeks)

2θ	d spacing (Å)	$I^{(rel)}$	Assignment
22.2	4.004	1	b ?
27.2	3.278	5	b
28.1	3.175	100	a
31.4	2.849	1	a ?
32.6	2.747	2	a
44.8	2.023	1	b,Al
45.0	2.014	1	b,Al
45.4	1.998	1	b,Al
46.6	1.949	57	a
53.4	1.716	1	b
55.3	1.661	13	a
55.8	1.647	2	a
58.0	1.590	3	a
58.1	1.588	2	a
65.0	1.435	1	b,Al
65.2	1.431	1	b,Al
68.0	1.379	3	b
68.2	1.375	2	b
68.7	1.366	1	a
75.0	1.266	6	b
75.2	1.263	5	a,b
77.3	1.234	2	b
77.6	1.230	1	b
78.3	1.221	1	a,Al
78.5	1.218	1	a
85.8	1.132	1	b
86.0	1.130	1	b
86.3	1.127	19	a,b ?
86.6	1.124	11	a
93.0	1.063	5	b
93.3	1.060	3	b
104.3	0.976	2	a ?
104.4	0.976	1	a ?
104.6	0.974	2	a ?
104.8	0.973	1	a
111.2	0.934	4	-
111.6	0.932	2	-
111.7	0.932	2	-
112.1	0.929	1	a,b ?
113.8	0.920	2	a,b
114.2	0.918	1	a,b

Table 3.1(b) (continued)

X-ray Diffraction Data
for the cooled melts from the
CaF_2 : LnF_3 Systems (Ln=La,Er,Nd)

85 mole% CaF_2 / LaF_3

2θ	d spacing (Å)	$I^{(rel)}$	Assignment
28.1	3.175	100	a
32.5	2.755	3	a
44.7	2.027	1	b,Al
46.6	1.949	44	a
55.0	1.670	15	a
57.7	1.616	3	b
67.7	1.380	2	b
74.7	1.271	4	b
74.9	1.268	2	b
77.0	1.238	1	b ?
85.9	1.131	5	b
86.1	1.129	4	b
92.5	1.067	4	b ?
92.7	1.065	2	b ?
103.6	0.981	2	b ?
104.0	0.978	1	a ?
110.6	0.938	2	-
111.0	0.935	1	-
123.0	0.877	3	b
123.4	0.876	2	b
131.2	0.847	1	b

Table 3.1(b) (continued)

X-ray Diffraction Data for the cooled melts from the CaF_2 : LnF_3 Systems (Ln=La,Er,Nd)

85 mole% CaF_2 / LaF_3 (annealed for 3 days)

2θ	d spacing (Å)	$I^{(rel)}$	Assignment
22.1	4.022	3	-
22.7	3.917	2	-
24.3	3.663	39	b
24.9	3.576	13	b
26.2	3.401	3	-
27.8	3.209	61	b
28.3	3.153	100	a
32.1	2.788	2	a ?
32.3	2.771	5	a ?
32.6	2.747	2	a ?
32.8	2.730	1	a
35.0	2.564	6	b
39.7	2.270	2	b
41.9	2.156	2	b ?
42.2	2.141	2	-
43.8	2.067	19	b
44.9	2.019	27	b
45.9	1.977	5	Al ?
46.3	1.961	10	a ?
47.0	1.933	49	a
49.7	1.834	7	b
49.8	1.831	4	b
50.7	1.801	10	b
52.6	1.740	6	b
54.5	1.684	1	b
54.9	1.672	4	b ?
55.1	1.667	2	a ?
55.7	1.650	11	a
56.4	1.631	2	b
57.3	1.608	1	b
64.5	1.445	4	b
68.6	1.368	5	a
69.1	1.359	3	b
69.3	1.356	2	b
70.8	1.331	4	b
74.0	1.281	1	b
74.5	1.274	3	b
74.8	1.269	2	b
75.8	1.255	4	a
78.1	1.224	2	a,b,Al
81.2	1.185	3	b
85.5	1.136	3	b
85.8	1.132	3	b
87.7	1.117	6	a
94.0	1.054	1	a,b
103.0	0.985	1	b
105.6	0.968	1	a
112.8	0.926	2	a,b
125.8	0.866	2	a

Table 3.1(b) (continued)

X-ray Diffraction Data for the cooled melts from the CaF_2 : LnF_3 Systems (Ln=La,Er,Nd)

85 mole% CaF_2 / LaF_3 (annealed for 9 days)

2θ	d spacing (Å)	$I^{(rel)}$	Assignment
27.8	3.209	100	b
32.3	2.771	6	a
46.2	1.965	29	a ?
54.8	1.675	14	b
55.0	1.670	8	a
57.5	1.603	2	b
57.7	1.598	1	b
67.4	1.389	2	b
67.5	1.388	1	b
74.4	1.275	9	b
74.6	1.272	6	b
76.7	1.242	2	a
76.9	1.240	1	a,b
85.6	1.135	29	b
85.9	1.131	14	b
92.3	1.069	4	-
92.6	1.066	2	-
103.4	0.982	2	b
103.8	0.980	1	b
110.3	0.939	4	-
110.7	0.937	2	-
112.6	0.927	2	a,b
113.0	0.924	1	a
122.6	0.879	2	b
123.1	0.877	1	b
131.0	0.847	1	b
133.9	0.838	2	b
134.6	0.836	1	b

Table 3.1(b) (continued)

X-ray Diffraction Data
for the cooled melts from the
CaF_2 : LnF_3 Systems (Ln=La,Er,Nd)

85 mole% CaF_2 / LaF_3 (annealed for 3 weeks)

2θ	d spacing (Å)	$I^{(rel)}$	Assignment
26.2	3.401	2	-
26.5	3.363	1	-
26.6	3.351	1	-
27.1	3.290	2	b
27.8	3.209	100	b
32.2	2.780	5	a ?
44.3	2.045	1	b,Al
44.6	2.032	1	b,Al
46.2	1.965	52	a
46.9	1.937	2	a
47.0	1.933	1	a
54.8	1.675	36	a,b ?
55.3	1.661	1	a,b
57.4	1.605	3	b
57.6	1.600	2	b
67.4	1.389	4	b
67.6	1.386	3	b
74.4	1.275	7	b
74.6	1.272	6	b
76.6	1.244	2	a
76.9	1.240	1	a,b ?
78.2	1.222	1	a
85.6	1.135	8	b
85.9	1.131	6	b
92.2	1.070	4	-
92.5	1.067	3	-
103.4	0.982	2	b
103.8	0.980	3	b
104.1	0.978	1	-
110.2	0.940	4	-
110.6	0.938	2	-
110.7	0.937	3	-
112.6	0.927	1	a,b
113.0	0.924	1	a,b
113.3	0.923	1	a,b
122.6	0.879	3	b
123.0	0.877	2	b
123.1	0.877	2	b
123.2	0.876	2	b
123.5	0.875	1	b
130.8	0.848	2	b
131.2	0.847	1	b
131.5	0.846	1	b
131.7	0.845	1	b
131.9	0.844	1	b
133.8	0.838	2	b
134.0	0.837	2	b
134.5	0.836	1	a,b
134.6	0.836	1	a,b

Table 3.1(b) (continued)

X-ray Diffraction Data for the cooled melts from the CaF_2 : LnF_3 Systems (Ln=La,Er,Nd)

80 mole% CaF_2 / LaF_3

2θ	d spacing (Å)	$I^{(rel)}$	Assignment
27.8	3.209	100	b
32.1	2.788	5	a,?
44.7	2.027	5	b
46.0	1.973	46	a,?
54.5	1.684	20	b
57.2	1.610	3	b
57.3	1.608	2	b
67.0	1.397	2	-
67.2	1.393	2	-
74.0	1.281	6	b
74.2	1.278	4	b
76.2	1.249	2	a
76.4	1.247	2	a
85.1	1.140	10	b
85.3	1.138	5	b
91.6	1.075	4	-
91.8	1.073	3	-
102.6	0.988	2	b
102.9	0.986	2	b
109.4	0.945	4	-
109.7	0.943	3	-
111.7	0.932	1	-
112.2	0.929	1	a,b,?
121.4	0.884	1	-
129.6	0.852	3	b,?
130.2	0.850	2	-

Table 3.1(b) (continued)

X-ray Diffraction Data for the cooled melts from the CaF_2 : LnF_3 Systems (Ln=La,Er,Nd)

80 mole% CaF_2 / LaF_3 (annealed for 3 days)

2θ	d spacing (Å)	$I^{(rel)}$	Assignment
27.4	3.255	100	b
31.8	2.814	5	a,?
44.6	2.032	7	b
45.7	1.985	51	a,b,Al
54.2	1.692	26	b
54.4	1.687	15	b
56.9	1.618	4	b
57.0	1.616	2	b
66.8	1.400	4	Al,?
67.0	1.397	2	-
73.7	1.285	10	b
73.9	1.282	5	b
76.0	1.252	2	a
76.2	1.249	1	a
84.9	1.142	6	b
85.1	1.140	4	b
91.4	1.077	8	-
91.7	1.074	4	-
102.0	0.989	3	b
102.8	0.986	2	b
109.2	0.946	5	-
109.6	0.943	2	-
111.5	0.933	2	-
111.9	0.930	1	a,b,?
121.3	0.884	4	b,?
121.8	0.882	2	b,?
129.4	0.853	2	b,?
130.0	0.851	1	-
132.2	0.843	1	b
132.9	0.841	1	b

Table 3.1(b) (continued)

X-ray Diffraction Data for the cooled melts from the CaF_2 : LnF_3 Systems (Ln=La,Er,Nd)

80 mole% CaF_2 / LaF_3 (annealed for 9 days)

2θ	d spacing (Å)	$I^{(rel)}$	Assignment
27.8	3.209	100	b
32.2	2.780	5	a
46.1	1.969	52	a
54.6	1.681	17	b
54.7	1.678	13	b
57.2	1.610	5	b
57.4	1.605	3	b
67.1	1.395	3	b
74.0	1.281	5	b
74.3	1.277	4	b
76.3	1.248	2	a
76.5	1.245	1	a
85.1	1.140	10	b
85.4	1.137	5	b
91.7	1.074	5	?
92.0	1.072	3	-
102.6	0.988	2	b
102.8	0.986	1	b
103.0	0.985	2	b
109.4	0.945	3	-
109.8	0.942	2	-
111.8	0.931	2	b,?
112.2	0.929	1	a,b
121.5	0.884	4	b,?
122.0	0.881	2	b
129.6	0.852	1	b

Table 3.1(b) (continued)

X-ray Diffraction Data for the cooled melts from the CaF_2 : LnF_3 Systems (Ln=La,Er,Nd)

80 mole% CaF_2 / LaF_3 (annealed for 3 weeks)

2θ	d spacing (Å)	$I^{(rel)}$	Assignment
27.0	3.302	2	a,b
27.9	3.198	100	a,b
32.2	2.780	8	a
44.6	2.032	2	b,Al
44.8	2.023	1	b,Al
46.1	1.969	44	a,?
54.6	1.681	26	b
57.4	1.605	6	b
65.0	1.435	1	Al
65.2	1.431	1	Al
65.3	1.429	1	Al
67.1	1.395	2	b,?
67.2	1.393	3	b,?
74.1	1.279	10	b
74.3	1.277	7	b
76.3	1.248	1	a,b
76.4	1.247	2	a,b
76.5	1.245	2	a,b
76.6	1.244	1	a,b
78.2	1.222	1	a
85.2	1.139	8	b
85.4	1.137	6	b
91.7	1.074	3	b,?
92.0	1.072	7	b,?
92.3	1.069	3	b,?
102.7	0.987	2	b
103.1	0.984	1	b
109.4	0.945	3	-
109.6	0.943	2	-
109.8	0.942	2	-
110.0	0.941	1	-
111.7	0.932	1	-
111.9	0.930	2	-
112.2	0.929	1	a,b
112.3	0.928	1	a,b
121.5	0.884	2	?
121.7	0.883	1	?
121.9	0.882	1	?
122.1	0.881	1	b
122.3	0.881	1	b
129.8	0.851	2	b,?
130.4	0.849	1	-
132.6	0.842	1	b
132.8	0.841	1	b
133.1	0.840	1	b

Table 3.1(b) (continued)

X-ray Diffraction Data for the cooled melts from the CaF_2 : LnF_3 Systems (Ln=La,Er,Nd)

75 mole% CaF_2 / LaF_3

2θ	d spacing (Å)	$I^{(rel)}$	Assignment
27.7	3.220	100	b
31.9	2.805	5	a,?
44.6	2.032	5	b
45.8	1.981	33	-
54.3	1.689	12	b
56.9	1.618	4	b
57.0	1.616	3	b
66.8	1.400	1	-
67.0	1.397	1	-
73.6	1.287	6	b
73.8	1.284	4	b
75.8	1.255	1	a
84.6	1.145	5	b,?
84.8	1.143	4	b
91.1	1.080	3	b,?
91.3	1.078	2	b,?
101.9	0.993	1	b
102.3	0.990	1	b
108.7	0.949	2	-
109.1	0.946	1	-
110.9	0.936	1	-
120.6	0.887	1	b
128.6	0.856	1	b

Table 3.1(b) (continued)

X-ray Diffraction Data
for the cooled melts from the
CaF_2 : LnF_3 Systems (Ln=La,Er,Nd)

75 mole% CaF_2 / LaF_3 (annealed for 3 days)

2θ	d spacing (Å)	$I^{(rel)}$	Assignment
27.6	3.232	100	b
31.9	2.805	4	a,?
43.6	2.076	4	b
45.8	1.981	69	-
54.2	1.692	24	b
54.4	1.687	12	b
56.8	1.621	4	b
57.0	1.616	2	b
66.7	1.402	1	-
66.9	1.399	1	-
73.6	1.287	9	b
73.8	1.284	5	b
75.8	1.255	3	a
76.0	1.252	1	a
84.6	1.145	10	b,?
84.8	1.143	5	b
91.0	1.081	7	b,?
91.4	1.077	4	-
102.0	0.992	5	b
102.3	0.990	2	b
108.7	0.949	5	-
109.1	0.946	3	-
111.0	0.935	1	a,b,?
120.6	0.887	2	b
121.1	0.885	1	-
128.5	0.856	3	b
129.1	0.854	1	b
131.3	0.846	1	b

Table 3.1(b) (continued)

X-ray Diffraction Data
for the cooled melts from the
CaF_2 : LnF_3 Systems (Ln=La,Er,Nd)

70 mole% CaF_2 / LaF_3

2θ	d spacing (Å)	$I^{(rel)}$	Assignment
27.3	3.267	100	b
31.8	2.814	11	a,?
44.6	2.032	7	b
45.4	1.998	37	b,?
54.0	1.698	20	b,?
56.6	1.626	3	b
56.8	1.621	2	b
66.4	1.408	2	-
73.2	1.293	5	b
73.3	1.291	5	b
75.4	1.261	2	a
84.1	1.151	10	b,?
90.6	1.085	3	b,?
101.0	0.996	1	b
107.8	0.954	3	b,?
108.2	0.952	3	-
110.3	0.939	2	-
119.6	0.892	1	b
120.0	0.890	1	b
127.3	0.860	3	b,?
127.8	0.858	1	b

Table 3.1(b) (continued)

X-ray Diffraction Data for the cooled melts from the CaF_2 : LnF_3 Systems (Ln=La,Er,Nd)

70 mole% CaF_6 / LaF_3 (annealed for 3 days)

2θ	d spacing (Å)	$I^{(rel)}$	Assignment
27.3	3.267	100	b
31.2	2.867	1	a,?
31.6	2.831	15	a,?
36.2	2.481	1	-
44.6	2.032	7	b
45.4	1.998	53	b,?
53.8	1.704	22	b,?
54.0	1.698	12	b,?
56.4	1.631	5	b
56.6	1.626	3	b
66.2	1.412	4	b,?
66.4	1.408	2	b,?
73.0	1.296	13	b,?
73.2	1.293	6	b
75.2	1.263	3	a,b
75.5	1.259	2	a
84.0	1.152	11	b,?
84.2	1.150	5	b,?
90.4	1.086	5	b
90.7	1.084	3	b,?
101.2	0.998	2	b
101.6	0.995	1	b
107.8	0.954	5	b,?
108.2	0.952	3	-
110.1	0.941	3	-
110.6	0.938	1	-
119.6	0.892	4	b
120.0	0.890	2	b
127.3	0.860	3	b,?
127.8	0.858	2	b
130.0	0.851	1	-
130.7	0.848	1	-

Table 3.1(b) (continued)

X-ray Diffraction Data
for the cooled melts from the
CaF_2 : LnF_3 Systems (Ln=La,Er,Nd)

65 mole% CaF_2 / LaF_3

2θ	d spacing (Å)	$I^{(rel)}$	Assignment
27.1	3.290	100	b
31.4	2.849	17	a,?
44.7	2.023	4	b
45.1	2.010	54	b,?
53.5	1.713	26	-
56.1	1.639	5	b
56.2	1.637	4	b
65.8	1.419	7	Al,?
66.0	1.415	4	Al,?
72.6	1.302	12	-
72.8	1.299	5	b,?
74.8	1.269	4	b
83.5	1.158	5	b
83.6	1.157	6	b
89.8	1.092	4	b
90.0	1.090	3	b
100.4	1.003	1	b
100.8	1.001	1	b
107.0	0.959	4	b
107.4	0.957	3	b
109.3	0.945	3	-
109.7	0.943	2	-
118.6	0.897	3	b,?
119.0	0.895	2	b
126.5	0.865	2	a
126.6	0.863	2	a
129.0	0.854	1	b
140.8	0.818	1	b

Table 3.1(b) (continued)

X-ray Diffraction Data for the cooled melts from the CaF_2 : LnF_3 Systems (Ln=La,Er,Nd)

65 mole% CaF_2 / LaF_3 (annealed for 3 days)

2θ	d spacing (Å)	$I^{(rel)}$	Assignment
24.3	3.663	1	b
27.4	3.255	100	b
31.7	2.823	14	a,?
45.4	1.998	49	b,Al
53.8	1.704	17	b
56.3	1.634	6	b
56.5	1.629	5	b
66.1	1.414	5	Al,?
66.3	1.410	3	-
72.8	1.299	10	b
73.0	1.296	5	b
75.1	1.265	2	a,b
75.3	1.262	1	a,b
83.7	1.155	5	b
84.0	1.152	3	b
91.0	1.081	10	b,?
91.4	1.077	5	-
100.8	1.001	3	b
101.1	0.998	2	b
107.3	0.957	6	b
107.7	0.955	4	b
109.5	0.944	2	-
110.0	0.941	1	-
118.9	0.895	2	b
119.4	0.893	1	b
126.4	0.864	2	a
127.0	0.861	1	a
129.1	0.854	2	b
129.7	0.852	1	b,?
140.8	0.818	1	b

Table 3.1(b) (continued)

X-ray Diffraction Data for the cooled melts from the CaF_2 : LnF_3 Systems (Ln=La,Er,Nd)

65 mole% CaF_2 / LaF_3 (annealed for 9 days)

2θ	d spacing (Å)	$I^{(rel)}$	Assignment
27.4	3.255	100	b
31.7	2.823	12	a,?
45.4	1.998	93	b
53.8	1.704	33	b,?
53.9	1.701	20	b,?
56.3	1.634	5	b
56.5	1.629	3	b
66.0	1.415	3	Al,?
66.2	1.412	2	Al,?
72.8	1.299	10	b,?
73.0	1.296	6	b
75.0	1.266	4	a,b
75.3	1.262	3	a
83.6	1.157	12	b
84.0	1.152	6	b
90.0	1.090	7	b
90.4	1.086	3	b
100.6	1.002	10	b
101.0	0.999	6	b
107.2	0.958	7	b
107.6	0.955	5	b
118.8	0.896	5	b,?
119.3	0.893	3	b
126.7	0.864	2	a
129.0	0.854	1	b

Table 3.1(b) (continued)

X-ray Diffraction Data for the cooled melts from the CaF_2 : LnF_3 Systems (Ln=La,Er,Nd)

65 mole% CaF_2 / LaF_3 (annealed for 3 weeks)

2θ	d spacing (Å)	$I^{(rel)}$	Assignment
27.4	3.255	100	b
28.3	3.153	1	a
29.2	3.058	1	a,?
31.0	2.885	1	-
31.3	2.858	1	-
31.8	2.814	8	a,?
38.5	2.338	1	b,Al
44.8	2.023	2	b,Al
45.4	1.998	61	b,Al
53.8	1.704	12	b
56.4	1.631	4	b
56.6	1.626	3	b
65.1	1.433	2	b,Al
65.3	1.429	1	b,Al
66.1	1.414	3	Al,?
73.0	1.296	5	b
75.2	1.263	3	a,b
75.4	1.261	3	a
75.5	1.259	2	a
75.7	1.256	1	a
78.2	1.222	2	a,Al
78.3	1.221	1	a,Al
78.5	1.218	1	a,Al
83.8	1.154	5	b
83.9	1.153	4	b
84.0	1.152	3	b,?
84.4	1.148	2	b,?
90.1	1.089	5	b
90.4	1.086	8	b
90.6	1.085	3	b
100.8	1.001	1	b
101.0	0.999	1	b
107.3	0.957	4	b
107.7	0.955	3	b
108.2	0.952	5	b,?
108.6	0.949	2	b,?
109.6	0.943	1	-
109.8	0.942	1	-
110.0	0.941	1	-
118.8	0.896	1	b
119.4	0.893	1	b
126.4	0.864	8	a
127.0	0.861	4	a
127.3	0.860	2	a
127.9	0.858	1	b,?
129.4	0.853	1	b,?

Table 3.1(b) (continued)

X-ray Diffraction Data
for the cooled melts from the
CaF_2 : LnF_3 Systems (Ln=La,Er,Nd)

60 mole% CaF_2 / LaF_3

2θ	d spacing (Å)	$I^{(rel)}$	Assignment
27.0	3.302	100	b
27.7	3.220	2	b
31.3	2.858	17	a,?
44.6	2.032	11	b
44.9	2.019	77	b
53.2	1.722	31	b,?
55.8	1.647	4	b
65.4	1.427	4	-
72.2	1.308	10	-
72.4	1.305	10	-
74.4	1.275	4	b
83.0	1.163	6	b
89.5	1.095	4	b
99.9	1.007	3	b
106.4	0.963	6	b
108.6	0.949	3	-
117.7	0.901	2	b
127.9	0.858	1	b

Table 3.1(b) (continued)

X-ray Diffraction Data for the cooled melts from the CaF_2 : LnF_3 Systems (Ln=La,Er,Nd)

60 mole% CaF_2 / LaF_3 (annealed for 3 days)

2θ	d spacing (Å)	$I^{(rel)}$	Assignment
24.4	3.648	8	b
25.1	3.548	3	b
27.6	3.232	100	b
28.0	3.187	14	a
31.8	2.814	10	a,?
35.2	2.550	1	b
44.1	2.053	6	b
44.7	2.027	7	b
45.1	2.010	9	b,?
45.5	1.993	43	b,?
49.9	1.828	1	b
51.0	1.791	4	b
52.9	1.731	2	b
53.8	1.704	20	b,?
54.0	1.698	15	b,?
56.4	1.631	6	b
56.6	1.626	5	b
64.8	1.439	1	b
66.2	1.412	2	-
68.5	1.370	1	a,b
69.3	1.356	1	b
71.1	1.326	1	b
72.9	1.298	9	b,?
73.1	1.294	6	b
75.2	1.263	3	a,b
75.3	1.262	2	a
81.6	1.180	1	b,?
83.7	1.155	7	b,?
84.0	1.152	5	b,?
85.8	1.132	1	b,?
90.2	1.088	5	b
90.4	1.086	4	b
100.8	1.001	1	b
107.3	0.957	3	b
107.7	0.955	2	b,?
109.5	0.944	1	-
109.9	0.942	1	-
118.8	0.896	2	b,?
119.2	0.894	1	b
126.2	0.864	4	a
126.8	0.862	2	a,?
140.9	0.818	2	b
141.8	0.816	2	b

Table 3.1(b) (continued)

X-ray Diffraction Data
for the cooled melts from the
CaF_2 : LnF_3 Systems (Ln=La,Er,Nd)

60 mole% CaF_2 / LaF_3 (annealed for 9 days)

2θ	d spacing (Å)	$I^{(rel)}$	Assignment
24.3	3.663	51	b
24.9	3.576	33	b
27.4	3.255	79	b
27.8	3.209	100	b
28.2	3.164	26	a
31.6	2.831	12	a
35.1	2.557	9	b
43.9	2.062	37	b
45.0	2.014	44	b
45.3	2.002	27	b,?
45.5	1.993	26	b,?
45.6	1.989	26	b,?
46.5	1.953	9	b,?
46.7	1.945	12	a
46.8	1.941	14	a
47.0	1.933	11	a
49.7	1.834	7	b
50.8	1.797	19	b
52.7	1.737	12	b
53.8	1.704	26	b
53.9	1.701	21	b
56.4	1.631	6	b
64.6	1.443	9	b
65.9	1.417	5	Al,?
66.1	1.414	5	Al,?
68.4	1.372	9	a,b
69.3	1.356	5	b
70.9	1.329	9	b
72.8	1.299	7	b
73.0	1.296	7	b
75.0	1.266	3	a,b
80.4	1.194	5	b
81.0	1.187	5	b
81.2	1.185	7	b
81.4	1.182	7	b
81.5	1.181	5	b
83.6	1.157	7	b
83.7	1.155	7	b
83.9	1.153	6	b
85.6	1.135	9	b
90.0	1.090	7	b
90.2	1.088	7	b
94.1	1.053	5	a,b
107.2	0.958	3	b
118.6	0.897	2	b
126.2	0.864	2	a
128.8	0.855	5	b
129.5	0.852	2	b,?

Table 3.1(b) (continued)

X-ray Diffraction Data for the cooled melts from the CaF_2 : LnF_3 Systems (Ln=La,Er,Nd)

60 mole% CaF_2 / LaF_3 (annealed for 3 weeks)

2θ	d spacing (Å)	$I^{(rel)}$	Assignment
22.0	4.040	2	-
24.3	3.663	3	b
24.9	3.576	2	b
25.2	3.534	1	b
27.3	3.267	100	b
27.8	3.209	4	a,b
28.2	3.164	3	a
31.2	2.867	4	-
31.6	2.831	12	-
43.9	2.062	2	b
44.6	2.032	10	b,Al
44.8	2.023	8	b,Al
45.0	2.014	9	b,Al
45.3	2.002	51	b
46.8	1.941	3	a
47.0	1.933	2	a
47.1	1.929	2	a
47.4	1.918	1	a
50.8	1.797	1	b
52.8	1.734	3	b
53.0	1.728	4	b
53.1	1.725	3	b
53.2	1.722	3	b
53.7	1.707	29	b
53.8	1.704	27	b
55.5	1.656	1	a
56.2	1.637	4	b
56.4	1.631	4	b
64.6	1.443	1	b
64.8	1.439	1	b
65.0	1.435	3	b
71.7	1.316	1	b,?
72.6	1.302	6	b,?
72.8	1.299	7	b,?
73.1	1.294	4	b,?
73.3	1.291	2	b
74.9	1.268	3	a,b
75.0	1.266	4	a,b
75.3	1.262	3	a,b
75.6	1.258	1	a
83.7	1.155	6	b
83.9	1.153	4	b
90.0	1.090	3	b
90.3	1.087	2	b
90.4	1.086	4	b
90.7	1.084	2	b
100.8	1.001	2	b,Al

Table 3.1(b) (continued)

X-ray Diffraction Data for the cooled melts from the CaF_2 : LnF_3 Systems (Ln=La,Er,Nd)

60 mole% CaF_2 / LaF_3 (annealed for 3 weeks) continued

2θ	d spacing (Å)	$I^{(rel)}$	Assignment
107.2	0.958	4	b
107.4	0.957	3	b
107.6	0.955	2	b
107.8	0.954	1	b
109.5	0.944	2	-
118.4	0.897	2	b,?
118.8	0.896	3	b,?
119.1	0.894	2	b
119.3	0.893	2	b
119.7	0.892	1	b
126.3	0.864	2	a
128.8	0.855	1	b
129.5	0.852	1	b,?

Table 3.1(b) (continued)

X-ray Diffraction Data
for the cooled melts from the
CaF_2 : LnF_3 Systems (Ln=La,Er,Nd)

55 mole% CaF_2 / LaF_3

2θ	d spacing (Å)	$I^{(rel)}$	Assignment
24.2	3.678	8	b
24.9	3.576	3	b
27.1	3.290	100	b
27.8	3.209	12	a
31.4	2.849	15	a,?
35.1	2.557	1	b
44.0	2.058	5	b
44.6	2.032	12	b
45.0	2.014	59	b,?
49.7	1.834	1	b
50.9	1.794	2	b
52.9	1.731	2	b
53.3	1.719	24	b,?
55.9	1.645	4	b
64.8	1.439	1	b
65.5	1.425	4	-
68.5	1.370	1	a,b
69.3	1.356	1	b
71.2	1.324	1	b,?
72.2	1.308	8	-
72.4	1.305	6	-
74.4	1.275	3	b
78.1	1.224	1	a,b,Al
82.9	1.165	6	b
83.2	1.161	4	b
89.2	1.098	4	b,?
89.5	1.095	3	b
99.0	1.014	1	b,Al
99.8	1.008	2	b
100.1	1.006	2	b
106.2	0.964	5	b
106.6	0.961	3	b
108.4	0.950	2	-
108.8	0.948	1	-
117.5	0.902	2	b
118.0	0.899	1	b

Table 3.1(b) (continued)

X-ray Diffraction Data for the cooled melts from the CaF_2 : LnF_3 Systems (Ln=La,Er,Nd)

55 mole% CaF_2 / LaF_3 (annealed for 3 days)

2θ	d spacing (Å)	$I^{(rel)}$	Assignment
24.3	3.663	21	b
25.0	3.562	9	b
27.4	3.255	100	b
27.8	3.209	32	a
31.6	2.831	10	a,?
35.1	2.557	3	b
43.9	2.062	15	b
44.9	2.019	19	b
45.3	2.002	55	b,?
49.7	1.834	3	b
50.8	1.797	7	b
52.7	1.737	6	b
53.7	1.707	25	b,?
53.8	1.704	18	b,?
56.2	1.637	5	b
56.4	1.631	5	b
64.6	1.443	3	b
64.7	1.441	3	b
65.9	1.417	3	-
66.1	1.414	2	-
68.4	1.372	2	a,b
69.2	1.358	2	b
70.9	1.329	3	b
71.1	1.326	2	b
72.8	1.299	10	b,?
73.0	1.296	6	b,?
75.0	1.266	3	b
75.2	1.263	2	a,b
78.1	1.224	1	a,b,Al
80.6	1.192	1	b
81.3	1.183	2	b
81.6	1.180	1	b,?
83.6	1.157	8	b
83.8	1.154	5	b,?
85.7	1.134	2	b,?
86.0	1.130	1	b,?
90.0	1.090	4	b
90.2	1.088	3	b
94.1	1.053	1	b
100.6	1.002	2	b
101.0	0.999	2	b
101.7	0.994	2	b
103.3	0.983	1	b,?
107.2	0.958	4	b,?
107.6	0.955	3	b,?
109.4	0.945	2	-
109.8	0.942	1	-
114.0	0.919	1	b

Table 3.1(b) (continued)

X-ray Diffraction Data for the cooled melts from the CaF_2 : LnF_3 Systems (Ln=La,Er,Nd)

55 mole% CaF_2 / LaF_3 (annealed for 3 days) continued

2θ	d spacing (Å)	$I^{(rel)}$	Assignment
116.4	0.907	1	b
116.9	0.905	1	b
118.7	0.896	2	b
119.2	0.894	1	b
126.2	0.864	2	a
128.8	0.855	1	a,?
129.0	0.854	2	b
129.5	0.852	1	b,?

Table 3.1(b) (continued)

X-ray Diffraction Data for the cooled melts from the CaF_2 : LnF_3 Systems (Ln=La,Er,Nd)

55 mole% CaF_2 / LaF_3 (annealed for 9 days)

2θ	d spacing (Å)	$I^{(rel)}$	Assignment
22.1	4.022	2	-
24.4	3.648	68	b
25.1	3.548	32	b,?
27.5	3.243	29	b
27.9	3.198	100	b
28.3	3.153	22	a
31.8	2.814	5	a
35.2	2.550	10	b
44.0	2.058	44	b,Al
45.0	2.014	61	b,Al
45.4	1.998	15	b,Al
45.6	1.989	14	b,Al
45.7	1.985	13	b,Al
45.9	1.977	12	b,Al
47.0	1.933	12	a
49.8	1.831	5	b
50.8	1.797	27	b
52.8	1.775	12	b
53.0	1.728	10	b
53.9	1.701	10	b
55.6	1.653	5	a
55.8	1.647	5	a
56.4	1.631	7	b
56.6	1.626	6	b
64.7	1.441	12	b
68.6	1.368	12	b
69.3	1.356	10	b
69.5	1.352	6	b
69.7	1.349	4	b
71.0	1.328	10	b
78.2	1.222	2	a
80.6	1.192	5	b
80.9	1.188	5	b
81.3	1.183	10	b
83.7	1.155	5	b
83.9	1.153	4	b
85.3	1.138	2	b
85.5	1.136	5	b
85.6	1.135	10	a,b
85.8	1.132	7	a,b
90.1	1.089	5	b
90.4	1.086	5	b
94.2	1.052	7	a,b
100.0	1.006	5	b
101.7	0.994	10	b

Table 3.1(b) (continued)

X-ray Diffraction Data
for the cooled melts from the
CaF_2 : LnF_3 Systems (Ln=La,Er,Nd)

55 mole% CaF_2 / LaF_3 (annealed for 3 weeks)

2θ	d spacing (Å)	$I^{(rel)}$	Assignment
24.4	3.648	4	b
25.0	3.562	3	b
27.3	3.267	100	b
27.8	3.209	13	b
31.6	2.831	13	a
35.1	2.557	2	b
35.2	2.550	1	b
43.8	2.067	2	b
44.0	2.058	3	b,Al
45.2	2.006	37	b,Al
49.7	1.834	1	b
50.4	1.811	1	b
50.8	1.797	3	b
52.8	1.734	2	b
53.6	1.710	17	b
56.2	1.637	4	b
57.2	1.610	1	b
57.4	1.605	1	b
64.6	1.443	2	b
64.7	1.441	1	b
65.0	1.435	2	Al
65.2	1.431	1	Al
65.5	1.425	1	Al,?
65.7	1.421	2	Al,?
65.8	1.419	3	Al,?
66.0	1.415	2	Al,?
66.3	1.410	1	Al,?
66.6	1.404	1	Al,?
66.9	1.399	1	Al,?
68.4	1.372	1	a,b
69.2	1.358	1	b
69.4	1.354	1	b
69.8	1.347	1	b
71.0	1.328	2	b
72.7	1.301	7	b,?
74.8	1.269	2	b
78.2	1.222	1	a
81.4	1.182	1	b
83.4	1.159	5	b
83.5	1.158	5	b
83.6	1.157	5	b
83.8	1.154	3	b
84.1	1.151	1	b
85.6	1.135	1	b
89.6	1.094	3	b
89.9	1.091	4	b
90.2	1.088	2	b

Table 3.1(b) (continued)

X-ray Diffraction Data
for the cooled melts from the
CaF_2 : LnF_3 Systems (Ln=La,Er,Nd)

55 mole% CaF_2 / LaF_3 (annealed for 3 weeks) continued

2θ	d spacing (Å)	$I^{(rel)}$	Assignment
94.2	1.052	1	a,b
94.5	1.050	1	a,b
100.0	1.006	1	b
100.2	1.005	1	b
100.3	1.004	1	b
100.6	1.002	1	b
101.0	0.999	1	b
101.7	0.994	1	b
105.4	0.969	1	a
105.8	0.967	1	a
106.4	0.963	2	b
106.5	0.962	2	b
106.8	0.960	3	b
107.0	0.959	3	b
107.1	0.958	2	b
109.2	0.946	1	-
118.4	0.897	2	b,?
125.6	0.867	1	a
125.8	0.866	1	a

Table 3.1(b) (continued)

X-ray Diffraction Data
for the cooled melts from the
CaF_2 : LnF_3 Systems (Ln=La,Er,Nd)

50 mole% CaF_2 / LaF_3

2θ	d spacing (Å)	$I^{(rel)}$	Assignment
24.3	3.663	35	b
25.0	3.562	15	b
27.2	3.278	100	b
27.9	3.198	45	a
31.5	2.840	19	a,?
35.2	2.550	4	b
44.1	2.053	18	b
44.6	2.032	10	b
45.1	2.010	79	b,?
49.8	1.831	4	b
51.0	1.791	13	b
52.9	1.731	7	b
53.4	1.716	16	-
53.5	1.713	18	-
56.1	1.639	4	b
56.5	1.629	2	b
64.8	1.439	4	b
65.7	1.421	4	-
68.6	1.368	3	a,b
69.3	1.356	4	b
69.5	1.352	3	b,?
71.2	1.324	4	b,?
72.4	1.305	7	-
74.5	1.274	2	b
81.0	1.187	1	b
81.7	1.179	3	b,?
83.2	1.161	5	b
86.1	1.129	2	b,?
89.7	1.093	3	b
94.5	1.050	2	b
99.7	1.009	4	b
100.1	1.006	4	b
106.7	0.961	3	b

Table 3.1(b) (continued)

X-ray Diffraction Data for the cooled melts from the CaF_2 : LnF_3 Systems (Ln=La,Er,Nd)

50 mole% CaF_2 / LaF_3 (annealed for 3 days)

2θ	d spacing (Å)	$I^{(rel)}$	Assignment
24.4	3.648	32	b
25.0	3.562	14	b
27.4	3.255	100	b
27.9	3.198	52	a
31.7	2.823	9	a,?
35.2	2.550	4	b
44.0	2.058	20	b
44.7	2.027	9	b
45.0	2.014	30	b,?
45.4	1.998	40	b,?
49.8	1.831	4	b
50.8	1.797	13	b
52.8	1.734	8	b
53.8	1.704	15	-
53.9	1.701	13	-
56.4	1.631	6	b
56.6	1.626	5	b
57.4	1.605	1	b
64.6	1.443	5	b
66.1	1.414	3	-
66.2	1.412	2	-
68.4	1.372	4	a,b
69.3	1.356	3	b
71.0	1.328	4	b
71.1	1.326	2	b
72.9	1.298	7	b,?
73.1	1.294	5	b
75.1	1.265	2	b
80.6	1.192	1	b
81.4	1.182	4	b
81.6	1.180	2	b,?
83.8	1.154	6	b,?
84.0	1.152	4	b,?
85.7	1.134	2	b,?
90.1	1.089	4	b
90.4	1.086	3	b
94.2	1.052	2	b
94.5	1.050	1	b
100.1	1.006	1	b
100.9	1.000	2	b
101.7	0.994	2	b
103.3	0.983	2	b,?
107.3	0.957	3	b,?
107.7	0.955	2	b,?
109.5	0.944	1	b,?
114.0	0.919	1	b
118.9	0.895	1	b

Table 3.1(b) (continued)

X-ray Diffraction Data
for the cooled melts from the
CaF_2 : LnF_3 Systems (Ln=La,Er,Nd)

50 mole% CaF_2 / LaF_3 (annealed for 3 days) continued

2θ	d spacing (Å)	$I^{(rel)}$	Assignment
119.4	0.893	1	b
126.4	0.864	1	a
129.0	0.854	1	b
133.6	0.839	1	b
141.1	0.818	2	b
141.8	0.816	2	b

Table 3.1(b) (continued)

X-ray Diffraction Data for the cooled melts from the CaF_2 : LnF_3 Systems (Ln=La,Er,Nd)

The CaF_2/ErF_3 System:

95 mole% CaF_2 / ErF_3

2θ	d spacing (Å)	$I^{(rel)}$	Assignment
28.2	3.164	100	a
32.7	2.739	1	a
47.0	1.933	44	a
55.7	1.650	13	a
55.8	1.647	7	a
58.4	1.580	1	a
58.5	1.578	1	a
68.5	1.370	1	a
68.7	1.366	1	a
75.7	1.256	4	a,c
75.9	1.254	2	a
87.2	1.118	4	a
87.4	1.116	2	a
93.9	1.055	2	a
94.0	1.054	2	a
94.3	1.054	1	a
105.5	0.970	1	a
105.9	0.970	1	a
112.8	0.930	1	a,c,?
113.2	0.920	1	a

Table 3.1(c)

X-ray Diffraction Data
for the cooled melts from the
CaF_2 : LnF_3 Systems (Ln=La,Er,Nd)

95 mole% CaF_2 / ErF_3 (annealed for 3 days)

2θ	d spacing (Å)	$I^{(rel)}$	Assignment
28.3	3.153	100	a
32.8	2.730	1	a
47.0	1.933	48	a
55.7	1.650	11	a
55.8	1.647	6	a
58.4	1.580	3	a
58.6	1.575	2	a
68.6	1.368	3	a
68.8	1.365	1	a
75.7	1.256	8	a,c
76.0	1.252	4	a
87.2	1.118	8	a
87.5	1.115	4	a
94.0	1.054	9	a
94.4	1.051	4	a
105.6	0.968	2	a
106.0	0.965	1	a
112.7	0.926	3	c
113.2	0.923	2	a
115.2	0.913	1	a
115.7	0.911	1	a

Table 3.1(c) continued

X-ray Diffraction Data
for the cooled melts from the
CaF_2 : LnF_3 Systems (Ln=La,Er,Nd)

90 mole% CaF_2 / ErF_3

2θ	d spacing (Å)	$I^{(rel)}$	Assignment
28.2	3.164	100	a
32.7	2.739	1	a
47.0	1.933	35	a
55.7	1.650	27	a
58.4	1.580	2	a
58.5	1.578	1	a
68.5	1.370	2	a
68.6	1.368	1	a
75.7	1.256	4	a,c
75.9	1.254	2	a
78.0	1.225	1	a
78.2	1.222	1	a,Al
87.2	1.118	5	a
87.4	1.116	3	a
94.0	1.054	3	a
94.3	1.052	2	a
105.5	0.968	1	a
105.8	0.967	1	a
112.4	0.928	1	c
112.6	0.927	3	c
113.1	0.924	2	a
115.2	0.913	1	a
115.6	0.911	1	a

Table 3.1(c) continued

X-ray Diffraction Data for the cooled melts from the CaF_2 : LnF_3 Systems (Ln=La,Er,Nd)

90 mole% CaF_2 / ErF_3 (annealed for 3 days)

2θ	d spacing (Å)	$I^{(rel)}$	Assignment
26.0	3.427	1	c
28.2	3.164	100	a
32.7	2.739	3	a
46.8	1.941	35	a
55.5	1.656	11	a
55.7	1.650	9	a
58.2	1.585	3	c
58.4	1.580	2	a
68.3	1.373	2	a
68.5	1.370	3	a
75.4	1.261	15	c
75.6	1.258	6	c
77.7	1.229	1	a
77.9	1.226	1	a
86.5	1.125	1	a
86.9	1.121	10	a
87.2	1.118	4	a
93.6	1.058	4	c
93.9	1.055	2	a
105.0	0.972	1	a
105.2	0.970	1	a
112.2	0.929	2	c
112.6	0.927	2	c
114.6	0.916	1	a,?
115.0	0.914	1	a

Table 3.1(c) continued

X-ray Diffraction Data
for the cooled melts from the
CaF_2 : LnF_3 Systems (Ln=La,Er,Nd)

85 mole% CaF_2 / ErF_3

2θ	d spacing (Å)	$I^{(rel)}$	Assignment
28.0	3.187	100	a,c
32.4	2.763	3	a
46.6	1.949	42	a
55.3	1.661	14	c
58.0	1.590	3	c
58.1	1.588	2	c
68.1	1.377	2	a,c
75.2	1.263	8	c
75.4	1.261	3	c
77.6	1.230	1	a,c
77.8	1.228	1	a
86.6	1.124	4	a
86.9	1.121	2	a
93.4	1.059	2	c
93.5	1.058	2	c
93.7	1.057	1	a,c
104.9	0.972	3	a,c
105.2	0.970	1	a
112.1	0.929	2	c
112.4	0.928	1	c

Table 3.1(c) continued

X-ray Diffraction Data for the cooled melts from the CaF_2 : LnF_3 Systems (Ln=La,Er,Nd)

85 mole% CaF_2 / ErF_3 (annealed for 3 days)

2θ	d spacing (Å)	$I^{(rel)}$	Assignment
28.2	3.164	100	a
32.6	2.747	3	a
46.8	1.941	42	a
55.5	1.656	14	a,c
55.6	1.653	13	a
58.2	1.585	3	c
58.3	1.583	2	c
68.2	1.375	2	a
68.3	1.373	3	a
68.6	1.368	1	a
75.4	1.261	6	c
75.7	1.256	3	a,c
77.7	1.229	1	a
77.9	1.226	1	a
86.8	1.122	4	a
87.1	1.119	2	a
93.6	1.058	3	c
93.7	1.057	4	a,c
94.0	1.054	2	a
105.1	0.971	1	a
105.2	0.970	1	a
112.2	0.929	8	c
112.6	0.927	3	c
114.6	0.916	1	a,?
115.0	0.914	1	a

Table 3.1(c) continued

X-ray Diffraction Data
for the cooled melts from the
CaF_2 : LnF_3 Systems (Ln=La,Er,Nd)

80 mole% CaF_2 / ErF_3

2θ	d spacing (Å)	$I^{(rel)}$	Assignment
28.0	3.187	100	a,c
32.3	2.771	4	a
46.5	1.953	36	a
55.2	1.664	16	c
55.3	1.661	12	c
57.8	1.595	2	c
58.0	1.590	1	c
68.0	1.379	2	c
75.1	1.265	7	c
75.3	1.262	4	c
77.4	1.233	2	c
77.5	1.232	1	c
77.7	1.229	1	a
86.5	1.125	9	a
86.8	1.122	5	a
93.3	1.060	3	c
93.6	1.058	1	c
104.7	0.974	2	c
105.1	0.971	1	a
111.8	0.931	5	c
112.2	0.929	2	c
114.2	0.918	1	-
114.7	0.916	1	a,?

Table 3.1(c) continued

X-ray Diffraction Data for the cooled melts from the CaF_2 : LnF_3 Systems (Ln=La,Er,Nd)

80 mole% CaF_2 / ErF_3 (annealed for 3 days)

2θ	d spacing (Å)	$I^{(rel)}$	Assignment
28.2	3.164	100	a
32.6	2.747	6	a
46.8	1.941	38	a
55.5	1.656	15	a,c
58.2	1.585	4	c
58.4	1.580	2	a
68.2	1.375	2	a
68.4	1.372	1	a
75.4	1.261	6	c
75.6	1.258	3	c
77.6	1.230	1	a,c
77.9	1.226	1	a
86.8	1.122	7	a
87.0	1.120	4	a
93.5	1.058	4	c
93.8	1.056	2	a
104.9	0.972	3	a,c
105.3	0.970	2	a
111.9	0.930	3	c
112.3	0.928	2	c
114.4	0.917	1	-
114.9	0.915	1	a

Table 3.1(c) continued

X-ray Diffraction Data
for the cooled melts from the
CaF_2 : LnF_3 Systems (Ln=La,Er,Nd)

75 mole% CaF_2 / ErF_3

2θ	d spacing (Å)	$I^{(rel)}$	Assignment
28.1	3.175	100	a,c
32.5	2.755	11	a
46.6	1.949	55	a
55.3	1.661	16	c
58.0	1.590	2	c
68.1	1.377	2	a,c
68.3	1.373	1	a
75.2	1.263	9	c
75.4	1.261	5	c
77.4	1.233	1	c
77.7	1.229	1	a
86.6	1.124	6	a
86.9	1.121	4	a
93.0	1.063	1	c
93.2	1.061	2	c
93.5	1.060	1	c
104.4	0.976	1	c
104.6	0.974	1	c
105.0	0.972	1	a
111.7	0.932	2	c
112.1	0.929	1	c
114.1	0.919	1	-
114.6	0.916	1	a,?

Table 3.1(c) continued

X-ray Diffraction Data
for the cooled melts from the
CaF_2 : LnF_3 Systems (Ln=La,Er,Nd)

75 mole% CaF_2 / ErF_3 (annealed for 3 days)

2θ	d spacing (Å)	$I^{(rel)}$	Assignment
28.2	3.164	100	a
29.0	3.079	1	a
32.7	2.739	9	a
46.7	1.945	51	a
55.4	1.658	16	c
55.6	1.653	10	a
68.2	1.375	5	a
68.4	1.372	3	a
75.2	1.263	5	c
75.4	1.261	3	c
77.6	1.230	5	a,c
77.8	1.228	2	a
86.6	1.124	11	a
86.8	1.122	5	a
93.4	1.059	5	c
93.7	1.057	3	a,c
104.6	0.974	2	c
105.0	0.972	1	a
111.7	0.932	4	c
112.2	0.929	2	c
114.2	0.918	2	-
114.6	0.916	1	a,?

Table 3.1(c) continued

X-ray Diffraction Data for the cooled melts from the CaF_2 : LnF_3 Systems (Ln=La,Er,Nd)

70 mole% CaF_2 / ErF_3

2θ	d spacing (Å)	$I^{(rel)}$	Assignment
28.0	3.187	100	a,c
32.4	2.763	11	a
46.5	1.953	40	a
55.2	1.664	14	c
55.3	1.661	15	c
57.9	1.593	7	c
67.9	1.380	3	c
68.1	1.377	1	a,c
75.0	1.266	4	c
75.2	1.263	2	c
77.3	1.234	1	c
77.5	1.232	1	c
86.4	1.126	9	a,?
86.6	1.124	5	a
93.0	1.063	7	c
104.4	0.976	1	c
104.6	0.974	1	c
111.3	0.934	2	c
111.7	0.932	1	c

X-ray Diffraction Data for the cooled melts from the CaF_2 : LnF_3 Systems (Ln=La,Er,Nd)

70 mole% CaF_2 / ErF_3 (annealed for 3 days)

2θ	d spacing (Å)	$I^{(rel)}$	Assignment
28.1	3.175	100	a,c
32.5	2.755	7	a
46.6	1.949	52	a
55.3	1.661	29	c
55.4	1.660	15	c
57.9	1.590	3	c
58.1	1.590	2	c
68.0	1.380	2	c
68.2	1.370	1	a
75.1	1.260	5	c
75.3	1.260	3	c
77.4	1.230	2	c
77.6	1.230	1	a,c
86.4	1.130	6	a,?
86.5	1.120	3	a
93.1	1.060	3	c
93.4	1.060	2	c
104.4	0.980	4	c
104.8	0.970	2	c
111.4	0.930	3	c
111.8	0.930	1	c
113.8	0.920	1	a
114.4	0.920	1	-

X-ray Diffraction Data
for the cooled melts from the
CaF_2 : LnF_3 Systems (Ln=La,Er,Nd)

65 mole% CaF_2 / ErF_3

2θ	d spacing (Å)	$I^{(rel)}$	Assignment
25.8	3.453	2	c
26.2	3.401	1	c
28.0	3.187	100	a,c
29.2	3.058	1	a
29.6	3.018	1	-
32.4	2.763	17	a
46.4	1.957	42	a
55.1	1.667	32	c
55.2	1.664	21	c
57.8	1.595	5	c
57.9	1.593	3	c
67.8	1.382	3	c
68.1	1.377	1	a,c
74.8	1.269	9	c
75.1	1.265	5	c
77.2	1.236	2	c
77.4	1.233	1	c
86.2	1.128	6	-
86.4	1.126	3	a,?
92.9	1.064	3	c
93.2	1.061	2	c
104.1	0.978	3	c
104.5	0.975	1	c
111.2	0.934	3	c
111.6	0.932	1	c
113.6	0.921	2	a
114.1	0.919	1	-

Table 3.1(c) continued

X-ray Diffraction Data
for the cooled melts from the
CaF_2 : LnF_3 Systems (Ln=La,Er,Nd)

65 mole% CaF_2 / ErF_3 (annealed for 3 days)

2θ	d spacing (Å)	$I^{(rel)}$	Assignment
10.7	8.268	2	-
11.7	7.563	2	-
20.2	4.396	2	-
21.4	4.152	2	-
28.0	3.187	100	a,c
32.4	2.763	19	a
46.5	1.953	47	a
55.2	1.664	23	c
57.8	1.595	5	c
57.9	1.593	3	c
67.8	1.382	3	c
68.1	1.377	2	a,c
74.9	1.268	7	c
75.1	1.265	5	c
77.2	1.236	5	c
77.4	1.233	3	c
86.2	1.128	6	-
86.4	1.126	3	a,?
92.8	1.065	3	c
93.1	1.062	2	c
104.1	0.978	1	c
104.5	0.975	1	c
111.2	0.934	3	c
111.6	0.932	2	c
113.6	0.921	2	a
114.0	0.919	1	a,?

Table 3.1(c) continued

X-ray Diffraction Data
for the cooled melts from the
CaF_2 : LnF_3 Systems (Ln=La,Er,Nd)

65 mole% CaF_2 / ErF_3 (annealed for 9 days)

2θ	d spacing (Å)	$I^{(rel)}$	Assignment
11.8	7.500	2	-
12.0	7.375	2	-
21.5	4.133	2	-
22.0	4.040	2	-
28.0	3.187	100	c
32.4	2.763	23	a
44.0	2.058	1	c
46.6	1.949	47	a
55.2	1.664	21	c
57.8	1.595	5	c
58.0	1.590	3	c
67.4	1.389	1	c
67.9	1.380	2	c
68.1	1.377	2	a,?
74.9	1.268	4	c
75.1	1.265	4	c
77.2	1.236	1	c
86.2	1.128	8	-
86.4	1.126	4	-
93.0	1.063	2	c
93.4	1.059	2	c
104.2	0.977	1	c
111.2	0.934	3	c
111.6	0.932	2	c

Table 3.1(c) continued

X-ray Diffraction Data
for the cooled melts from the
CaF_2 : LnF_3 Systems (Ln=La,Er,Nd)

65 mole% CaF_2 / ErF_3 (annealed for 3 weeks)

2θ	d spacing (Å)	$I^{(rel)}$	Assignment
10.7	8.268	1	-
10.9	8.117	2	-
11.2	7.900	2	-
11.5	7.695	3	-
11.8	7.500	4	-
12.4	7.138	1	-
12.6	7.025	1	-
13.5	6.559	1	-
14.1	6.281	1	-
16.2	5.471	1	-
16.4	5.405	1	-
17.2	5.155	1	-
20.0	4.439	4	-
20.4	4.353	3	-
20.6	4.311	2	-
20.8	4.270	2	-
21.0	4.230	2	-
21.4	4.152	4	-
21.6	4.114	4	-
21.8	4.077	4	-
22.0	4.040	2	-
22.3	3.986	1	-
22.5	3.952	1	-
23.2	3.834	1	-
24.2	3.678	1	c
24.9	3.576	1	c
25.2	3.534	1	c,?
25.8	3.453	29	c
26.2	3.401	6	c
28.0	3.187	100	a,c
28.3	3.153	48	a
28.9	3.089	30	a
29.3	3.048	14	a,?
30.6	2.921	1	c
32.4	2.763	23	c
33.3	2.691	4	-
37.1	2.423	1	c
40.7	2.217	3	c
42.6	2.122	1	-
43.5	2.080	2	c
44.2	2.049	2	c
45.4	1.998	1	c
46.4	1.957	40	-

Table 3.1(c) continued

X-ray Diffraction Data
for the cooled melts from the
CaF_2 : LnF_3 Systems (Ln=La,Er,Nd)

65 mole% CaF_2 / ErF_3 (annealed for 3 weeks) continued

2θ	d spacing (Å)	$I^{(rel)}$	Assignment
47.2	1.926	7	a,c
47.6	1.910	8	c
47.8	1.903	7	c
48.0	1.895	5	c
49.8	1.831	1	c
53.0	1.728	7	c
53.6	1.710	2	c
54.0	1.698	2	c,?
55.1	1.667	25	c
56.3	1.634	3	a
56.9	1.618	2	a,?
57.6	1.600	5	c
57.8	1.595	6	c
58.5	1.578	2	a
59.0	1.566	1	a
59.8	1.546	2	c
60.0	1.542	1	c
61.5	1.508	1	c,?
63.6	1.463	1	c
63.9	1.457	1	c
64.9	1.437	1	c,Al
65.8	1.419	1	c
67.8	1.382	3	c
68.2	1.375	1	a
68.4	1.372	1	a
68.6	1.368	1	a
69.9	1.346	1	c
70.2	1.341	1	c
71.3	1.323	1	c
71.5	1.319	1	c
73.2	1.293	1	c
73.4	1.290	1	c
73.5	1.288	1	c
74.0	1.281	1	c
74.8	1.269	7	c
75.8	1.255	2	a
76.0	1.252	2	a
76.3	1.248	2	a,c
77.1	1.237	5	c
77.3	1.234	4	c
84.0	1.152	2	-
86.0	1.130	5	-
86.2	1.128	5	-

Table 3.1(c) continued

X-ray Diffraction Data
for the cooled melts from the
CaF_2 : LnF_3 Systems (Ln=La,Er,Nd)

65 mole% CaF_2 / ErF_3 (annealed for 3 weeks) continued

2θ	d spacing (Å)	$I^{(rel)}$	Assignment
87.0	1.120	2	a
87.3	1.117	2	a
92.6	1.066	4	c
92.8	1.065	4	c
111.0	0.935	2	c

Table 3.1(c) continued

X-ray Diffraction Data
for the cooled melts from the
CaF_2 : LnF_3 Systems (Ln=La,Er,Nd)

60 mole% CaF_2 / ErF_3 (annealed for 3 days)

2θ	d spacing (Å)	$I^{(rel)}$	Assignment
11.8	7.500	3	-
17.4	5.096	1	-
20.1	4.418	3	-
21.5	4.133	3	-
21.9	4.058	2	-
25.3	3.520	1	c,?
25.9	3.440	2	c
26.4	3.376	1	c
27.0	3.302	1	c,?
28.0	3.187	100	a,c
29.5	3.028	2	a,?
30.8	2.903	1	c
32.5	2.755	17	a
33.2	2.698	1	a
43.6	2.076	1	c
44.4	2.040	1	c
46.6	1.949	37	a
55.2	1.664	19	c
57.7	1.598	4	c
57.9	1.593	4	c
67.8	1.382	3	c
68.0	1.379	2	c
74.8	1.269	4	c
75.0	1.266	4	c
77.0	1.238	2	c
77.2	1.236	2	c
77.4	1.233	2	c
86.0	1.130	3	c,?
86.3	1.127	3	-
92.9	1.064	2	c
110.8	0.937	2	c
111.1	0.935	2	c
111.3	0.934	2	c

Table 3.1(c) continued

X-ray Diffraction Data
for the cooled melts from the
CaF_2 : LnF_3 Systems (Ln=La,Er,Nd)

60 mole% CaF_2 / ErF_3 (annealed for 9 days)

2θ	d spacing (Å)	$I^{(rel)}$	Assignment
11.8	7.500	31	-
20.1	4.418	2	-
21.6	4.114	3	-
28.0	3.187	100	a,c
32.5	2.755	14	a
46.6	1.949	42	a
55.2	1.664	21	a,c,?
57.8	1.595	3	a,c,?
67.8	1.382	2	c
74.8	1.269	3	c
75.0	1.266	4	c,?
75.1	1.265	3	a,c,?
77.2	1.236	3	c
77.4	1.233	3	c
86.1	1.129	4	-
86.4	1.126	5	c,?
93.0	1.063	3	c
110.6	0.938	1	c,?
111.1	0.935	2	c
113.4	0.922	2	a

Table 3.1(c) continued

X-ray Diffraction Data
for the cooled melts from the
CaF_2 : LnF_3 Systems (Ln=La,Er,Nd)

60 mole% CaF_2 / ErF_3 (annealed for 3 weeks)

2θ	d spacing (Å)	$I^{(rel)}$	Assignment
11.8	7.500	1	-
14.3	6.194	1	-
16.5	5.372	2	-
20.1	4.418	2	-
21.5	4.133	2	-
23.3	3.802	1	-
26.3	3.389	1	c
28.1	3.175	100	a
28.9	3.089	19	a
32.6	2.747	16	a
33.3	2.691	3	a,?
40.8	2.212	3	-
42.8	2.113	1	c,?
43.6	2.076	1	c
44.2	2.049	1	c
44.6	2.032	1	c,Al
46.6	1.949	37	a,?
47.2	1.926	7	a,c
47.7	1.907	3	c
48.1	1.892	3	c
48.3	1.884	2	c,?
49.9	1.828	1	c
52.9	1.731	1	c
55.3	1.661	20	a,c
56.4	1.631	3	a,?
56.5	1.629	2	a,?
56.9	1.618	2	-
58.0	1.590	4	c
58.5	1.578	2	a
58.6	1.575	2	a
58.7	1.573	2	a
59.8	1.546	1	c
61.6	1.506	2	c,?
63.7	1.461	1	c
65.0	1.435	1	c,Al
68.0	1.379	3	a,c
71.5	1.319	1	c
75.0	1.266	5	c
76.2	1.249	1	a
77.4	1.233	3	c
77.6	1.230	3	a,c
78.2	1.222	2	a,Al
86.4	1.126	5	-

Table 3.1(c) continued

X-ray Diffraction Data
for the cooled melts from the
CaF_2 : LnF_3 Systems (Ln=La,Er,Nd)

60 mole% CaF_2 / ErF_3 (annealed for 3 weeks) continued

2θ	d spacing (Å)	$I^{(rel)}$	Assignment
93.0	1.063	3	c
103.6	0.981	1	c
104.6	0.974	1	c
111.5	0.933	2	c
113.8	0.920	2	a

Table 3.1(c) (continued)

X-ray Diffraction Data
for the cooled melts from the
CaF_2 : LnF_3 Systems (Ln=La,Er,Nd)

55 mole% CaF_2 / ErF_3

2θ	d spacing (Å)	$I^{(rel)}$	Assignment
11.6	7.628	2	-
19.9	4.462	2	-
20.0	4.439	2	-
20.4	4.353	2	-
21.4	4.152	2	-
21.7	4.095	2	-
25.8	3.453	20	c
26.2	3.401	7	c
26.6	3.351	1	c
27.9	3.198	100	c
29.2	3.058	14	a,?
29.6	3.018	10	-
32.4	2.763	21	a
37.0	2.430	1	c
43.4	2.085	1	c
43.6	2.076	1	c
44.2	2.049	1	c
45.9	1.977	2	c
46.4	1.957	38	a
47.6	1.910	5	c
47.9	1.899	4	c
53.0	1.728	2	c
53.4	1.716	1	c
54.1	1.695	2	c
55.0	1.670	27	c
55.6	1.653	3	a
57.5	1.603	2	c
67.5	1.388	2	c
67.6	1.386	2	c
74.8	1.269	7	c
77.0	1.238	3	c
77.2	1.236	2	c
86.0	1.130	3	c,?
86.2	1.128	2	-
92.6	1.066	3	c
92.7	1.065	3	c
93.0	1.063	2	c
103.8	0.980	1	c
104.0	0.978	1	c
111.0	0.935	2	c
111.4	0.933	1	c
113.3	0.923	1	a
113.6	0.921	1	a

Table 3.1(c) continued

X-ray Diffraction Data
for the cooled melts from the
CaF_2 : LnF_3 Systems (Ln=La,Er,Nd)

55 mole% CaF_2 / ErF_3 (annealed for 3 days)

2θ	d spacing (Å)	$I^{(rel)}$	Assignment
11.6	7.628	3	-
19.9	4.462	2	-
20.4	4.353	2	-
21.4	4.152	3	-
21.7	4.095	2	-
25.8	3.453	18	c
26.2	3.401	5	c
27.9	3.198	100	c
29.2	3.058	15	a,?
29.6	3.018	9	-
32.4	2.763	21	a
37.0	2.430	2	c
46.5	1.953	50	a
47.7	1.907	6	c
53.0	1.728	2	c
53.5	1.713	1	c
54.0	1.698	2	c
55.1	1.667	18	c
55.7	1.650	2	a
57.7	1.598	4	c
67.7	1.384	2	c
74.8	1.269	5	c
77.2	1.236	2	c
86.1	1.129	4	-
86.3	1.127	4	-
92.8	1.065	3	c
111.1	0.935	2	c

Table 3.1(c) continued

X-ray Diffraction Data
for the cooled melts from the
CaF_2 : LnF_3 Systems (Ln=La,Er,Nd)

55 mole% CaF_2 / ErF_3 (annealed for 9 days)

2θ	d spacing (Å)	$I^{(rel)}$	Assignment
11.0	8.043	1	-
11.3	7.830	1	-
11.5	7.695	2	-
11.7	7.563	3	-
11.9	7.437	4	-
20.2	4.396	2	-
20.6	4.311	2	-
21.8	4.077	4	-
26.0	3.427	14	c
26.4	3.376	6	c
28.2	3.164	100	a
29.5	3.028	18	-
32.6	2.747	18	a
33.7	2.659	1	a,?
37.3	2.411	2	c
37.5	2.398	2	c
46.6	1.949	3	a
47.9	1.899	6	c
48.0	1.895	8	c
53.2	1.722	2	c
53.3	1.719	2	c
53.7	1.707	2	c
54.2	1.692	3	c,?
54.3	1.689	4	-
55.3	1.661	19	c
56.0	1.642	3	a
56.2	1.637	2	a
57.8	1.595	5	c
58.0	1.590	4	c
60.2	1.537	1	c
60.4	1.533	1	c
67.9	1.380	5	c
68.1	1.377	4	a,c,?
68.9	1.363	1	a
73.0	1.296	1	c,?
73.2	1.293	1	c,?
73.3	1.291	1	c
73.4	1.290	1	c
73.6	1.287	1	c
74.9	1.268	4	c
75.1	1.265	4	c
77.3	1.234	2	c
86.2	1.128	5	-

Table 3.1(c) continued

X-ray Diffraction Data
for the cooled melts from the
CaF_2 : LnF_3 Systems (Ln=La,Er,Nd)

55 mole% CaF_2 / ErF_3 (annealed for 9 days) continued

2θ	d spacing (Å)	$I^{(rel)}$	Assignment
86.4	1.126	4	-
92.8	1.065	3	c
93.0	1.063	3	c
93.1	1.062	3	c
103.7	0.980	1	c
104.0	0.978	1	c
104.2	0.977	1	c
111.1	0.935	2	c
111.2	0.934	2	c

Table 3.1(c) continued

X-ray Diffraction Data
for the cooled melts from the
CaF_2 : LnF_3 Systems (Ln=La,Er,Nd)

55 mole% CaF_2 / ErF_3 (annealed for 3 weeks)

2θ	d spacing (Å)	$I^{(rel)}$	Assignment
14.2	6.237	2	-
16.4	5.405	2	-
22.0	4.040	1	-
23.2	3.834	1	-
28.2	3.164	100	a
28.9	3.089	67	a
29.3	3.048	6	-
32.2	2.780	2	a
32.6	2.750	17	a
33.4	2.680	16	a,?
34.0	2.640	1	c,?
34.3	2.610	1	c
36.4	2.470	2	c
36.8	2.440	1	c,?
40.8	2.210	5	-
41.4	2.180	1	c
41.5	2.180	1	c
41.8	2.160	1	c
43.3	2.090	2	c
43.5	2.082	2	c
46.8	1.940	52	a,c
47.6	1.910	12	c
48.2	1.890	12	c
48.7	1.870	1	c,?
49.0	1.860	1	c
49.9	1.830	1	c
50.8	1.800	1	c,?
51.3	1.780	1	c
52.7	1.740	1	c
53.0	1.730	1	c
55.6	1.650	23	a
56.4	1.631	6	a,?
56.9	1.618	8	-
58.2	1.585	2	c
58.3	1.583	2	a,c
58.5	1.578	3	a
58.9	1.568	2	a
59.1	1.563	1	a,c
59.8	1.546	4	c
60.6	1.528	1	c
61.2	1.514	1	c
61.6	1.506	2	c
61.8	1.501	1	c

Table 3.1(c) continued

X-ray Diffraction Data
for the cooled melts from the
CaF_2 : LnF_3 Systems (Ln=La,Er,Nd)

55 mole% CaF_2 / ErF_3 (annealed for 3 weeks) continued

2θ	d spacing (Å)	$I^{(rel)}$	Assignment
63.7	1.461	1	c
63.8	1.459	1	c
64.7	1.441	1	c
64.8	1.439	1	c
64.9	1.437	1	c
65.1	1.433	1	c,Al
66.8	1.400	1	c
68.3	1.373	1	a
68.4	1.372	3	a
68.7	1.366	2	a
70.0	1.344	3	c
71.1	1.326	1	c
71.4	1.321	2	c
71.6	1.318	1	c
74.3	1.277	1	c
74.5	1.274	1	c
75.4	1.261	5	c
75.6	1.258	4	c
75.9	1.254	3	a
76.0	1.252	2	a
76.6	1.244	1	a,c
77.2	1.236	2	c
77.7	1.229	4	a,Al
78.2	1.222	2	a,Al
79.0	1.212	1	a,Al
79.3	1.208	1	c
80.0	1.199	2	c
80.1	1.198	1	c
86.8	1.122	4	a,?
87.0	1.120	5	a
87.1	1.119	4	a
89.3	1.097	2	c,?
89.6	1.094	2	c
92.5	1.067	1	c,?
93.5	1.058	3	c
93.8	1.056	2	a
94.0	1.054	2	a
94.3	1.052	1	a
94.4	1.051	2	a
94.8	1.047	1	c
96.7	1.032	2	c
96.9	1.030	1	c
98.7	1.016	1	Al

Table 3.1(c) continued

X-ray Diffraction Data
for the cooled melts from the
CaF_2 : LnF_3 Systems (Ln=La,Er,Nd)

55 mole% CaF_2 / ErF_3 (annealed for 3 weeks) continued

2θ	d spacing (Å)	$I^{(rel)}$	Assignment
98.9	1.015	1	Al
99.1	1.013	1	Al
99.5	1.010	1	Al
99.8	1.008	1	Al,?
100.0	1.006	1	c,?
100.2	1.005	1	c,?
100.3	1.004	1	c
100.7	1.001	1	c
105.0	0.972	2	a,?
105.1	0.971	2	a,?
105.4	0.969	2	a
105.7	0.967	1	a
106.0	0.965	1	a
106.3	0.963	1	a,?
112.1	0.929	3	c,?
112.6	0.927	2	c
112.8	0.926	1	c
113.1	0.924	1	a
114.4	0.917	1	-
114.6	0.916	1	-
114.8	0.915	2	a,?
115.2	0.913	1	a
116.6	0.906	1	-
116.8	0.905	1	-
117.0	0.904	1	-
117.1	0.904	1	-

Table 3.1(c) continued

X-ray Diffraction Data
for the cooled melts from the
CaF_2 : LnF_3 Systems (Ln=La,Er,Nd)

50 mole% CaF_2 / ErF_3

2θ	d spacing (Å)	$I^{(rel)}$	Assignment
11.8	7.500	5	-
20.1	4.418	4	-
20.5	4.332	4	-
21.5	4.133	4	-
21.9	4.058	4	-
22.0	4.040	4	-
25.9	3.440	51	c
26.3	3.389	25	c
26.8	3.326	4	c
28.1	3.175	100	a,c
28.8	3.100	2	a
29.4	3.038	50	-
29.8	2.998	31	-
32.5	2.755	30	a
37.2	2.417	6	c
42.6	2.122	2	c,?
43.7	2.071	3	c
46.0	1.973	11	c
46.6	1.949	62	c
46.9	1.937	19	a
47.8	1.903	17	c
48.0	1.895	13	c
48.8	1.866	3	c
53.1	1.725	8	c
53.5	1.713	5	c
54.3	1.689	7	c
55.2	1.664	43	c
55.7	1.650	8	a
56.8	1.621	2	a,?
57.8	1.595	4	c
60.2	1.537	1	c
67.8	1.382	5	c
68.0	1.379	5	c
68.7	1.366	1	a
73.4	1.290	2	c
74.0	1.281	2	c
74.2	1.278	3	c
74.9	1.268	10	c
75.0	1.266	8	c
77.2	1.236	2	c
84.0	1.152	1	c,?
86.2	1.128	6	-
92.8	1.065	4	c
93.2	1.061	2	c
104.0	0.978	2	c
109.1	0.946	6	c

Table 3.1(c) continued

X-ray Diffraction Data
for the cooled melts from the
CaF_2 : LnF_3 Systems (Ln=La,Er,Nd)

50 mole% CaF_2 / ErF_3 (annealed for 3 days)

2θ	d spacing (Å)	$I^{(rel)}$	Assignment
11.8	7.500	3	-
20.4	4.353	2	-
21.5	4.133	2	-
25.8	3.453	42	c
26.2	3.401	18	c
28.0	3.187	100	a,c
28.6	3.121	2	a
29.3	3.048	40	a,?
29.6	3.018	22	-
32.4	2.763	27	a
37.1	2.423	3	c
40.8	2.212	2	c
42.4	2.132	2	-
43.5	2.080	4	c
46.1	1.969	7	c
46.5	1.953	58	a
47.6	1.910	14	c
47.8	1.903	16	c
47.9	1.899	15	c
52.4	1.746	1	c
52.7	1.737	2	c
53.1	1.725	6	c
53.6	1.710	5	c
54.1	1.695	8	c
55.1	1.667	30	c
55.7	1.650	6	a
56.4	1.631	3	a
57.8	1.595	4	c
60.1	1.539	2	c
67.7	1.384	3	c
68.7	1.366	2	a
72.8	1.299	2	c
73.2	1.293	3	c
74.2	1.278	3	c
74.9	1.268	6	c
77.2	1.236	2	-
86.2	1.128	4	c
92.8	1.065	3	c
111.0	0.935	6	

Table 3.1(c) continued

X-ray Diffraction Data for the cooled melts from the CaF_2 : LnF_3 Systems (Ln=La,Er,Nd)

The CaF_2 / NdF_3 System:

95 mole% CaF_2 / NdF_3

2θ	d spacing (Å)	$I^{(rel)}$	Assignment
28.1	3.175	100	a,d
32.6	2.747	1	a
44.6	2.032	2	d,Al
46.8	1.941	29	a
55.5	1.656	6	a
55.6	1.653	3	a
58.2	1.585	1	a,d
58.4	1.580	1	a,d
68.3	1.373	1	a
68.5	1.370	1	a
75.4	1.261	4	a,d
75.7	1.256	2	a,d
86.9	1.121	5	a
87.2	1.118	3	a
93.5	1.058	4	a
94.0	1.054	2	a
105.1	0.971	5	a,d,?
105.5	0.968	3	a,d
112.3	0.928	2	a
112.7	0.926	1	a
114.7	0.916	1	a,?
115.2	0.913	1	a

Table 3.1(d)

X-ray Diffraction Data for the cooled melts from the CaF_2 : LnF_3 Systems (Ln=La,Er,Nd)

95 mole% CaF_2 / NdF_3 (annealed for 3 days)

2θ	d spacing (Å)	$I^{(rel)}$	Assignment
28.2	3.164	100	a,d
31.3	2.858	1	-
32.6	2.747	1	a
36.3	2.475	1	d
44.6	2.032	1	d,Al
46.8	1.941	40	a
55.5	1.656	13	a
55.7	1.650	7	a
58.2	1.585	1	a,d
58.4	1.580	1	a,d
68.3	1.373	2	a
68.5	1.370	1	a
75.4	1.261	4	a,d
75.7	1.256	2	a,d
86.9	1.121	5	a
87.2	1.118	3	a
93.7	1.057	2	a
94.0	1.054	1	a
105.1	0.971	2	a,d
105.5	0.968	1	a,d
112.3	0.928	3	a
112.7	0.926	1	a

Table 3.1(d) continued

X-ray Diffraction Data
for the cooled melts from the
CaF_2 : LnF_3 Systems (Ln=La,Er,Nd)

90 mole% CaF_2 / NdF_3

2θ	d spacing (Å)	$I^{(rel)}$	Assignment
28.0	3.187	100	a,d
32.4	2.763	1	a
44.6	2.032	1	d,Al
46.5	1.953	54	a
55.2	1.664	14	a
55.4	1.658	8	a
57.9	1.593	1	a,d
58.1	1.588	1	a,d
68.0	1.379	3	a
68.2	1.375	2	a
75.1	1.265	3	a,d
75.3	1.262	2	a,d
86.4	1.126	4	d
86.7	1.123	2	a
93.1	1.062	3	d
93.5	1.058	1	a
104.5	0.975	1	d
104.9	0.972	1	d
111.6	0.932	2	-
112.0	0.930	1	a,?
114.0	0.919	1	a,?
114.5	0.917	1	-

Table 3.1(d) continued

X-ray Diffraction Data
for the cooled melts from the
CaF_2 : LnF_3 Systems (Ln=La,Er,Nd)

90 mole% CaF_2 / NdF_3 (annealed for 3 days)

2θ	d spacing (Å)	$I^{(rel)}$	Assignment
28.1	3.175	100	a,d
32.5	2.755	2	a
44.6	2.032	1	d,Al
46.6	1.949	50	a
55.3	1.661	7	a
55.4	1.658	5	a
56.0	1.642	1	a
56.2	1.637	1	a
68.0	1.379	1	a
68.2	1.375	1	a
75.1	1.265	3	a,d
75.4	1.261	2	a,d
86.5	1.125	4	a,d
86.7	1.123	2	a
93.2	1.061	3	d
93.5	1.058	1	a
104.6	0.974	1	d
105.0	0.972	1	d
111.6	0.932	1	-
112.0	0.930	1	a,?
114.0	0.919	1	a,?

Table 3.1(d) continued

X-ray Diffraction Data
for the cooled melts from the
CaF_2 : LnF_3 Systems (Ln=La,Er,Nd)

85 mole% CaF_2 / NdF_3

2θ	d spacing (Å)	$I^{(rel)}$	Assignment
28.2	3.164	100	a
32.6	2.747	1	a
46.6	1.949	15	a
55.2	1.664	6	a
55.4	1.658	3	a
57.9	1.593	2	d
58.1	1.588	1	a,d
68.0	1.379	1	a
68.1	1.377	1	a
75.0	1.266	3	a,d
75.2	1.263	2	a,d
86.0	1.130	2	d
86.3	1.127	3	d
86.6	1.124	2	a,?
92.9	1.064	1	d
93.2	1.061	1	d
93.3	1.060	1	d
104.1	0.978	1	d
111.0	0.935	2	-
111.2	0.934	3	-
111.6	0.932	1	-
115.6	0.911	1	a

Table 3.1(d) continued

X-ray Diffraction Data
for the cooled melts from the
CaF_2 : LnF_3 Systems (Ln=La,Er,Nd)

85 mole% CaF_2 / NdF_3 (annealed for 3 days)

2θ	d spacing (Å)	$I^{(rel)}$	Assignment
27.9	3.198	100	a,d
32.4	2.763	2	a
44.6	2.032	1	d,Al
46.4	1.957	38	a,d
55.1	1.667	7	a
57.7	1.598	2	d
67.8	1.382	1	a,?
68.0	1.379	1	a
74.8	1.269	4	a,d,?
74.9	1.268	7	a,d,?
75.1	1.265	4	a,d
77.1	1.237	1	d
77.3	1.234	1	d
86.0	1.130	4	d
86.3	1.127	3	d
92.7	1.065	5	d
93.0	1.063	2	d
104.1	0.978	1	d
110.6	0.938	1	-
111.1	0.935	4	-
111.5	0.933	2	-
113.5	0.922	1	a

Table 3.1(d) continued

X-ray Diffraction Data
for the cooled melts from the
CaF_2 : LnF_3 Systems (Ln=La,Er,Nd)

85 mole% CaF_2 / NdF_3 (annealed for 9 days)

2θ	d spacing (Å)	$I^{(rel)}$	Assignment
28.2	3.164	100	a,d
32.6	2.747	2	a
44.7	2.027	1	d,Al
46.7	1.945	20	a
55.3	1.661	7	a
55.4	1.658	4	a
58.0	1.590	2	a,d
58.2	1.585	1	a,d
65.1	1.433	2	d,Al
65.2	1.431	1	d,Al
68.0	1.379	1	a
75.0	1.266	6	a,d
75.2	1.263	3	a,d
77.3	1.234	1	a,d,Al
77.5	1.232	1	a,d,Al
78.2	1.222	1	a,Al
78.4	1.220	1	a,Al
86.3	1.127	16	d
86.6	1.124	8	d
92.9	1.064	2	d
93.2	1.061	1	d
104.2	0.977	1	d
104.5	0.975	1	d
111.1	0.935	3	-
111.6	0.932	2	-
113.5	0.922	1	a

Table 3.1(d) continued

X-ray Diffraction Data
for the cooled melts from the
CaF_2 : LnF_3 Systems (Ln=La,Er,Nd)

85 mole% CaF_2 / NdF_3 (annealed for 3 weeks)

2θ	d spacing (Å)	$I^{(rel)}$	Assignment
28.0	3.187	100	a,d
32.4	2.763	5	a
38.2	2.356	1	Al
44.5	2.036	2	d,Al
46.5	1.953	58	a
55.1	1.667	22	a
57.7	1.598	3	d
57.9	1.593	4	d
64.9	1.437	3	d,?
65.0	1.435	2	d
65.1	1.433	1	d
67.8	1.382	4	a,?
68.0	1.379	3	a
74.8	1.269	6	d,?
75.0	1.266	4	d
77.1	1.237	3	d
77.3	1.234	2	d
78.0	1.225	2	a,Al
78.3	1.221	1	a,Al
86.2	1.128	12	d
86.4	1.126	6	d
92.8	1.065	11	d
93.1	1.062	5	d
104.1	0.978	5	d
104.4	0.976	3	d
111.0	0.935	2	-
111.4	0.933	2	-
113.4	0.922	2	a
113.9	0.920	1	a

Table 3.1(d) continued

X-ray Diffraction Data
for the cooled melts from the
CaF_2 : LnF_3 Systems (Ln=La,Er,Nd)

80 mole% CaF_2 / NdF_3

2θ	d spacing (Å)	$I^{(rel)}$	Assignment
27.9	3.198	100	a,d
32.3	2.771	3	a
32.4	2.763	2	a
44.6	2.032	2	d,Al
46.3	1.961	19	a,Al
54.9	1.672	11	a,?
57.5	1.603	2	d
57.7	1.598	1	d
67.5	1.388	2	-
67.7	1.384	1	a,?
74.4	1.275	2	-
74.6	1.272	3	-
74.8	1.269	2	a,d,?
76.9	1.240	1	d
85.6	1.135	4	d
85.8	1.132	7	d
86.1	1.129	3	d
92.2	1.070	1	d
92.4	1.068	2	d
92.8	1.065	1	d
103.6	0.981	1	d
104.0	0.978	1	d
110.4	0.939	2	-
110.6	0.938	2	-
111.0	0.935	1	-
113.0	0.924	1	a

Table 3.1(d) (continued)

X-ray Diffraction Data
for the cooled melts from the
CaF_2 : LnF_3 Systems (Ln=La,Er,Nd)

80 mole% CaF_2 / NdF_3 (annealed for 3 days)

2θ	d spacing (Å)	$I^{(rel)}$	Assignment
27.8	3.209	100	a,d
32.2	2.780	14	a
44.6	2.032	2	a,Al
46.2	1.965	60	d
54.8	1.675	42	a,d,?
54.9	1.672	22	a,?
57.4	1.605	6	d
57.6	1.600	5	d
67.4	1.389	11	-
67.6	1.386	6	-
74.4	1.275	9	-
74.5	1.274	12	-
74.7	1.271	5	-
76.7	1.242	4	d
77.0	1.238	3	d
85.6	1.135	8	d
85.7	1.134	7	d
85.9	1.131	5	d
92.3	1.069	10	d
92.6	1.066	6	d
103.4	0.982	3	d
103.8	0.980	2	d
110.4	0.939	11	-
110.8	0.937	6	-
112.7	0.926	2	a
113.1	0.924	1	a

Table 3.1(d) continued

X-ray Diffraction Data
for the cooled melts from the
CaF_2 : LnF_3 Systems (Ln=La,Er,Nd)

75 mole% CaF_2 / NdF_3

2θ	d spacing (Å)	$I^{(rel)}$	Assignment
27.7	3.220	100	a,d
32.1	2.788	3	a
44.6	2.032	1	d,Al
46.0	1.973	26	d
54.6	1.681	10	d
57.1	1.613	2	d
57.3	1.608	3	d
67.1	1.395	1	d,?
67.2	1.393	1	d,?
74.1	1.279	2	-
74.2	1.278	2	-
76.4	1.247	1	d
76.6	1.244	1	d
85.4	1.137	5	d
91.8	1.073	1	d
92.1	1.071	1	d
102.6	0.988	1	d
102.7	0.987	1	d
102.9	0.986	1	d
103.1	0.984	1	d
109.8	0.942	1	-

Table 3.1(d) continued

X-ray Diffraction Data
for the cooled melts from the
CaF_2 : LnF_3 Systems (Ln=La,Er,Nd)

75 mole% CaF_2 / NdF_3 (annealed for 3 days)

2θ	d spacing (Å)	$I^{(rel)}$	Assignment
27.8	3.209	100	a,d
32.2	2.780	4	a
44.6	2.032	3	d,Al
46.1	1.969	27	d
54.6	1.681	10	d
57.2	1.610	4	d
57.4	1.605	2	d
67.2	1.393	3	-
67.4	1.389	1	-
74.2	1.278	4	-
74.4	1.275	2	-
76.4	1.247	1	d
76.6	1.244	1	d
85.3	1.138	4	d
85.5	1.136	2	d
91.9	1.073	6	d
92.2	1.070	3	d
103.0	0.985	2	d
103.3	0.983	1	d
103.4	0.982	1	d
109.8	0.942	1	-
110.2	0.940	1	-
112.1	0.929	4	-
112.5	0.927	2	-

Table 3.1(d) continued

X-ray Diffraction Data
for the cooled melts from the
CaF_2 : LnF_3 Systems (Ln=La,Er,Nd)

75 mole% CaF_2 / NdF_3 (annealed for 9 days)

2θ	d spacing (Å)	$I^{(rel)}$	Assignment
28.0	3.187	100	a,d
29.4	3.038	2	-
30.6	2.921	2	-
32.4	2.763	7	a
46.2	1.965	41	d
54.8	1.675	26	a,d,?
54.9	1.672	17	a
57.4	1.605	4	d
57.6	1.600	3	d
67.3	1.391	3	-
67.5	1.388	2	-
74.4	1.275	31	-
74.6	1.272	16	-
76.6	1.244	1	d
85.4	1.137	9	d
85.7	1.134	5	d
92.0	1.072	4	d
92.3	1.069	3	d
103.1	0.984	3	d
103.5	0.982	2	d
109.9	0.942	8	-
110.3	0.939	4	-
112.3	0.928	2	a
112.7	0.926	1	a

Table 3.1(d) continued

X-ray Diffraction Data for the cooled melts from the CaF_2 : LnF_3 Systems (Ln=La,Er,Nd)

75 mole% CaF_2 / NdF_3 (annealed for 3 weeks)

2θ	d spacing (Å)	$I^{(rel)}$	Assignment
27.9	3.198	100	a,d
32.2	2.780	8	a
46.2	1.965	48	d
54.7	1.678	39	d
57.3	1.608	5	d
57.5	1.603	3	d
67.2	1.393	4	-
67.4	1.389	3	-
74.2	1.278	9	-
74.4	1.275	6	-
76.5	1.245	2	d
76.7	1.242	1	d
85.4	1.137	11	d
85.6	1.135	5	d
92.0	1.072	5	d
92.1	1.071	4	d
103.0	0.985	2	d
103.4	0.982	1	d
109.8	0.942	8	-
110.2	0.940	4	-
112.2	0.929	3	a
112.6	0.927	2	a

Table 3.1(d) continued

X-ray Diffraction Data
for the cooled melts from the
CaF_2 : LnF_3 Systems (Ln=La,Er,Nd)

70 mole% CaF_2 / NdF_3

2θ	d spacing (Å)	$I^{(rel)}$	Assignment
27.6	3.232	100	a,d
32.0	2.797	7	a
44.7	2.027	2	d,Al
45.9	1.977	35	d
46.0	1.973	37	d
54.4	1.687	9	d
57.0	1.616	6	d
57.2	1.610	4	d
67.0	1.397	2	d
73.7	1.285	3	-
73.8	1.284	4	-
76.0	1.252	1	d
76.2	1.249	1	d
84.8	1.143	4	d
85.0	1.141	4	d
85.1	1.140	4	d
91.5	1.076	6	d,?
102.6	0.988	1	d
108.9	0.948	1	-
109.2	0.946	2	-
111.4	0.933	1	-

Table 3.1(d) continued

X-ray Diffraction Data for the cooled melts from the CaF_2 : LnF_3 Systems (Ln=La,Er,Nd)

70 mole% CaF_2 / NdF_3 (annealed for 3 days)

2θ	d spacing (Å)	$I^{(rel)}$	Assignment
27.8	3.209	100	a,d
32.2	2.780	10	a
44.6	2.032	1	a,Al
45.5	1.993	2	d
46.0	1.973	72	d
54.5	1.684	24	d
57.2	1.610	6	d
57.3	1.608	4	d
67.0	1.397	3	d,?
67.2	1.393	2	?
73.0	1.296	10	d
73.2	1.293	5	d
76.2	1.249	3	d
76.4	1.247	2	d
85.1	1.140	14	d
85.3	1.138	6	d
91.6	1.075	6	d
91.9	1.073	3	d
102.5	0.989	3	d
102.6	0.988	3	d
102.9	0.986	2	d
103.0	0.985	2	d
109.3	0.945	6	-
109.4	0.945	6	-
109.7	0.943	3	-
111.6	0.932	4	-
112.0	0.930	2	a,?

Table 3.1(d) continued

X-ray Diffraction Data
for the cooled melts from the
CaF_2 : LnF_3 Systems (Ln=La,Er,Nd)

65 mole% CaF_2 / NdF_3

2θ	d spacing (Å)	$I^{(rel)}$	Assignment
27.7	3.220	100	a,d
32.0	2.797	13	a
44.6	2.032	2	d,Al
45.9	1.977	39	d
54.3	1.689	14	d
57.0	1.616	4	d
66.6	1.404	2	d
66.8	1.400	3	d
73.6	1.287	6	-
73.8	1.284	7	-
75.9	1.254	2	d
76.1	1.251	2	a
84.6	1.145	3	d,?
84.8	1.143	3	d
91.2	1.079	4	-
91.6	1.075	1	d
101.7	0.994	2	d
101.9	0.993	2	d
102.2	0.991	2	d
108.5	0.950	2	-
108.7	0.949	2	-
108.9	0.948	2	-
109.3	0.945	1	-
111.1	0.935	2	-

Table 3.1(d) continued

X-ray Diffraction Data
for the cooled melts from the
CaF_2 : LnF_3 Systems (Ln=La,Er,Nd)

65 mole% CaF_2 / NdF_3 (annealed for 3 days)

2θ	d spacing (Å)	$I^{(rel)}$	Assignment
24.3	3.663	1	d
27.5	3.243	100	a,d
31.9	2.805	9	a
44.6	2.032	1	d,Al
45.8	1.981	70	d
54.2	1.692	25	d
54.3	1.689	13	d
56.8	1.621	10	d
56.9	1.618	5	d
66.6	1.404	3	d
66.8	1.400	2	d
73.6	1.287	21	-
73.8	1.284	10	-
75.8	1.255	4	d,?
76.0	1.252	2	a,d
84.6	1.145	11	d,?
84.8	1.143	6	d
93.0	1.063	6	d
93.3	1.060	4	d
103.9	0.979	3	d
104.2	0.977	2	d
110.7	0.937	10	-
111.1	0.935	6	-
112.9	0.925	7	a
113.4	0.922	4	a

Table 3.1(d) continued

X-ray Diffraction Data
for the cooled melts from the
CaF_2 : LnF_3 Systems (Ln=La,Er,Nd)

65 mole% CaF_2 / NdF_3 (annealed for 9 days)

2θ	d spacing (Å)	$I^{(rel)}$	Assignment
27.8	3.209	100	a,d
28.6	3.121	3	a,d
32.2	2.780	15	a
45.8	1.981	12	d
46.1	1.969	48	d
54.2	1.692	4	d
54.6	1.681	22	d
54.7	1.678	15	d
57.1	1.613	3	d
67.0	1.397	6	d
67.2	1.393	3	d
73.5	1.288	7	d,?
73.7	1.285	4	-
73.9	1.282	9	-
74.2	1.278	6	-
75.8	1.255	1	a,d
76.1	1.251	4	a,d
76.4	1.247	3	a,d
85.0	1.141	7	d
85.2	1.139	4	d
90.9	1.082	2	-
91.2	1.079	1	-
91.3	1.078	2	d,?
91.5	1.076	3	d
91.6	1.075	2	d
91.8	1.073	1	d
102.4	0.989	1	d
108.4	0.950	1	-
109.2	0.946	4	-
109.6	0.943	2	-
111.4	0.933	17	-
111.9	0.930	9	-

Table 3.1(d) continued

X-ray Diffraction Data
for the cooled melts from the
CaF_2 : LnF_3 Systems (Ln=La,Er,Nd)

65 mole% CaF_2 / NdF_3 (annealed for 3 weeks)

2θ	d spacing (Å)	$I^{(rel)}$	Assignment
27.8	3.209	100	a,d
28.5	3.132	5	a,d
32.1	2.788	14	a
46.0	1.973	45	d
54.5	1.684	18	d
54.6	1.681	19	d
56.8	1.621	3	d
57.1	1.613	4	d
65.1	1.433	1	d
67.0	1.397	4	d,?
67.2	1.393	3	-
73.8	1.284	16	-
74.0	1.281	10	-
75.7	1.256	2	a,d
76.2	1.249	4	a,d
76.4	1.247	3	a,d
84.9	1.142	6	d
85.2	1.139	5	d
90.9	1.082	2	-
91.2	1.079	3	-
91.4	1.077	4	d
91.6	1.075	3	d
91.9	1.073	2	d
101.8	0.993	3	d
102.1	0.991	1	d
102.3	0.990	2	d
102.6	0.988	1	d
108.4	0.950	1	-
109.1	0.946	4	-
109.5	0.944	5	-
110.0	0.941	3	-

Table 3.1(d) continued

X-ray Diffraction Data
for the cooled melts from the
CaF_2 : LnF_3 Systems (Ln=La,Er,Nd)

60 mole% CaF_2 / NdF_3

2θ	d spacing (Å)	$I^{(rel)}$	Assignment
24.7	3.604	2	d
25.5	3.493	1	d
27.1	3.290	2	-
27.4	3.255	100	a,d
28.4	3.143	4	a,d
31.8	2.814	10	a,?
44.6	2.032	3	d,Al
44.7	2.027	2	d,Al
45.0	2.014	3	d
45.6	1.989	73	d
52.1	1.755	1	d
54.1	1.695	23	d
56.6	1.626	6	a,d
56.8	1.621	7	d
66.4	1.408	4	d
66.6	1.404	2	d
73.3	1.291	9	d
73.5	1.288	7	d,?
75.5	1.259	4	d
75.7	1.256	4	a,d
75.9	1.254	1	d,?
84.3	1.149	7	d,?
84.5	1.147	5	d,?
90.8	1.083	4	-
108.2	0.952	6	-
108.6	0.949	4	-
110.5	0.938	4	-
110.6	0.938	3	-
111.0	0.935	2	-

Table 3.1(d) continued

X-ray Diffraction Data
for the cooled melts from the
CaF_2 : LnF_3 Systems (Ln=La,Er,Nd)

60 mole% CaF_2 / NdF_3 (annealed for 3 days)

2θ	d spacing (Å)	$I^{(rel)}$	Assignment
24.8	3.590	3	d
25.5	3.493	1	d
27.6	3.232	100	a,d
28.4	3.143	4	d
31.9	2.805	13	a
45.0	2.014	2	d
45.6	1.989	44	d
52.0	1.759	1	d
54.1	1.695	25	d
56.3	1.634	1	a
56.7	1.623	9	a,d
56.9	1.618	5	d
66.5	1.406	4	d
66.7	1.402	2	d
66.9	1.399	1	a,d
72.8	1.299	1	d
73.1	1.294	1	d
73.4	1.290	16	d
73.6	1.287	8	d,?
75.6	1.258	4	a,d
75.9	1.254	3	a,d
77.1	1.237	1	d
84.3	1.149	5	d
84.6	1.145	4	d
90.8	1.083	5	-
91.1	1.080	3	-
101.6	0.995	4	d
102.0	0.992	2	d
108.3	0.951	6	-
108.7	0.949	3	-
110.6	0.938	2	-
111.0	0.935	1	-

Table 3.1(d) continued

X-ray Diffraction Data
for the cooled melts from the
CaF_2 : LnF_3 Systems (Ln=La,Er,Nd)

55 mole% CaF_2 / NdF_3

2θ	d spacing (Å)	$I^{(rel)}$	Assignment
25.0	3.562	7	d
25.8	3.453	4	d
27.7	3.220	100	a,d
28.7	3.110	11	d
32.0	2.797	13	a
45.3	2.002	6	d,Al
45.8	1.981	65	d
46.2	1.965	7	d
52.3	1.749	3	d
54.2	1.692	32	d
56.8	1.621	6	a,d
56.9	1.618	4	d
66.5	1.406	3	d
73.4	1.290	10	d,?
73.6	1.287	6	?
75.6	1.258	4	a,d
75.8	1.255	3	a,d
84.3	1.149	9	d,?
84.6	1.145	5	d,?
90.7	1.084	5	-
91.0	1.081	4	-
101.5	0.995	4	d
101.8	0.993	3	d
108.1	0.952	6	-
108.5	0.950	4	-
108.7	0.949	1	-
110.4	0.939	3	-
110.8	0.937	2	-
119.8	0.891	4	-

Table 3.1(d) continued

X-ray Diffraction Data
for the cooled melts from the
CaF_2 : LnF_3 Systems (Ln=La,Er,Nd)

55 mole% CaF_2 / NdF_3 (annealed for 3 days)

2θ	d spacing (Å)	$I^{(rel)}$	Assignment
25.0	3.562	12	d
25.7	3.466	7	d
27.7	3.220	100	a,d
28.6	3.121	23	a,d
32.1	2.788	16	a
36.0	2.495	2	d
45.1	2.010	7	d,Al
45.3	2.002	5	d
45.8	1.981	71	d
46.2	1.965	14	d
51.0	1.791	3	d
52.2	1.752	6	d
52.3	1.749	4	d
54.3	1.689	38	d
54.5	1.684	25	d
56.9	1.618	7	d
57.1	1.613	4	d
66.4	1.408	3	d
66.5	1.406	3	d
66.7	1.402	5	d
66.9	1.399	4	d
70.3	1.339	2	d
70.5	1.336	1	d
71.0	1.328	1	d
71.2	1.324	1	d
73.0	1.296	3	d
73.2	1.293	2	d
73.6	1.287	11	-
73.8	1.284	7	-
75.7	1.256	5	a,d
76.0	1.252	4	a,d
84.6	1.145	12	d,?
84.8	1.143	7	d
90.9	1.082	9	-
91.2	1.079	4	-
101.8	0.993	6	d
102.1	0.991	4	d
108.4	0.950	7	-
108.8	0.948	4	-
110.8	0.937	2	-
111.1	0.935	3	-

Table 3.1(d) continued

X-ray Diffraction Data
for the cooled melts from the
CaF_2 : LnF_3 Systems (Ln=La,Er,Nd)

50 mole% CaF_2 / NdF_3

2θ	d spacing (Å)	$I^{(rel)}$	Assignment
24.8	3.590	26	d
25.6	3.480	10	d
27.4	3.255	100	a,d
28.5	3.132	42	d
31.8	2.814	26	a,?
35.9	2.501	4	d
44.7	2.027	5	d,Al
45.1	2.010	19	d
45.6	1.989	62	d
46.0	1.973	21	d
50.8	1.797	3	d
52.1	1.755	12	d
54.0	1.698	42	d
56.6	1.626	6	a,d
66.4	1.408	10	d
66.5	1.406	7	d
70.2	1.341	3	d
70.4	1.337	3	d
70.9	1.329	6	d
71.1	1.326	6	d
73.1	1.294	13	d
73.2	1.293	13	d
73.4	1.290	10	d
75.5	1.259	3	a,d
75.6	1.258	3	a,d
83.7	1.155	3	d
84.1	1.151	11	d
84.3	1.149	8	d,?
90.6	1.085	8	-
90.8	1.083	5	-
108.0	0.953	6	-
108.4	0.950	4	-
110.2	0.940	3	-

Table 3.1(d) continued

X-ray Diffraction Data
for the cooled melts from the
CaF_2 : LnF_3 Systems (Ln=La,Er,Nd)

50 mole% CaF_2 / NdF_3 (annealed for 3 days)

2θ	d spacing (Å)	$I^{(rel)}$	Assignment
24.8	3.590	24	d
25.5	3.493	5	d
27.5	3.243	100	a,d
28.4	3.143	48	a,d
31.3	2.858	3	-
31.8	2.814	17	a,?
35.9	2.501	4	d
44.9	2.019	19	d,Al
45.6	1.989	69	d
45.9	1.977	31	d
50.8	1.797	4	d
52.0	1.759	12	d
54.0	1.698	31	d
56.8	1.621	10	a,d,?
56.9	1.618	6	d
57.7	1.598	2	d
66.2	1.412	6	d
66.4	1.408	4	d
66.6	1.404	4	d
66.7	1.402	2	d
70.2	1.341	4	d
70.8	1.331	4	d
72.8	1.299	6	d
73.0	1.296	4	d
73.4	1.290	12	d
73.6	1.287	8	?
75.6	1.258	4	a,d
75.9	1.254	4	a,d
83.6	1.157	4	d
83.8	1.154	4	d
84.4	1.148	12	d,?
84.6	1.145	9	d,?
88.2	1.108	2	d
90.9	1.082	12	-
91.2	1.079	6	-
108.4	0.950	6	-
108.8	0.948	4	-
110.6	0.938	4	-
111.0	0.935	3	-
111.2	0.934	2	-

Table 3.1(d) continued

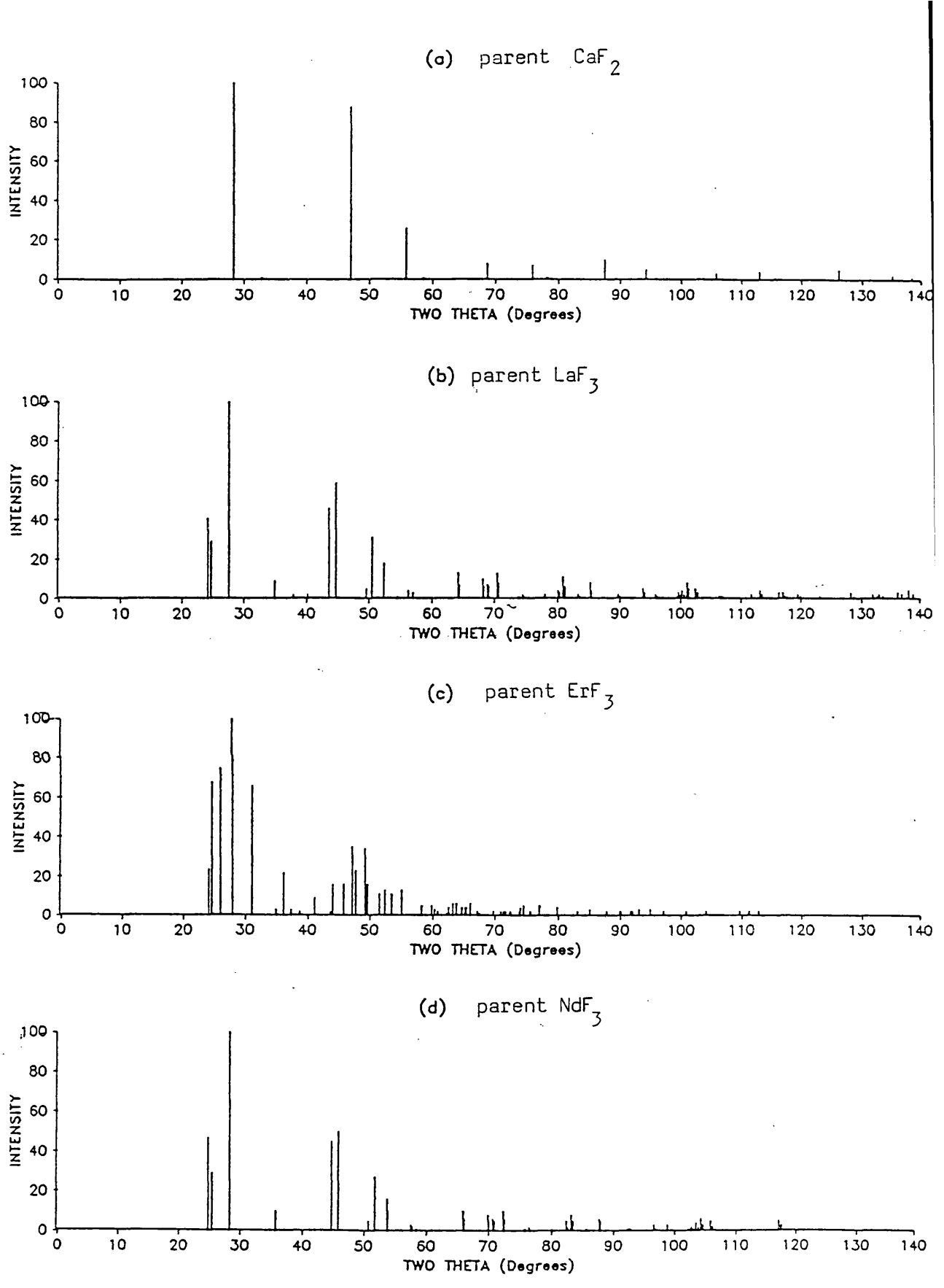

FIG. 3.3(a): Stick-diagrams of parent compounds

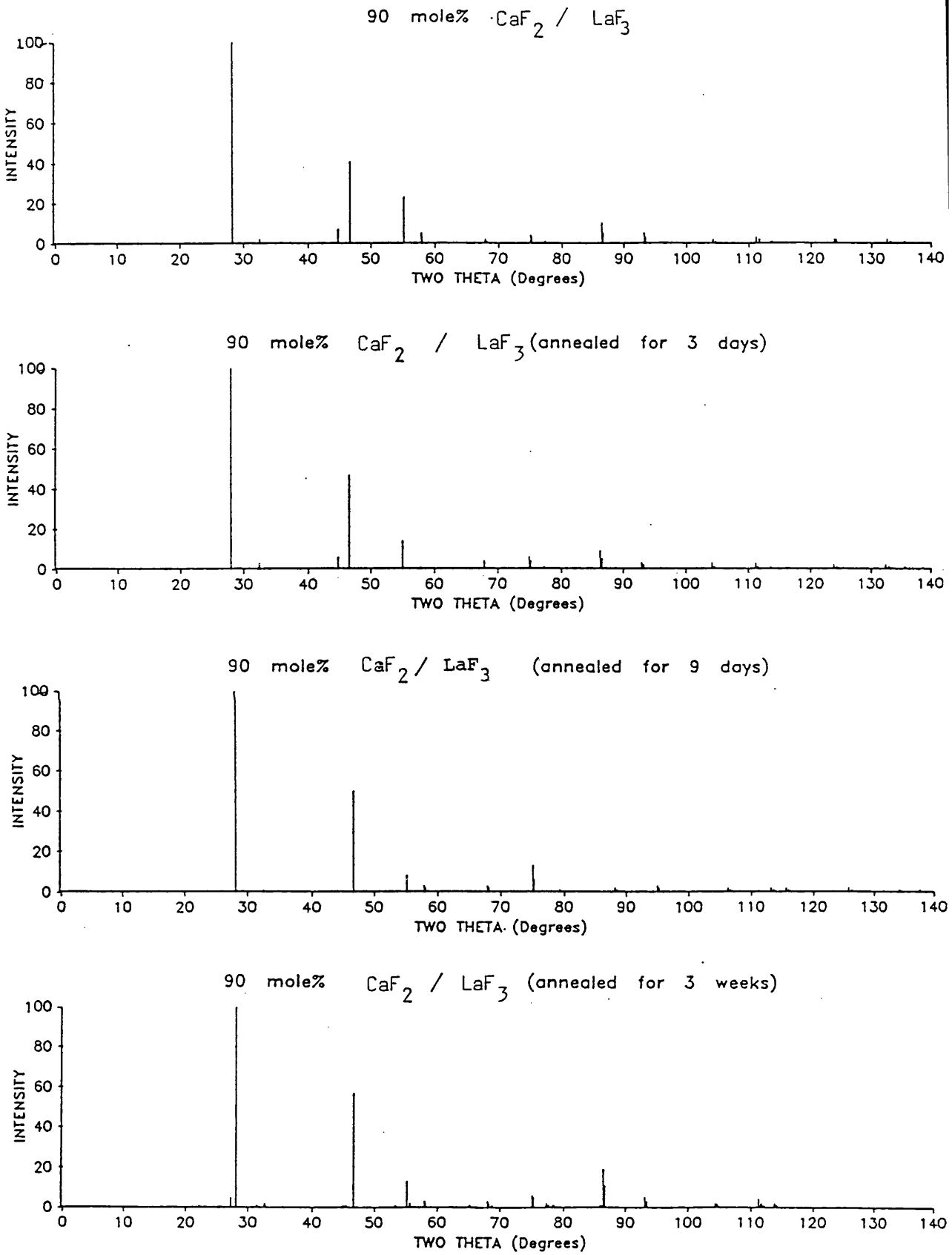

FIG. 3.3(b): Stick-diagrams of selected molar percentages in the CaF_2/LaF_3

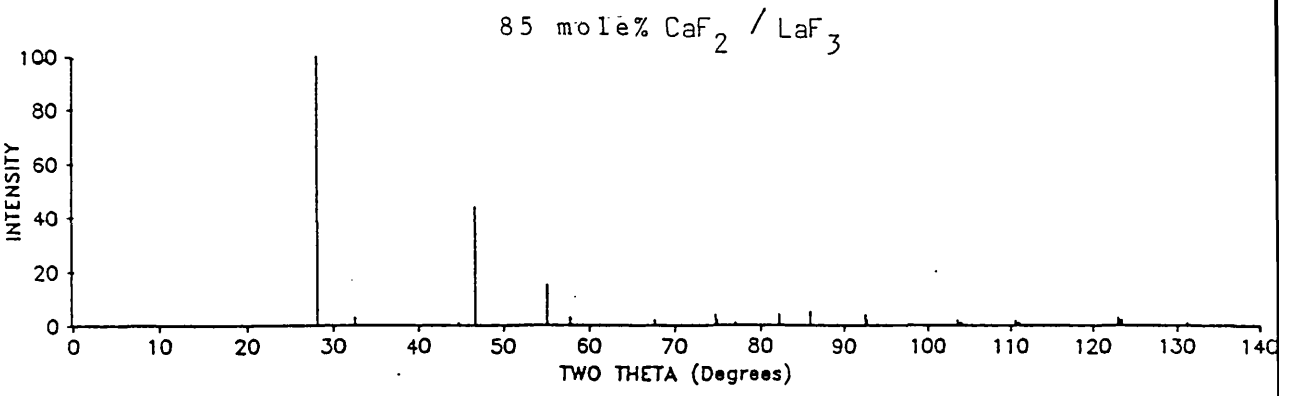

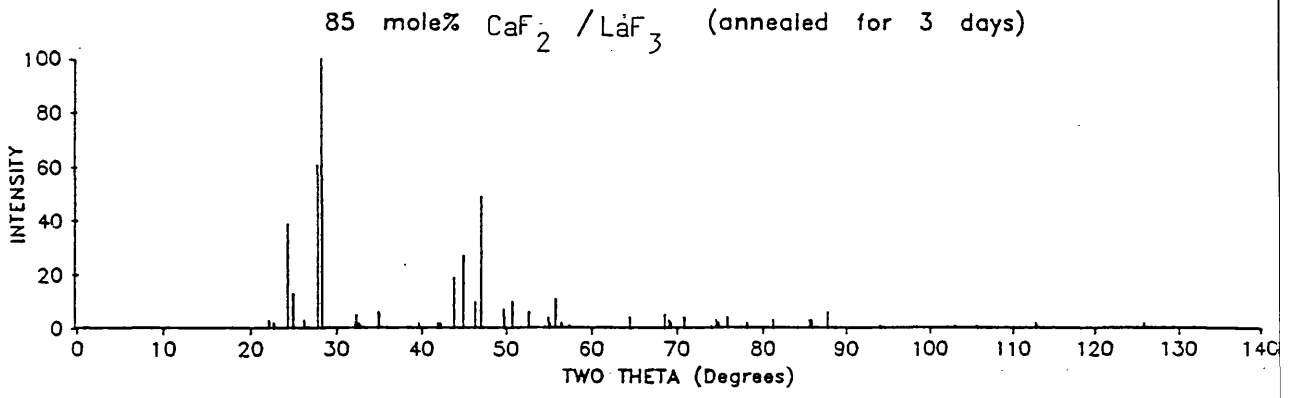

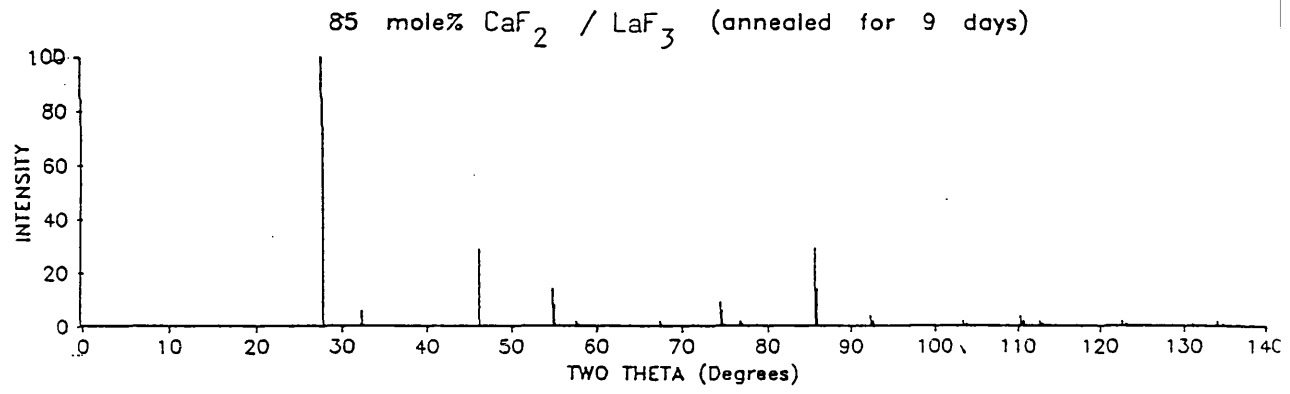

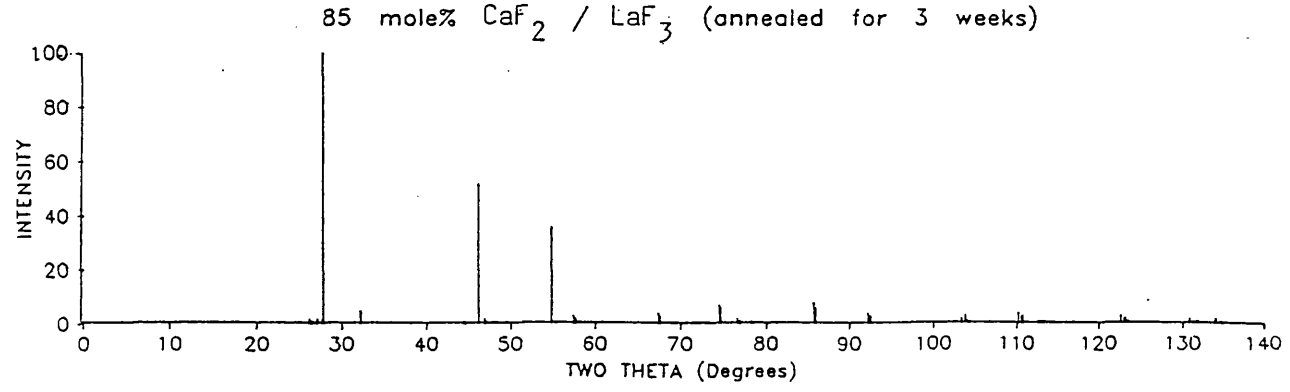

FIG. 3.3(b): Stick-diagrams of selected molar percentages in the CaF_2/LaF_3 system.

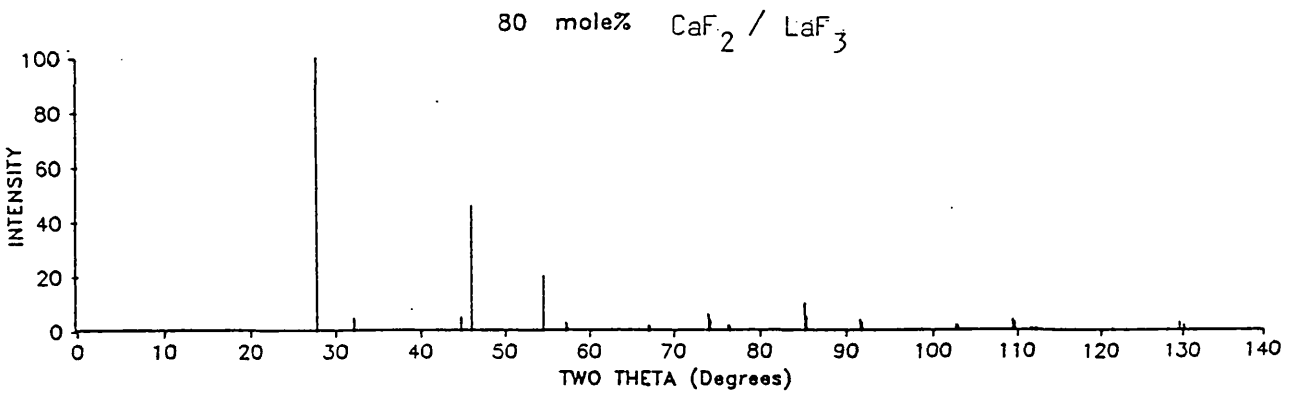

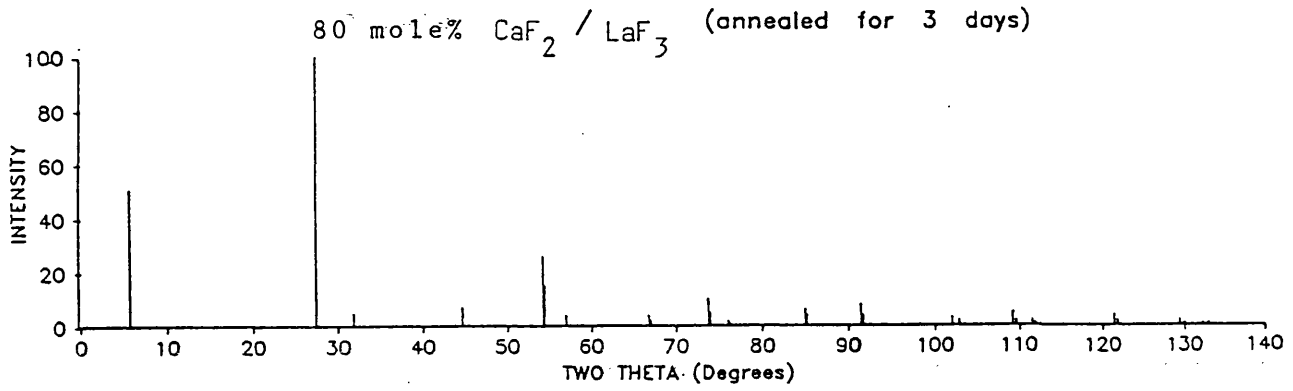

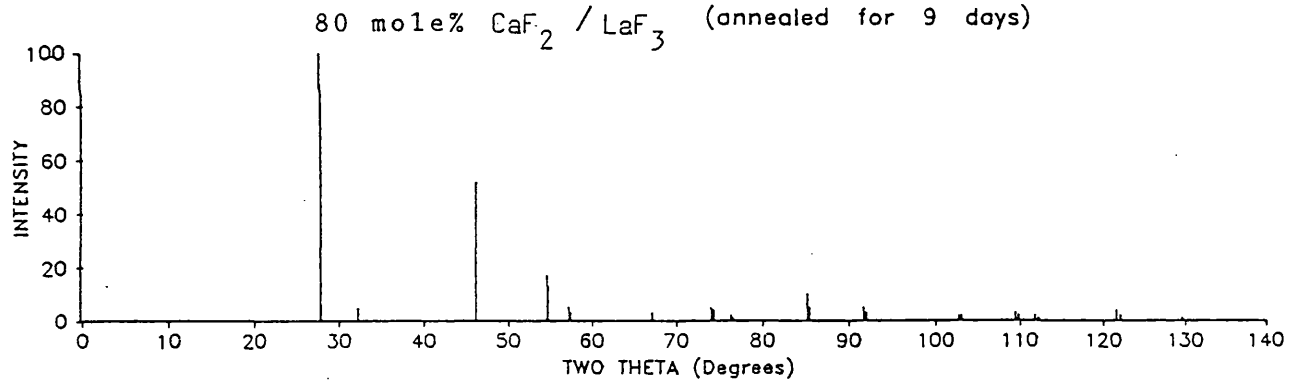

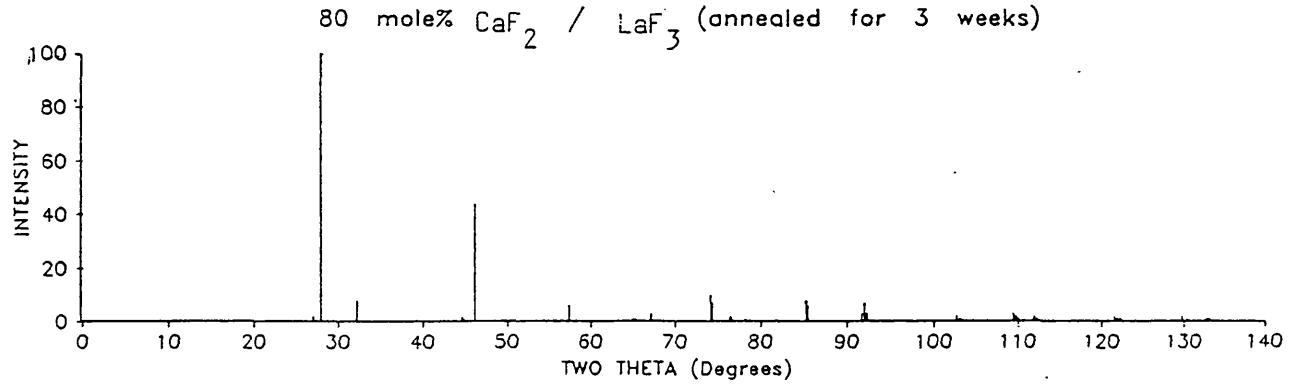

FIG. 3.3 (b): Stick-diagrams of selected molar percentages in the CaF_2/LaF_3 system.

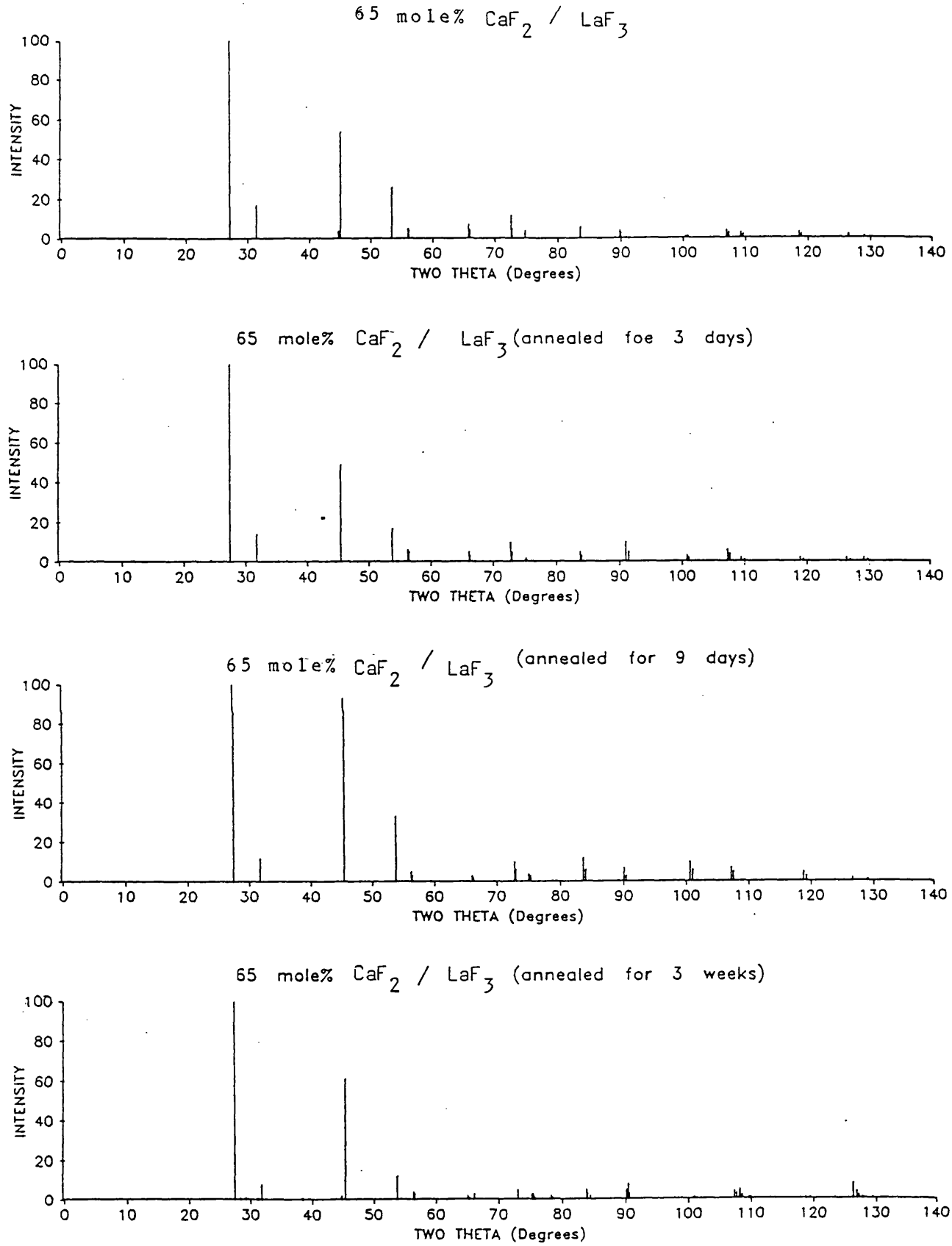

FIG. 3.3 (b): Stick-diagrams of selected molar percentages in the CaF_2/LaF_3 system.

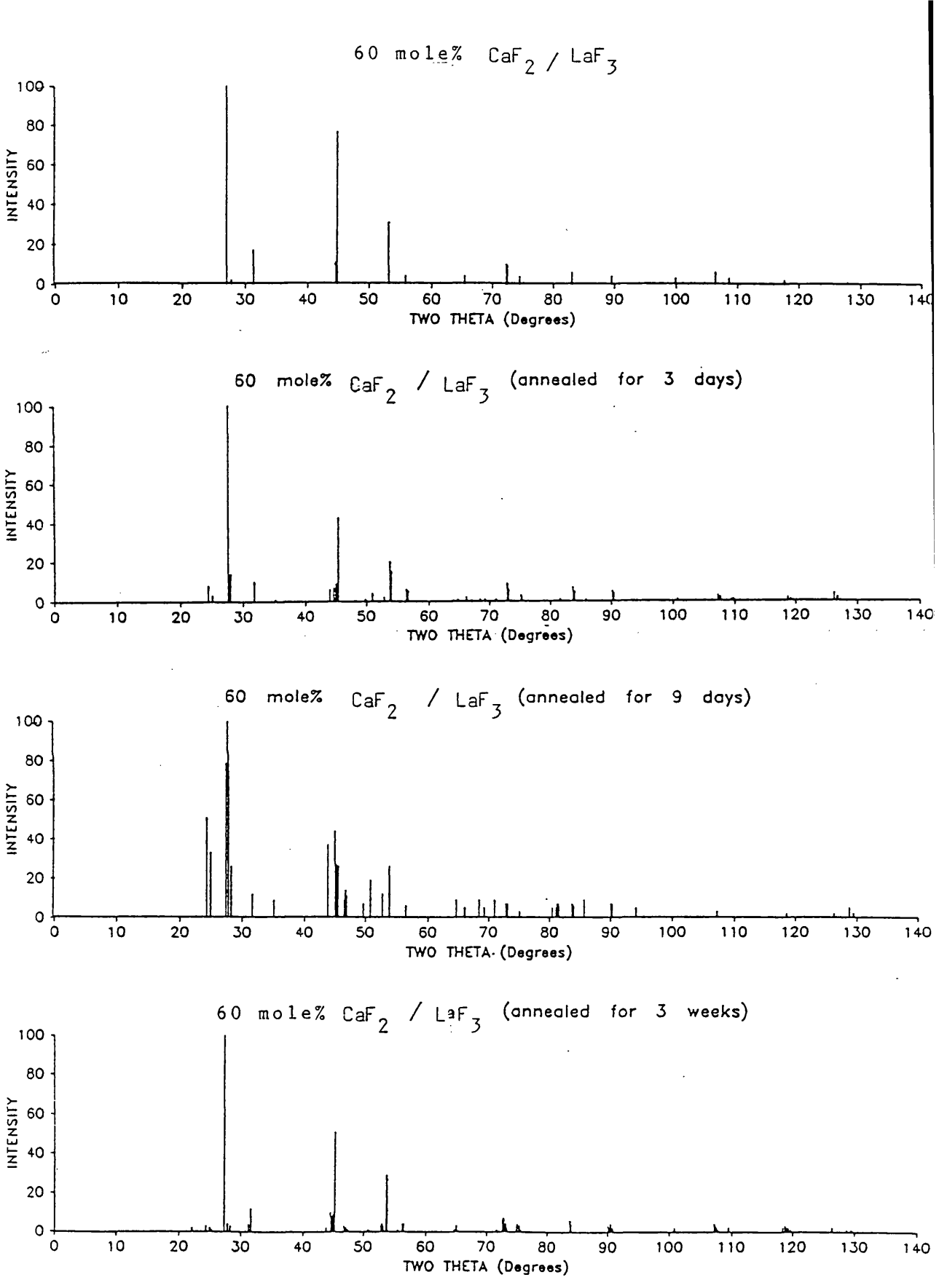

FIG. 3.3 (b): Stick-diagrams of selected molar percentages in the CaF_2/LaF_3 system.

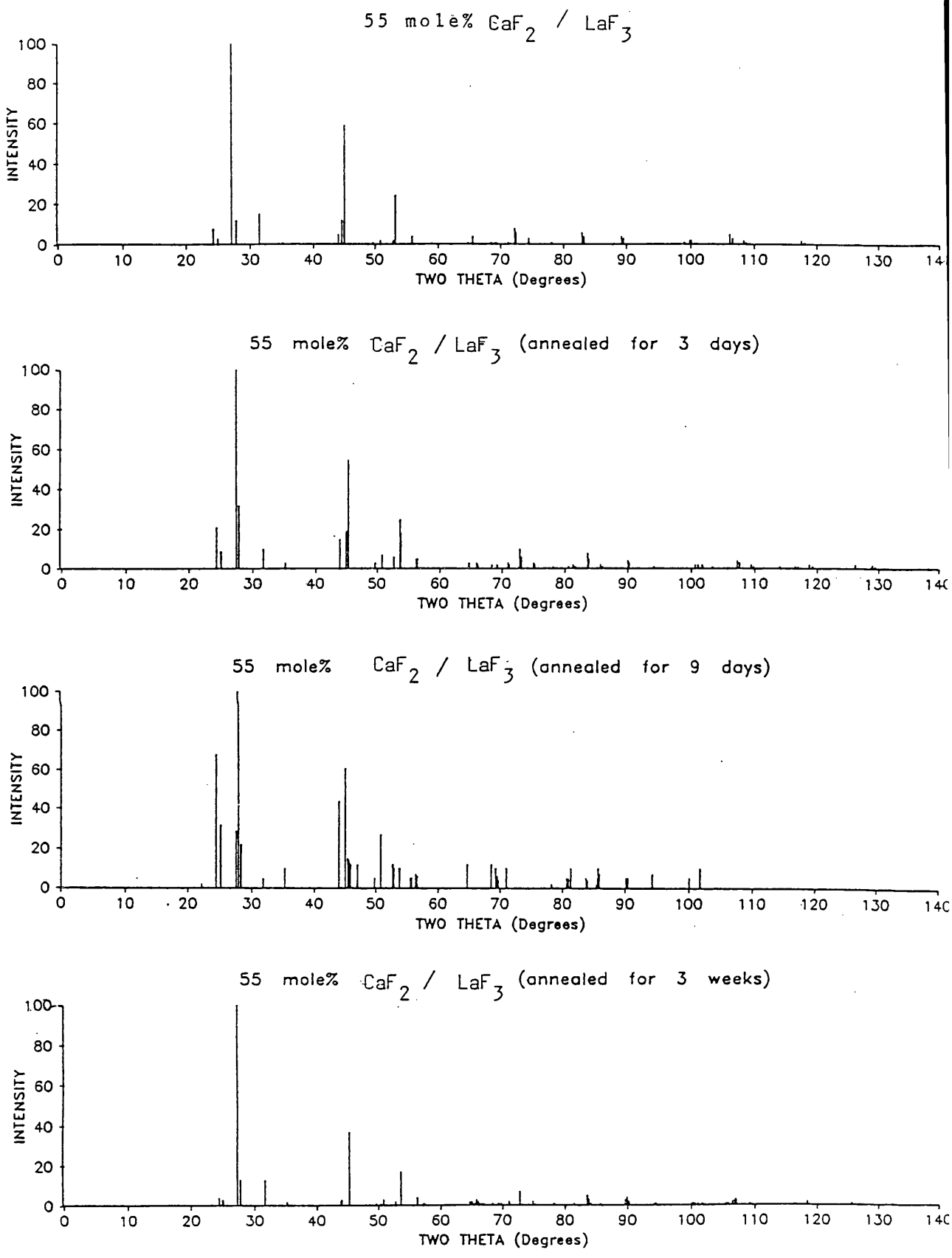

FIG. 3.3 (b): Stick-diagrams of selected molar percentages in the CaF_2/LaF_3 system.

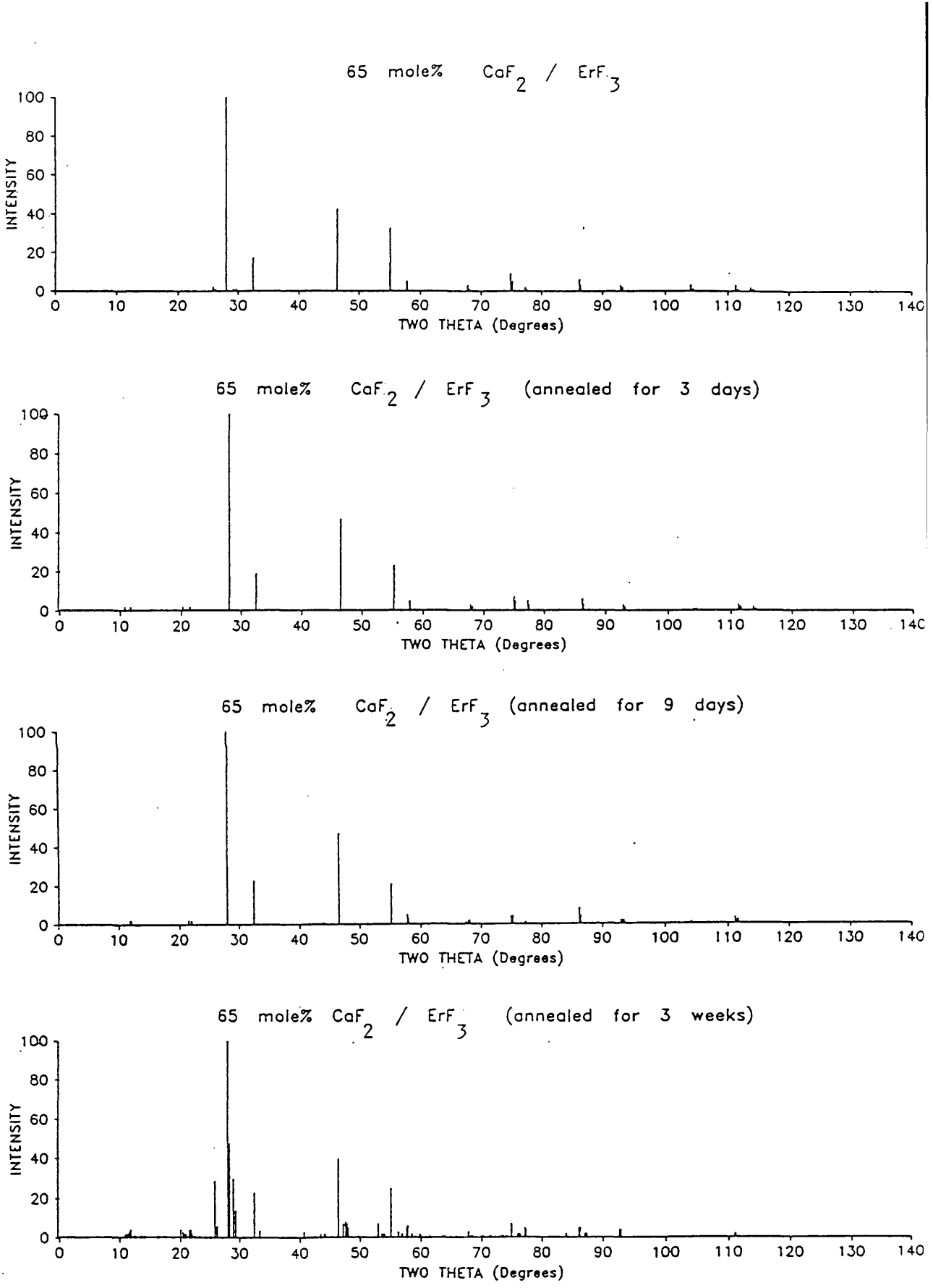

FIG. 3.3(c): Stick-diagrams of selected molar percentages in the CaF_2/ErF_3 system.

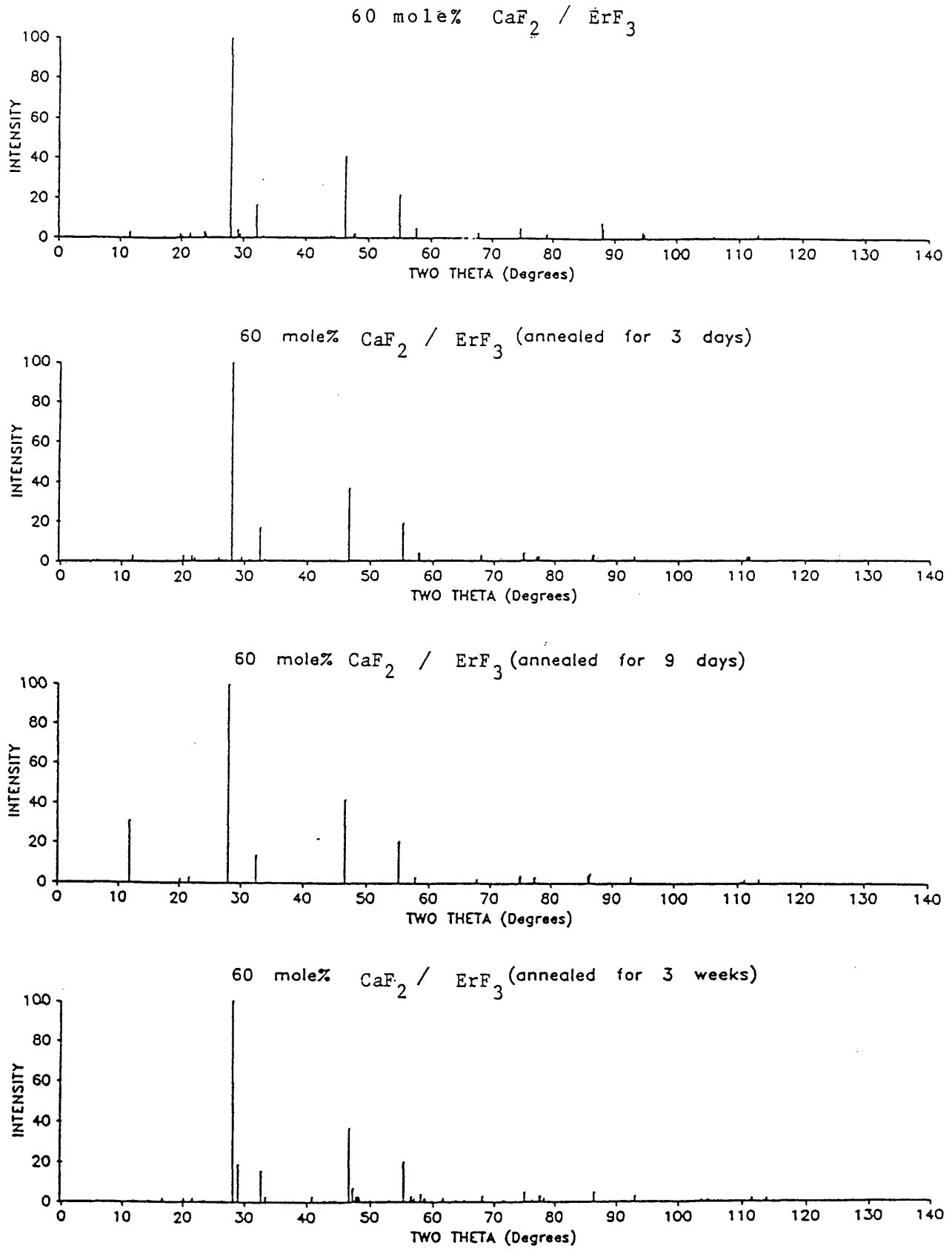

FIG. 3.3 (c): Stick-diagrams of selected molar percentages in the CaF_2 /ErF_3 system

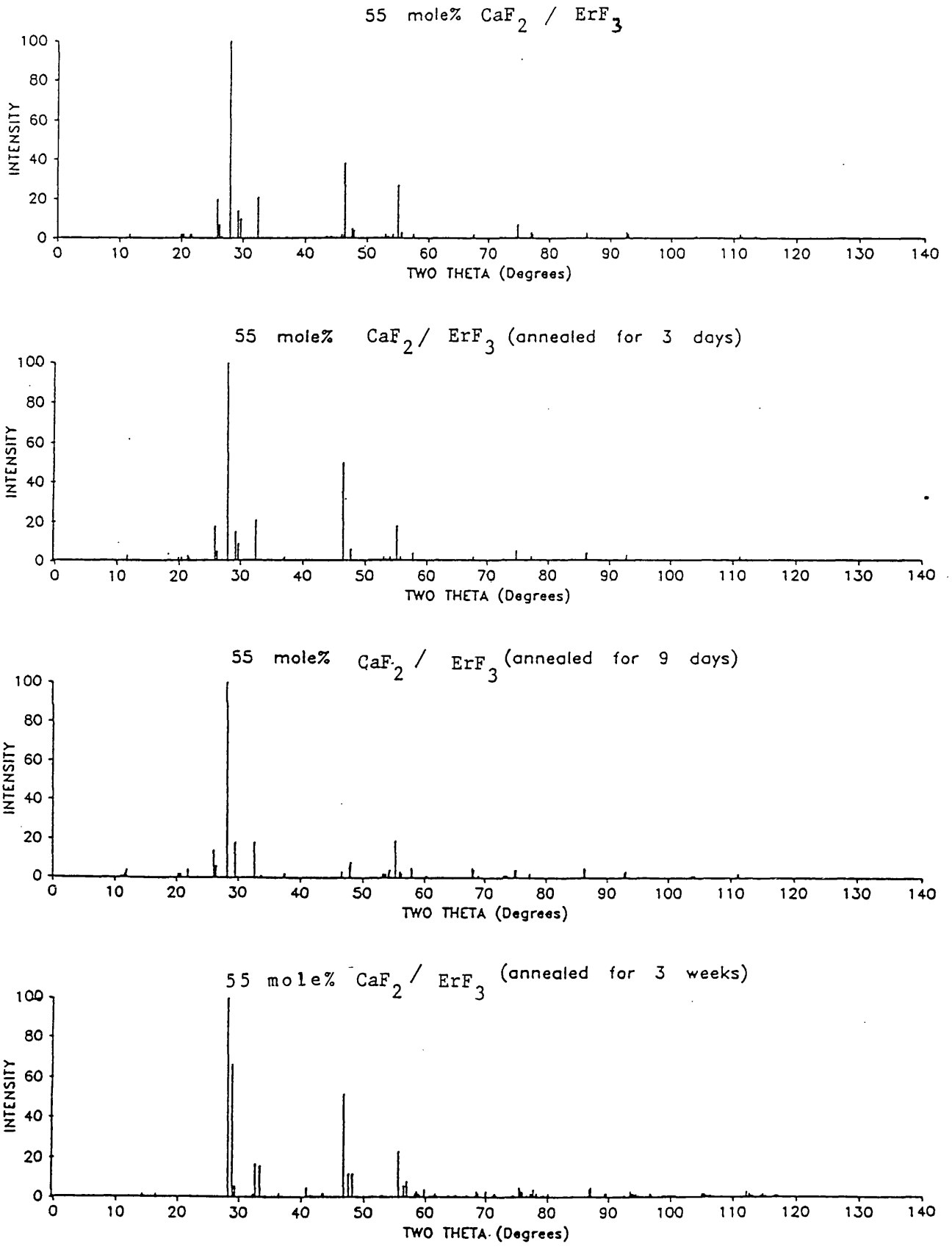

FIG. 3.3(c): Stick-diagrams of selected molar percentages in the CaF_2/ErF_3 system

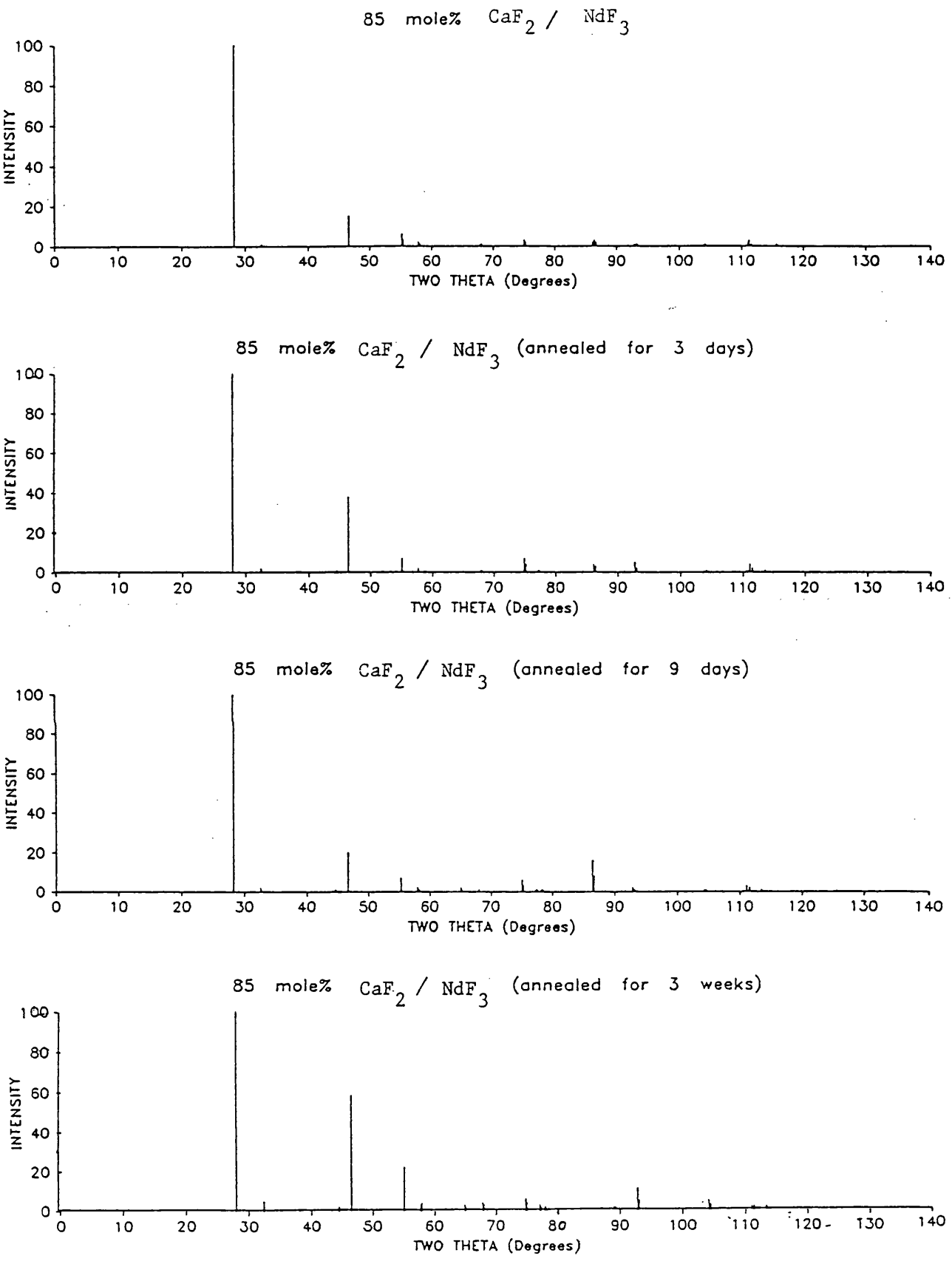

FIG. 3.3 (d): Stick-diagrams of selected molar percentages in the CaF_2/NdF_3 system.

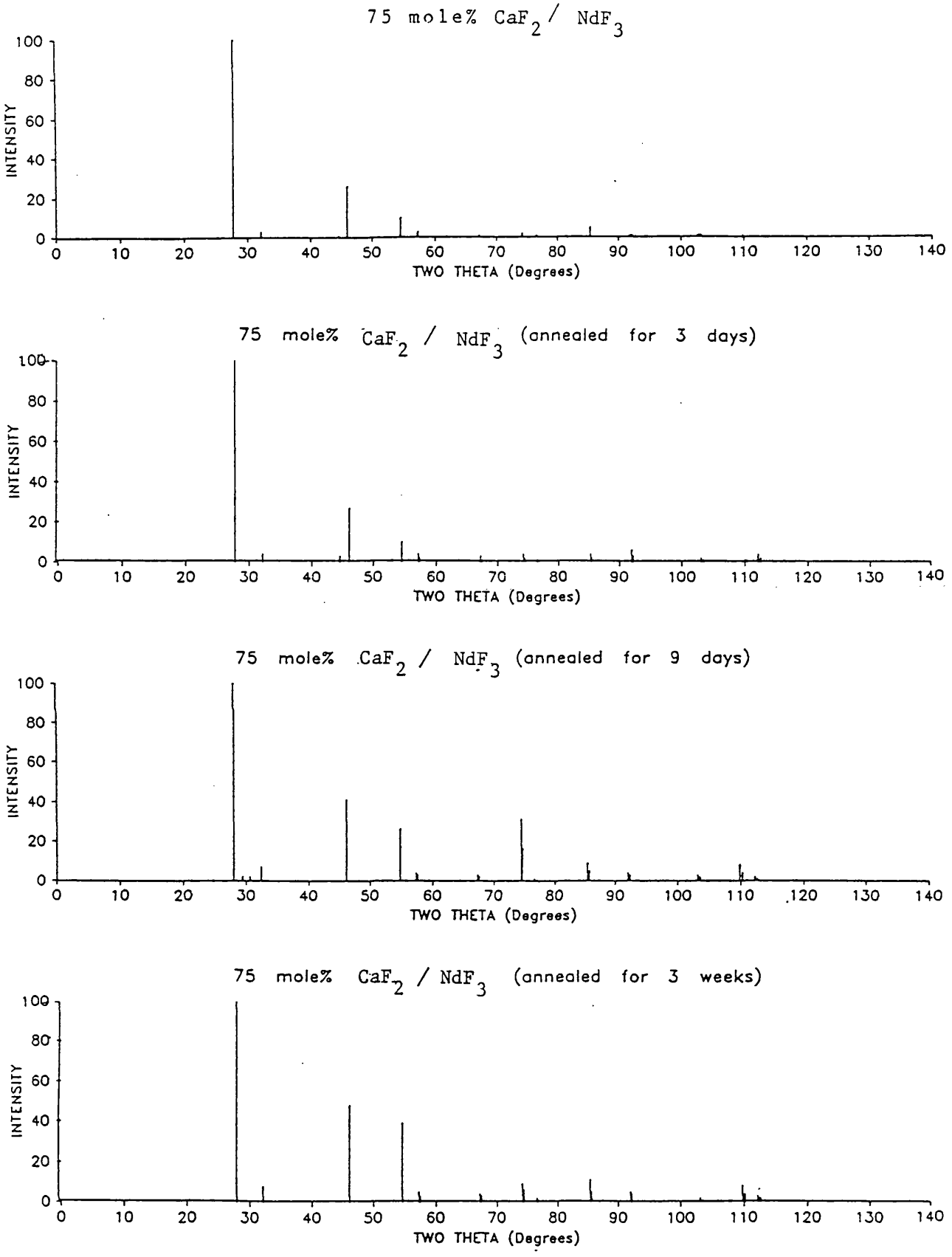

FIG. 3.3 (d): Stick-diagrams of selected molar percentages in the CaF_2/NdF_3 system.

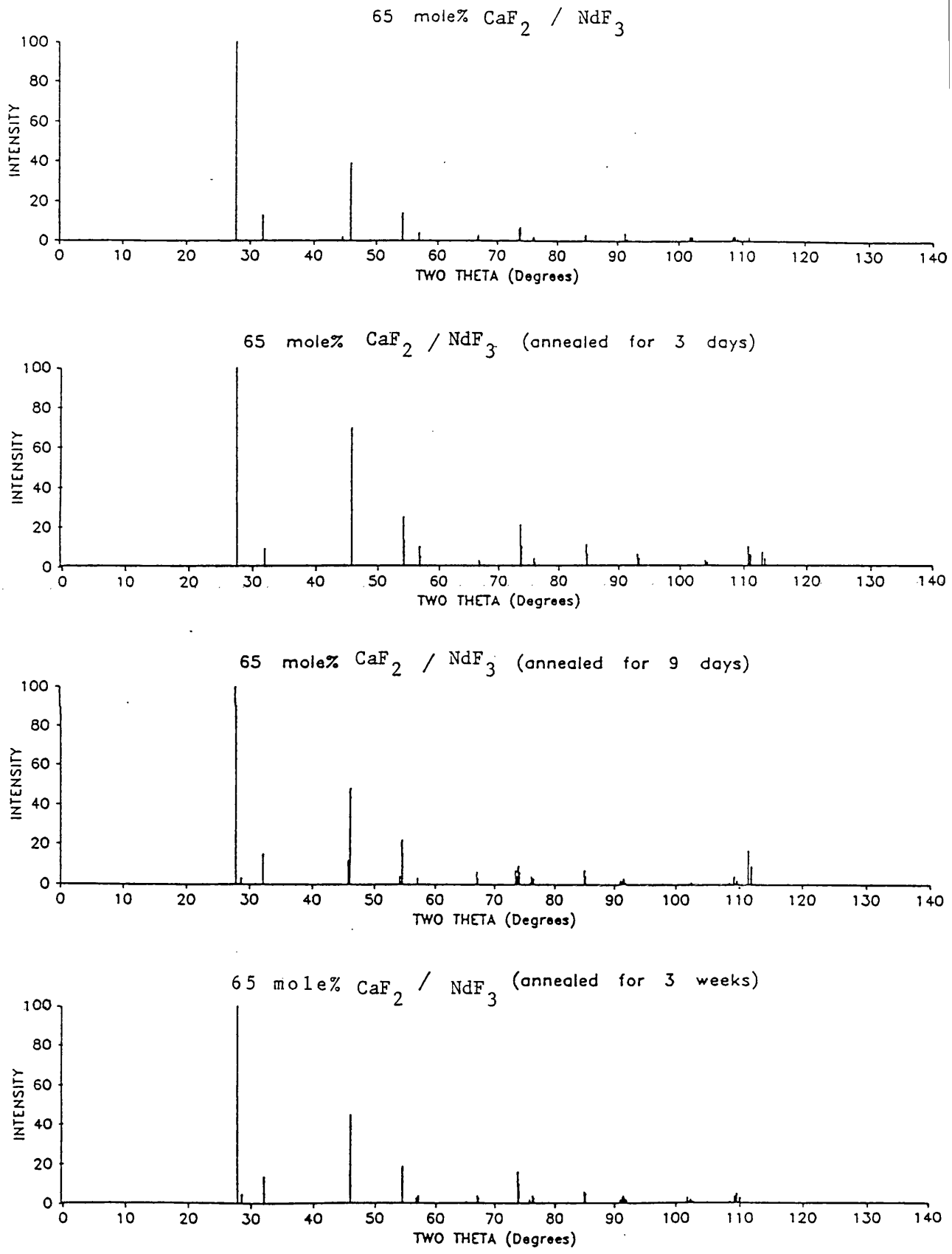

FIG. 3.3 (d): Stick-diagrams of selected molar percentages in the CaF_2/NdF_3 system.

CHAPTER 4

THE ANION DISORDER OF THE PEROVSKITE FLUORIDE $KCaF_3$

4.1 Introduction

The alkaline earth fluorides are well known to exhibit fast ion conduction over a range of a few hundred degrees, up to their melting points [146]. In the study of these fluorite structured materials the combination of a.c. electrical conductivity and N.M.R. techniques has been shown to be a particularly powerful tool in evaluating the diffusion mechanism [147]. Many materials exhibit the perovskite structure, ABX_3, both oxides and halides and fast ion conduction might be anticipated in such systems [53,55], which have an open lattice reminiscent of the fluorite structure. In particular perovskite fluorides, ABF_3 (A = alkali metal, B = divalent cation) have invoked considerable interest following the suggestion [53] that the perovskite structure is conductive to fast anion conduction. In this context it was noted that high pressure $MgSiO_3$ has a distorted perovskite structure; fast ion conduction in this material, which is thought to be a major constituent of the earths inner mantle Fig. 4.1 could have important geophysical implications. Indeed fast-ion motion has been claimed in $NaMgF_3$ [53], however more recent work [54] did not show the phenomenon to be present in $NaMgF_3$ and $KMgF_3$. There is good evidence for high temperature fast ion conduction in $KCaF_3$ [54] and $CsPbF_3$ [55] suggesting that the nature of the B ion plays an

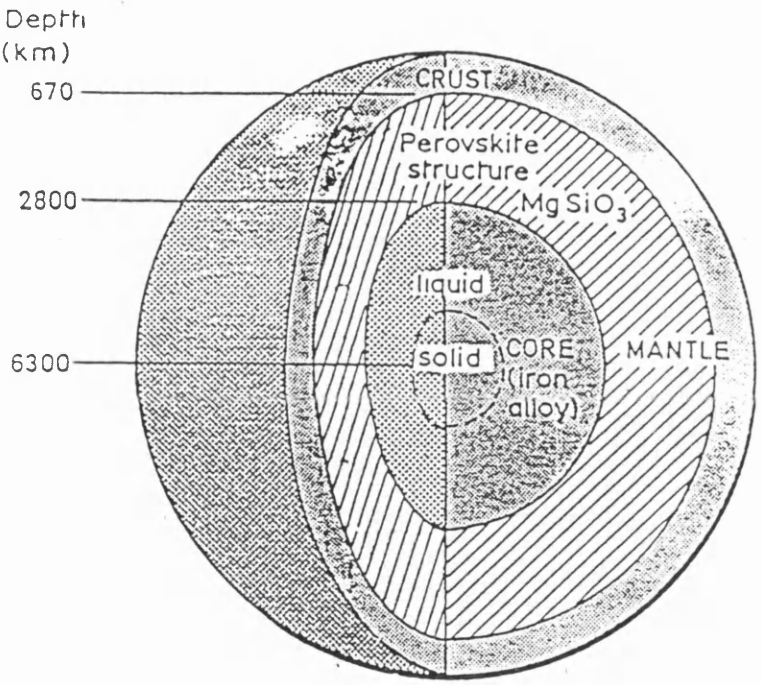

FIG. 4.1: The commonest stuff in the world: perovskite makes up more than half the planet.

important role in transport. At low temperatures the mobile defect is the F^- vacancy [54]. The results of conductivity and N.M.R. [54] are consistent with a vacancy diffusion mechanism. These results also confirm the theoretical predictions [148] that the F^- interstitial ion is the more mobile defect, however, little is known about the defect structure of these materials.

4.2 Investigation of Anion Disorder in $KCaF_3$

The results obtained by applying a.c. electrical and N.M.R. techniques to single crystals of this perovskite structured material show that it displays ionic conductivities Fig.4.2 comparable to the more extensively studied superionic fluorite structured phases [149,150].

The perovskite ABX_3 compounds have been extensively studied by N.M.R. and neutron diffraction techniques in order to relate the phase transitions in these systems to the rotation of the BX_6 octahedra. The N.M.R. studies, using ^{19}F relaxation techniques, give information on the dynamics of the fluorine sublattice. Relaxation time N.M.R. measurements in $KCaF_3$ [54] could not be interpreted in terms of short range rotational motions, but only in terms of long range diffusional modes for the fluorine ions, coupled with a large amount of disorder on the anion sublattice. This interpretation is underpinned by the results obtained from the electrical measurements [54]. Similar behaviour has been reported for the analogous

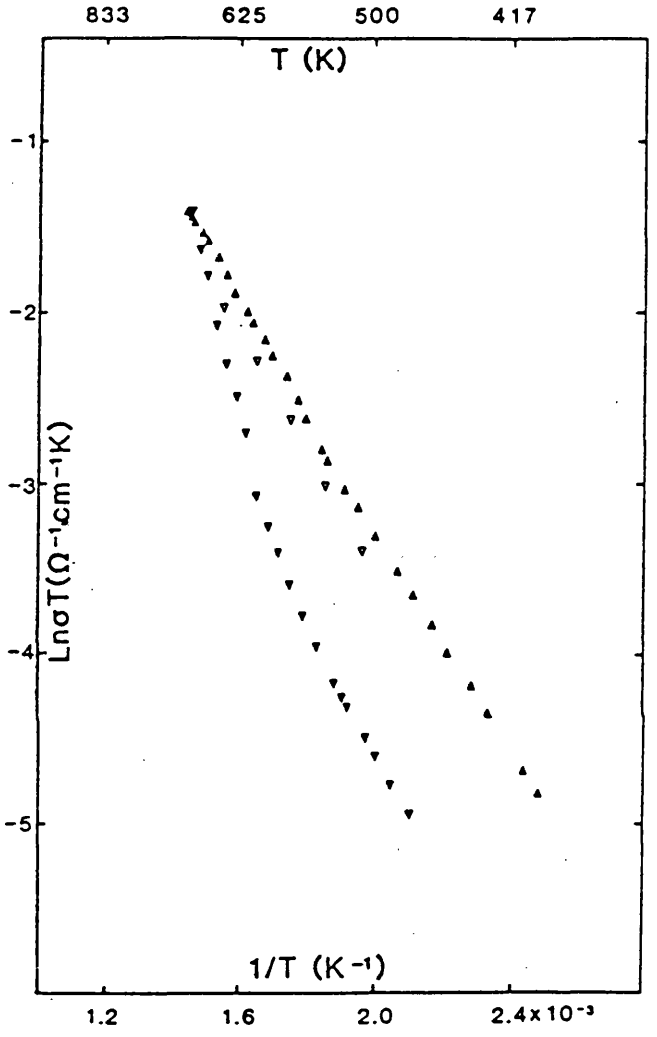

FIG. 4.2: Ionic Conductivity plotted versus reciprocal temperature for $KCaF_3$

system $CsPbF_3$ [55].

The data collected and the open lattice of $KCaF_3$ suggest fast ionic conductivity. This is also confirmed by calculations of the defect energies performed and published for the fluoride perovskite, $KMnF_3$, using the HADES program [148]. Both the data collected and the calculations of defect energies suggest that the conductivity is governed by the migration of thermally generated point defects. The predominant point defects are thought to be of the anion Frenkel type, $F_V^{\cdot}$ vacancy and $F_i^{\cdot}$ interstitial; the $F_i^{\cdot}$ interstitial ion being the more mobile defect even at room temperature. At low temperature the conductivity and N.M.R. results suggest extrinsic behaviour, the F^- motion being dominated by residual impurities. Fast-ionic conduction is observed at high temperatures. In crystals deliberately doped with oxygen the compensating defect is expected to be the $F^{\cdot}$ vacancy. The results of conductivity and N.M.R. are consistent with a vacancy diffusion mechanism. The calculated defect energies in $KMnF_3$ ie. o.41eV for $F^{\cdot}$ vacancies and 1.63eV for K^+ vacancies are of comparable magnitude to the measured value of 0.66eV for $KCaF_3$. Similar experiments for $NaMgF_3$ and $KMgF_3$ revealed no detectable $F^{\cdot}$ion motion even at high temperatures. This is perhaps surprising, particularly for $KMgF_3$ which has a similar structure to $KCaF_3$ and the difference must reflect the relative chemical nature and size of the Ca and Mg ions.

The general aim of this experiment is to identify the nature and concentration of these defects, as has been achieved using single crystal neutron techniques for the high temperature superionic fluorites [56]. A powder experiment on D1A to investigate the variation of the ferroelastic effect with temperature in this system has been reported [151]. However, the long wavelength used in this study means that it would be unsuitable for detecting the lattice defects expected in this kind of system.

X-ray and neutron diffraction studies on single and polycrystal samples of the high temperature fluorite structured materials PbF_2, CaF_2 and SrF_2 [56,86,150] in their high conductivity phases have highlighted several important points that have influenced this study. The main crystallographic point which arose from these studies was the need for single crystal neutron measurements using short wavelengths in order to obtain high resolution for the structure, thus permitting differentiation between the point defect formations and the large dynamic effects observed at high temperature in these superionic systems. A rerun of the powder study at the lowest wavelength on D1A of 1.3Å was unsuitable and a neutron single crystal investigation, for which D9 was the ideal instrument, was necessary for results of the required quality. The fact that fluorine has a higher scattering length than either Ca or K is an additional feature which favoured a neutron study. The evolution of the defect structure in this

material with temperature is currently being investigated by Molecular Dynamics (MD) methods and the results of these investigations will be available to guide the interpretation of the high temperature structures. The same combination of MD studies and diffraction has proved particularly powerful in the study of superionic fluorides [152].

A further motivation for this study or as mentioned earlier in the introduction, is that the material is an analogue of the high pressure modification of the mineral Magnesium Silicate, which is thought to comprise a large percentage of the earths mantle Fig. 4.1. It has been suggested [53] that if the material is superionic then an alternative mechanism for the retention of electrical neutrality in the mantle is possible, and if this could be shown to be true then this concept could have major geophysical implications.

This experiment therefore offered an excellent opportunity to investigate a simple member of a potentially larger and important class of high temperature superionics.

4.3 Experimental

4.3.1 Preparation of $KCaF_3$ and Experimental Procedure on the D9

Single crystals, 6mm diameter x 30mm long, were grown from powders by the Stöckbarger technique using high-purity

graphite crucibles (Ultra-Carbon, UF4S for sugar grade) and a radio-frequency induction furnace [153]. The atmosphere inside the growth chamber was flowing argon gas. The relevant high-purity powders (B.D.H. Optran crystal - growing grade) were intimately mixed prior to crystal growth. A growth speed of 0.05mm/min was employed and generally this produced transparent single crystals. The crystals had good cleavage planes and could be cut into regular cubes.

X-ray characterisations have demonstrated the high quality of these crystals. A crystal was mounted in a sealed tube Fig. 4.3 onto the D9 diffractometer at the ILL. The tube (6mm diameter) contains a cubic crystal located within two pieces of graphite, as shown in the figure, placed at the bottom of the tube. The two pieces of graphite "sandwiched" the crystal and were pressed together by a silica rod. A cubic crystal is preferred since a spherical crystal in a similar environment would move around during the passage of the neutron beam. The tube was evacuated and sealed by fusing the tube and rod together and drawing off, as shown in Fig.4.3.b.

Knowing the space-group (Fm3m) and lattice parameters of the sample, the program Dragon [154] was used to generate the Miller indices and the 2θ value of the Bragg reflection. The diffractometer was calibrated by recording the T_{set} and T_{obs} values. The maximum temperature that was

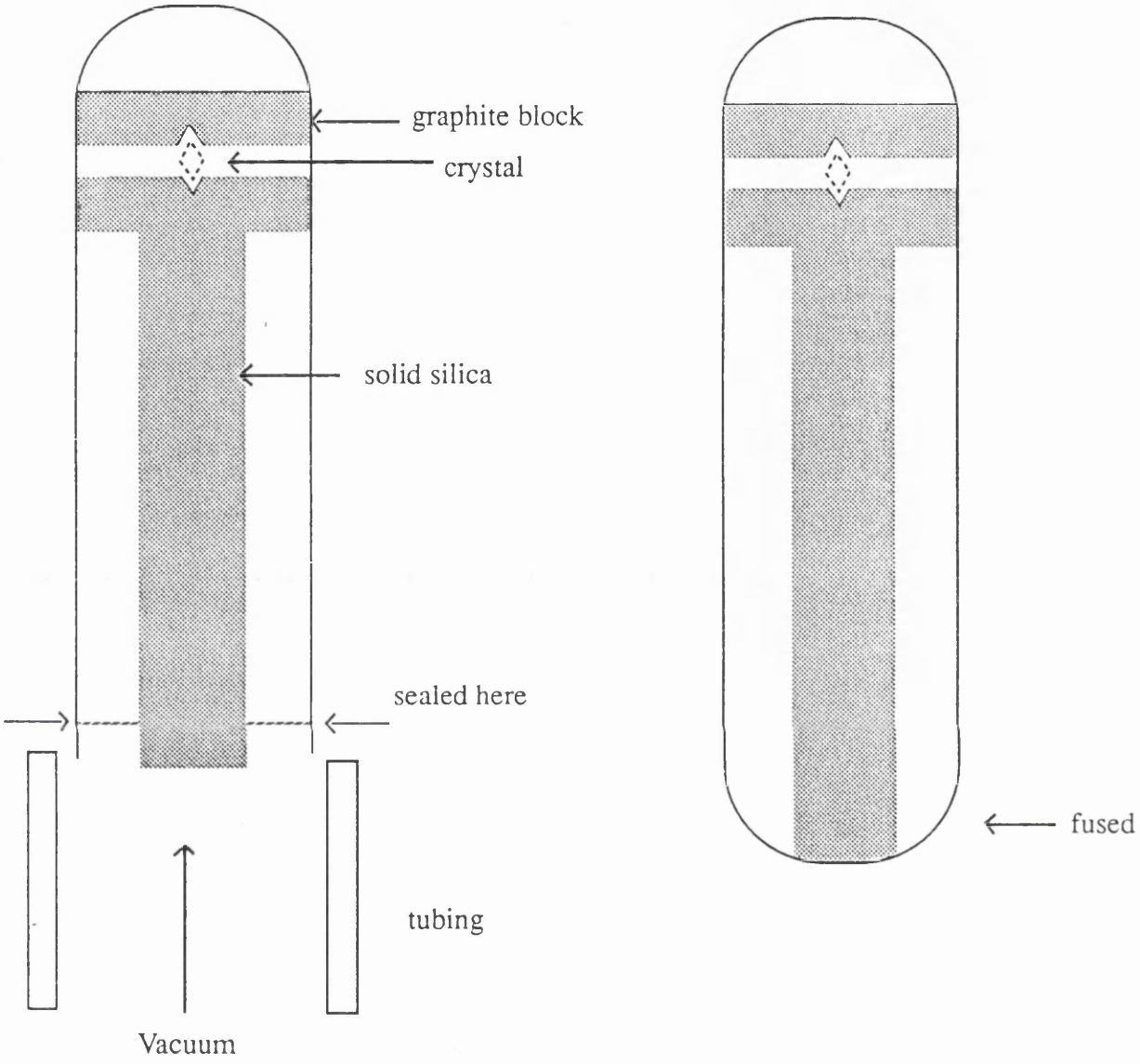

(a) Preparation of Sample (b) Final Sample

Fig. 4.3: Mounting of crystal onto the D9 Diffractometer

reasonable on the D9 was 700°C. The system was tested with a thermocouple placed inside a dummy silica tube, the same dimensions as the sample holder. Calibration checks showed that the temperature inside the silica tube was considerably less than the setting on the controller of the soufflet at temperatures of >500°C. The calibration table values are shown in Table 4.1.

TABLE 4.1 Calibration values

T_{set} °C	T_{obs} (in thick tube) °C	T_{obs} (bare thermometer) °C
100		
200	206	
300	280	
400	358	
500	420	
600	500	
700	545	
800	595	785
900	662	883
950	696	858
1000		
1050		
1100		

The maximum setting on the controller was 950°C which gave a temperature of 696°C on the sample. Once the diffractometer was calibrated the crystal was mounted, aligned optically and the temperature was raised slowly to T_{set} = 500°C (T_{obs} = 420°C) to ensure that the crystal was in the cubic phase before looking for reflections. The wavelength used was λ = 0.7025Å. Readings were taken at 400°C and in the superionic region at 700°C respectively and the high angle data were checked. The single crystal data collected over a period of 24 hours at 400°C and 700°C

were refined using the program UPALS [155] and at least 130 independent reflections were observed at each temperature.

4.4 Results and Discussion

The final least squares atomic and harmonic thermal parameters, the observed and calculated intensities, the delta and weighted residual values obtained from the refinements of the data measured at 400°C and 700°C are given in Tables 4.2(a),(b),(c), 4.4(a),(b) and (c) respectively. The corresponding values for the anharmonic refinements are given in Tables 4.3(a),(b),(c), 4.5(a),(b) and (c) respectively.

The quality of the fit for both the 400°C and 700°C data is fairly good. The final refinement of the 400°C data for the harmonic thermal parameters gave a weighted residual, Rw =17% (Table 4.2(c)). Including anharmonic thermal parameters in the refinements seems to improve the quality of the fit and Rw =10% (Table 4.3(c)) giving evidence of some degree of anharmonicity. Considering the 700°C data, there is less evidence of anharmonicity as the weighted R-factor obtained for the harmonic model, Rw = 14% (Table 4.4(c)) is only slightly higher than the anharmonic model were Rw = 10% (Table 4.5(c)) although still favouring anharmonic behaviour. In general the Rw factors are fairly good with no interstitial occupancy.

There are two pairs of Fourier maps (FCALC) for each set of

the data at 400°C and 700°C. Considering the 400°C data and looking at the Fourier section along the 001 and -110 directions there are two harmonic thermal factors, one along the 001 direction Figure 4.4(a) and one along the -110 direction Figure 4.4(b). Similarly there are also two anharmonic thermal factors, one along the 001 direction Figure 4.4(c) and one along the -110 direction Figure 4.4(d).

Considering the 700°C data, and looking at the Fourier section along the 001 and -110 directions there are two harmonic thermal factors along each direction respectively Fig. 4.5(a) and Fig. 4.5(b). Similarly there are also two anharmonic thermal factors one along the 001 direction Fig. 4.5(c) and one along the -110 direction Fig. 4.5(d). Considering both the 400°C and 700°C data it can be seen that the Ca^{2+} and K^{+} cations are spherically symmetrical (see Figures 4.4(b), (d), 4.5(b), (d). However the F^{-} anions appear to have an oblate ellipsoid discus like shape. This can be seen in all the F-maps (Figs 4.4(a) to 4.5(d)). It is not easy to understand the diffusion pathway. Anharmonicity would have been expected if the fluoride ion vibrated towards the nearest fluoride neighbouring site (nns). Due to the oblate ellipsoid like vibration it may seem that the fluoride ion is vibrating towards a saddle point ie. towards the K^{+} cation at the centre of a cube face. It is assumed, therefore, that the F^{-} anion is vibrating with an oblate ellipsoid discus-like fashion with

the larger axis in the 100 plane and the smaller in the 110 plane for a ½00F^- (Fig. 4.6). In this proposed vacancy mechanism the F^- jumps are either to the next nearest neighbour in the 110 plane ie. a 110 type jump (the saddle point being at ½ 0½ for ½00F^- where $1/\sqrt{2}a = 0.7a$) or towards the centre, K^+ saddle point, in the 100 plane in which case the F^- could possibly jump straight across the cube face. From above it can be seen that the K^+ and Ca^{2+} cations are fairly rigidly fixed on their sites. The F^- anions show anharmonic oblate ellipsoid discus-like vibrations with no obvious move towards a saddle point but could be expansible for conductivity and do not behave like other fluorides which easily move off their sites. The discussion of the F-maps and the proposed vacancy mechanism is also consistent with the refinement of the data in which the Rw factors were fairly good with no interstitial occupancy. In conclusion $KCaF_3$ is a straightforward structure with a low concentration of defects. Although there is some evidence for vacancies there is no significant occupation of interstitial sites. All the ions show a small amount of anharmonic behaviour and it is possible that the high conductivity could be due to a small population of highly mobile vacancies. For future work molecular dynamics or static simulation could be used to locate saddle points in possible migration pathways.

Table 4.2(a) $KCaF_3$ rectangular crystal at 400°C (harmonic thermal parameters)

ATOMIC PARAMETERS

Ca Atom No. 1 Parameters 10 to 19

	X	Y	Z	G	B11	B22	B33	B12	B13	B23
VALUE	0.000000	0.000000	0.000000	0.020833	0.023047	0.023047	0.023047	0.000000	0.000000	0.000000
E.S.D.	0.000000	0.000000	0.000000	0.000000	0.000910	0.000910	0.000910	0.000000	0.000000	0.000000
	BIJ/(2*PI**2*ASTAR(I)*ASTAR(J))			$**2	0.023208	0.023208	0.023208	0.000000	0.000000	0.000000

K Atom No. 2 Parameters 20 to 29

	X	Y	Z	G	B11	B22	B33	B12	B13	B23
VALUE	0.500000	0.500000	0.500000	0.020833	0.066051	0.066051	0.066051	0.000000	0.000000	0.000000
E.S.D.	0.000000	0.000000	0.000000	0.000000	0.002134	0.002134	0.002134	0.000000	0.000000	0.000000
	BIJ/(2*PI**2*ASTAR(I)*ASTAR(J))			$**2	0.066514	0.066514	0.066514	0.000000	0.000000	0.000000

F Atom No. 3 Parameters 30 to 39

	X	Y	Z	G	B11	B22	B33	B12	B13	B23
VALUE	0.500000	0.000000	0.000000	0.062500	0.016839	0.140795	0.140795	0.000000	0.000000	0.000000
E.S.D.	0.000000	0.000000	0.000000	0.000000	0.000973	0.002977	0.002977	0.000000	0.000000	0.000000
	BIJ/(2*PI**2*ASTAR(I)*ASTAR(J))			$**2	0.016956	0.141780	0.141780	0.000000	0.000000	0.000000

Table 4.2(b) $KCaF_3$ rectangular crystal at 400°C
(IOE, IC and Delta values for harmonic thermal parameters)

H	K	L	IOE	IC	DELTA
1	0	0	32.54	31.12	1.413
1	1	0	4.67	6.44	-1.769
1	1	1	139.68	122.24	17.444
2	0	0	325.58	362.57	-36.999
2	1	0	35.51	35.08	0.429
2	1	1	26.20	27.58	-1.383
2	2	0	216.90	199.22	17.685
2	2	1	31.34	28.74	2.603
2	2	2	114.02	111.02	3.003
3	0	0	0.00	0.07	-0.068
3	1	0	2.21	1.97	0.237
3	1	1	21.45	19.17	2.284
3	2	0	2.86	2.85	0.015
3	2	1	9.91	9.11	0.803
3	2	2	4.06	4.95	-0.888
3	3	0	3.27	4.32	-1.045
3	3	1	0.25	0.51	-0.262
3	3	2	7.42	7.18	0.242
3	3	3	2.92	0.72	2.202
4	0	0	103.77	103.74	0.029
4	1	0	30.81	33.50	-2.694
4	1	1	47.54	43.69	3.854
4	2	0	54.53	55.26	-0.721
4	2	1	20.25	19.18	1.075
4	2	2	29.87	31.49	-1.618
4	3	0	7.64	8.50	-0.859
4	3	1	18.44	14.48	3.959
4	3	2	6.19	6.37	-0.180
4	3	3	10.10	7.21	2.885
4	4	0	13.44	14.15	-0.718
4	4	1	8.41	6.75	1.662
4	4	2	6.47	9.34	-2.878
4	4	3	7.22	3.46	3.762
4	4	4	0.00	3.69	-3.686
5	0	0	1.31	1.78	-0.471
5	1	0	0.08	0.01	0.070
5	1	1	0.30	1.17	-0.864
5	2	0	0.31	0.01	0.299
5	2	1	2.81	1.37	1.438
5	2	2	0.92	0.72	0.200
5	3	0	3.10	2.22	0.882
5	3	1	1.35	0.55	0.801
5	3	2	3.74	2.92	0.814
5	3	3	0.70	1.50	-0.803
5	4	0	5.79	2.00	3.791
5	4	1	3.31	3.41	-0.103
5	4	2	2.93	2.00	0.930
5	4	3	1.29	2.55	-1.251
5	4	4	2.25	1.48	0.769
5	5	0	1.27	2.16	-0.893
5	5	1	4.88	1.41	3.462
5	5	2	7.22	1.95	5.276
5	5	3	3.30	1.25	2.057
5	5	4	3.08	1.21	1.876

Table 4.2(b) (Continued)

H	K	L	IOE	IC	DELTA
5	5	5	-0.54	0.70	-1.232
6	0	0	30.42	31.77	-1.353
6	1	0	18.67	19.72	-1.051
6	1	1	23.38	21.24	2.139
6	2	0	20.81	16.18	4.626
6	2	1	13.49	10.19	3.301
6	2	2	8.56	9.11	-0.553
6	3	0	7.08	5.74	1.343
6	3	1	10.72	6.72	3.995
6	3	2	1.84	3.70	-1.865
6	3	3	7.86	3.04	4.816
6	4	0	6.77	3.81	2.960
6	4	1	7.28	2.67	4.606
6	4	2	3.26	2.70	0.564
6	4	3	-2.18	1.52	-3.696
6	4	4	2.62	1.22	1.397
6	5	0	1.31	1.45	-0.142
6	5	1	-1.37	1.67	-3.043
6	5	2	-0.08	1.18	-1.252
6	5	3	0.80	1.06	-0.264
6	5	4	-1.36	0.67	-2.021
6	5	5	-1.61	0.47	-2.085
6	6	0	-0.70	1.01	-1.708
6	6	1	-3.07	0.84	-3.905
6	6	2	1.47	0.80	0.668
6	6	3	1.92	0.56	1.356
6	6	4	-0.44	0.44	-0.876
7	0	0	-3.23	1.06	-4.290
7	1	0	-1.00	0.22	-1.224
7	1	1	2.04	0.24	1.792
7	2	0	4.40	0.00	4.396
7	2	1	3.61	0.09	3.529
7	2	2	1.28	0.19	1.091
7	3	0	-0.43	0.44	-0.871
7	3	1	0.64	0.33	0.314
7	3	2	-2.74	0.70	-3.439
7	3	3	6.28	0.64	5.632
7	4	0	2.40	0.62	1.779
7	4	1	3.81	0.80	3.005
7	4	2	1.14	0.66	0.471
7	4	3	0.47	0.72	-0.247
7	4	4	1.38	0.51	0.867
7	5	0	0.15	0.71	-0.556
7	5	1	0.08	0.60	-0.521
7	5	2	5.49	0.62	4.868
7	5	3	4.40	0.47	3.933
7	5	4	3.99	0.38	3.610
7	6	0	-2.53	0.44	-2.974
7	6	1	-2.97	0.46	-3.430
7	6	2	2.93	0.38	2.556
8	0	0	8.37	9.62	-1.246
8	1	0	7.58	7.38	0.196
8	1	1	8.95	6.60	2.353
8	2	0	7.16	4.67	2.489
8	2	1	5.19	3.66	1.529

Table 4.2(b) (Continued)

H	K	L	IOE	IC	DELTA
8	2	2	8.29	2.52	5.764
8	3	0	2.56	2.02	0.537
8	3	1	3.77	1.93	1.845
8	3	2	1.09	1.25	-0.152
8	3	3	0.36	0.83	-0.462
8	4	0	3.48	0.99	2.488
8	4	1	4.63	0.84	3.793
8	4	2	-0.39	0.70	-1.086
8	4	3	1.23	0.46	0.774
8	5	0	5.59	0.46	5.137
8	5	1	1.02	0.45	0.563
8	5	2	2.75	0.36	2.387
9	0	0	1.58	0.50	1.085
9	1	0	4.14	0.25	3.893
9	1	1	-2.71	0.15	-2.857
9	2	0	-5.73	0.02	-5.752
9	2	1	-0.29	0.00	-0.290
9	2	2	-0.76	0.02	-0.787
9	3	0	2.79	0.05	2.746
9	3	1	-1.51	0.06	-1.564

Table 4.2(c) $KCaF_3$ Rectangular crystal at 400°C (residual values for harmonic thermal parameters)

THIS IS CYCLE 4 OF SERIES 1 FOR $KCaF_3$ at 400°C

AGREEMENT FACTORS BASED ON PARAMETERS BEFORE CYCLE 4

SUM(IOE) = 1637.121, SUM(IOE-IC) = 268.940, SLMAX = , 0.0000

R = SUM(IOE-IC)/SUM(IOE) = 0.16428, NO. OF REFL. = 118
R (INCLUDING ZERO WEIGHT DATA) = 0.18117, NO. OF REFL. = 129

R = SQRT(SUM(WTG*(IOE-IC)**2)/SUM(WTG*IOE**2)) = 0.17160

SUM(WTG*(IOE-IC)**2) IS 1592.86743
SQRT(SUM(WTG*(IOE-IC)**2/(NO. OF OBSERVATIONS-NO. OF PARAMETERS VARIED)) IS 3.77121

Table 4.3(a) $KcaF_3$ rectangular crystal at 400°C (anharmonic thermal parameters)

ATOMIC PARAMETERS

Ca Atom No. 1 Parameters 10 to 44

	X	Y	Z	G	B11	B22	B33	B12	B13	B23
VALUE	0.000000	0.000000	0.000000	0.020833	0.021110	0.021110	0.021110	0.000000	0.000000	0.000000
E.S.D.	0.000000	0.000000	0.000000	0.000000	0.001478	0.001478	0.001478	0.000000	0.000000	0.000000
	BIJ/(2*PI**2*ASTAR(I)*ASTAR(J))			$**2	0.021258	0.021258	0.021258	0.000000	0.000000	0.000000

10**2*	D1111	D2222	D3333	D1112	D1222	D1113	D1333	D2223	D2333	D1122
VALUE	0.010108	0.010108	0.010108	0.000000	0.000000	0.000000	0.000000	0.000000	0.000000	-0.002945
E.S.D.	0.004601	0.004601	0.004601	0.000000	0.000000	0.000000	0.000000	0.000000	0.000000	0.001470

10**2*	D1133	D2233	D1123	D1223	D1233
VALUE	-0.002945	-0.002945	0.000000	0.000000	0.000000
E.S.D.	0.001470	0.001470	0.000000	0.000000	0.000000

G111 to G123 = 0

Table 4.3(a) (Continued)

ATOMIC PARAMETERS

K Atom No. 2 Parameters 45 to 79

	X	Y	Z	G	B11	B22	B33	B12	B13	B23
VALUE	0.500000	0.500000	0.500000	0.020833	0.060550	0.060550	0.060550	0.000000	0.000000	0.000000
E.S.D.	0.000000	0.000000	0.000000	0.000000	0.002747	0.002747	0.002747	0.000000	0.000000	0.000000
	BIJ/(2*PI**2*ASTAR(I)*ASTAR(J))			$**2	0.060974	0.060974	0.060974	0.000000	0.000000	0.000000

10**2*	D1111	D2222	D3333	D1112	D1222	D1113	D1333	D2223	D2333	D1122
VALUE	0.015873	0.015873	0.015873	0.000000	0.000000	0.000000	0.000000	0.000000	0.000000	-0.013839
E.S.D.	0.015331	0.015331	0.015331	0.000000	0.000000	0.000000	0.000000	0.000000	0.000000	0.005078

10**2*	D1133	D2233	D1123	D1223	D1233
VALUE	-0.013839	-0.013839	0.000000	0.000000	0.000000
E.S.D.	0.005078	0.005078	0.000000	0.000000	0.000000

G111 to G123 = 0

Table 4.3(a) (Continued)

ATOMIC PARAMETERS

F Atom No. 3 Parameters 80 to 114

	X	Y	Z	G	B11	B22	B33	B12	B13	B23
VALUE	0.500000	0.000000	0.000000	0.062500	0.019307	0.113989	0.113989	0.000000	0.000000	0.000000
E.S.D.	0.000000	0.000000	0.000000	0.000000	0.001562	0.002492	0.002492	0.000000	0.000000	0.000000
	BIJ/(2*PI**2*ASTAR(I)*ASTAR(J))			$**2	0.019442	0.114787	0.114787	0.000000	0.000000	0.000000

10**2*	D1111	D2222	D3333	D1112	D1222	D1113	D1333	D2223	D2333	D1122
VALUE	-0.005330	-0.137409	-0.137409	0.000000	0.000000	0.000000	0.000000	0.000000	0.000000	0.000236
E.S.D.	0.004777	0.015772	0.015772	0.000000	0.000000	0.000000	0.000000	0.000000	0.000000	0.002719

10**2*	D1133	D2233	D1123	D1223	D1233
VALUE	0.000236	-0.106464	0.000000	0.000000	0.000000
E.S.D.	0.002719	0.008518	0.000000	0.000000	0.000000

G111 to G123 = 0

Table 4.3(b) $KCaF_3$ rectangular crystal at 400°C
(IOE, IC and Delta values for anharmonic thermal parameters)

H	K	L	IOE	IC	DELTA
1	0	0	33.74	34.06	-0.319
1	1	0	4.67	6.55	-1.791
1	1	1	149.90	134.88	15.023
2	0	0	361.00	386.87	-25.872
2	1	0	36.40	35.25	1.146
2	1	1	26.76	25.45	1.307
2	2	0	227.88	219.97	7.914
2	2	1	32.15	31.96	0.191
2	2	2	118.79	119.01	-0.221
3	0	0	0.00	0.60	-0.604
3	1	0	2.25	2.39	-0.145
3	1	1	21.95	21.85	0.099
3	2	0	2.91	2.63	0.280
3	2	1	10.11	10.50	-0.389
3	2	2	4.13	4.19	-0.056
3	3	0	3.33	2.98	0.350
3	3	1	0.25	0.28	-0.028
3	3	2	7.56	7.51	0.051
3	3	3	2.98	2.70	0.279
4	0	0	106.89	106.69	0.201
4	1	0	31.45	31.95	-0.496
4	1	1	48.76	49.62	-0.855
4	2	0	56.04	57.33	-1.291
4	2	1	20.69	21.75	-1.057
4	2	2	30.49	29.20	1.285
4	3	0	7.73	8.05	-0.273
4	3	1	18.84	19.21	-0.367
4	3	2	6.30	6.05	0.246
4	3	3	10.29	9.24	1.045
4	4	0	13.68	13.19	0.493
4	4	1	8.57	8.14	0.428
4	4	2	6.58	6.62	-0.048
4	4	3	7.34	3.12	4.224
4	4	4	0.00	1.79	-1.788
5	0	0	1.33	1.22	0.110
5	1	0	0.08	0.59	-0.506
5	1	1	0.31	0.24	0.064
5	2	0	0.31	0.00	0.314
5	2	1	2.86	2.55	0.313
5	2	2	0.93	0.48	0.452
5	3	0	3.15	2.65	0.507
5	3	1	1.37	1.63	-0.253
5	3	2	3.80	3.90	-0.101
5	3	3	0.71	3.74	-3.025
5	4	0	5.89	1.92	3.965
5	4	1	3.37	4.60	-1.231
5	4	2	2.98	2.05	0.934
5	4	3	1.32	3.29	-1.977
5	4	4	2.29	1.53	0.755
5	5	0	1.29	2.95	-1.663
5	5	1	4.96	2.81	2.150
5	5	2	7.35	2.78	4.568
5	5	3	3.36	2.50	0.864
5	5	4	3.14	1.48	1.660

Table 4.3(b) (Continued)

H	K	L	IOE	IC	DELTA
5	5	5	-0.55	1.08	-1.626
6	0	0	30.99	31.12	-0.130
6	1	0	19.03	19.25	-0.223
6	1	1	23.89	26.22	-2.336
6	2	0	21.22	17.22	3.994
6	2	1	13.74	11.39	2.350
6	2	2	8.71	9.27	-0.560
6	3	0	7.21	6.84	0.369
6	3	1	10.92	9.37	1.553
6	3	2	1.87	4.16	-2.293
6	3	3	7.99	3.70	4.294
6	4	0	6.89	3.95	2.940
6	4	1	7.40	3.14	4.267
6	4	2	3.32	2.28	1.038
6	4	3	-2.22	1.45	-3.672
6	4	4	2.66	0.79	1.872
6	5	0	1.33	1.87	-0.541
6	5	1	-1.39	2.19	-3.587
6	5	2	-0.08	1.38	-1.460
6	5	3	0.81	1.15	-0.341
6	5	4	-1.38	0.65	-2.028
6	5	5	-1.64	0.43	-2.064
6	6	0	-0.71	1.06	-1.772
6	6	1	-3.12	0.97	-4.094
6	6	2	1.50	0.73	0.771
6	6	3	1.95	0.55	1.405
6	6	4	-0.45	0.31	-0.759
7	0	0	-3.29	0.01	-3.301
7	1	0	-1.02	0.41	-1.427
7	1	1	2.07	0.17	1.901
7	2	0	4.48	0.22	4.252
7	2	1	3.68	1.05	2.632
7	2	2	1.30	0.76	0.546
7	3	0	-0.43	1.44	-1.876
7	3	1	0.65	1.26	-0.605
7	3	2	-2.78	1.74	-4.523
7	3	3	6.38	1.65	4.736
7	4	0	2.44	1.21	1.238
7	4	1	3.87	1.60	2.275
7	4	2	1.16	1.27	-0.111
7	4	3	0.48	1.28	-0.804
7	4	4	1.40	0.82	0.577
7	5	0	0.15	1.33	-1.172
7	5	1	0.08	1.27	-1.183
7	5	2	5.59	1.11	4.471
7	5	3	4.48	0.88	3.597
7	5	4	4.06	0.52	3.539
7	6	0	-2.57	0.75	-3.322
7	6	1	-3.02	0.73	-3.749
7	6	2	2.98	0.59	2.394
8	0	0	8.52	10.05	-1.533
8	1	0	7.71	7.69	0.023
8	1	1	9.11	8.09	1.020
8	2	0	7.29	6.00	1.291
8	2	1	5.28	4.65	0.626

Table 4.3(b) (Continued)

H	K	L	IOE	IC	DELTA
8	2	2	8.43	3.51	4.928
8	3	0	2.61	3.01	-0.407
8	3	1	3.84	3.04	0.801
8	3	2	1.11	1.84	-0.722
8	3	3	0.37	1.21	-0.841
8	4	0	3.54	1.59	1.950
8	4	1	4.71	1.34	3.373
8	4	2	-0.39	1.00	-1.392
8	4	3	1.25	0.63	0.626
8	5	0	5.69	0.79	4.899
8	5	1	1.04	0.75	0.287
8	5	2	2.79	0.55	2.243
9	0	0	1.61	0.41	1.201
9	1	0	4.21	0.63	3.580
9	1	1	-2.76	0.55	-3.311
9	2	0	-5.83	0.62	-6.451
9	2	1	-0.29	0.81	-1.100
9	2	2	-0.78	0.78	-1.558
9	3	0	2.84	0.85	1.922
9	3	1	-1.53	0.80	-2.333

Table 4.3(c) $KCaF_3$ Rectangular crystal at 400°C (residual values for anharmonic thermal parameters)

THIS IS CYCLE 4 OF SERIES 2 FOR $KCaF_3$ at 400°C

AGREEMENT FACTORS BASED ON PARAMETERS BEFORE CYCLE 4

SUM(IOE) = 1717.480, SUM(IOE-IC) = 210.899, SLMAX = , 0.0000

R = SUM(IOE-IC)/SUM(IOE) = 0.12280, NO. OF REFL. = 118
R (INCLUDING ZERO WEIGHT DATA) = 0.13876, NO. OF REFL. = 129

R = SQRT(SUM(WTG*(IOE-IC)**2)/SUM(WTG*IOE**2)) = 0.09551

SUM(WTG*(IOE-IC)**2) IS 493.49585
SQRT(SUM(WTG*(IOE-IC)**2/(NO. OF OBSERVATIONS-NO. OF PARAMETERS VARIED)) IS 2.17834

Table 4.4(a) $KCaF_3$ rectangular crystal at 700°C (harmonic thermal parameters)

ATOMIC PARAMETERS

Ca Atom No. 1 Parameters 10 to 19

	X	Y	Z	G	B11	B22	B33	B12	B13	B23
VALUE	0.000000	0.000000	0.000000	0.020833	0.033175	0.033175	0.033175	0.000000	0.000000	0.000000
E.S.D.	0.000000	0.000000	0.000000	0.000000	0.000800	0.000800	0.000800	0.000000	0.000000	0.000000
	BIJ/(2*PI**2*ASTAR(I)*ASTAR(J))			$**2	0.033407	0.033407	0.033407	0.000000	0.000000	0.000000

K Atom No. 2 Parameters 20 to 29

	X	Y	Z	G	B11	B22	B33	B12	B13	B23
VALUE	0.500000	0.500000	0.500000	0.020833	0.092299	0.092299	0.092299	0.000000	0.000000	0.000000
E.S.D.	0.000000	0.000000	0.000000	0.000000	0.002417	0.002417	0.002417	0.000000	0.000000	0.000000
	BIJ/(2*PI**2*ASTAR(I)*ASTAR(J))			$**2	0.092945	0.092945	0.092945	0.000000	0.000000	0.000000

F Atom No. 3 Parameters 30 to 39

	X	Y	Z	G	B11	B22	B33	B12	B13	B23
VALUE	0.500000	0.000000	0.000000	0.062500	0.026932	0.148909	0.148909	0.000000	0.000000	0.000000
E.S.D.	0.000000	0.000000	0.000000	0.000000	0.000923	0.002582	0.002582	0.000000	0.000000	0.000000
	BIJ/(2*PI**2*ASTAR(I)*ASTAR(J))			$**2	0.027121	0.149951	0.149951	0.000000	0.000000	0.000000

Table 4.4(b) $KCaF_3$ rectangular crystal at 700°C
(IOE, IC and Delta values for harmonic thermal parameters)

H	K	L	IOE	IC	DELTA
1	0	0	32.48	31.33	1.156
1	0	0	32.31	31.33	0.986
0	1	0	33.99	31.33	2.663
0	0	1	29.53	31.33	-1.797
2	0	0	312.17	329.98	-17.810
2	0	0	313.22	329.98	-16.759
0	2	0	337.98	329.98	7.997
-2	0	0	312.31	329.98	-17.668
0	-2	0	334.24	329.98	4.266
0	0	2	300.15	329.98	-29.827
2	2	0	178.52	165.00	13.526
0	2	2	174.45	165.00	9.450
2	0	2	175.36	165.00	10.361
-2	-2	0	177.76	165.00	12.767
-2	2	0	177.34	165.00	12.343
1	1	0	4.59	5.68	-1.086
1	1	1	130.01	113.11	16.898
2	1	0	34.55	34.09	0.462
2	1	1	22.64	21.99	0.655
2	2	1	27.92	26.71	1.207
2	2	2	83.20	83.61	-0.407
3	0	0	0.16	0.29	-0.129
3	1	0	1.16	1.00	0.156
3	1	1	14.55	13.84	0.715
3	2	0	3.27	3.12	0.156
3	2	1	6.06	5.49	0.579
3	2	2	3.74	4.55	-0.805
3	3	0	1.56	2.15	-0.586
3	3	1	0.07	0.17	-0.100
3	3	2	3.81	3.67	0.134
3	3	3	2.02	0.61	1.406
4	0	0	71.69	71.36	0.330
4	1	0	24.42	26.25	-1.824
4	1	1	28.79	27.60	1.191
4	2	0	35.09	34.71	0.386
4	2	1	15.40	14.26	1.142
4	2	2	16.48	18.05	-1.565
4	3	0	5.90	6.04	-0.141
4	3	1	8.97	7.55	1.419
4	3	2	3.85	4.18	-0.330
4	3	3	4.37	3.18	1.181
4	4	0	7.22	6.84	0.379
4	4	1	4.39	4.00	0.387
4	4	2	2.96	4.14	-1.187
4	4	3	5.59	1.72	3.866
4	4	4	-0.86	1.29	-2.149
5	0	0	0.45	0.71	-0.260
5	1	0	-0.47	0.01	-0.483
5	1	1	0.25	0.46	-0.210
5	2	0	0.19	0.05	0.141
5	2	1	0.68	0.50	0.177
5	2	2	-0.65	0.52	-1.167
5	3	0	0.25	0.85	-0.601
5	3	1	0.89	0.37	0.516

Table 4.4(b) (Continued)

H	K	L	IOE	IC	DELTA
5	3	2	0.79	1.12	-0.329
5	3	3	-0.20	0.73	-0.926
5	4	0	4.59	1.02	3.569
5	4	1	2.56	1.27	1.290
5	4	2	1.01	0.91	0.100
5	4	3	0.43	0.83	-0.403
5	4	4	1.31	0.51	0.799
5	5	0	-0.70	0.69	-1.392
5	5	1	1.37	0.56	0.814
5	5	2	4.24	0.59	3.653
5	5	3	0.52	0.41	0.114
5	5	4	0.34	0.30	0.040
5	5	5	0.45	0.16	0.293
6	0	0	14.41	14.56	-0.142
6	1	0	9.18	9.98	-0.798
6	1	1	9.75	9.29	0.463
6	2	0	10.90	6.83	4.073
6	2	1	8.98	4.83	4.146
6	2	2	2.46	3.53	-1.075
6	3	0	3.13	2.53	0.600
6	3	1	4.48	2.49	1.994
6	3	2	-0.93	1.51	-2.442
6	3	3	4.83	0.96	3.869
6	4	0	3.95	1.26	2.694
6	4	1	4.66	1.00	3.657
6	4	2	1.69	0.82	0.869
6	4	3	-1.01	0.47	-1.485
6	4	4	1.87	0.29	1.579
6	5	0	0.27	0.45	-0.185
6	5	1	-0.36	0.45	-0.812
6	5	2	-0.33	0.34	-0.669
6	5	3	0.85	0.25	0.601
6	5	4	0.73	0.15	0.582
6	5	5	-2.84	0.08	-2.916
6	6	0	-0.49	0.23	-0.718
6	6	1	-1.94	0.20	-2.137
6	6	2	0.25	0.17	0.086
6	6	3	2.01	0.11	1.895
6	6	4	0.79	0.07	0.717
7	0	0	-0.90	0.34	-1.237
7	1	0	-2.62	0.11	-2.732
7	1	1	-0.69	0.07	-0.756
7	2	0	2.81	0.00	2.815
7	2	1	3.47	0.02	3.456
7	2	2	0.04	0.07	-0.026
7	3	0	-0.74	0.11	-0.855
7	3	1	0.53	0.11	0.420
7	3	2	-0.96	0.18	-1.139
7	3	3	-0.82	0.17	-0.999
7	4	0	-1.89	0.18	-2.069
7	4	1	0.55	0.19	0.353
7	4	2	0.97	0.17	0.800
7	4	3	-0.01	0.15	-0.157
7	4	4	0.72	0.10	0.616
7	5	0	0.74	0.15	0.590

Table 4.4(b) (Continued)

H	K	L	IOE	IC	DELTA
7	5	1	0.25	0.14	0.108
7	5	2	0.67	0.12	0.547
7	5	3	1.63	0.09	1.545
7	5	4	1.12	0.06	1.058
7	6	0	-2.79	0.08	-2.869
7	6	1	-2.93	0.08	-3.005
7	6	2	1.21	0.06	1.144
8	0	0	0.67	2.58	-1.910
8	1	0	1.11	2.04	-0.926
8	1	1	3.75	1.70	2.047
8	2	0	2.29	1.16	1.134
8	2	1	2.08	0.94	1.138
8	2	2	0.63	0.58	0.050
8	3	0	0.79	0.48	0.310
8	3	1	0.79	0.42	0.366
8	3	2	0.26	0.27	-0.010
8	3	3	1.31	0.15	1.154
8	4	0	1.53	0.19	1.336
8	4	1	1.15	0.17	0.977
8	4	2	-1.16	0.13	-1.286
8	4	3	0.90	0.08	0.825
8	5	0	-0.65	0.08	-0.732
8	5	1	1.84	0.07	1.763
8	5	2	4.08	0.06	4.028
9	0	0	2.63	0.09	2.539
9	1	0	1.00	0.05	0.951
9	1	1	-0.34	0.03	-0.371
9	2	0	-0.57	0.00	-0.574
9	2	1	-1.41	0.00	-1.412
9	2	2	-0.31	0.00	-0.315
9	3	0	1.02	0.01	1.009
9	3	1	2.27	0.01	2.263

Table 4.4(c) $KCaF_3$ Rectangular crystal at 700°C (residual values for harmonic thermal parameters)

THIS IS CYCLE 4 OF SERIES 13 FOR $KCaF_3$ at 700°C

AGREEMENT FACTORS BASED ON PARAMETERS BEFORE CYCLE 4

SUM(IOE) = 3618.035, SUM(IOE-IC) = 279.713, SLMAX = , 0.0000

R = SUM(IOE-IC)/SUM(IOE) = 0.07731, NO. OF REFL. = 130
R (INCLUDING ZERO WEIGHT DATA) = 0.08692, NO. OF REFL. = 141

R = SQRT(SUM(WTG*(IOE-IC)**2)/SUM(WTG*IOE**2)) = 0.13884

SUM(WTG*(IOE-IC)**2) IS 1712.77466
SQRT(SUM(WTG*(IOE-IC)**2/(NO. OF OBSERVATIONS-NO. OF PARAMETERS VARIED)) IS 3.71654

Table 4.5(a) $KCaF_3$ rectangular crystal at 700°C (anharmonic thermal parameters)

ATOMIC PARAMETERS

Ca Atom No. 1 Parameters 10 to 44

	X	Y	Z	G	B11	B22	B33	B12	B13	B23
VALUE	0.000000	0.000000	0.000000	0.020833	0.031612	0.031612	0.031612	0.000000	0.000000	0.000000
E.S.D.	0.000000	0.000000	0.000000	0.000000	0.001649	0.001649	0.001649	0.000000	0.000000	0.000000
	BIJ/(2*PI**2*ASTAR(I)*ASTAR(J))			$**2	0.031833	0.031833	0.031833	0.000000	0.000000	0.000000

10**2*	D1111	D2222	D3333	D1112	D1222	D1113	D1333	D2223	D2333	D1122
VALUE	0.007967	0.007967	0.007967	0.000000	0.000000	0.000000	0.000000	0.000000	0.000000	-0.000588
E.S.D.	0.006565	0.006565	0.006565	0.000000	0.000000	0.000000	0.000000	0.000000	0.000000	0.002105

10**2*	D1133	D2233	D1123	D1223	D1233
VALUE	-0.000588	-0.000588	0.000000	0.000000	0.000000
E.S.D.	0.002105	0.002105	0.000000	0.000000	0.000000

G111 to G123 = 0

Table 4.5(a) (Continued)

ATOMIC PARAMETERS

K Atom No. 2 Parameters 45 to 79

	X	Y	Z	G	B11	B22	B33	B12	B13	B23
VALUE	0.500000	0.500000	0.500000	0.020833	0.089347	0.089347	0.089347	0.000000	0.000000	0.000000
E.S.D.	0.000000	0.000000	0.000000	0.000000	0.004172	0.004172	0.004172	0.000000	0.000000	0.000000
	BIJ/(2*PI**2*ASTAR(I)*ASTAR(J))			$**2	0.089972	0.089972	0.089972	0.000000	0.000000	0.000000

10**2*	D1111	D2222	D3333	D1112	D1222	D1113	D1333	D2223	D2333	D1122
VALUE	0.050113	0.050113	0.050113	0.000000	0.000000	0.000000	0.000000	0.000000	0.000000	-0.017970
E.S.D.	0.036409	0.036409	0.036409	0.000000	0.000000	0.000000	0.000000	0.000000	0.000000	0.008831

10**2*	D1133	D2233	D1123	D1223	D1233
VALUE	-0.017970	-0.017970	0.000000	0.000000	0.000000
E.S.D.	0.008831	0.008831	0.000000	0.000000	0.000000

G111 to G123 = 0

Table 4.5(a) (Continued)

ATOMIC PARAMETERS

F Atom No. 3 Parameters 80 to 114

	X	Y	Z	G	B11	B22	B33	B12	B13	B23
VALUE	0.500000	0.000000	0.000000	0.062500	0.026590	0.130719	0.130719	0.000000	0.000000	0.000000
E.S.D.	0.000000	0.000000	0.000000	0.000000	0.001641	0.003067	0.003067	0.000000	0.000000	0.000000
	BIJ/(2*PI**2*ASTAR(I)*ASTAR(J))			$**2	0.026776	0.131633	0.131633	0.000000	0.000000	0.000000

10**2*	D1111	D2222	D3333	D1112	D1222	D1113	D1333	D2223	D2333	D1122
VALUE	-0.010695	-0.102315	-0.102315	0.000000	0.000000	0.000000	0.000000	0.000000	0.000000	-0.000105
E.S.D.	0.006001	0.022362	0.022362	0.000000	0.000000	0.000000	0.000000	0.000000	0.000000	0.003354

10**2*	D1133	D2233	D1123	D1223	D1233
VALUE	-0.000105	-0.097521	0.000000	0.000000	0.000000
E.S.D.	0.003354	0.009730	0.000000	0.000000	0.000000

G111 to G123 = 0

Table 4.5(b) $KCaF_3$ rectangular crystal at 700°C
(IOE, IC and Delta values for anharmonic thermal parameters)

H	K	L	IOE	IC	DELTA
1	0	0	33.77	33.18	0.583
1	0	0	33.59	33.18	0.407
0	1	0	35.23	33.18	2.049
0	0	1	30.61	33.18	-2.571
2	0	0	332.18	346.26	-14.072
2	0	0	333.30	346.26	-12.954
0	2	0	356.29	346.26	10.036
-2	0	0	332.34	346.26	-13.921
0	-2	0	352.36	346.26	6.103
0	0	2	316.54	346.26	-29.718
2	2	0	186.23	176.34	9.893
0	2	2	181.68	176.34	5.341
2	0	2	183.52	176.34	7.182
-2	-2	0	185.44	176.34	9.101
-2	2	0	185.02	176.34	8.683
1	1	0	4.74	5.62	-0.880
1	1	1	136.89	120.80	16.096
2	1	0	35.73	34.40	1.331
2	1	1	23.37	21.25	2.121
2	2	1	28.91	29.39	-0.484
2	2	2	86.34	85.87	0.461
3	0	0	0.17	0.59	-0.421
3	1	0	1.20	1.12	0.080
3	1	1	15.04	15.04	-0.004
3	2	0	3.37	2.80	0.575
3	2	1	6.26	6.33	-0.067
3	2	2	3.86	4.10	-0.242
3	3	0	1.61	1.54	0.069
3	3	1	0.07	0.04	0.034
3	3	2	3.93	4.05	-0.120
3	3	3	2.08	1.90	0.181
4	0	0	74.23	74.68	-0.449
4	1	0	25.21	25.59	-0.387
4	1	1	29.79	31.54	-1.754
4	2	0	36.29	36.20	0.091
4	2	1	15.91	15.83	0.080
4	2	2	17.00	16.97	0.028
4	3	0	6.09	5.96	0.130
4	3	1	9.26	9.77	-0.510
4	3	2	3.97	4.18	-0.205
4	3	3	4.50	4.14	0.367
4	4	0	7.45	6.79	0.655
4	4	1	4.53	4.72	-0.192
4	4	2	3.05	3.36	-0.316
4	4	3	5.77	1.74	4.025
4	4	4	-0.89	0.92	-1.812
5	0	0	0.46	0.56	-0.096
5	1	0	-0.49	0.10	-0.588
5	1	1	0.26	0.14	0.110
5	2	0	0.20	0.03	0.168
5	2	1	0.70	1.01	-0.311
5	2	2	-0.67	0.51	-1.171
5	3	0	0.25	1.13	-0.872
5	3	1	0.92	0.87	0.044

Table 4.5(b) (Continued)

H	K	L	IOE	IC	DELTA
5	3	2	0.81	1.67	-0.860
5	3	3	-0.21	1.63	-1.838
5	4	0	4.73	1.14	3.593
5	4	1	2.64	1.83	0.810
5	4	2	1.05	1.10	-0.058
5	4	3	0.44	1.24	-0.800
5	4	4	1.35	0.66	0.689
5	5	0	-0.72	1.06	-1.782
5	5	1	1.41	1.04	0.372
5	5	2	4.38	0.97	3.404
5	5	3	0.54	0.81	-0.279
5	5	4	0.35	0.48	-0.134
5	5	5	0.47	0.30	0.167
6	0	0	14.87	14.55	0.322
6	1	0	9.47	9.54	-0.068
6	1	1	10.07	10.83	-0.763
6	2	0	11.25	7.36	3.888
6	2	1	9.26	5.16	4.100
6	2	2	2.54	3.71	-1.178
6	3	0	3.23	2.91	0.320
6	3	1	4.62	3.29	1.336
6	3	2	-0.96	1.68	-2.648
6	3	3	4.98	1.21	3.769
6	4	0	4.08	1.46	2.615
6	4	1	4.80	1.21	3.592
6	4	2	1.74	0.86	0.888
6	4	3	-1.04	0.54	-1.584
6	4	4	1.93	0.31	1.621
6	5	0	0.28	0.64	-0.362
6	5	1	-0.37	0.67	-1.041
6	5	2	-0.34	0.46	-0.808
6	5	3	0.87	0.36	0.518
6	5	4	0.75	0.21	0.542
6	5	5	-2.92	0.13	-3.054
6	6	0	-0.51	0.32	-0.829
6	6	1	-2.00	0.29	-2.290
6	6	2	0.26	0.23	0.031
6	6	3	2.07	0.17	1.906
6	6	4	0.81	0.10	0.709
7	0	0	-0.93	0.00	-0.930
7	1	0	-2.70	0.08	-2.788
7	1	1	-0.71	0.06	-0.767
7	2	0	2.90	0.11	2.791
7	2	1	3.58	0.30	3.277
7	2	2	0.05	0.31	-0.263
7	3	0	-0.77	0.42	-1.188
7	3	1	0.55	0.40	0.144
7	3	2	-0.99	0.51	-1.502
7	3	3	-0.85	0.47	-1.316
7	4	0	-1.95	0.38	-2.336
7	4	1	0.56	0.45	0.117
7	4	2	1.00	0.38	0.624
7	4	3	-0.01	0.34	-0.344
7	4	4	0.74	0.21	0.528
7	5	0	0.76	0.33	0.437

Table 4.5(b) (Continued)

H	K	L	IOE	IC	DELTA
7	5	1	0.25	0.31	-0.056
7	5	2	0.69	0.27	0.420
7	5	3	1.69	0.20	1.483
7	5	4	1.15	0.13	1.027
7	6	0	-2.87	0.17	-3.043
7	6	1	-3.02	0.16	-3.182
7	6	2	1.25	0.13	1.113
8	0	0	0.69	2.15	-1.464
8	1	0	1.15	1.70	-0.558
8	1	1	3.87	1.64	2.227
8	2	0	2.37	1.21	1.153
8	2	1	2.14	0.97	1.172
8	2	2	0.65	0.68	-0.030
8	3	0	0.82	0.61	0.212
8	3	1	0.82	0.57	0.247
8	3	2	0.27	0.36	-0.087
8	3	3	1.35	0.23	1.124
8	4	0	1.58	0.30	1.274
8	4	1	1.18	0.26	0.922
8	4	2	-1.20	0.19	-1.390
8	4	3	0.93	0.12	0.807
8	5	0	-0.67	0.15	-0.822
8	5	1	1.89	0.14	1.755
8	5	2	4.21	0.10	4.108
9	0	0	2.72	0.14	2.581
9	1	0	1.03	0.16	0.876
9	1	1	-0.35	0.15	-0.503
9	2	0	-0.59	0.15	-0.738
9	2	1	-1.46	0.17	-1.622
9	2	2	-0.32	0.16	-0.478
9	3	0	1.05	0.15	0.896
9	3	1	2.34	0.15	2.196

Table 4.5(c) $KCaF_3$ Rectangular crystal at 700°C (residual values for anharmonic thermal parameters)

THIS IS CYCLE 4 OF SERIES 12 FOR $KCaF_3$ at 700°C

AGREEMENT FACTORS BASED ON PARAMETERS BEFORE CYCLE 4

SUM(IOE) = 3800.339, SUM(IOE-IC) = 245.463, SLMAX = , 0.0000

R = SUM(IOE-IC)/SUM(IOE) = 0.06459, NO. OF REFL. = 130
R (INCLUDING ZERO WEIGHT DATA) = 0.07373, NO. OF REFL. = 141

R = SQRT(SUM(WTG*(IOE-IC)**2)/SUM(WTG*IOE**2)) = 0.09587

SUM(WTG*(IOE-IC)**2) IS 816.67444
SQRT(SUM(WTG*(IOE-IC)**2/(NO. OF OBSERVATIONS-NO. OF PARAMETERS VARIED)) IS 2.65336

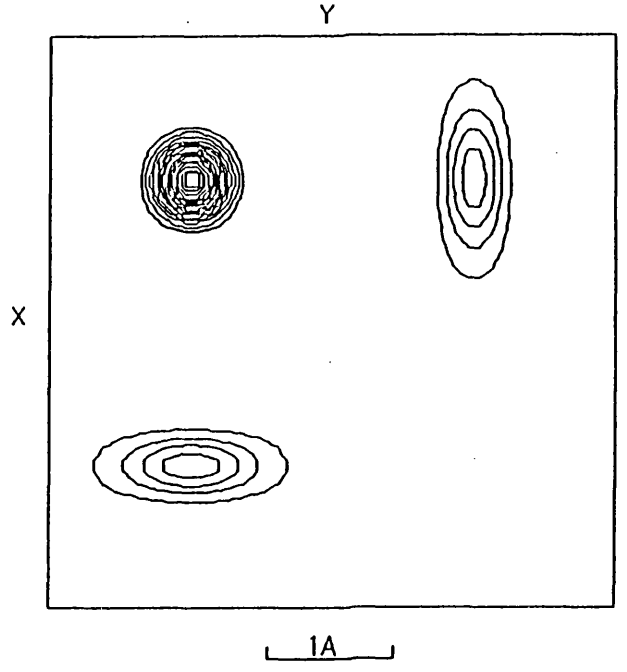

CONTOURS
2
6
10
14
18
22
26
30
34
38
42
46
50
54
58
62

FOURIER SECTION AT	0	ON	0	0	1
X parallel to	1	0	0	from −0.25	to 0.75
Y parallel to	0	1	0	from −0.25	to 0.75
Coefficients are FCALC multiplied by 1					
and averaged over a cube of edge 0.05					

FIG. 4.4(a): $KCaF_3$ 400°C harmonic

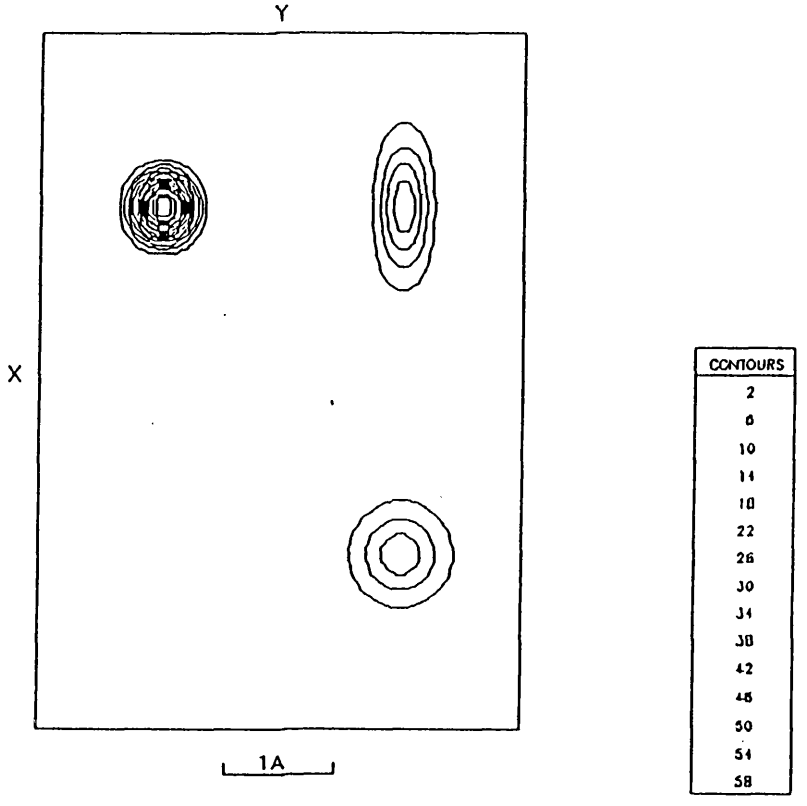

FOURIER SECTION AT	0	ON	-1	1	0
X parallel to	1	1	0	from −0.25	to 0.75
Y parallel to	0	0	1	from −0.25	to 0.75
Coefficients are FCALC mulliplied by 1					
and averaged over a cube of edge 0.05					

FIG. 4.4 (b): $KCaF_3$ 400°C Harmonic

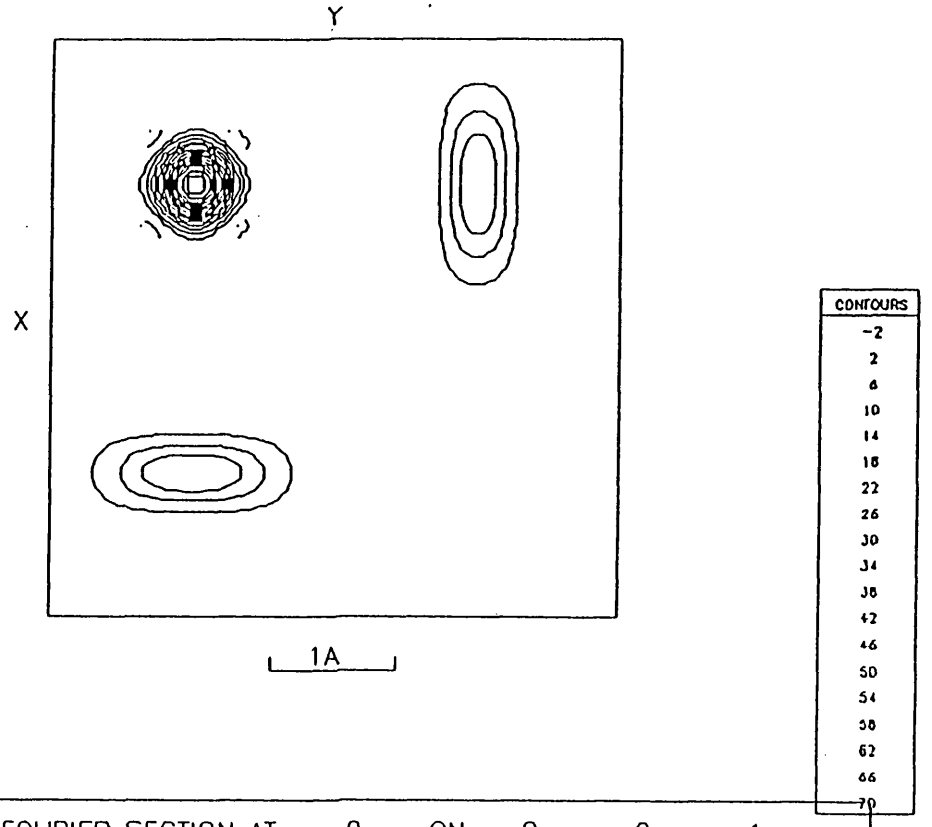

FOURIER SECTION AT	0	ON	0	0	1
X parallel to	1	0	0	from −0.25	to 0.75
Y parallel to	0	1	0	from −0.25	to 0.75
Coefficients are FCALC multiplied by 1					
and averaged over a cube of edge 0.05					

FIG. 4.4 (c): $KCaF_3$ 400°C Anharmonic

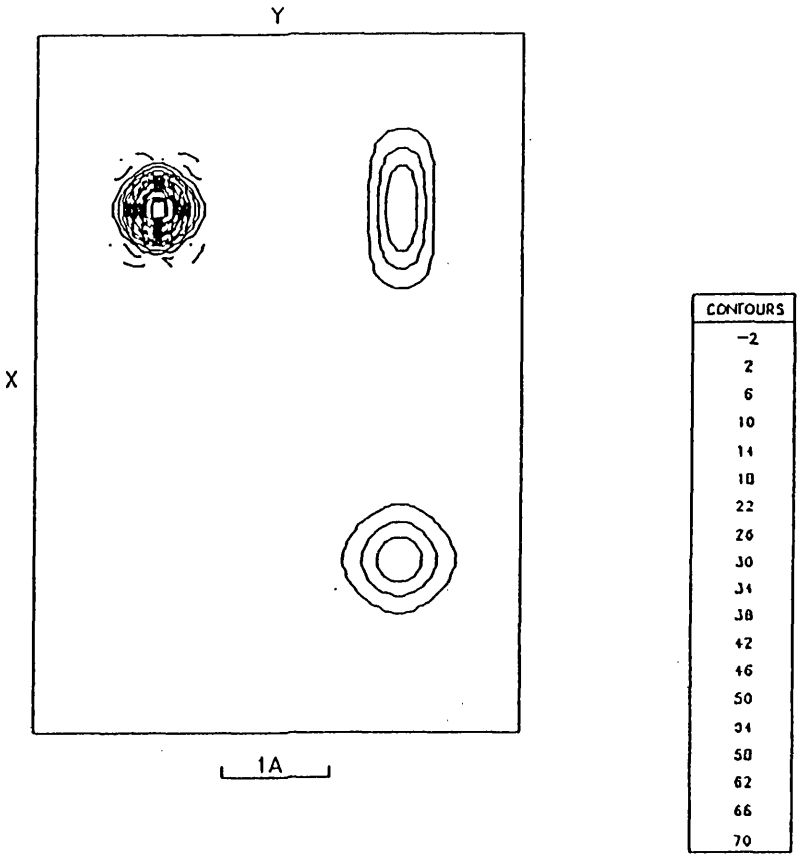

FOURIER SECTION AT	0	ON	-1	1	0
X parallel to	1	1	0	from -0.25	to 0.75
Y parallel to	0	0	1	from -0.25	to 0.75
Coefficients are FCALC multiplied by 1					
and averaged over a cube of edge 0.05					

FIG. 4.4 (d): $KCaF_3$ 400°C Anharmonic

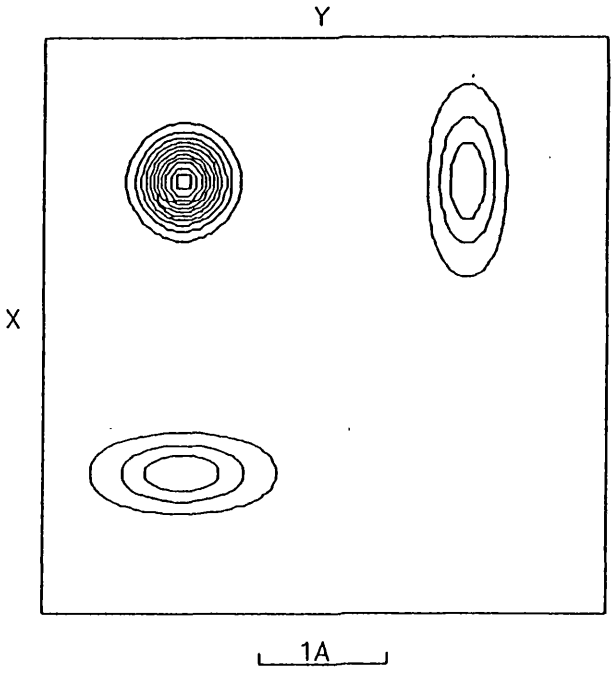

CONTOURS
2
6
10
14
18
22
26
30
34
38
42

FOURIER SECTION AT	0	ON	0	0	1
X parallel to	1	0	0	from −0.25	to 0.75
Y parallel to	0	1	0	from −0.25	to 0.75
Coefficients are FCALC multiplied by 1					
and averaged over a cube of edge 0.05					

FIG 4.5 (a): $KCaF_3$ 700^{o}C Harmonic

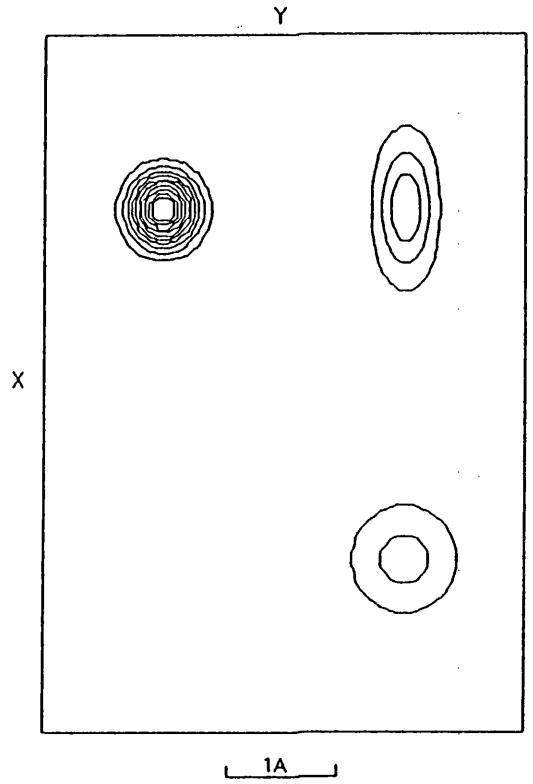

CONTOURS
2
6
10
14
18
22
26
30
34
38

FOURIER SECTION AT	0	ON	-1	1	0
X parallel to	1	1	0	from -0.25	to 0.75
Y parallel to	0	0	1	from -0.25	to 0.75
Coefficients are FCALC multiplied by 1 and averaged over a cube of edge 0.05					

FIG. 4.5 (b): $KCaF_3$ 700°C Harmonic

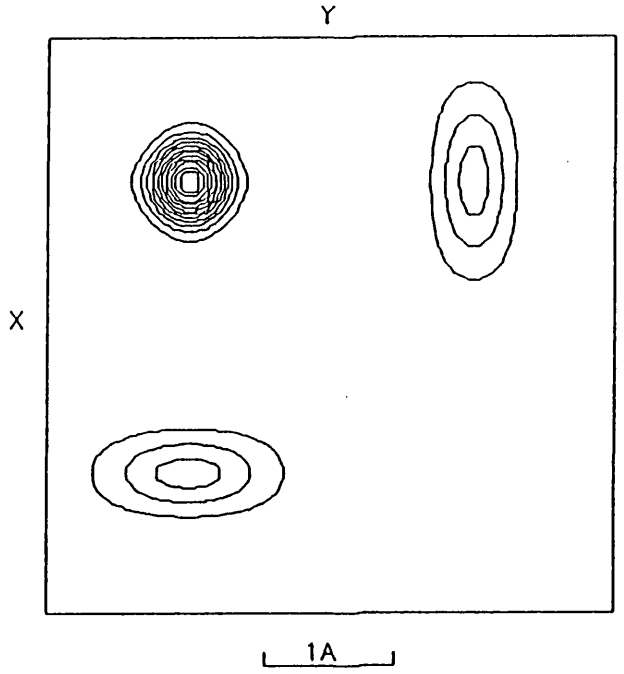

CONTOURS
2
6
10
14
18
22
26
30
34
38
42
46

FOURIER SECTION AT	0	ON	0	0	1
X parallel to	1	0	0	from −0.25	to 0.75
Y parallel to	0	1	0	from −0.25	to 0.75
Coefficients are FCALC multiplied by 1					
and averaged over a cube of edge 0.05					

FIG. 4.5 (c): $KCaF_3$ 700°C Anharmonic

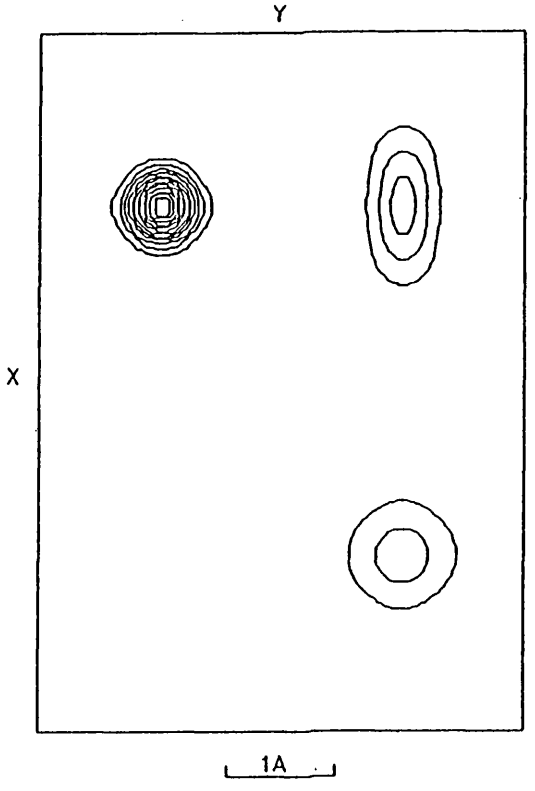

CONTOURS
2
6
10
14
18
22
26
30
34
38
42
46

FOURIER SECTION AT	0	ON	−1	1	0
X parallel to	1	1	0	from −0.25	to 0.75
Y parallel to	0	0	1	from −0.25	to 0.75
Coefficients are FCALC multiplied by 1					
and averaged over a cube of edge 0.05					

FIG. 4.5 (d): $KCaF_3$ 700°C Anharmonic

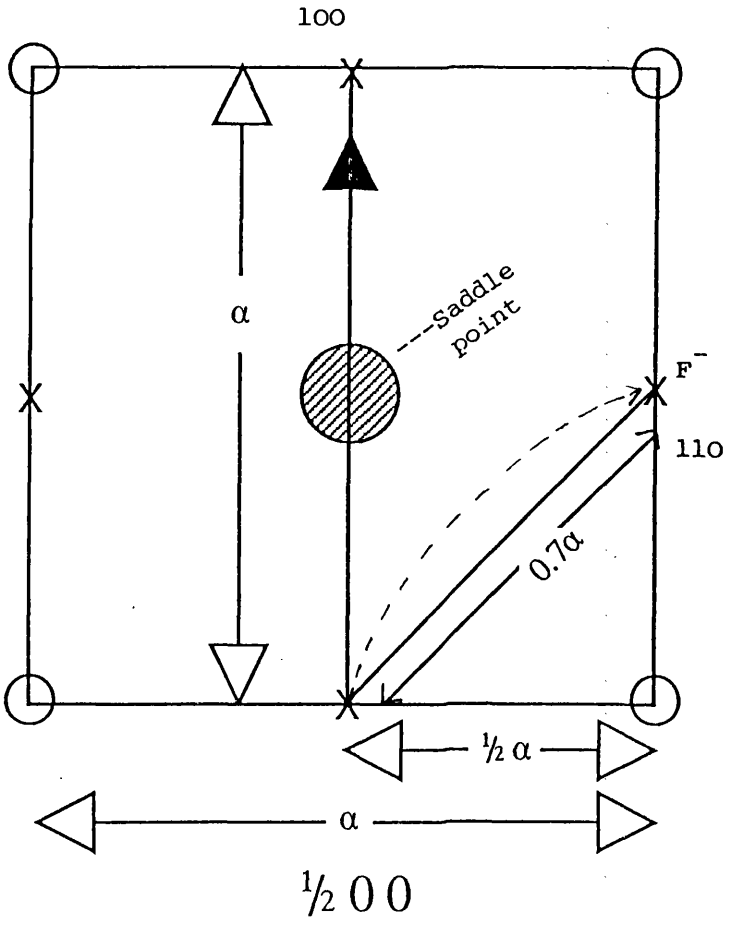

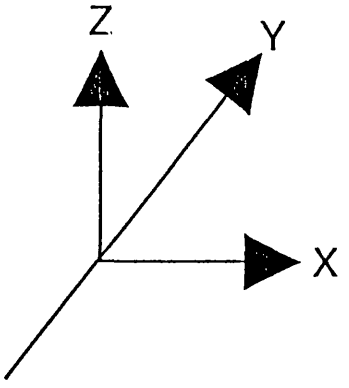

= K^+

= Ca^{2+}

X = F^-

Major axis of oblate ellipsoid is in zy plane (011) direction

FIG. 4.6: Possible vacancy mechanisms for F^- migration

CHAPTER 5

THE ELPASOLITES: $A_2^{+1}B^{+1}RE^{+3}X_6^{-1}$

5.1 Introduction

The elpasolites represent a huge group of compounds, not only halides, but also oxides, sulfides, nitrates, and cyanides. In this chapter however only halides will be considered. These materials, which are known to be good fluoride ion conductors [57] are of general formula A_2BReX_6 (where A and B are monovalent ions and Re is a rare earth cation) with a perovskite related structure. Several members of this class of materials are known to undergo a number of phase transitions involving distortion of the ReX_6 octahedra. The majority of the compounds A_2BReF_6 and A_2BReCl_6 crystallise with the elpasolite structure, space group O^5_h [58]. Only a very few insulating rare-earth compounds with cubic point symmetry are known (mainly spinels and divalent fluorites RF_2) and the present isostructural series provides a basis for the systematic study of the effect of changing the rare-earth ion. The symmetry is the same as in previously examined rock-salt structures for which physical phenomena associated with crystal field effects have been very satisfactorily explained using simple theoretical models. There have been several recent studies of the crystallographic [58-62], optical [63,64], magnetic [65-67], and spectroscopic [68,69], properties of these classes of compounds.

The main theme of this chapter is concerned with the structural studies of several members of the A_2BReX_6 system which have been investigated by High Resolution X-ray Diffraction using the synchrotron radiation source at the Daresbury Laboratory.

5.2 Structural Considerations

The structural family of the elpasolites as a whole can neither be classified by structure field maps nor by Goldschmidt's tolerance factor t', both based on ionic radii [156]. For each class, say Cs_2BReCl_6, and Rb_2BReCl_6 and Cs_2BReBr_6, respectively, one would have to evaluate the tolerance factor ranges, which makes the concept difficult to handle and rather impractical, see Fig. 5.1.

The mineral elpasolite, K_2NaAlF_6, named after El Paso, Texas, was originally said to crystallize in the cubic space group Pa3 [157]. More recent work on synthetic K_2NaAlF_6 [158] could not establish any deviations from the symmetry of the cubic face-centred space group Fm3m. The crystal structure, see Fig. 5.2 may be understood as a substitutional variant of the cubic perovskite. According to

$$2A^{+1}RE^{+2}X_3 = A_2^{+1}RE_2^{+2}X_6 = A_2^{+1}B^{+1}RE^{+3}X_6$$

The divalent cations in the octahedral interstices are substituted in an ordered way by half monovalent and half trivalent cations of nearly equal size. The character of a close-packed structure remains although the repeat

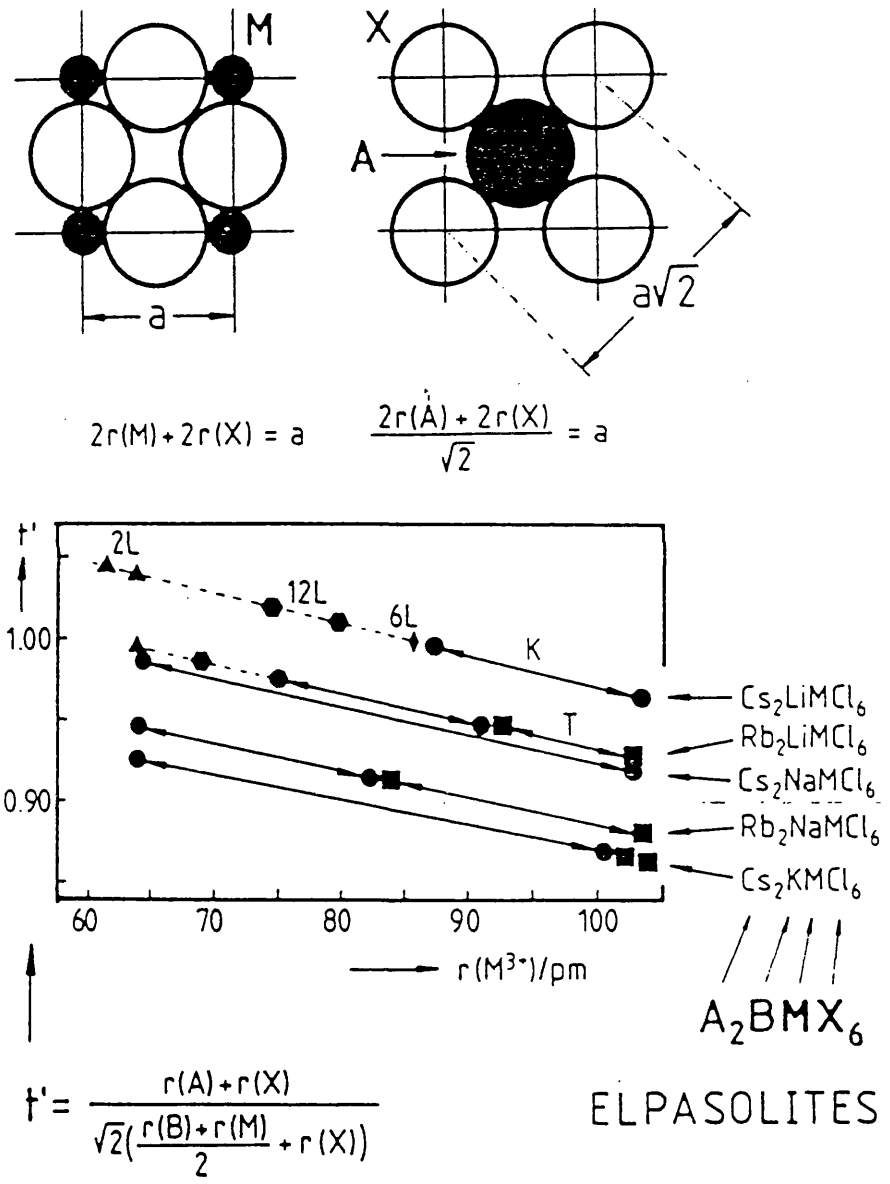

FIG. 5.1: The derivation of Goldschmidt's tolerance factor t' (above) and its (useless) application to chloro-epasolites

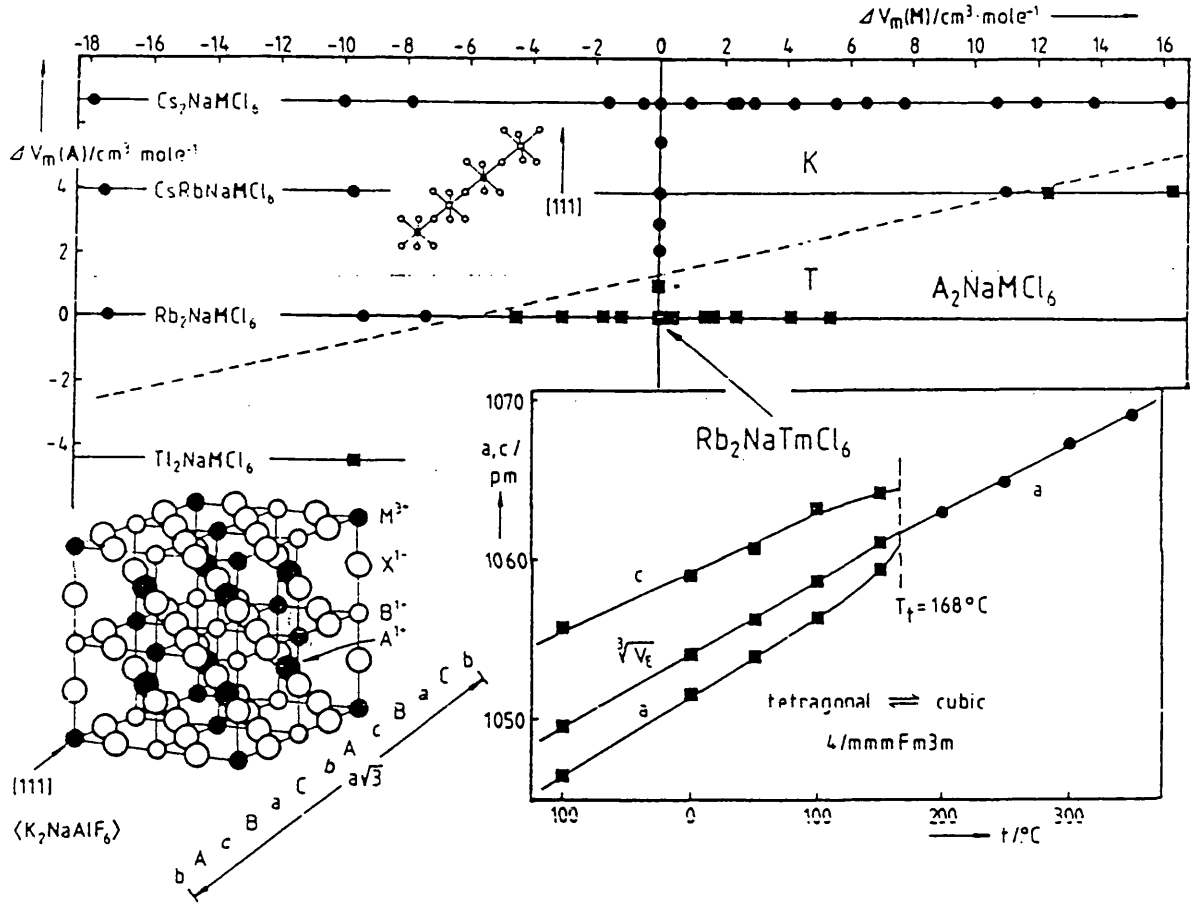

FIG. 5.2: A Structure Field Map for A_2NaMCl_6 compounds (M= RE, In), above. For the crystal structure of the cubic face-centered (K) and tetragonally distorted (T) elpasolites see lower left. For thermal expansion of $Rb_2NaTmCl_6$ see lower right.

distance has to be doubled. Cubic stacking of AX_3 layers takes place in the [111] direction and the sequence is as indicated in Fig. 5.2. All cations are in special positions, there is only one free structural parameter, $X(X^-) \approx 0.25$, that adjusts to the 'sizes' of the B^+ and RE^{3+} cations. There are many known cubic face-centred elpasolites, and halides of this type have appeared in the literature [159]

As is the case with the perovskites, variants of lower symmetry occur depending upon composition, temperature, and pressure. One phase transition that is frequently observed reduces the symmetry of the cubic face-centred aristotype (paraelastic phase) to a presumably tetragonal hettotype (ferroelastic phase) [160]. For $Cs_2NaRECl_6$ compounds the transition temperatures were found to be rather low. Splittings of epr fine-structure lines were observed for $Gd^{3+}:Cs_2NaLaCl_6$ and $Gd^{3+}:Cs_2NaPrCl_6$ between room temperature and 77K, but not for $Gd^{3+}:Cs_2NaYCl_6$ [161]. Conclusions that were drawn from these experiments are : the phase transitions are 'small' and reversible, a centre of inversion is preserved at the rare-earth site, the relative size of the trivalent ion seems to be the determining factor whether or not a phase transition is observed. This view is supported by the transition temperature as far as they were determined: 158K for $Cs_2NaPrCl_6$ and 138K for $Cs_2NaNdCl_6$ [162]. As is shown in Fig. 5.3 the transition temperature for bromo-elpasolites

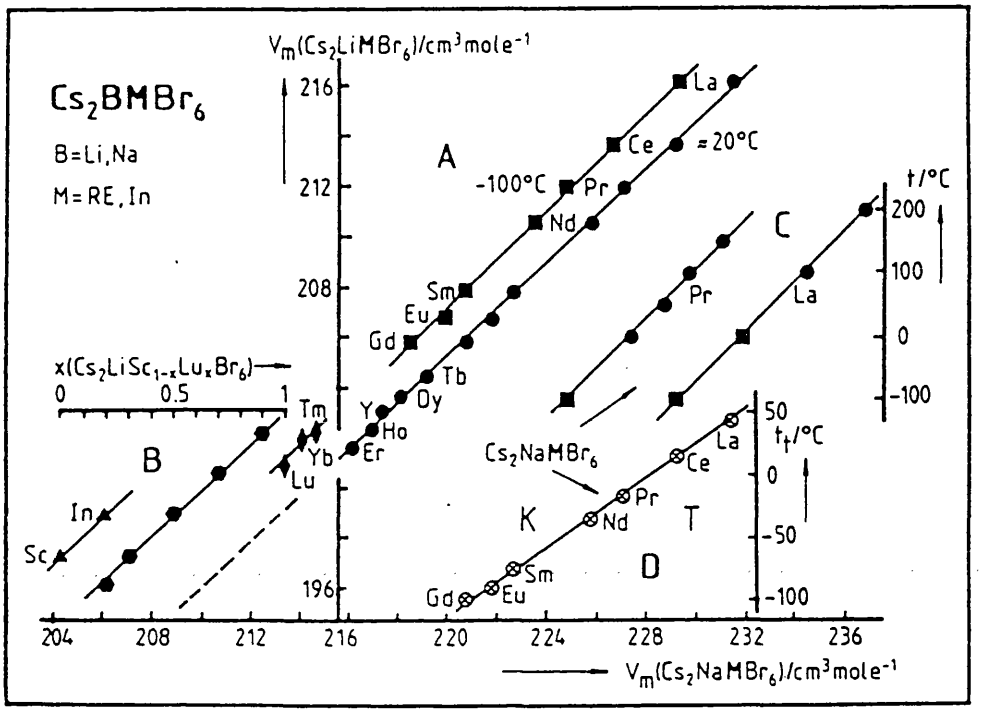

FIG. 5.3: Relationships between the molar volumes V_m of Cs_2NaMBr_6 (M= RE,In) and those of cubic (filled circles, part A; filled squares represent $V_m(Cs_2NaMBr_6)$ at -100°C) and hexagonal (part B, ◆: 6 L, ⬢: 12 L, ▲: 2 L type structures) Cs_2LiMBr_6 compounds. Part C: temperature dependence of the molar volumes of $Cs_2NaPrBr_6$ and $Cs_2NaLaBr_6$ (●: cubic, ■: tetragonal). Part D: dependence of the transition temperature t_t (cubic to tetragonal) upon the respective molar volume of Cs_2NaMBr_6

$Cs_2NaREBr_6$ [163] is strongly dependent upon the size of the trivalent rare-earth ion, which is represented by the molar volume of the respective compounds: the transition temperature decreases rapidly from +43°C ($Cs_2NaLaBr_6$) to -100°C ($Cs_2NaGdBr_6$). There are also examples for transitions above room temperature: 168°C for $Rb_2NaTmCl_6$ [160], see Fig.5.2; and 110°C for Cs_2NaErI_6 [164]. For $Rb_2NaTmCl_6$ no evidence was found that would demand a crystal system of lower symmetry than tetragonal [160]. Powder patterns of this material show only a few line splittings and one very weak extra line, which is consistent with tetragonal symmetry. Difference reflections on single crystal exposures correspond to a unit cell of size almost equal to that of the cubic aristotype, and the space group is found to be P4/nbm [160]. The paraelastic-ferroelastic character of the phase transition causes severe strain in the crystals, which usually gives rise to multiple twinning. However, the space group and the transition order remain contradictory: the low temperature space group of $Cs_2NaPrCl_6$ was said to be 14/mmm and the transition of first order [162]. From epr spectra and optical spectroscopy of the doped elpasolites mentioned above, it seems to be likely that 14/m would be more appropriate [161].

Investigation of thermal expansion in the -100 to +350°C range yielded expansion coefficients of $\alpha_{11}=4.78\times10^{-5}\ K^{-1}$ and $\alpha_{33}=3.51\times10^{-5}\ K^{-1}$ for tetragonal $Rb_2NaTmCl_6$-I and

$\alpha_{11}=3.83\times10^{-5}$ K^{-1} for the isotropic $Rb_2NaTmCl_6$-II. As no volume discontinuity could be detected (see Fig.5.2) at the transition point, the transition is presumably of second order.

Those compounds that crystallize tetragonally at ambient temperature are included in the literature [159]. The structure field map for $A_2NaRECl_6$ compounds as shown in Fig.5.2 indicates the cubic to tetragonal border. To summarize: chloro-elpasolites become tetragonal when A^+ is sufficiently small, and RE^{3+} and B^+ sufficiently large. The results as described for $Rb_2NaTmCl_6$ make it clear that the tetragonal to cubic border is very sensitive to temperature and, in an inverse manner, to static pressure. Higher temperatures favour the cubic aristotype and the border is moved eg. in the $A_2NaRECl_6$ map to the 'south-east'.

On the other hand, the stability of the cubic elpasolite type is limited when B^+ and RE^{3+} become too small or in turn A^+ and/or X^- too large and polarizable. Three stacking variants have been observed for the fluorides HT-K_2LiAlF_6 [165], Cs_2NaCrF_6 and Cs_2LiGaF_6 [166]. Whereas the elpasolite exhibits all octahedra corner-sharing, the latter, the Cs_2LiGaF_6 type is determined by all $[BX_6]$ and $[REX_6]$ octahedra sharing common faces which leads to infinite chains of face-sharing octahedra in the [00.1] direction with voids occupied alternatively by B^+ and RE^{3+}.

As a consequence, the molar volume is some 3% larger than expected by extrapolation of linear relations of commensurate series of compounds, eg. from a plot of the molar volumes of $Cs_2LiREBr_6$ against $Cs_2NaREBr_6$ (see Fig.5.3).

The K_2NaAlF_6 and Cs_2LiGaF_6 types may be understood as polymorphs. Direct phase transitions between these two are not known and are not likely because two stacking variants or polytypes occur between these polymorphs. These stacking variants have one third hexagonal/two thirds cubic stacking (HT-K_2LiAlF_6 or 6L type [165] and equal parts of hexagonal and cubic stacking (Cs_2NaCrF_6 or 12L type [166].

Increases in molar volumes as compared with the K_2NaAlF_6 type are around 1 and 2% respectively. The principal parts of the four structure types are compared which differ in the stacking sequences of AX_3 'layers' and are shown in Fig.5.4.

Strictly speaking all A_2BREX_6 compounds belong to the group of nesohalides, ie. they do not have a secondary structure. Therefore the only way to a structural classification is obtained by using field maps. Two more are shown in Figs.5.4 and 5.5 for the compounds $A_2LiRECl_6$ and Cs_2NaREX_6, respectively. The first one contains the five structure types to be considered here and makes it

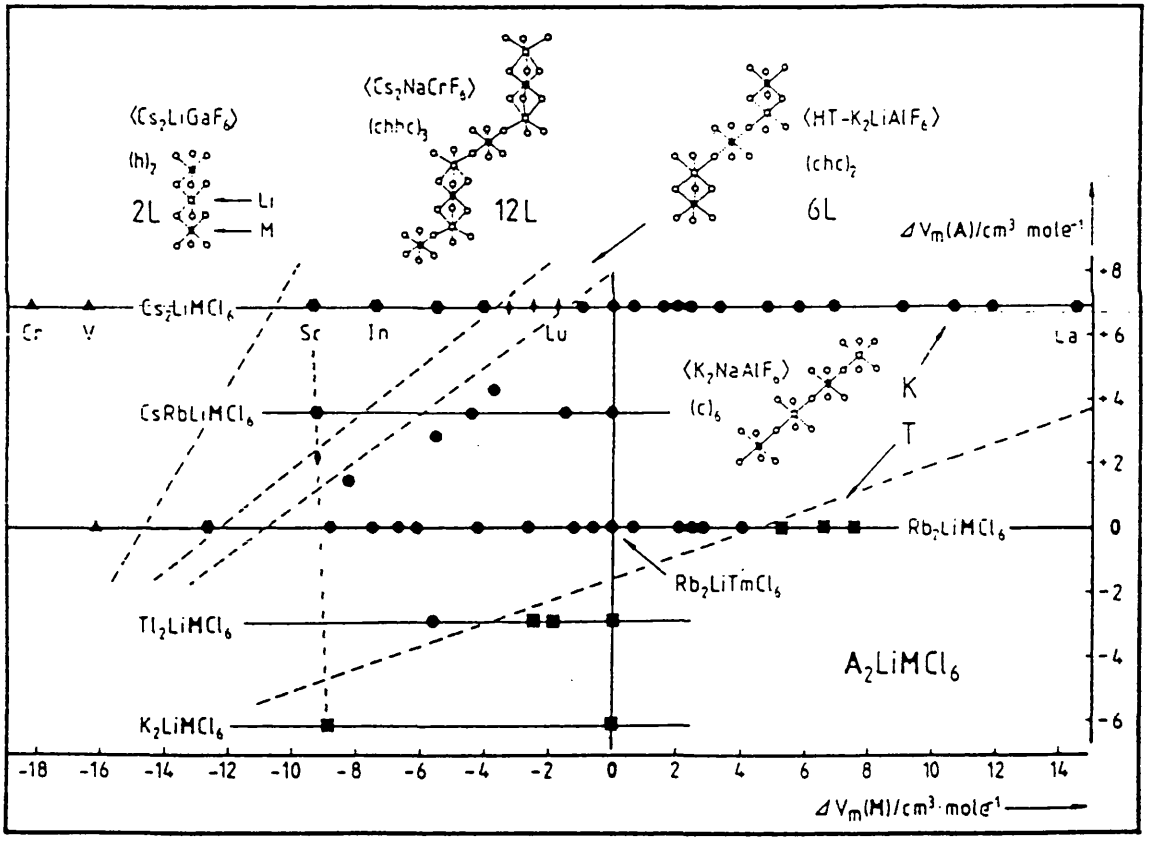

FIG. 5.4: Structure Field Map for A_2LiMCl_6 compounds (M= RE, Cr,V,In) together with structural details for the four stacking variants observed for elpasolites

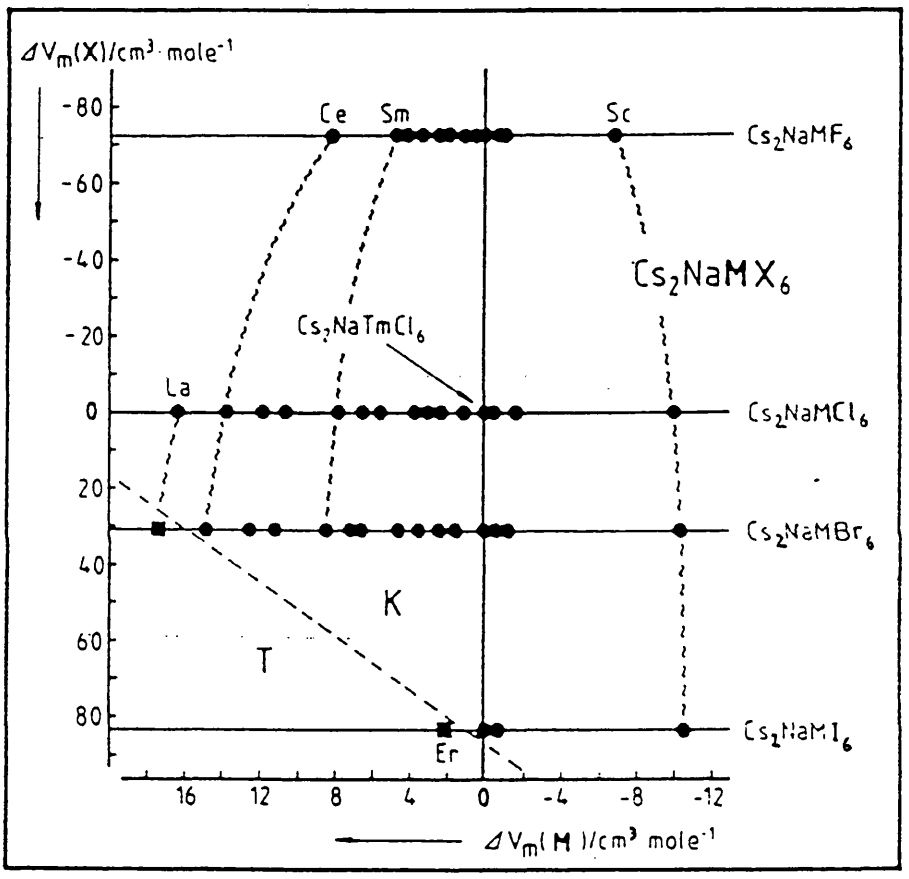

FIG. 5.5: Structure Field Map for Cs_2NaREX_6 compounds showing the effect of polarizability on differences in molar volumes especially when proceeding from fluorides to the heavier halides (M ≡ RE)

clear that the structure types 6L and 12L are not very stable intermediates. Especially the stability range of the 6L type is very small. The latter map combines halides of all kinds and it shows that fluorides are not much affected by the actual 'size' of the RE^{3+} ion as are increasingly chlorides, bromides, and iodides. Clearly, this is due to the ascending polarizability in that order.

Phase transitions from the cubic elpasolite to the so-called hexagonal elpasolites have been observed. These, and their pressure and temperature dependence, have been described in some detail by Babel [167] for the respective transition and post-transition metal containing compounds. With rare earths, transitions were observed for $Cs_2LiErBr_6$ as well as for solid solutions $Cs_2LiTm_{1-x}Er_xBr_6$, $Cs_2Li_{1-y}Na_yTmBr_6$, and for $Cs_2LiYbCl_6$ (all cubic to 6L) [168].6L to 12L transitions were observed within the $Cs_2LiSc_{1-x}Yb_xCl_6$ system [169].

Note that it is always the modification with the higher expected molar volume that occurs as the high-temperature polymorph. A series of phase transitions which is puzzling was established for $Cs_2LiLuCl_6$ [170]: two modifications occur with two transitions in the solid state below the melting point (675°C). At ambient temperature $Cs_2LiLuCl_6$ crystallizes with the 6L type, named $Cs_2LiLuCl_6$-I,L. At about 325°C a reversible 6L to cubic phase transition occurs which is surprising in that

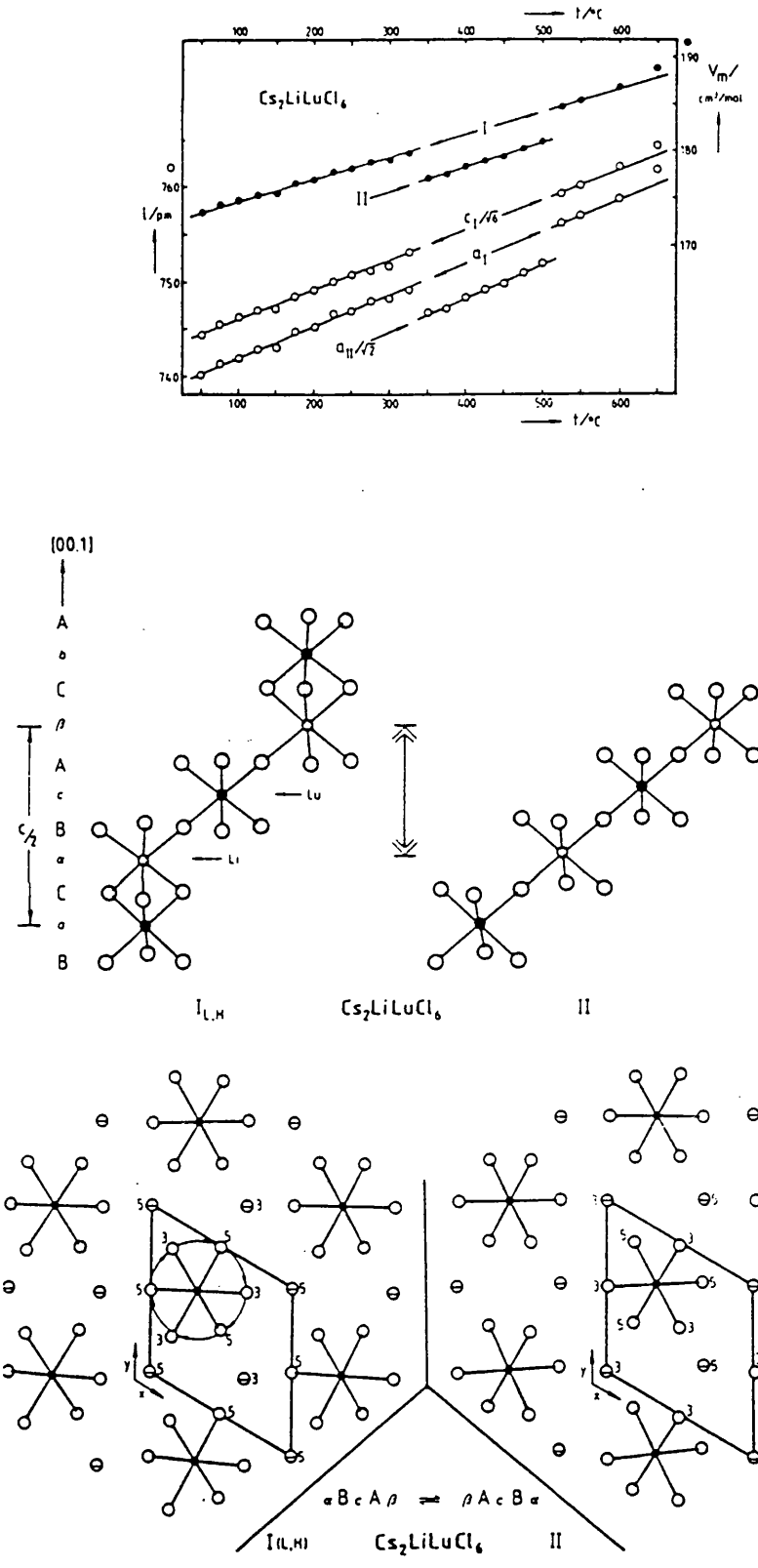

FIG.5.6: The enigmatic structural phase transitions in $Cs_2LiLuCl_6$: a) lattice constants and molar volume vs. temperature; b) characteristic structural features of $Cs_2LiLuCl_6$-I,L and -I,H (both 6 L type) and -II (cubic face-centered); c) a proposed rotational mechanism of the phase transitions

the molar volume shows a sharp decrease (see Fig.5.6). The transition temperature is strongly dependent upon the actual conditions such as heating or cooling rates and also what is called the 'history of the sample'. The cubic to 6L transition shows a tendency to supercool so that upon rapid cooling the cubic modification, named $Cs_2LiLuCl_6$-II, may be retained in a metastable form for some days. The transition is of first order and a simple model is shown schematically in Fig.5.6.60° rotations take place within the close-packed $CsCl_3$ layers with [00.1] as rotation axis. The double layer BA in ..aC∝BcAβCbAγBa.. ($Cs_2LiLuCl_6$-I, a,b,c represent Lu^{3+}, ∝,β,γ Li^+ with the same x,y - coordinates as Cs^+ in the respective layers A,B,C) undergoes a concerted rotation to AB which yields ..aCβAcB∝CbAγBa.., ie the cubic stacking in $Cs_2LiLuCl_6$-II. The Lu^{3+} positions remain unchanged, the Li^+ positions ∝ and β rotate to β and ∝ respectively. Note that for a better comparison shifts in origin were made in [00.1] direction compared to the usual descriptions for the stacking sequences. At about 510°C a second phase transition from cubic back to 6L is observed with a positive volume discontinuity. This is the 'normal' high-temperature transition that one would expect and which is in fact observed for the adjacent $Cs_2LiYbCl_6$, although at a slightly higher transition temperature (580°C)[171], attesting to the higher stability of the cubic phase with increasing size of the RE^{3+} cation.

5.3 Preparation of A_2BRECl_6 Compounds

A_2BRECl_6 compounds have been prepared by many workers using a variety of straightforward techniques [172]. Most commonly these compounds are synthesised by reacting the three chloride compounds according to the equation:

$$2ACl+BCl+RECl_3 \rightarrow A_2BRECl_6$$

The chlorides were added to a small quantity of HCl and the solution was evaporated to dryness using electrical heating. The solid or crystalline elpasolites were thus obtained. In this work, the following elpasolite compounds were prepared:

$Cs_2AgNdCl_6$	K
$Cs_2NaNdCl_6$	K
Cs_2KNdCl_6	K
$Rb_2NaErCl_6$	T

where K = cubic face- centred K_2NaAlF_6 type;

T = tetragonal, isotypic with $Rb_2NaTmCl_6$

The compounds were characterized by High Resolution X-rays using the High Resolution 9.1 powder diffractometer at SRS Daresbury.

5.4 Results and Discussion

Plots of the data are shown in Figures 5.7(a), (b), (c) and (d) respectively.

Looking carefully at all the patterns it can be seen that High Resolution X-ray diffraction demonstrates a great complexity in all cases. This is due to the multiphase present in all the compounds. Rietvield analysis [111] was attempted but the minority phases could not be identified. Apart from the multiphase difficulty there is also a problem due to small traces of unreacted materials e.g. alkali-halides and the rare-earth halides. The only solution to this problem will be the preparation of single crystals of the elpasolites using a melt growth method [145]. The growth process should zone-refine the material to produce a portion of pure elpasolite. This, however, would require a considerable amount of work as the growth conditions would have to be determined for each of the different materials. Future work should take this approach. However, due to the time involved, the studies would have to concentrate on one particular elpasolite. Experiments can be performed on both fluoride and chloride members of this class at several temperatures, including the high temperature superionic region.

In addition <u>elpasolite fluorides</u> $A_2A'CF_3$ (A,A' = alkali metals, C = trivalent metal) can be investigated in terms of transport phenomena but this is not the concern of this thesis. The work therefore performed in this chapter provides a basis for the further systematic investigation of these systems.

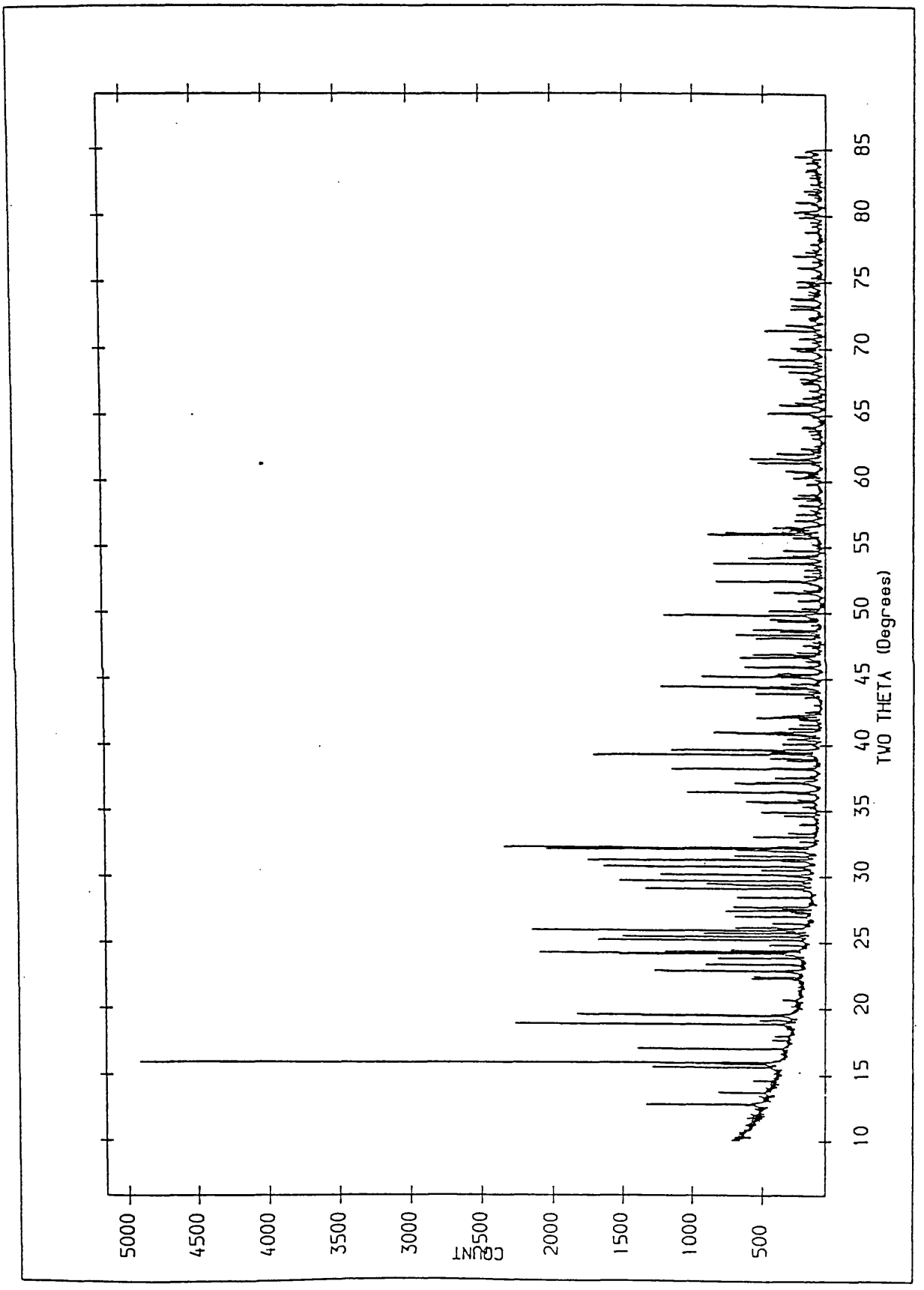

FIG. 5.7(a) Elpasolite $Cs_2AgNdCl_6$

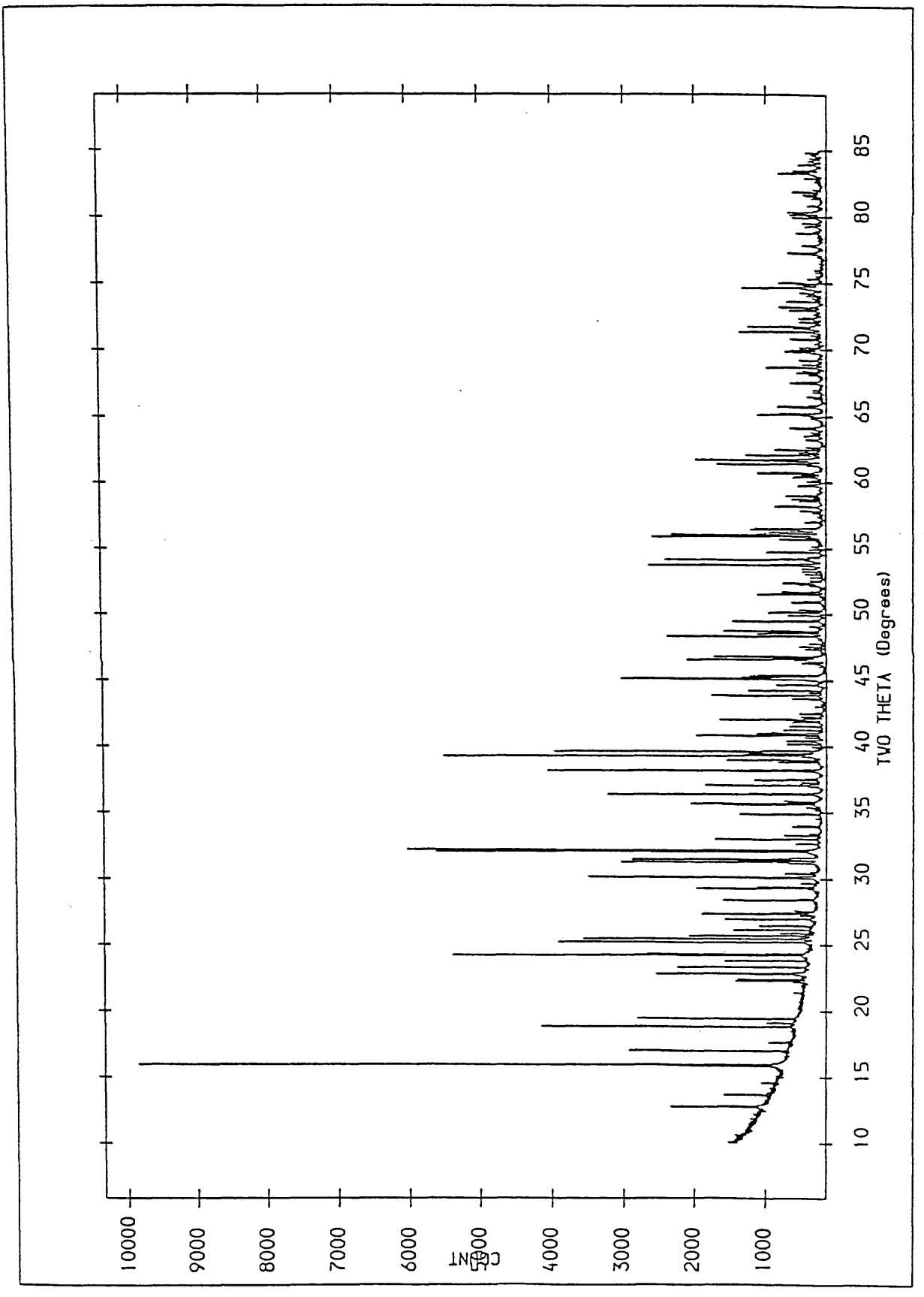

FIG. 5.7(b) Elpasolite $Cs_2NaNdCl_6$

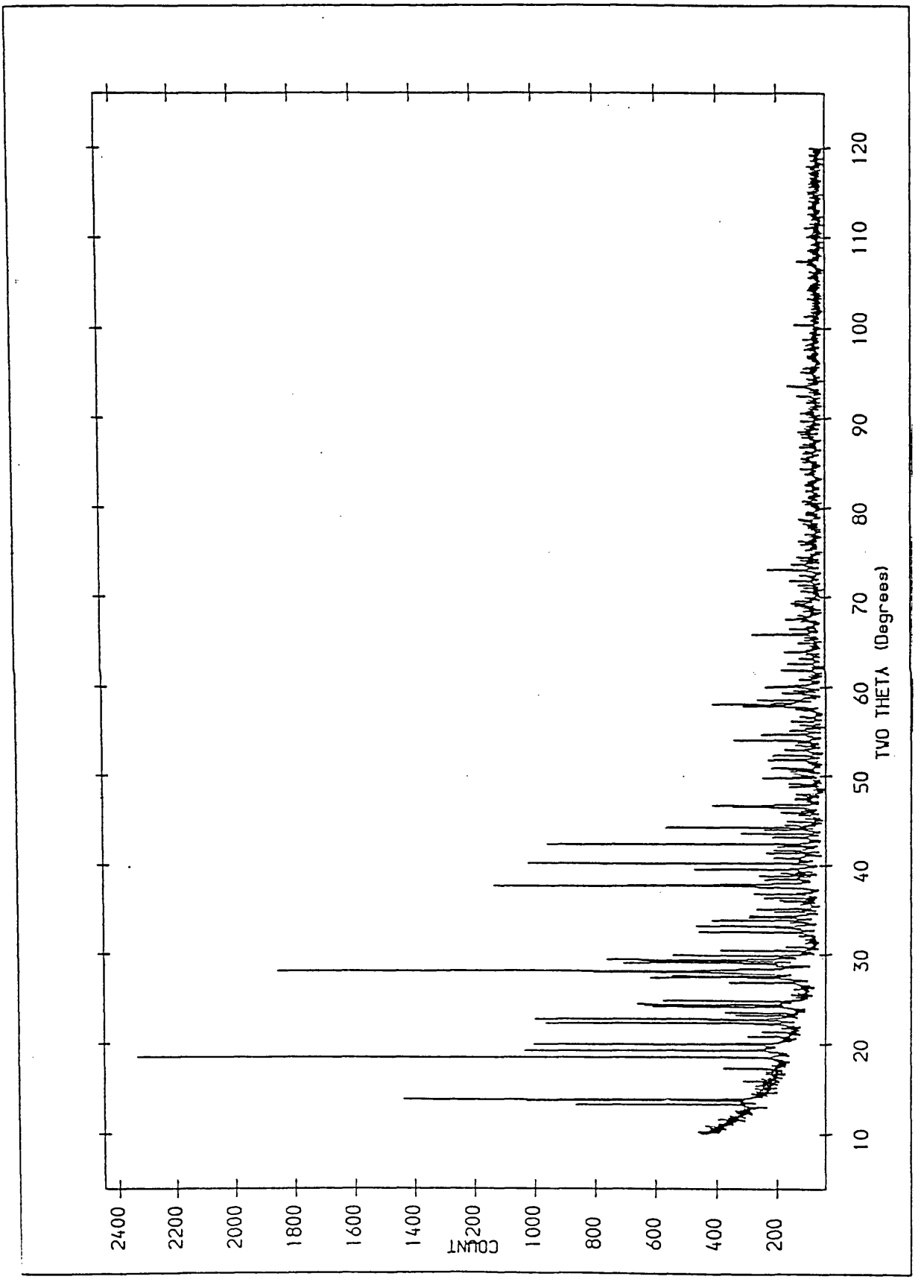

FIG. 5.7(c): Elpasolite Cs_2KNdCl_6

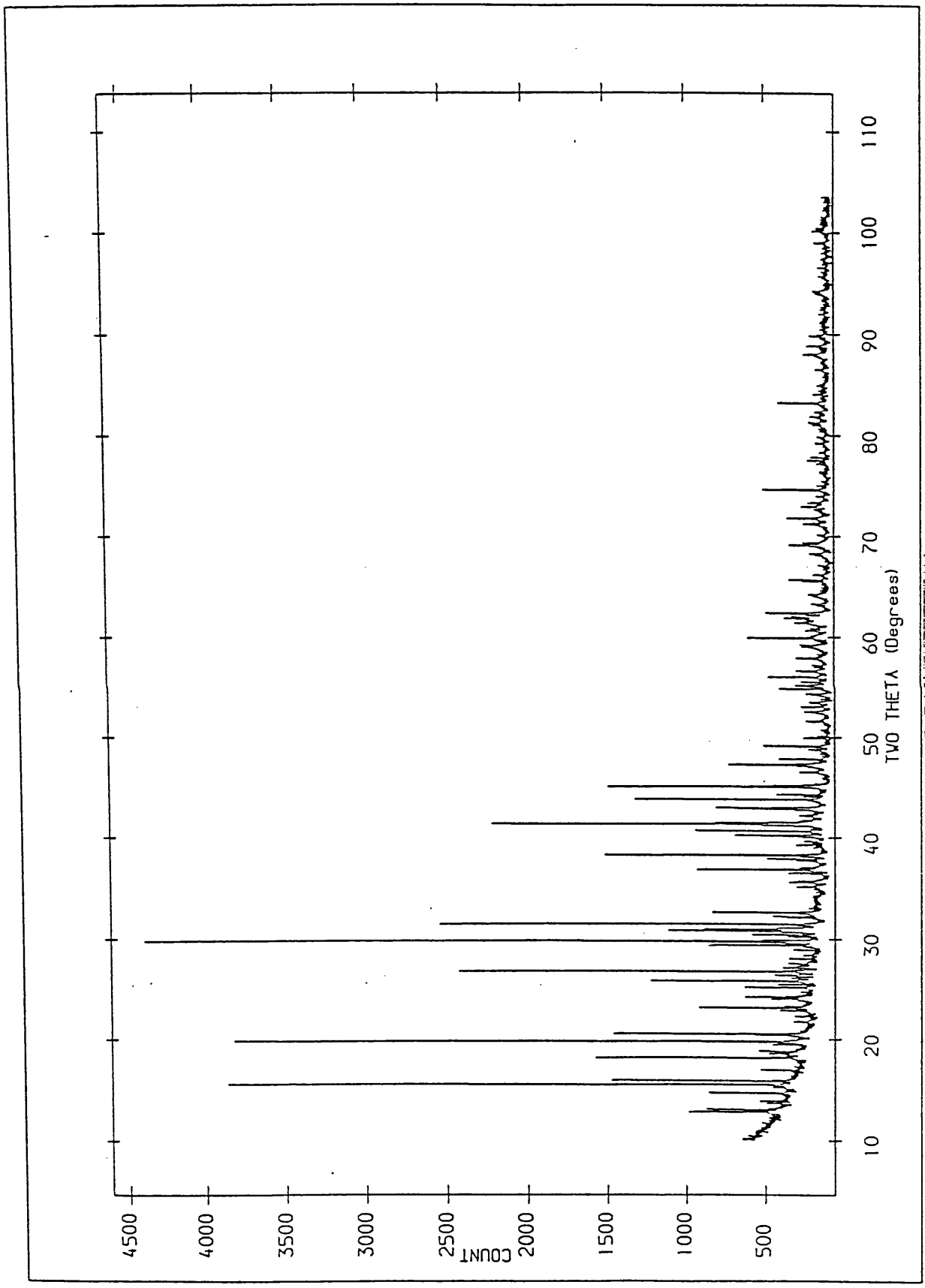

FIG. 5.7(d) Elpasolite $Rb_2NaErCl_6$

CHAPTER 6

CONCLUSION AND SUGGESTIONS FOR FURTHER WORK

In this thesis the structural properties of solid ionic halides and in particular several classes of fluorite structured materials have been investigated. The systems studied include: rare-earth fluorides and the anion excess alkaline earth fluorides, perovskite and elpasolite structured halides.

The work involved in Chapter 3 of this thesis determines the effects of ageing (investigated by annealing samples at high temperatures for variable times) and dopant ion radius on the defect structures of the solid solutions of composition 95-50 mole per cent CaF_2 - $(Ln)F_3$ where Ln = La, Er and Nd. The prepared and annealed compounds were characterised by X-ray powder diffraction. The results show that:

(i) In the CaF_2/LaF_3 system new compounds may be present in the region of 90-80 mole% CaF_2 and 65-55 mole% CaF_2. The stick diagrams of these two regions Fig 3.3(b) confirm that prolonged annealing clearly shows ion and vacancy movements. It can also be seen that annealing initially decreases the symmetry, perhaps by domain formation although the final annealing product i.e. the three-week annealed compounds, again has

a relatively simple cubic structure. In general a minor phase seems to have been formed. Therefore for future work it is worthwhile investigating these two regions even further by undertaking a High Resolution X-ray diffraction study.

(ii) In the CaF_2/ErF_3 system a new compound may be present in the 65-55 mole% CaF_2 region. The stick diagrams of this region Fig 3.3(c) show that prolonged annealing produces new phases within the lattice. In this case however we are not dealing with a simple tetragonal distortion of the lattice but with a possible orthorhombic or even domain formation of a new phase. Again for future work the 65-55 mole% CaF_2 region is worth investigating further.

(iii) In the CaF_2/NdF_3 system a new compound is not clearly evident. Prolonged annealing of three possible compounds namely 85, 75 and 65% mole% CaF_2 was undertaken. The stick diagrams Fig 3.3(d) show that annealing has made things more complicated with either a new phase or more domains of impurities. For this reason further investigation of this system by High Resolution X-ray diffraction is required.

It is also worthwhile mentioning that the results in this

chapter are consistent with radius-ratio considerations. Despite intensive investigations of these classic disordered solid phases, there remain several puzzles in understanding their complex defect structures. Early work, using both neutron diffraction [45] and computer modelling methods, [46] supported the formation of dopant/interstitial dimers and trimers in systems containing 5-10 mole% of the trivalent ion, dissolved substitutionally in the fluorite structured host. Recent work [47] has proposed more complex structures, in particular the cubo-octahedral structure containing 6 dopant ions. Computer modelling studies [48] have suggested that the relative stability of the different cluster types depends on the radius of the dopant ion, with clusters of the 2:2:2 and 4:3:2 type being stable for the larger dopant ions (e.g. La^{3+}) and the cubo-octahedral aggregates having greater stability for the smaller dopant ions (e.g. Y^{3+}, Er^{3+}). These predictions have been supported by EXAFS studies [49] and by recent single crystal neutron diffraction work [50,51]. Further neutron work is, however, needed with the following aims (i) to increase our knowledge of the variation of cluster structure with dopant radius, (ii) to study the effects of the host lattice-parameter on cluster structure experiments on doped SrF_2 and BaF_2, (iii) to investigate the temperature dependence of the cluster structure and (iv) to determine the effects of ageing on the defect structure of the solid solutions.

The possibility of very rapid data collection on D9 offers the unique opportunity of solving these problems and obtaining a definitive understanding of the structural properties of these important and complex solid solutions. The single crystal neutron work can be carried out in conjunction with computer modelling and EXAFS studies - a combination which has proved particularly effective in recent work on these systems [49]. The feedback from these studies into the analysis of existing high quality conductivity data will enable the mechanisms of F^- transport in these systems to be resolved. In addition future workers can explore the use of N.M.R. studies to ascertain the local environments of the paramagnetic rare earth ions. This technique has considerable potential as a structural tool and can be thoroughly tested for these materials against well-characterized systems.

Several halides that have the fluorite (CaF_2) structure may be classified as solid electrolytes at high temperatures because they have high halide ion conductivity. The hope of discovering a suitable solid with a high F^- ion conductivity is not beyond reach. The F^- ion is the smallest of the anions, and it possesses a single charge. As a consequence, fluorides can be predicted as the best anionic conductors. However in the case of defect complexes the details of the sites occupied are not known, especially in the more disordered structures at high temperatures. In the case of $KCaF_3$, dealt within Chapter 4

of this thesis, the results show that $KCaF_3$ is a straightforward structure with a low concentration of defects. Although there is some evidence for vacancies there is no significant occupation of interstitial sites. All the ions show a small amount of anharmonic behaviour and it is possible that the high conductivity could be due to a small population of highly mobile vacancies. The K^+ and Ca^{2+} cations are fairly rigidly fixed on their sites and the F^- anions show anharmonic oblate ellipsoid discus-like vibrations with no obvious move towards a saddle point (see proposed mechanism in Chapter 4); although expansible for conductivity $KCaF_3$ does not behave like other fluorides in which the F^- anions move off their sites. The $KCaF_3$ structure is probably a Schottky rather than a Frenkel disordered system. Although the F^- anions are vibrating in the superionic state and there appears to be lattice premelting or sublattice melting, a considerable number of F^- anions are still on their sites. For future work molecular dynamics or static simulation could be used to locate saddle points in possible migration pathways.

Several elpasolite structured halides, of general formula A_2BReX_6 (where A and B are monovalent ions and Re is a rare-earth cation) were prepared, and investigated in Chapter 5. High Resolution X-ray diffraction demonstrated a great complexity in all cases due to the multiphase present in all the compounds. The minority phases could not be identified using the Rietvield method [111]. For

future work however the problem can be overcome by preparing single crystals of the elpasolites using a melt growth method [145]. However due to the time involved, the studies would have to concentrate on one particular elpasolite. Experiments can be performed on both fluoride and chloride members of this class at several temperatures, including the high temperature superionic region. The work therefore presented in this chapter provides a basis for the further systematic investigation of these systems.

References

1. D.F. Shriver and G.C. Farrington, "Solid Ionic Conductors", Chem. and Eng. News, May 1985, 42.

2. P. Hagenmuller and W. van Gool, "Solid Electrolytes", 1978, Academic Press, New York.

3. P. Vashishta, J.N. Mundy and G.K. Shenoy, "Fast Ion Transport in Solids", 1979, North-Holland Publ., Amsterdam.

4. C.E. Subbarao, "Solid Electrolytes and their Applications", 1980, Plenum, New York.

5. B.J. Bates and G.C. Farrington, "Fast Ionic Transport In Solids", 1981, North-Holland Publ., Amsterdam.

6. T.H. Etsell and S.N. Flengas, Chem. Rev., 1970, 70, 339.

7. A.S. Nowick and D.S. Park, "Super Ionic Conductors" (G.D. Mahan and W.L. Roth, eds.), 1976, p. 395, Plenum, New York.

8. D.Y. Wang, D.S. Park, J. Griffith and A.S. Nowick, Solid State Ionics, 1981, 2, 95.

9. J.M. Réau and J. Portier, "Solid Electrolytes" (P. Hagenmuller and W. van Gool, eds), 1978, p. 313, Academic Press, New York.

10. J. Schoonman, J. Electrochem. Soc., 1976, 123, 1772.

11. J. Schoonman and A. Wolfert, Solid State Ionics, 1981, 314, 373.

12. J. Portier, J.M. Réau, S. Matar, J.L. Soubeyroux and P. Hagenmuller, Solid State Ionics, 1983, 11, 83.

13. A.B. Lidiard, "Crystals with the Fluorite Structure" (W.Hayes, ed.), 1974, Oxford Univ. Press (Clarendon), London and New York.

14. F. Bénière and C.R.A. Catlow "Mass Transport in Solids, Series B, Physics", 1983, 97, Plenum, New York.

15. V.M. Goldschmidt, T. Barth, G. Lunde and W. Zachariasen, Skr. Nor. Vidensk. Akad. Oslo, 1926, 1, 1.

16. A.A. Kaminskii and V.V. Osiko, Izv. Akad. Nauk SSSR, Neorgan. Mat., 1965, 1, 2049.

17. A.A. Kaminskii and V.V. Osiko, Isv. Akad, Nauk SSSR, Neorgan. Mat., 1967, 3, 417.

18. A.A. Kaminskii and V.V. Osiko, Isv. Akad, Nauk SSSR, Neorgan. Mat., 1970, 6, 629.

19. L.F. Johnson and H.J. Guggenheim, Appl. Phys. Lets., 1972, 20, 474.

20. L.F. Johnson and H.J. Guggenheim, Appl. Phys. Lets., 1973, 23, 96.

21. A.A. Kaminskii, S.É Sarkisov, K.B. Seiranyan, and B.P. Sobolev, Izv. Akad, Nauk SSSR, Neorgan. Mat., 1973, 9, 340.

22. A.A. Kaminskii, S.É. Sarkisov, K.B. Seiranyan, and B.P. Sobolev, Kvant. Elektron. (Mosc.), 1974, 1, 187. [Sov. J. Quant. Electron., 1974, 4, 112.]

23. H.J. Guggenheim and L.F. Johnson, Appl. Phys. Lets., 1969, 15, 51.

24. L.F. Johnson, J.E. Geusic, H.J. Guggenheim, T. Kushida, S. Singh, and L.G. Van Uitert, Appl. Phys. Lets., 1969, 15, 48.

25. A. Vecht and A. Hickey, J. Electrochem. Soc., 1971, 118, 71c.

26. Y. Mita, E. Nagasawa, K. Shiroki, Y. Ohono, and T. Matsubava, Appl. Phys. Lets., 1973, 23, 173.

27. J.D. Kingsley, G.E. Fennet, and S.V. Galginatis, Appl. Phys. Lets., 1969, 15, 115.

28. L.G. Van Uitert, L. Pictorski, and W.H. Grodkiewicz, Mater. Res. Bull., 1969, 4, 777.

29. R.A. Hewes and J.F. Sarver, Phys. Rev., 1969, 182, 427.

30. M. Tomkus and S. Natanson, J. Electrochem. Soc., 1971, 118, 70c.

31. V.V. Ovsyankin and P.P. Feofilov, Opt. Spekt., 1971, 31, 944.

32. V.V. Ovsyankin and P.P. Feofilov, ZhETF Pis. Red., 1966, 3, 494 [JETP Lett., 1966, 8, 322.

33. O. Adametz, Kristal. Teknik, 1972, 7, 1297.

34. Hj. Bernhardt, P.Görlich, and G. Kötitz, Phys. Status Solidi, 1971, a6, 479.

35. F.S. Maddocks and R.E. Than, J. Electrochem Soc., 1962, 109, 99.

36. V.S. Krikorov and V.G. Krasov, Transactions of Second All-Union Symposium on the Chemistry of Inorganic Fluorides [in Russian], In-t Obshchei Neorgan. Khim., 1970, p.133, Moscow.

37. B.P. Sobolev, P.P. Fedorov, B. Serianian and N.L. Tkachenko, J. Sol. State Chem., 1976, 17, 201.

38. R.E. Thoma, Rev. Chim. Miner., 1973, 10, 363.

39. R.H. Nafziger and N. Riazance, J. Am. Ceram. Soc., 1972, 55, 130.

40. P.P. Fedorov, O.E. Izotova, V.B. Alexandrov and B.P. Sobolev, J. Solid State Chem., 1974, 9, 368.

41. B.P. Sobolev and P.P. Fedorov, J. Less-Common Metals, 1978, 60, 33.

42. J.M. Short and R. Roy, J. Phys. Chem., 1963, 67, 1860.

43. N.L. Tkachenko, L.S. Garashina, O.E.Izotova, v.B. Alexandrov and B.P. Sobolev, J. Solid State Chem., 1973, 8, 213.

44. K.B. Seiranian, P.P. Fedorov, L.S. Garashina, G.V. Molev, V.V. Karelin and B.P. Sobolev, J. Cryst. Growth, 1974, 26, 61.

45. A.K. Cheetham, B.E.F. Fender and M.J. Cooper, J. Phys. C., 1971, 4, 3107.

46. C.R.A. Catlow, J. Phys. C., 1973, 6, L64.

47. P.J. Bendall, C.R.A. Catlow and B.E.F. Fender, J. Phys. C., 1984, 17, 797.

48. J. Corish, C.R.A. Catlow and P.W.M. Jacobs, Phys. Rev. B, 1982, 25, 6425.

49. L.M. Moroney, C.R.A. Catlow, A.V. Chadwick and G.N. Greaves, Radiation Effects, 1983, 75, 159.

50. C.R.A. Catlow, A.V. Chadwick and J. Corish, J. Solid State Chem., 1983, 48, 65.

51. C.R.A. Catlow, A.V. Chadwick and J. Corish, Radiation Effects, 1983, 75, 61.

52. J.A. Archer, A.V. Chadwick, I.R. Jack and B. Zeqiri, Solid State Ionics, 1983, 9 and 10, 505.

53. M. O'Keefe and T.O. Bovin, Science, 1979, 206, 599.

54. A.V. Chadwick, J.H. Strange, G. Ranieri and M. Terenzi, Solid State Ionics, 1983, 9 and 10, 555.

55. V.M. Bouznik, Y.N. Moskvich and V.N. Voronov, Chem. Phys. Lett., 1976, 37, 464.

56. H. Schutz and R. Bachmann, 'Fluorine distribution in the fast ionic conductor δPbF_2, ILL. Expt. no. 05-15-201 (1982 Annual Report) and Private Communication.

57. B.R. McGarvey and A. Reuvehi, J. Mag. Res., 1979, 34, 181.

58. L.R. Morss, M. Siegal, L. Stenger and N. Edelstein, Inorg. Chem., 1970, 9, 1771.

59. J.P. Besse and M. Capestan, C.R. Acad. Sci. (Paris), 1968, C266, 551.

60. A. Vedrine, J.P. Besse, G. Band and M. Capestan, Rev. Chim. Miner., 1970, 7, 593.

61. A. Vedrine, J.P. Besse, G. Band and M. Capestan, Rev. Chim. Miner., 1971, 8, 663.

62. S. Aleonard and C. Pouzet, J. Appl. Crystallography, 1968, 1, 113.

63. C. Cheng and P.B. Dorain, J. Chem. Phys., 1976, 65, 785.

64. H.D. Amberger and G.G. Rosenbauer, J. Phys. Chem. Solids, 1977, 38, 379.

65. E. Bucher, H.J. Guggenheim, K. Andres, G.W. Hull, Jnr. and A.S. Cooper, Phys. Rev. B, 1974, 10, 2945.

66. M.V. Hoehn and D.G. Karraker, J. Chem. Phys., 1974, 60, 393.

67. B.D. Dunlop and G.H. Shenoy, Phys. Rev. B, 1975, 12, 2716.

68. R.W. Schwartz, S.F. Watkins, C.J. O'Connor and R.L. Carbin, J. Chem. Soc. Faraday Trans. II, 1976, 72 565.

69. G.E. Fish and H.J. Stapleton, J. Chem. Phys. 1976, 65, 785.

70. R.W.G. Wyckoff, "Crystal Structures", 2nd Ed., 1965, Vol. 1, p.239, Interscience.

71. A.B. Lidiard, "Handbuch der Physik" (S. Flügge, ed.), 1957, Vol. 20, p.507. Springer-Verlag, Berlin and New York.

72. C.R.A. Catlow, Comments Solid State Phys., 1980, 9, 157.

73. A.V. Chadwick, Radiat. Eff.,1983, 74, 17.

74. C.R.A. Catlow, "Non-stoichiometric Oxides" (O.T. Sorensen, ed.), 1981, Academic Press, New York.

75. W. Hayes and A.M. Stoneham, "Crystals with the Fluorite Structure" (W. Hayes, ed.), 1974, p.472. Oxford Univ. Press, London and New York.

76. W. Hayes and I. Staebler, "Crystals with the Fluorite Structure" (W. Hayes, ed.), 1974, Oxford Univ. Press, London and New York.

77. R.M. Dell and A. Hooper, "Solid Electrolytes", eds., 1978, P. Hayenmuller and W. van Gool, (Academic Press, New York, ch. 18).

78. P.P. Sorokin and M.J. Stevenson, IBM J. Res. Develop., 1961, 5, 56.

79. C.R.A. Catlow, PhD. Thesis, University of Oxford, 1974.

80. A.S. Dworkin and M.A. Bredig, J. Phys Chem., 1968, 72, 1277.

81. W. Schroter and J. Nolting, J. Phys. (Paris), 1980, 41, C6-20.

82. C.E. Derrington, A. Lindner and M. O'Keeffe, J. Solid State Chem., 1975, 15, 171.

83. M.H. Dickens, W. Hayes, M.T. Hutchings and C. Smith, J. Phys. C., 1979, 12, L97.

84. M. Dixon and M.J. Gillan, J. Phys. C., 1980a, 13, 1901.

85. M. Dixon and M.J. Gillan, J. Phys. C., 1980b, 13, 1919.

86. M.H. Dickens, W. Hayes, M.T. Hutchings and C. Smith, J. Phys. C., 1982, 15, 4043.

87. C.R.A. Catlow, and W. Hayes, J. Phys. C., 1982, 15, L9.

88. W.G. Lyon, D.W. Osborne, H.E. Flotow and F. Grandjean, J. Chem. Phys., 1978, 68, 167.

89. J.M. Baker, "Crystals with the Fluorite Structure" (W. Hayes, Ed.), 1974, Oxford Univ. Press, London and New York.

90. B.T.M. WIllis, Proc. Bri. Ceram. Soc., 1964, 1, 9.

91. C.R.A. Catlow, J. Phys. C., 1976, 9, 1845.

92. P. Gettman and O. Greiss, J. Solid State Chem., 1978, 26, 255.

93. D.J.M. Bevan, J. Strähle and O. Greiss, J. Solid State Chem., 1982, 44, 75.

94. C.R.A. Catlow, J. Corish and P.W.M. Jacobs, J. Solid State Chem., 1984, 51, 159.

95. J. Schoonman, Solid State Ionics, 1980, 1, 123.

96. C. Kittel, "An Introduction to Solid State Physics", 6th edition, 1986, Ch.2, Wiley, New York.

97. A.K. Cheetham in "Thermal Neutron Diffraction", 1970, (ed. B.T.M. Willis), Ch.10, Oxford University Press.

98. W.J.A.M. Peterse and J.H. Palm, Acta Cryst., 1966, 20, 147.

99. B.T.M. Willis, Acta Cryst., 1969, A25, 277.

100. B.E.F. Fender in "Thermal Neutron Diffraction", (ed. B.T.M. Willis), 1970, Ch.11, Oxford University Press.

101. J.M. Cowley, Phys. Rev., 1950, 77, 669.

102. G.E. Bacon, "Neutron Diffraction", 3rd edition, 1975, Clarendon Press, Oxford.

103. B.T.M. Willis, Acta Cryst.,1970, A26, 396.

104. P.M. de Wolff, Acta Cryst., 1957, 10, 590, 590; 1958, 11, 664.

105. "Ortec Instruments for Research" Catalogue 1002.

106. G. Caglioti, A. Paoletti and F.P. Ricci, Nucl. Instrum., 1958, 3, 223.

107. C.G. Windsor, "Pulsed Neutron Scattering", 1981, Taylor and Francis, London.

108. G.E. Bacon, "X-ray and Neutron Diffraction", 1966, Pergammon Press, Oxford.

109. H. Lipson and W. Cochran "The Determination of Crystal Structures", 1953, Bell and Sons, London.

110. J.W. Visser, J. Appl. Cryst., 1969, 2, 89.

111. H.M. Rietveld, J. Appl. Cryst., 1969, 2, 65.

112. H.P. Klug and L.E. Alexander. "X-ray Diffraction Procedures", 2nd edition, 1959, Wiley, New York.

113. J.S. Rollet, "Computing Methods in Crystallography", 1965, pp. 32-37, Pergammon Press, Oxford.

114. P.J. Bendall, D. Phil Thesis, University of Oxford, 1980.

115. P.J. Bendall, A.N. Fitch and B.E.F. Fender, J. Appl. Cryst., 1983, 16, 164.

116. A. Albinati and B.T.M. Willis, J. Appl. Cryst., 1982, 15, 361.

117. A.K. Cheetham and J.C. Taylor, J. Solid State Chem., 1977, 21, 253.

118. T. Vogt, Neues Jahrb. Mineral. Abh., 1914, 2, 9.

119. J.A.A. Ketelaar and P.J.H. Williams, Rec. Trav. Chim. Pays-Bas, 1937, 56, 29.

120. E. Zintl and A. Udgard, Z. Anorg. Chem., 1939, 240, 150.

121. R.W.M. D'Eye and F.S. Martin, J. Chem. Soc., 1957, 61, 1847.

122. M. Rubenstein and E. Banks, J. Electrochem. Soc., 1959, 106, 404.

123. R.W.M. D'Eye and I.F. Ferguson, J. Chem. Soc., 1959, 63, 3401.

124. D.M. Roy and R. Roy, J. Electrochem Soc., 1964, 111, 421.

125. J.P. Besse and M. Capestan, Bull. Soc. Chim. Fr., 1967, 4, 1341.

126. E. Catalano, R.G. Bedford, V.C. Silvera and H.H. Wickman, J. Phys. Chem. Solids, 1969, 30, 1613.

127. H. Hahn, W. Seeman and H.L. Kohyn, Z. Anorg. Chem., 1969, 369, 48.

128. A.D. Franklin and R. Spal, Am. Ceram. Soc. Bull., 1972, 51, 320.

129. R.C. Pastor, A.C. Pastor and K.T. Miller, Mater. Res. Bull., 1974, 9, 1247.

130. V.B. Alexandrov and L.S. Garashina, Dokl. Akad. Nauk SSSR, 1969, 189, 307.

131. A.K. Cheetham, B.E.F. Fender, D. Steele, R.I. Taylor and B.T.M. Willis, Solid State Commun, 1970, 8, 171.

132. Kh. S. Bagdasarov, Yu.K.Voronko, A.A. Kaminskii, V.V. Osiko and A.M. Prokhorov, Kristallografiya, 1965, 10, 746.

133. P.P. Sorokin and M.J. Stevenson, Phys. Rev. Lett., 1960, 5, 557.

134. A.A. Kaminskii, Lazernye Kristally, 1975, Nauka, Moscow.

135. R.E. Thoma and G.D. Brunton, Inorg. Chem., 1966, 5, 1937.

136. D.P. Devor and M. Robinson, Phys. Rev. Letters, 1969, 23, 704.

137. I.N. Seleznev and N.N. Shuikin, Krantoraya Elektron., 1974, 1, 1485.

138. T.N. Rezukhina, Zh. Neorg. Khim., 1972, 46, 1565.

139. L.E. Nagel and M. O'Keeffe, in W. van Gool (ed.), Fast Ion Transport in Solids, Solid State Batteries and Devices, Proc. NATO Adv. Study Inst., 1972, Belgirate, North-Holland Publ. Co., 1973, Amsterdam.

140. A.R. Patel and C.C. Desai, J. Phys. D, 1970, 3, 1645.

141. F.H. Spedding and A.H. Daane, Prog. Nucl. Energy, Ser.5, 1956, 1, 413.

142. J.P. Laval and B. Frit, J. Solid State Chem., 1983, 49, 237.

143. O. Greis, Rev. Chim. Miner., 1978, 15, 481.

144. J. Czochralski, Z. Phy. Chem., 1917, 92, 219.

145. D.C. Stöckbarger, Rev. Sci. Instrum., 1936, 7, 133.

146. W. Hayes, Superionic Conductors, Contemporary Physics, 1978, 19, 469.

147. R.E. Gordon and J.H. Strange, Self-diffusion Studies in solids using N.M.R. techniques, Faraday Symposium, 1979, 13, 153.

148. J.A. Kilner, The calculation of defect energies in the perovskite fluoride $KMnF_3$, Philos. Mag., 1980, A43, 1473.

149. M.T. Hutchings in Proc. Symp. Neutron Scattering, Argonne Nat. Lab., AIP Conf. Proc. 1981.

150. M.H. Dickens, W. Hayes, C. Smith and M.T. Hutchings in 'Fast Ion Transport in Solids', eds. P. Vashishta, J.N. Mundy and G.K. Shenoy (North Holland 1979), 225.

151. A. Bulou, J. Novet, A.W. Hewat and F.J. Schafer, Ferroelectrics, 1980, 25, 375.

152. M. Dixon and M.J. Gillan, J. Phys.,1979, C11, L165.

153. D.R. Figueroa, A.V. Chadwick and J.H. Strange, N.M.R. relaxation, ionic conductivity and the self-diffusion process in barium fluoride, J. Phys. C., 1978, 11, 55.

154. J.K. Cockcroft, Reflection Generation Program, I.L.L., Grenobol, France.

155. J.O. Lundgren, Institute of Chemistry, 1972, Uppsala, extinction correction and refinement according to the Becker-Coppens formalism added by K. Hermansson, 1978, Uppsala, anharmonic thermal tensor refinement modified by G.J. McIntyre, 1981.

156. G. Meyer, "the synthesis and structures of complex rare-earth halides", Prog. Solid St. Chem., 1982, 14, 177.

157. G. Menzer, Fortschr. Mineral, 1932, 17, 61.

158. L.R. Morss, J. Inorg. Nucl. Chem., 1974, 36, 3876.

159. G. Meyer, "the synthesis and structures of complex rare-earth halides", Prog. Solid St. Chem., 1982, 14, 141.

160. G. Meyer and E. Dietzel, Rev. Chim. Miner., 1979, 16, 189.

161. R.W. Schwartz, S.F. Watkins, C.J. O'Connor and R.L. Carlin, J. Chem. Soc. Faraday II, 1976, 72, 565.

162. K.S. Aleksandrov, A.T. Anistratov, V.I. Zinenko, I.M. Iskornev, S.V. Misul and L.A. Shabanova, Ferroelectrics, 1980, 26, 653.

163. G. Meyer and H.-C. Gaebell, Z. Naturfor sch., 1978, 33b, 1476.

164. G. Meyer, Z. Naturforsch., 1980, 35b, 394.

165. H.G.F. Winkler, Acta Crystallogr., 1954, 7, 33.

166. D. Babel and R. Haegele, J. Solid State Chem., 1976, 18, 39.

167. J. Arndt, D. Babel, R. Haegele and N. Rombach, Z. anorg. allg. Chem., 1975, 418, 193.

168. G. Meyer and W. Moritz, unpublished research, 1980.

169. G. Meyer and H.-C. Gaebell, unpublished research, 1978.

170. G. Meyer and W. Duesmann, Z. anorg. allg. chem., 1982, 485, 133.

171. G. Meyer, unpublished research, 1979.

172. L.R. Morss, M. Siegal, L. Stenger and N. Edelstein, "Preparation of cubic Chloro Complex Compounds of Trivalent Metals: Cs_2NaMCl_6, Inorganic Chemistry, 1970, 9, 1771.